To the Graduate Council:

I am submitting herewith a thesis written by Manish Sangal entitled "In-Line Monitoring of Partially Miscible Molten Polymer Blends." I have examined the final copy of this thesis for form and content and recommend that it is accepted in partial fulfillment of the requirements for the degree of Master of Science, with a major in Chemical Engineering.

Marion G. Hansen, Major Professor

We have read this thesis
and recommend its acceptance:

Accepted for the Council:

Associate Vice Chancellor
and Dean of The Graduate School

IN-LINE MONITORING OF PARTIALLY MISCIBLE MOLTEN POLYMER BLENDS

A Thesis
presented for the
Master of Science
Degree

The University of Tennessee, Knoxville

Manish Sangal
December, 1995

ACKNOWLEDGMENTS

The author would like to thank his major professor, Dr. Marion G. Hansen for his guidance, patience and encouragement throughout this research. The author also wishes to thank his committee members, Dr. T. W. Wang and Dr. E. S. Clark for their guidance, comments, and assistance. A special note of thanks to all fellow graduate students for their help and encouragement. The financial support from the Chemical Engineering department and Center for Computer Integrated Engineering, University of Tennessee is gratefully acknowledged. Finally, the author wishes to thank his family and close friends for their continual support and encouragement at all times, without which this work could not have been accomplished.

ABSTRACT

High quality products, lower costs, reduction in waste, and improved profitability are important concerns of industries in plastics manufacturing. *In-situ* or in-line monitoring of flowing molten polymers by fiber optic near infrared (NIR) spectroscopy offers all these advantages along with ease of handling molten polymers during the manufacture of plastics.

The objective of this research is to demonstrate the viability of using NIR spectroscopy coupled with fiber optics, for in-line composition monitoring of partially miscible polymer blends. Studies on blends of styrene-acrylonitrile (SAN)/acrylonitrile-butadiene-styrene (ABS), SAN/polycarbonate (PC), and PC/ABS were performed.

Absorbance data for the molten blends was recorded in the NIR region from 1200 nm to 2400 nm. Multivariate analysis by partial least squares (PLS) and principal component regression (PCR) of the spectroscopic data was carried out to develop robust calibration models, which were subsequently used for predicting the composition of unknown samples of the polymer blends. For the partially miscible blend systems, qualitative and quantitative interpretation of loadings and scores showed meaningful contributions from the first three factors for ABS/SAN and SAN/PC blends and from the first two factors for PC/ABS blends. Standard errors of calibration (SEC) and standard error of prediction (SEP) values were also calculated based on the optimal number of factors for the calibration and prediction sets, respectively.

TABLE OF CONTENTS

Chapter		*Page*
1.	INTRODUCTION	1
2.	NIR BACKGROUND	3
2.1	Introduction to the Near Infrared (NIR) region	3
2.2	Theory	4
2.3	Spectral analysis: Band Assignments	11
2.4	Process analysis, Sampling Techniques, and Instrumentation	21
2.5	Advantages of NIR spectroscopy	26
3.	CHEMOMETRICS: MULTIVARIATE ANALYSIS OF SPECTRAL DATA	28
3.1	Overview of techniques used	30
3.2	Data analysis of spectral data	41
4.	APPLICATIONS OF NIR SPECTROSCOPY	47
4.1	Polymers	47
4.2	Miscellaneous	65
5.	EXPERIMENTAL SETUP FOR IN-LINE MONITORING OF POLYMER BLENDS	70
5.1	Equipment and Experimental Setup	70

5.2 Rugged Probes and Optical Fibers 72
5.3 Overview of the Polymer Blend Systems used for Experimental Research 76

6. IN-LINE MONITORING OF ACRYLONITRILE-BUTADIENE STYRENE (ABS)-STYRENE/ACRYLONITRILE (SAN) BLENDS 78

7. IN-LINE MONITORING OF STYRENE-ACRYLONITRILE (SAN)/ POLYCARBONATE (PC) BLENDS 122

8. IN-LINE MONITORING OF POLYCARBONATE (PC)/ACRYLONITRILE-BUTADIENE STYRENE (ABS) BLENDS 160

9. CONCLUSIONS AND FUTURE WORK 194

REFERENCES 198

APPENDICES 207
A. DATA ANALYSIS 208
B. COMPUTER CODES 213

VITA 233

LIST OF TABLES

Table *Page*

6.1 Percent variances explained by the PLS and PCR models for increasing number of factors in the analysis of the overtone region (1600 nm to 1800 nm) for ABS/SAN blends 92

6.2 Comparison of calibration and prediction errors using PLS and PCR in the overtone and combination regions for ABS/SAN blends 99

6.3 Percent variances explained by the PLS and PCR models for increasing number of factors in the full spectrum analysis (1200 nm to 2400 nm) for ABS/SAN blends 110

6.4 Comparison of calibration and prediction errors using PLS and PCR in the region from 1200 nm to 2400 nm for ABS/SAN blends 113

7.1 Percent variances explained by the PLS and PCR models for increasing number of factors in the analysis of the overtone region (1600 nm to 1800 nm) for SAN/PC blends 136

7.2 Comparison of calibration and prediction errors using PLS and PCR in the overtone and combination regions for SAN/PC blends 143

7.3 Percent variances explained by the PLS and PCR models for increasing number of factors in the full spectrum analysis (1200 nm to 2400 nm) for SAN/PC blends..... 154

7.4 Comparison of calibration and prediction errors using PLS and PCR in the region from 1200 nm to 2400 nm for SAN/PC blends..... 157

8.1 Percent variances explained by the PLS and PCR models for increasing number of factors in the analysis of the overtone region (1600 nm to 1800 nm) for ABS/PC blends..... 173

8.2 Comparison of calibration and prediction errors using PLS and PCR in the overtone and combination regions for ABS/PC blends..... 187

8.3 Percent variances explained by the PLS and PCR models for increasing number of factors in the full spectrum analysis (1200 nm to 2400 nm) for ABS/PC blends..... 188

8.4 Comparison of calibration and prediction errors using PLS and PCR in the region from 1200 nm to 2400 nm for ABS/PC blends..... 190

LIST OF FIGURES

Figure *Page*

2.1 The electromagnetic radiation spectrum [4] 5

2.2 Energy diagram for an ideal and anharmonic oscillator [5] 9

2.3 Chemical structures of functional groups absorbing in the NIR region [12] 15

2.4 Spectra-structure correlations and average molar absorptivity data [10] 22

3.1 Representation of principal component analysis with a 3-dimensional object [30] 37

4.1 Epoxy resin curing study [6] 50

4.2 PS/PPO blends in the region from 1600 nm to 1800 nm [2] 64

4.3 On-line NIR measurements of research octane number (RON) over time [63] 67

5.1 Experimental setup for in-line monitoring of molten polymers 71

5.2 Fiber optic probe for *in-situ* monitoring [2] 74

5.3 Schematic diagram of an optical fiber [54] 75

5.4 Polymer resins in the partially miscible polymer blend systems 77

6.1 Chemical structures of styrene-acrylonitrile (SAN) and acrylonitrile-butadiene-styrene (ABS). x, y, and z represent the number of repeat units in the two polymers 83

6.2 Overlaid NIR absorbance spectra (averaged raw data) of pure SAN and pure ABS in the region from 1200 nm to 2400 nm @ 250 °C 85

6.3 Overlaid NIR absorbance spectra (averaged raw data) for each of the ABS/SAN blend compositions in the region from 1200 nm to 2400 nm @ 250 °C 86

6.4 Plot of variance in absorbance vs. wavelength for the ABS/SAN blend compositions (averaged raw data) in the region from 1200 nm to 2400 nm @ 250 °C 88

6.5 Overlaid NIR absorbance spectra (smoothed and baseline corrected data) for each of the ABS/SAN blend compositions in the overtone region from 1600 nm to 1800 nm 90

6.6 Overlaid NIR absorbance spectra (smoothed and baseline corrected data) for each of the ABS/SAN blend compositions in the combination region from 2075 nm to 2215 nm 91

6.7 Variances explained by the wavelengths after considering, (a) First factor only, (b) Second factor only, for the ABS/SAN blends in the region from 1600 nm to 1800 nm 93

6.8 Overall variances explained by the wavelengths after considering, (a) First two factors, (b) First three factors for the ABS/SAN blends in the region from 1600 nm to 1800 nm 94

6.9 PRESS values for leave-a-sample (LAS) and leave-a-group (LAG) cross-validation methods using PLS, for the ABS/SAN blends in the overtone region from 1600 nm to 1800 nm 96

6.10 Plot of SEC and SEP for calibration and validation sets, respectively, for increasing number of factors using PLS, for the ABS/SAN blends in the overtone region from 1600 nm to 1800 nm 97

6.11 Model predictions for the calibration set (based on absorbance data) using PLS, plotted against the reference (actual) concentrations for the ABS/SAN blends in the region from 1600 nm to 1800 nm 100

6.12 Model predictions for the validation set (based on absorbance data) using PLS, plotted against the reference (actual) concentrations for the ABS/SAN blends in the region from 1600 nm to 1800 nm..... 101

6.13 Loadings plot for first, second, and third factors for samples in the calibration set (based on absorbance data) using PLS, for ABS/SAN blends in the overtone region from 1600 nm to 1800 nm..... 102

6.14 Scores plot for first, second, and third factors for samples in the calibration set (based on absorbance data) using PLS, for ABS/SAN blends in the overtone region from 1600 nm to 1800 nm..... 103

6.15 First, second, and third factor scores for samples in the calibration set for the ABS/SAN blends using PLS in the region from 1600 nm to 1800 nm..... 105

6.16 First factor vs second factor scores for samples in the calibration set, for the ABS/SAN blends using PLS in the overtone region from 1600 nm to 1800 nm..... 106

6.17 (a) projection of scores on second and third factors, (b) projection of scores on first and third factors, for the ABS/SAN blends using PLS in the region from 1600 nm to 1800 nm..... 107

6.18 First factor vs second factor scores for samples in the calibration set, for the ABS/SAN blends using PCR in the region from 1600 nm to 1800 nm..... 109

6.19 Scores plot for first, second, and third factors for full spectral analysis (based on absorbance data) using PLS in the region from 1200 nm to 2400 nm for samples in the calibration set, for ABS/SAN blends 111

6.20 Overlaid NIR absorbance spectra (average data) of PET with varying TiO_2 content in the region from 1200 nm to 2400 nm 115

6.21 Loadings plot for first, second, and third factors for samples in the calibration set (based on absorbance data) using PLS in the region from 1200 nm to 2400 nm, for PET with varying TiO_2 content 117

6.22 Scores plot for first, second, and third factors for samples in the calibration set (based on absorbance data) using PLS in the region from 1200 nm to 2400 nm, for PET with varying TiO_2 content 118

6.23 Difference in absorbance for the ABS/SAN blends compared to the absorbance of an ideal blend of the same composition (based on the absorbances of pure SAN and pure ABS), in the region from 1200 nm to 2400 nm 119

6.24 Mean-centered and normalized spectra for PET with varying TiO_2 content in the region from 1200 nm to 2400 nm [26] 121

7.1 Chemical structures of styrene-acrylonitrile (SAN) and bisphenol-A polycarbonate (PC). x, y, and n represent the number of repeat units in the two polymers..... 123

7.2 Overlaid NIR absorbance spectra (averaged raw data) of pure SAN and pure PC in the region from 1200 nm to 2400 nm @ 260 °C..... 129

7.3 Overlaid NIR absorbance spectra (averaged raw data) for each of the SAN/PC blend compositions in the region from 1200 nm to 2400 nm @ 260 °C..... 130

7.4 Plot of variance in absorbance vs. wavelength for the SAN/PC blend compositions (averaged raw data) in the region from 1200 nm to 2400 nm @ 260 °C..... 131

7.5 Overlaid first derivative NIR absorbance spectra for each of the SAN/PC blend compositions in the overtone region from 1600 nm to 1800 nm..... 133

7.6 Overlaid first derivative NIR absorbance spectra for each of the SAN/PC blend compositions in the combination region from 2065 nm to 2185 nm..... 134

7.7 Variances explained by the wavelengths after considering, (a) First factor only, (b) Second factor only, for the SAN/PC blends in the region from 1600 nm to 1800 nm..... 137

7.8 Overall variances explained by the wavelengths after considering, (a) First two factors, (b) First three factors for the SAN/PC blends in the region from 1600 nm to 1800 nm 138

7.9 PRESS values for leave-a-sample (LAS) and leave-a-group (LAG) cross-validation methods using PLS, for the SAN/PC blends in the overtone region from 1600 nm to 1800 nm 141

7.10 Plot of SEC and SEP for calibration and validation sets, respectively, for increasing number of factors using PLS, for the SAN/PC blends in the overtone region from 1600 nm to 1800 nm 142

7.11 Model predictions for the calibration set (based on first derivative absorbance data) using PLS, plotted against the reference (actual) concentrations for the SAN/PC blends in the region from 1600 nm to 1800 nm 144

7.12 Model predictions for the validation set (based on first derivative absorbance data) using PLS, plotted against the reference (actual) concentrations for the SAN/PC blends in the region from 1600 nm to 1800 nm 145

7.13 Loadings plot for first, second, and third factors for samples in the calibration set (based on first derivative absorbance data) using PLS, for SAN/PC blends in the overtone region from 1600 nm to 1800 nm 146

7.14 Scores plot for first, second, and third factors for samples in the calibration set (based on first derivative absorbance data) using PLS, for SAN/PC blends in the overtone region from 1600 nm to 1800 nm..... 148

7.15 First, second, and third factor scores for samples in the calibration set for the SAN/PC blends using PLS in the region from 1600 nm to 1800 nm..... 149

7.16 First factor vs. second factor scores for samples in the calibration set, for the SAN/PC blends using PLS in the overtone region from 1600 nm to 1800 nm..... 151

7.17 (a) projection of scores on second and third factors, (b) projection of scores on first and third factors, for the SAN/PC blends using PLS in the region from 1600 nm to 1800 nm..... 152

7.18 First factor vs second factor scores for samples in the calibration set, for the SAN/PC blends using PCR in the region from 1600 nm to 1800 nm..... 153

7.19 Scores plot for first, second, and third factors for full spectral analysis (based on first derivative absorbance data) using PLS in the region from 1200 nm to 2400 nm for samples in the calibration set, for SAN/PC blends... 156

7.20 Difference in absorbance for the SAN/PC blends compared to the absorbance of an ideal blend of the same composition (based on the absorbances of pure SAN and pure PC), in the region from 1200 nm to 2400 nm 158

8.1 Chemical structures of polycarbonate (PC) and acrylonitrile-butadiene-styrene (ABS). x, y, z, and n represent the number of repeat units in the two polymers 161

8.2 Overlaid NIR absorbance spectra (averaged raw data) of pure PC and pure ABS in the region from 1200 nm to 2400 nm @ 260 °C 166

8.3 Overlaid NIR absorbance spectra (averaged raw data) for each of the ABS/PC blend compositions in the region from 1200 nm to 2400 nm @ 260 °C 167

8.4 Plot of variance in absorbance vs. wavelength for the ABS/PC blend compositions (averaged raw data) in the region from 1200 nm to 2400 nm @ 260 °C 169

8.5 Overlaid first derivative NIR absorbance spectra for each of the ABS/PC blend compositions in the overtone region from 1600 nm to 1800 nm 171

8.6 Overlaid first derivative NIR absorbance spectra for each of the ABS/PC blend compositions in the combination region from 2050 nm to 2200 nm 172

8.7 Variances explained by the wavelengths after considering, (a) First factor only, (b) Second factor only, for the ABS/PC blends in the region from 1600 nm to 1800 nm 174

8.8 Overall variances explained by the wavelengths after considering, (a) First two factors, (b) First three factors for the ABS/PC blends in the region from 1600 nm to 1800 nm 176

8.9 PRESS values for leave-a-sample (LAS) and leave-a-group (LAG) cross-validation methods using PLS, for the ABS/PC blends in the overtone region from 1600 nm to 1800 nm 178

8.10 Plot of SEC and SEP for calibration and validation sets, respectively, for increasing number of factors using PLS, for the ABS/PC blends in the overtone region from 1600 nm to 1800 nm 179

8.11 Model predictions for the calibration set (based on first derivative absorbance data) using PLS, plotted against the reference (actual) concentrations for the ABS/PC blends in the region from 1600 nm to 1800 nm 180

8.12 Model predictions for the validation set (based on first derivative absorbance data) using PLS, plotted against the reference (actual) concentrations for the ABS/PC blends in the region from 1600 nm to 1800 nm 181

8.13 Loadings plot for first and second factors for samples in the calibration set (based on first derivative absorbance data) using PLS, for ABS/PC blends in the overtone region from 1600 nm to 1800 nm 182

8.14 First and second factor scores for samples in the calibration set (based on first derivative absorbance data) for the ABS/PC blends using PLS in the region from 1600 nm to 1800 nm 184

8.15 First factor vs. second factor scores for samples in the calibration set, for the ABS/PC blends using PLS in the overtone region from 1600 nm to 1800 nm 185

8.16 Scores plot for first and second factors for full spectral analysis (based on first derivative absorbance data) using PLS in the region from 1200 nm to 2400 nm for samples in the calibration set, for ABS/PC blends 189

8.17 Difference in absorbance for the ABS/PC blends compared to the absorbance of an ideal blend of the same composition (based on the absorbances of pure ABS and pure PC), in the region from 1200 nm to 2400 nm 192

1. INTRODUCTION

Control of continuous processes in the chemical industry requires measurement of the constituents in the process stream. Near infrared (NIR) spectroscopy along with fiber optics and computers provides an excellent analytical tool for measurements in real time. Such process control techniques provide quality products, minimize the waste generated by out of specification products and provide better control of the continuous process.

Real time monitoring of a process can result in better control and understanding of the process either through statistical process control or feedback loops. In-line analysis in real time enhances process control, thereby providing improved product quality, reducing waste, and resulting in improved profitability [1].

In-line monitoring of molten polymers is extremely useful for the production of uniform polymer products of consistent quality. In-line monitoring of extrusion processes reduces cost by minimizing the production of out of specification products in the plastics industry. It also decreases the time and effort required for sample preparation and analyses by the laboratory methods in off-line analyses. These advantages make in-line monitoring a cost effective and rapid analysis technique for monitoring polymeric processes [2].

What is In-Line NIR transmission spectroscopy?

In-line NIR transmission spectroscopy involves transmission of NIR light through the process stream, collecting the transmitted light and analyzing the NIR absorbance spectrum. The NIR spectra, is quantitatively analyzed by multivariate techniques to determine the composition of constituents in the process stream. At no time is a sample removed from the process stream even though the spectrometer is remote from the process stream. The calibration model formed as a result of this analysis is subsequently used for in-line composition predictions of the process stream based on the NIR absorbance spectra.

NIR instrumentation and analysis is now being used in many different applications ranging from rapid and precise quantitative analysis of food samples, to petrochemical process control operations, and in-line monitoring of polymeric melt processes. The availability of precision instrumentation, statistics and computer software are important factors for the growth of NIR analytical techniques in the last decade.

Recent advances in instrumentation and development of multivariate statistical analyses techniques have resulted in NIR spectroscopy as an important analytical tool for process monitoring and quality control applications. McClure reported that NIR spectroscopy was one of the fastest growing analytical technologies in the world. No doubt "the giant is running strong" [3].

2. NIR BACKGROUND

2.1 INTRODUCTION TO THE NEAR INFRARED (NIR) REGION

Early in the nineteenth century, in an attempt to determine the color within the visible spectrum responsible for the heat in sunlight, Sir William Herschel performed an experiment using a glass prism and a thermometer to separate the colors of the sun's "white" light. He observed that the temperature did not change much in the visible spectrum, but increased beyond the red end of the spectrum, indicating that there was energy beyond the red light. Being unable to see it, he named it infrared (IR) (Latin prefix meaning below) [4]. In 1990, Herschel was credited for his discovery of the NIR region; thereby the region from 700 nanometers (nm) to 1100 nm is often referred to as the "Herschel region" [3].

In about 1900, W. W. Coblentz built an IR spectrometer consisting of a rock salt prism and a sensitive thermopile as a detector, connected to a mirror galvanometer. The mid-IR spectra of hundreds of compounds between 10000-15000 nm was measured but no two compounds gave the same IR spectral readings. He observed that compounds with similar chemical groups had similar absorption bands. For instance, even though ethanol and methyl ether, have the same number of carbon (C), hydrogen (H), and oxygen (O) atoms, their IR spectra are very different. All alcohols, phenols, carboxylic acids have an absorption band near 2700 nm due to the presence of the hydroxyl (OH) groups.

This led to the important idea that if the spectrum of a compound could be measured, one could obtain some useful information about the structure of the compound.

Coblentz concluded that the IR spectrum of every compound is unique or is a "fingerprint." The region from 2000-15000 nm is still referred to as the fingerprint region [4].

Over the years, a great deal of information has been acquired about the electromagnetic spectrum. Figure 2.1 shows the entire electromagnetic radiation spectrum [4]. The infrared region is further subdivided into three regions: the near infrared (NIR) region from 750 nm to 2500 nm, the mid-infrared (mid-IR) region from 2500 nm to 15000 nm; and the far infrared (far IR) region from 15000 nm to 25000 nm.

The mid-IR region is marked by fundamental absorption bands, with high absorptivities. Sharp peaks, characteristic of a particular compound are observed in this region. Mid-IR spectra have also been used for the characterization of structures and product identification. The NIR region has overtone and combination bands arising due to the fundamental absorptions in the mid-IR. Bands in the NIR region are broad and overlapping, resulting in their limited qualitative interpretive value. However, the spectral bands in this region have enormous potential for quantitative analysis using multivariate techniques.

2.2 THEORY

Near infrared spectra is the result of light absorbed by organic molecules. Absorption bands in the NIR region are due to overtones and combination of fundamental absorption bands occurring in the mid-IR region (2500 nm-15000 nm) of the electromagnetic spectrum.

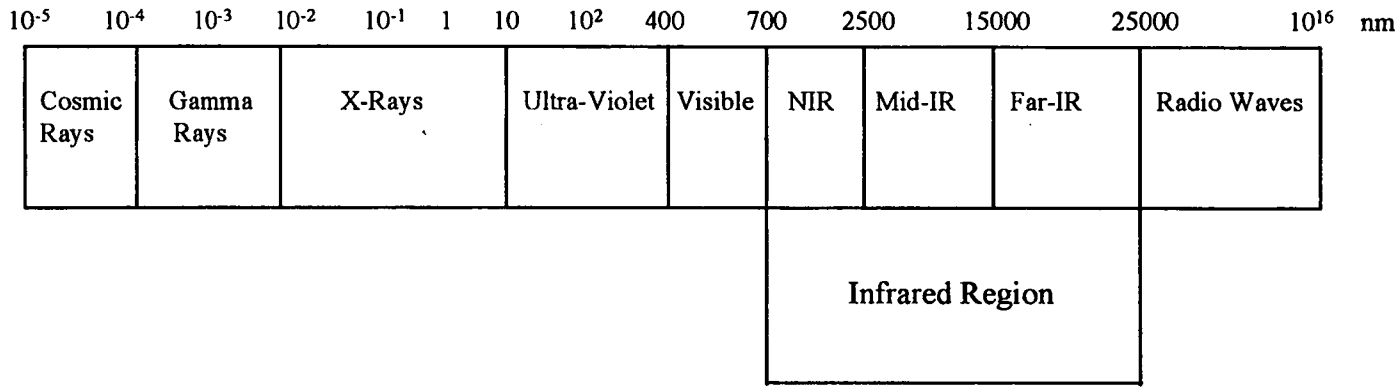


Figure 2.1 The electromagnetic radiation spectrum [4].

For an ideal diatomic harmonic oscillator obeying Hooke's law, the vibrational frequency is given by [5]:

$$\nu_{osc} = \frac{1}{2\pi}\sqrt{\frac{k}{u}} \tag{2.1}$$

where

ν_{osc} is the vibrational frequency of the oscillator

k is the classical force constant

u is the reduced mass of the two atoms

This classical spring model for molecular vibrations allows an infinite number of energy levels, but according to quantum theory only discrete energy levels are possible. In case of diatomic molecules, the energy levels are given by:

$$E_{\nu_{osc}} = (v + ½)h\nu_{osc} \tag{2.2}$$

where

$E_{\nu_{osc}}$ is the energy of vibration of the oscillator

ν_{osc} frequency of vibration of the oscillator

v is the vibrational quantum number

h is Planck's constant

The energy difference between successive levels is $h\nu_{osc}$.

For polyatomic molecules the possible energy levels are numerous, as they can be considered as a series of diatomic harmonic oscillators. The equation of energy for polyatomic molecules is given by [5]:

$$E_{\nu_{osc}}(v_1, v_2, \ldots) = \sum_{i=1}^{3N-6} (v_i + \tfrac{1}{2}) h\nu_{osci} \qquad (2.3)$$

where

$E_{\nu_{osc}}(v_1, v_2, \ldots)$ is the energy of vibration of the oscillator

$v_1, v_2, \ldots$ are vibration quantum numbers

N is the number of molecules in the polyatomic molecule

$3N-6$ are the total number of energy levels, when one vibrational quantum number is 1, and the others are 0

ν_{osci} is the frequency of vibration of the oscillator for quantum number i

h is Planck's constant

If the transition of an energy state is from 0 to 1 in any of the vibrational quantum states $(v_1, v_2, \ldots)$ the transition is *fundamental*. If the molecules were ideal oscillators only fundamental transitions would be observed as quantum mechanics selection rules do not allow transitions between non-adjacent energy levels [5].

In reality, the molecules are not ideal oscillators. In the molecules, electron clouds of the atoms limit their approach in the compression step, creating an energy barrier. During the extension step, the bond eventually breaks when the vibrational energy equals the dissociation energy. This is called *anharmonicity* and the molecules exhibiting this phenomenon are anharmonic oscillators. The energy levels for anharmonic oscillators are given by:

$$E_{\nu_{osc}} = (v + \tfrac{1}{2}) h\nu_{osc} - (v + \tfrac{1}{2})^2 \nu_{osc} X + \ldots. \text{ higher terms} \qquad (2.4)$$

where

$E_{v_{osc}}$ is the energy of vibration of the oscillator

v is the vibrational quantum number

v_{osc} is the vibrational frequency of the oscillator

X is the anharmonicity constant

h is Planck's constant

Figure 2.2 shows the energy diagram for an ideal and anharmonic diatomic oscillator [5]. The difference in energy between successive energy levels is $hv_{osc}(1-2X)$.

The anharmonic nature of molecular vibrations results in transitions between more than one energy level, giving rise to overtone and combination absorption bands [6]. If the transition is from the ground state ($V_i = 0$) to $V_i = 2, 3, \ldots$, and other quantum vibrational states are 0, the transition is an *overtone*. Transitions from the ground state ($V_i = 0$, $V_j = 0$) to V_i=1 and V_j=1 simultaneously result in *combination* bands.

The intensity of the first overtone band is an order of magnitude lower than the fundamental absorption band. Second and higher overtone bands are correspondingly lower in intensity than their preceding overtone bands. It is due to anharmonicity effects that overtones and combinations are observed, resulting in the NIR spectrum. Anharmonicity is usually between 1- 5% of the wavelength. Therefore, if the first overtone of a fundamental vibration is at 3500 nm the fundamental vibration would occur at wavelength (V),

$$v = \frac{3500}{2} + (3500 * [0.01.....0.05]) \qquad (2.5)$$

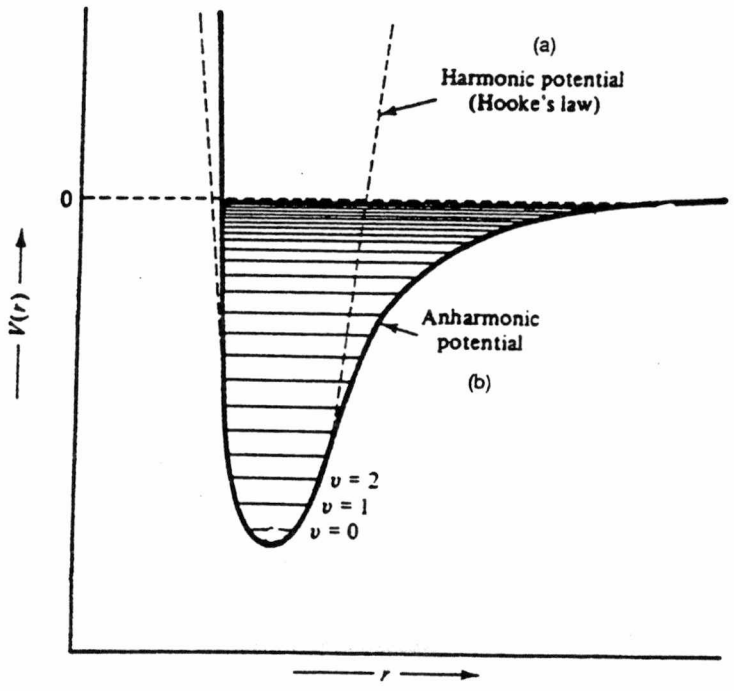


Figure 2.2 Energy diagram for an ideal and anhamonic oscillator [5].

depending on the percentage of the anharmonicity constant [5].

Beer-Lambert Law

In transmission spectroscopy of homogenous, non-scattering samples, Beer-Lambert law describes the ideal and exact relationship between absorbance and transmittance as [7]:

$$A(\lambda) = -\log_{10}\left(\frac{I(\lambda)}{I_o(\lambda)}\right) = \log_{10}\left(\frac{1}{T(\lambda)}\right) \tag{2.6}$$

where

$A(\lambda)$ is the absorbance at a particular wavelength (λ)

$I(\lambda)$ is the intensity of the incident light beam at λ

$I_o(\lambda)$ is the intensity of beam after absorption by the sample at λ

$T(\lambda)$ is the transmittance at λ

Beer-Lambert law of energy absorption also relates absorbance to concentration as [8]:

$$A(\lambda) = a(\lambda)bc \tag{2.7}$$

where

$A(\lambda)$ is the absorbance at a given wavelength (λ)

$a(\lambda)$ is the molar absorptivity at λ

b is the length of absorption cell or optical pathlength

c is the concentration of the sample

Therefore, if $a(\lambda)$ and b are fixed, change in absorbance $A(\lambda)$ at a given wavelength (λ) is proportional to c. This expression also suggests that absorbances at a particular wavelength are additive due to different absorbing constituents in the sample [7].

2.3 SPECTRAL ANALYSIS: BAND ASSIGNMENTS

NIR spectroscopy can be defined as the study of the low-energy electronic transitions, such as the overtones and combinations of essentially C-H, N-H, and O-H stretching and bending vibrational modes. The overlapping of bands in the NIR region result in NIR spectroscopy as primarily a quantitative technique rather than a qualitative technique.

The wavelength range of the NIR spectral region is defined from 700 nm to 2500 nm in the electromagnetic radiation spectrum. The absorption bands observed in the NIR region are primarily due to overtones and combinations of the fundamental mid-IR bands related to the O-H, C-H, and N-H groups. Other vibrations like C=O stretching have only second and third overtones in the NIR regions [6].

These overtones and combination bands are relatively weaker than the fundamental bands providing useful sampling advantages. Absorption bands in the NIR compared to the infrared region exhibit loss of sensitivity and abundance of overlapping bands, resulting in the absorption bands being non-selective in the NIR region [9].

In a comprehensive review by Robert F. Goddu [10], the qualitative and quantitative applications of near infrared spectrophotometry applied to chemical analysis were detailed and discussed. Whetsel [11] presented a detailed discussion on band assignments in the NIR region and reviewed the numerous organic and inorganic applications of NIR spectroscopy. Weyer discussed band assignments and NIR spectroscopy of organic substances [6].

Qualitative uses of NIR spectra

Most of the absorption bands in the NIR region are due to C-H, O-H, and N-H stretching vibrations or combination of these vibrations with other modes of vibration of the molecule. In general, NIR region primarily consists of overtones and combinations bands of fundamental C-H, O-H, and N-H stretching vibrations and is extremely valuable in the detection and subsequent determination of functional groups containing unique hydrogen atoms [10].

Quantitative organic functional group analysis

NIR spectroscopy has primary importance in the quantitative analysis of organic functional groups. NIR spectroscopy is primarily used for the determination and detection of hydrogen containing groups like C-H, N-H, and O-H. Some of the absorption bands of these groups are discussed in this section.

1. C-H vibrations

The fundamental stretching vibration bands of the C-H group lie outside the NIR region, between 3000 nm and 3600 nm. The first overtone stretching bands occurs between 1600 nm and 1800 nm; the second overtone occurs between 1100 nm and 1250 nm; and the combination band occurs between 2000 nm and 2400 nm. The first overtone band between 1600 nm and 1800 nm is more intense than the second overtone band between 1100 nm and 1200 nm and is generally used for spectral analysis [6, 10, 11].

A. Terminal Methylene Groups

a. Olefins

Terminal olefins have characteristic first overtone C-H stretching bands at 1620 nm and combination bands at 2110 nm due to terminal double bonds [10].

b. Epoxides

Terminal epoxide methylene groups have sharp bands at 1650 nm and 2200 nm as a result of the first overtone band of the methylene C-H stretching and due to a combination of C-H stretching and $-CH_2$ bending vibrations [10].

c. Cyclopropanes

Terminal cyclopropyl group have absorption bands at 1640 nm and 2240 nm.

B. Terminal Methyne or Acetylenic Groups

The terminal methyne or acetylenic groups have overtone C-H stretching vibrations at 1500 nm.

C. Unsaturated hydrocarbons

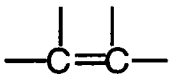
Cis and trans are configurations due to the restricted movement about the double bond. When a functional group is on the same side of the unsaturation, it is a cis configuration and when the group is on opposite sides of the double bond it is a trans configuration. Figure 2.3 shows a number of functional groups that have absorption bands in the NIR region [12]. Cis olefins show characteristic first overtone band at 1680 nm, second overtone band at 1180 nm and combination bands at 2150 nm and 2190 nm. The band at 2140 nm is primarily used for the analysis of cis-trans mixtures of olefins. The trans olefins do not have strong absorption bands in the NIR region. Terminal acetylenic groups exhibit a characteristic first overtone C-H stretching band at 1530 nm [10].

D. Aldehydic C-H and formates

Aldehydes have two absorption bands at 2210 nm and 2250 nm due to symmetric and unsymmetric C-H, C=O stretching. Formates exhibit a combination band at about 2150 nm.

E. Methyl and methylene vibrations

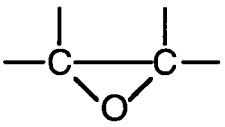
The first overtones of C-H stretching vibrations of aliphatic hydrocarbons are observed between 1600 nm and 1800 nm, second overtones between 1100 nm and 1250 nm and combination bands between 2000 nm and 2400 nm. Doublets due to first overtones of methyl and methylene C-H stretching occur from 1695 to 1705 nm and between 1725 nm and 1765 nm, respectively. Methyl and methylene groups also exhibit characteristic bands at 2270 nm and 2340 nm, respectively [10].



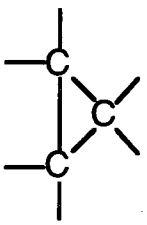
Olefins



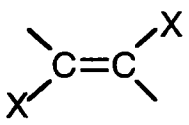
Acetylenic group



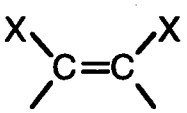
Epoxide (oxirane ring)



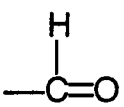
Cyclopropyl group



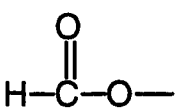
Cis Olefins



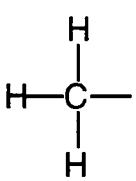
Trans Olefins



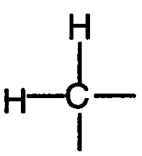
Aldehyde



Formates

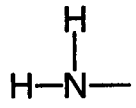


Methyl group

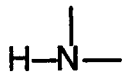


Methylene group

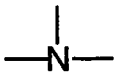
Figure 2.3 Chemical structures of functional groups absorbing in the NIR region [12].



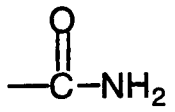
Primary amine



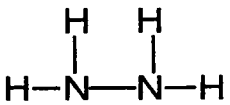
Secondary amine



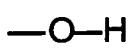
Tertiary amine



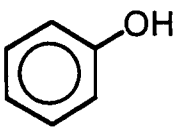
Amide group



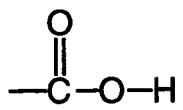
Hydrazine



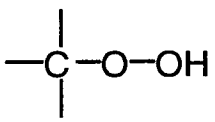
Alcohol



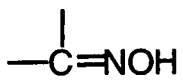
Phenol



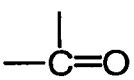
Carboxylic acid



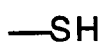
Hydroperoxide



Oxime



Carbonyl group



Thiol group

Figure 2.3 (cont.) Chemical structures of functional groups absorbing in the NIR region [12].

F. Aromatic hydrocarbons

The first and second overtones of aromatic C-H stretching absorptions occur at about 1685 nm and 1143 nm, respectively. Combination bands are observed at about 2150 nm and 2460 nm [6, 10].

2. N-H vibrations

The fundamental stretching vibrations bands of the N-H groups lie between 2800 nm to 3000 nm. The first overtone of N-H stretching occurs at 1500 nm, a weak second overtone occurs at about 1000 nm, and a combination band due to N-H bending and stretching modes is observed around 2000 nm [6, 10, 11].

A. Amines

The NIR spectral absorption bands of primary, secondary, and tertiary amines are very different. Primary amines have a couple of absorption bands between 2850 and 3050 nm, a first overtone doublet at 1530 nm and a single peak at about 1000 nm. A combination band at 2020 nm due to N-H bending and stretching modes is also observed. Secondary amines have single absorption bands at 1540 nm and 1000 nm and no absorption bands in the N-H combination band region around 2000 nm. Tertiary amines do not exhibit strong absorption bands in the NIR region. The intensities of the first overtone bands and fundamental bands of aliphatic N-H stretching vibrations are of the same order of magnitude. In this respect, these bands are unique. Aromatic amines have second overtone N-H stretching bands near 1020 nm.

B. Amides

The N-H vibrations for amides are similar to the amines although more complicated as secondary amides can be in either in a cis or trans form. Primary amides have two bands at 2820 nm and 2920 nm due to the fundamental N-H asymmetric and symmetric stretching vibrations, respectively. Primary amides exhibit two first overtone N-H stretching bands at 1460 nm and 1480 nm and two combination bands near 1960 nm and 2000 nm. Secondary amides exhibit a combination band around 2100 nm [6, 10, 11].

C. Hydrazines

Hydrazines have N-H overtone bands around 1500 nm and combination bands in the 2000 nm region [10].

3. O-H vibrations

Fundamental O-H stretching vibration occur between 2700 nm and 3000 nm. The first overtone of O-H stretching occurs at 1400 nm and a combination band occurs in the 1900 nm to 2000 nm range. The fundamental O-H stretching vibration band occurs around 2800 nm. The first and second overtone bands occur around 1400 nm and 1000 nm, respectively, and a combination band is observed near 2000 nm [6, 10, 11].

A. Alcohols

The fundamental O-H stretching in alcohols is observed around 2750 nm to 2770 nm. Primary alcohols absorb between 2748 and 2752, secondary alcohols between 2758 and 2762, and tertiary alcohol between 2763 and 2769, indicating a shift with alcohol type. The first and second overtone O-H stretching bands of alcohols are observed near 1410 nm and 970 nm respectively.

B. Phenols

Most phenols have fundamental OH absorption bands between 2769 nm and 2775 nm. A first overtone O-H stretching band of phenols occurs between 1404 and 1441 nm, and a combination O-H band is observed near 2000 nm.

C. Carboxylic Acids

The hydroxyl (O-H) group of carboxylic acids have the fundamental stretching vibrations between 2700 nm and 3000 nm. Carboxylic acids exhibit sharp first overtone and absorption bands due to O-H stretching at 1450 nm and 2100 nm, respectively. A characteristic second overtone carbonyl C=O stretching band for acids occurs at 1900 nm. A combination band is observed at 2100 nm due to C-H stretching and bending vibrations [6, 10].

D. Hydroperoxides

The fundamental O-H stretching vibration of the hydroperoxide group occurs between 2810 nm and 2840 nm. The first overtone occurs between 1450 nm and 1470 nm, while the combination band is observed between 2050 nm and 2070 nm [10].

E. Oximes

The first overtone of the fundamental hydroxyl (O-H) band of oximes occurs at about 1450 nm [10].

F. Water

Water has an O-H stretching first overtone at 1440 nm, a second overtone at 960 nm, and a strong combination band at 1940 nm. The absorptivity of the combination band is nearly twice as that of the first overtone O-H band. A weaker combination band is also observed at about 1200 nm. The combination band at 1940 nm is usually used in most applications for the determination of water [6, 11].

3. Silanols

The hydroxyl group in SiOH exhibits first overtones due to O-H stretching at 1385 nm. A combination band due to O-H stretching and O-H bending is observed at 2220 nm [6].

4. Thiols

A weak fundamental S-H stretching band occurs at 3900 nm and the first overtone is observed between 1970 nm and 1980 nm [10].

5. Carbonyls

The fundamental C=O stretching vibration of the carbonyl group has a first overtone between 2800 nm and 3000 nm and a weak second overtone between 1900 nm and 2000 nm [10].

6. Nitriles

The first and second overtones of the $C \equiv N$ stretching vibrations appear at 2250 nm and 1500 nm, respectively. Weak but characteristic bands due to nitriles are seen between 1800 nm and 2100 nm [10, 11].

7. Agricultural products

Carbohydrates show a strong O-H combination band at 2100 nm and a first overtone O-H stretching band at 1460 nm. Proteins, an important constituent of many agricultural products, exhibit a first overtone N-H stretching band at 1510 and a number of combination bands at 1980 nm, 2060 nm, and 2180 nm [6].

Figure 2.4 gives a large compilation of spectra-structure correlation data, giving valuable information about the absorption bands of the various functional groups absorbing in the NIR region [10].

2.4 PROCESS ANALYSIS, SAMPLING TECHNIQUES, AND INSTRUMENTATION

Process Analysis

Four different options for process analysis are discussed and evaluated by Mackinson *et al* [13]. The first option is the most commonly used off-line analysis. A sample is drawn from the process stream and analyzed in the laboratory. The drawbacks with this analysis include the overall time needed between obtaining the sample and reporting results in which the process conditions can change.

Off-line analysis is not an ideal method for reducing process variability, as it does not provide timely information concerning the dynamics of the process due to the considerable time lapse between the drawing of the sample and obtaining results [1].

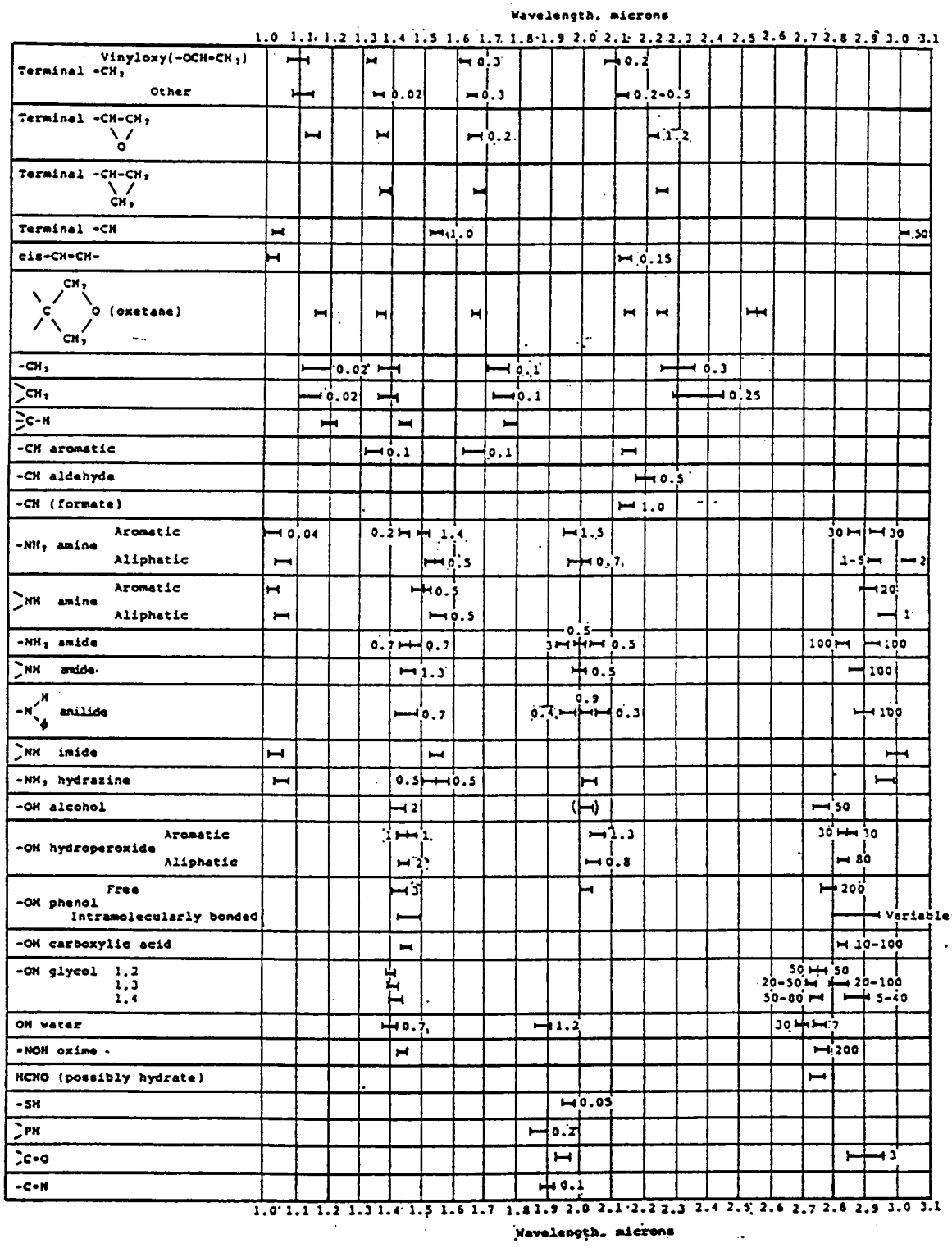


Figure 2.4 Spectra-structure correlations and average molar absorptivity data [10].

The second option is at-line analysis in which the analyzer is placed close to the process stream and is interfaced to the process stream by short fibers for spectroscopic measurements. The drawbacks include the proximity of the analyzer to the harsh processing environments and monitoring of only one process stream.

The third option is on-line analysis in which the analyzer is housed safely at a distance from the process and the sample is transferred to an analyzer by a "fast sample loop" [13]. Drawbacks include blocking of these sample loops, changes in the composition and properties of the material in the bleed streams after leaving the process stream resulting in erroneous results, and the additional cost for building analyzer houses away from the process stream.

The fourth option and the one used for these experiments is in-line measurements in the process stream. Rugged optical probes inserted directly in the process streams which are capable of withstanding high temperatures, pressures, and severe process environments are essential for in-line analysis. The fiber optic probes are connected to the spectrophotometer by optical fibers. Advantages of in-line measurements include rapid, safe, cost-effective, and accurate analysis of the process stream. This approach is being widely used for quality control and optimization in chemical analysis.

Sampling Techniques

Four different sampling methods [14] of NIR spectroscopy for the analysis of polymers are discussed in this section.

1. NIR transmission/absorbance spectroscopy

NIR transmission spectroscopy is used for analyzing bulk polymers, molten polymers, and polymer solutions. Pathlengths varying from 1 mm to several centimeters can be used owing to the low absorptivities in the NIR region. Beer-Lambert law (given by eqn. 2.7) relates the absorbance at a given wavelength to be directly proportion to the concentration of the sample [8].

2. NIR dichroism spectroscopy

NIR dichroism spectroscopy is used to determine the structure and orientation of functional groups in crystalline polymers [14].

3. NIR diffuse reflectance spectroscopy

NIR diffuse reflectance spectroscopy, which requires the presence of refractive index interfaces in the sample, can be used to analyze highly scattering semicrystalline bulk polymers, synthetic fibers, filled polymers, and colloidal suspensions. The intensity of the backscattered light from the sample is measured. The empirical expression relating the pseudoabsorbance value to the intensity of backscattered light is given by [14]:

$$A_r(\lambda) = -\log_{10}\left(\frac{R(\lambda)}{R_o(\lambda)}\right) \tag{2.8}$$

where

$A_r(\lambda)$ is the pseudoabsorbance value at wavelength λ

$R(\lambda)$ is the intensity of backscattered light at λ

$R_o(\lambda)$ is a reference intensity value at λ

4. NIR photoacoustic spectroscopy (NIR-PAS)

NIR-PAS involves the measurement of a sound waves emitted from the sample after it is exposed to NIR light. This technique can be used to analyze bulk polymer samples [14].

Instrumentation

Till the early 1950's very few analytical spectroscopists worked in the NIR region due to the lack of convenient instrumentation. In 1954, spectrophotometers containing quartz prisms and lead sulfide detectors were commercially available, leading to the beginning of a new era of analytical research in the near infrared region [10].

Recent advances in instrumentation and development of multivariate statistical analysis techniques have resulted in NIR spectroscopy as an important analytical tool for process monitoring and quality analysis applications [14].

LeFebre (1985) *et al* evaluated the design of an in-line scanning ultraviolet-visible-NIR process monitors for process control in hostile environments at distances of over 100 meters from the instrument [15]. Bickel (1989) compared and contrasted grating and filter-based NIR analyzers with respect to speed, ruggedness, accuracy, and reliability for

on-line analysis [16]. Kilham *et al* (1989) presented an account of on-line analyzers used for quality control and adjustment of process variables in extrusion operations, bypassing the need for laboratory analysis [17]. McDermott (1990) discussed the approaches and steps recommended for optimizing the instrument, for model calibration and validation, and for maintenance of the analyzer [18].

Modern NIR spectrophotometers give an insight into rapid, complex and inaccessible petrochemical, pharmaceutical, and polymeric reactions revealing the presence of unstable intermediates. Multivariate analysis of the data is further invaluable for industrial process monitoring and process control [9].

NIR instruments used for most polymer process monitoring applications should be accurate, rugged, and dependable as they are subject to high temperatures, pressures, and severe environments. Specially designed fiber optic probes [1, 2] are now being used to withstand the high temperatures and pressures in the flowing polymer streams in process monitoring applications [14].

2.5 ADVANTAGES OF NIR SPECTROSCOPY

NIR spectroscopy is emerging as a very useful technique for industrial quality control and quality assurance, where ease of sample preparation, speed of analysis and ruggedness of the NIR instrumentation are of great significance [7]. The multiplicity of analyses from a single spectrum and the non-destructive nature of sample handling are a few other advantages resulting in NIR spectroscopy as an attractive, and viable analytical technique for on-line analysis [3].

NIR spectroscopy can be used for liquid, semisolid, and solid samples. The lower intensity of bands in the NIR region are advantageous in polymer studies compared to the relatively higher intensity of bands in the mid-IR region [6]. Sampling advantages, along with the use of longer pathlengths owing to the low absorptivities, enables NIR spectroscopy for nondestructive and rapid analysis in process and quality controls applications [14]. NIR analysis can be used for simultaneous determination of multiple constituents, as it does not require reagents or other consumables for sample preparation. This saves operating expenses and eliminates hazardous wastes generated by other analytical techniques [7].

Measurements of chemical composition in real-time are important for understanding, improving, and controlling polymeric processes. NIR spectroscopy coupled with fiber optic probes and fibers is being used in-line for process control and quality improvement in the process industry. This technique extracts chemical information with minimum time delays and without physically removing the samples from the process stream [19].

McDermott (1990) discussed NIR spectroscopy as an analytical tool for real time process monitoring. Advantages for on-line analysis, such as rapid analysis, little or no sample preparation, non-destructive analysis, and easy operations in severe environments using fiber optics, are described in the article [18].

3. CHEMOMETRICS: MULTIVARIATE ANALYSIS OF SPECTRAL DATA

Near infrared spectroscopy, despite its advantages, was not used extensively as an analytical technique due to its lack in structural interpretive value compared to the mid-IR region. Although the overtone and combination bands contain a great deal of information, the complexity of the bands in the NIR region reduce its qualitative power compared to the mid-IR region.

However, using multivariate analytical techniques (chemometrics), the NIR spectral data can be analyzed to yield valuable information from the data [20]. Chemometrics is a discipline which generates correlations between experimental spectral data and the chemical composition (or other physical properties), for the extraction of useful chemical information using computers, mathematics and statistical procedures [2].

Although the NIR region appears to be a poor choice of spectral region for qualitative analysis it is extremely useful for quantitative analysis. The quantitative power of the NIR analysis is embedded in the computer-aided mathematical manipulations of the spectral data. Analysis can be performed in the quantitative format or the discriminate format. The quantitative format involves the determination of the actual composition in the process stream, whereas in the discriminate format, deviations from normal operating limits are of primary concern [21].

Quantitative analysis involves first selecting representative calibrating samples, acquiring spectral data and pretreating the data, developing a calibration model and validating the model by various methods. A large number of samples representing the

range of variation of interest in the constituents following the theory of factorial experimental design methods should be included in the calibration or training set for a robust calibration. The value of the property of interest of all calibration samples should be known a priori, for intelligent subsequent data analysis. The set of samples chosen for calibration should account for all the variation in the constituents being monitored by the technique for accurate predictions [22].

The two mathematical approaches for NIR spectral data analyses are discrete-wavelength approach, in which only a few wavelength responses are used, and the full-spectrum approach, which uses the entire spectrum [14]. The primary objective of wavelength selection and data treatment is to do away with the intercorrelation of the data and to reduce the effect caused by scattering.

NIR spectral data should be subjected to mathematical corrections to remove baseline variations for a consistent calibration. Non-reproducibility in spectra arises due to sample inhomogeneity, variations in sample thickness, and changes in scattering properties of the samples. Variables with little explainable variance can be removed without changing the model. The presence of these variables does not affect the predictability of the model. The reduction of the data set should be made only if there is a cost associated with a decrease in the number of variables in the model [23].

Derivative treatment of data and difference techniques are used to account for slight variations in sample presentations and particle sizes. Most models use first or second derivative treatment of absorbance data to compensate for baseline shifts or shape

changes in the spectrum, resulting in more wavelengths for calibration purposes [14], as well increase the calibration sensitivity to noise.

3.1 OVERVIEW OF TECHNIQUES USED

The efficiency of NIR spectroscopy partly depends on the quality of the statistical methods used for extracting qualitative and quantitative information from the spectral data. Some of these methods, such as Multiple Linear Regression (MLR), Principal Component Regression (PCR), and Partial Least Squares (PLS) are discussed in this section.

MLR is used when the spectral data obtained at the various wavelengths is independent of each other and when the number of samples used in the calibration is much greater than the number of wavelengths selected for the data analysis. PCR and PLS are techniques used to reduce the enormous but independent data set wavelengths to a smaller number of independent variables or "factors" while preserving most of the spectral variation information. The number of factors in these methods are significantly less than the original number of wavelengths or samples. As the factors are "hidden" in the spectral data, they are also termed as "latent factors" [7].

When the data is subjected to factor analysis, it is often found that the first few factors are associated with the systematic variation in the data and the remaining principal components are associated with random "noise" due to process and instrumental variations. Deleting some of the latter factors that account for little variance and contain mostly noise, does not significantly reduce the amount of useful information in the data.

This reduction in dimensionality is of primary importance in forming a robust mathematical model [24].

The principal components obtained from the NIR spectra are independent variations in the data set. Each principal component has a score vector which gives the relationship between the different samples relative to that principal component, and a loading vector which gives the contribution of the different wavelengths in making up that principal component. The scores or weighted sum of the original variables, are of great significance in the detection of outliers [25]. The total number of principal components or factors also represent the degrees of freedom for the data [26].

Calibration Techniques

Multivariate calibration techniques are applied for the analyses of data in situations where traditional univariate techniques do not give accurate results [27]. Some of these calibration techniques are discussed here.

1. Classical Least Squares (CLS)

Classical Least Squares (CLS) is a first order method that is based on the model given by:

$$X = YS^T + E_R \tag{3.1}$$

where

X (a m x n matrix) contains the spectral response of m samples at n wavelengths, Y (a m x p matrix) contains the concentrations of p constituents in m samples, S (a n x p

matrix) contains the pure spectral responses of the p constituents at the n wavelengths, and E_R (a m x n matrix) contains the residual errors [27]

The pure spectral responses of the constituents can be estimated by:

$$\hat{S} = X^T Y (Y^T Y)^{-1} \tag{3.2}$$

where

$\hat{S}$ (a n x p matrix) is the estimated analyte spectra coefficients for the unit concentration of the p constituents at the n wavelengths

The estimated pure response coefficients ($\hat{S}$) are used to predict the concentration of the p constituents in an unknown sample by [27]:

$$\hat{y}_{un} = x_{un} \hat{S} (\hat{S}^T \hat{S})^{-1} \tag{3.3}$$

where

$\hat{y}_{un}$ (a 1 x p matrix) is the predicted concentration of the unknown sample and x_{un} (a 1 x n matrix) is the spectral response of the unknown sample at n wavelengths

As the spectral responses at all the wavelengths are considered, a weighted signal-averaging effect can take place using this approach. The disadvantage of this method is that both $Y^T Y$ and $\hat{S}^T \hat{S}$ should be invertible for the estimation of the pure responses ($\hat{S}$) and the concentration of all the components that contribute to a response should be known a priori. This is difficult due to the presence of interferents in the samples and also due to the non-linear relationships between the responses and the concentrations of the constituents [27].

2. Multiple Linear Regression (MLR) or Inverse Least Squares (ILS)

Multiple linear regression (MLR), also known as Inverse Least Squares (ILS), is a method to model NIR data for predictions. Inverse Least Squares relates the property to be predicted and the spectral response by [27]:

$$Y = B_o + XB + E \tag{3.4}$$

where

Y (a m x p matrix) contains the concentration of the p analytes in the m samples, B_o (a m x p matrix) contains numerical constants equal to the n y-intercepts, X (a m x n matrix) contains the spectral responses of m samples at n wavelengths, B (a n x p matrix) contains the regression coefficients, and E (a m x p matrix) is the residual error

If the mean of each column in the concentration matrix (Y) is subtracted from each element in that column, and the mean of the spectral response for each wavelength is subtracted from each sample response, then B_o is zero. The estimated regression coefficients ($\hat{B}$) are then given by:

$$\hat{B} = (X^T X)^{-1} X^T Y \tag{3.5}$$

$X^T X$ must be full rank to be invertible. This results in the option of using only n limited number of wavelengths for the analysis, if the number of independently varying chemical components is n [27].

The estimated concentration of unknown samples is therefore given by:

$$\hat{y}_{un} = \bar{y} + x_{un}\hat{B} \tag{3.6}$$

where

$\hat{y}_{un}$ (a 1 x p matrix) is the predicted concentrations of the p constituents in the unknown sample, X_{un} (a 1 x n matrix) is the spectral response of the unknown sample at n wavelengths, $\hat{B}$ (a n x p matrix) contains the estimated regression coefficients, and $\bar{y}$ is the mean of the calibration concentration matrix Y

The choice of wavelengths for the analysis by ILS is very important to yield low standard-errors-of-calibration (SEC) and standard-errors-of-prediction (SEP), and to render the calibration model robust against minute changes in the calibrating concentrations. Collinearity among selected wavelengths, and overfitting of data by incorporating noise and random errors in the model may result in high SEPs and SECs during analyses by ILS. ILS can accommodate nonlinearities between the concentration and the responses. This method does not have any signal-averaging effects as only a few spectral responses are considered [27].

Principal component regression, and partial least squares are multivariate techniques where the original full spectrum data is transformed into new variables which are linear combination of the original variables. PCR and PLS are also called biased methods as some of the data is discarded in these approaches and therefore a biased least-squares estimate of the model parameters is calculated [27].

3. Principal Component Regression (PCR)

Principal component regression (PCR) is a method used to correlate between Y and X, but using the variance in a single data (absorbance) matrix X for the data reduction step. Principal component procedures determines mutually orthogonal vectors or principal components which describe the main variability in the data. The first principal component describes the direction of greatest variability in X [28].

The PCR method involves the decomposition of the spectral data matrix X in terms of a linear combination of orthogonal principal components with zero intercorrelation given by:

$$X = t_1 p_1 + t_2 p_2 + \ldots\ldots\ldots + t_r p_r + E \qquad (3.7)$$

i.e.

$$X = TP^T + E \qquad (3.8)$$

where

X (a m x n matrix) contains the spectral responses of the m calibration samples at n wavelengths, columns of T (a m x r matrix) are mutually orthogonal and orthonormal and contain the PCR scores (t_1, t_2,.... t_r) for the first r factors; where r is the number of factors to be retained in the calibration model, columns of P (a n x r matrix) are mutually orthogonal and orthonormal and contain the PCR loadings (p_1, p_2,.... p_r) for the first r factors, and E (a m x n matrix) contains the residuals [29]

The measured property of interest of the calibration samples contained in the (concentration) matrix Y, can be regressed against the PCR scores matrix T as:

$$Y = T\beta + F \tag{3.9}$$

where

Y (a m x p matrix) contains the concentrations of the p constituents in the m samples, β (a r x p matrix) contains the PCR regression coefficients, and F (a m x p matrix) contains the modeling errors

The matrices P and β can be used to predict the concentration ($\hat{y}_{un}$) of an unknown sample from its spectral response (x_{un}) by [29]:

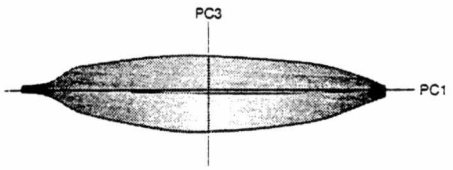
$$\hat{y}_{un} = x_{un} P\beta \tag{3.10}$$

where

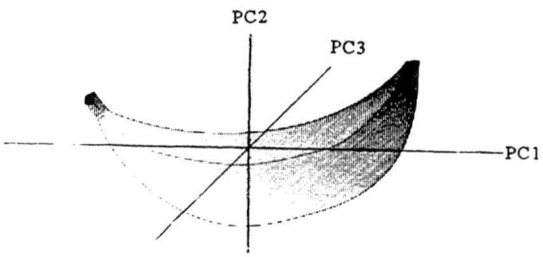
$\hat{y}_{un}$ (a 1 x p matrix) is the predicted concentration of the unknown sample by the PCR model and x_{un} (a 1 x n matrix) is the spectral response of the unknown sample at the n wavelengths

The first principal component is pointed in the direction of maximum variability in the data. Each subsequent principal component, orthogonal to the previous principal component, accounts for the maximum possible amount of the remaining variability. Figure 3.1 illustrates this concept as applied to a 3-D object. The figure shows that the first, second, and third principal components explain the variance in the object, regardless of its orientation [30].

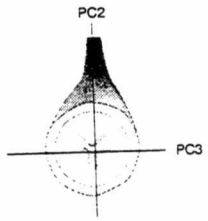
The orthogonality of the principal components in PCR eliminates collinearity among the principal variables without eliminating spectral information, resulting in a



Top view



3-D object



Side view

Figure 3.1 Representation of principal component analysis with a 3-dimensional object [30] .

robust model. Noise in the original data set is spread amongst the last principal components while the variation of interest is usually imbedded into the first few factors.

PLS and PCR differ in the decomposition of spectral data into principal components. In PCR, dimensionality reduction is performed using the X (absorbance) matrix without taking the Y (concentration) matrix into consideration, while PLS accounts for both X and Y matrices in the data analysis [22].

4. Partial Least Squares or Projection onto Latent Structures (PLS)

Partial least squares (PLS) is a latent variable or factor based method for modeling the relationship between spectral responses (X) and the concentration matrix (Y). PLS regression allows more variables than objects in the data and data is discarded prior to the regression step. PLS also considers collinearity present between X and Y [31].

The PLS method decomposes X and Y as:

$$X = TP^T + E \tag{3.11}$$

$$Y = RS^T + F \tag{3.12}$$

where

columns of matrices T (a m x r matrix) and R (a m x r matrix) are the scores of X and Y, respectively, columns of matrices P (a n x r matrix) and S (a p x r matrix) are the loadings of X and Y, respectively, and E (a m x n matrix) and F (a m x p matrix) are residual matrices [32]

Several algorithms are used for the decomposition of X and Y; some resulting in the columns of T being orthogonal while some resulting in the columns of P being orthogonal. In either case, the columns of T and P cannot be orthogonal simultaneously, as the PLS algorithm describes the maximum correlation between X and Y coordinatedly and not independently [32]. In PLS the factors are selected in such a way that there is a maximal reduction in the covariance X^TY of the spectral data. In this respect, PLS provides the minimum number of factors necessary for the analyses [33].

The error is distributed over all the components in PCR and PLS. Therefore if fewer components are needed by PLS compared to PCR, the predicted concentrations using PLS will contain less error [81]. The advantage of PLS over PCR is that in the calibration step more correlation information is incorporated into the model, as the factors are built using both X and Y matrices in partial least squares [24].

Several review papers on multivariate techniques have been published in recent years. Geladi and Kowalski [34] (1986) compared and contrasted several multivariate approaches and discussed the nonlinear iterative partial least squares (NIPALS) algorithm for PLS. Beebe and Kowalski (1987) discussed MLR, PCR, and PLS and presented an introduction of these techniques for multivariate calibration and predictions [24]. Lorber *et al* (1987) discussed a PLS algorithm based on the singular value decomposition (SVD) approach [35].

Helland *et al* (1988) demonstrated by simulation that the PLS regression algorithm needed fewer factors compared to other multivariate techniques like PCR for optimal

predictions. They obtained similar predictions and mean square errors (MSE) for optimal number of factors for both PLS and PCR [36]. A comprehensive account of multivariate calibration is given by Martens and Naes [37].

Sutter *et al* (1992) discussed an alternative approach for selecting the principal components for principal component regression. Traditionally, the principal components are selected by considering the most informative principal component (associated with the largest singular value) and proceeding to the least informative principal component (associated with the smallest singular value). They demonstrated that better predictions were possible with optimal subset selection of principal components opposed to subset selections made from top down in the principal component list [38].

PLS regression algorithms are mostly iterative. The classical PLS algorithm is based on the NIPALS method. Sijmen de Jong (1993) presented the simplified PLS (SIMPLS) algorithm for partial least squares. SIMPLS is one of the fastest algorithm in use for PLS regression [39]. Wold *et al* (1994) discussed a PLS algorithm based on small cross-product or "kernel" matrices [31].

Jong *et al* (1994) also proposed a kernel based PLS algorithm from the cross-product matrices X^TX and X^TY [32]. Results obtained from their approach were identical to the traditional NIPALS method. Wang *et al* (1994) proposed an efficient PLS algorithm based on the SVD approach called SVDPLS. The algorithm was found to be considerably faster than the traditional NIPALS approach [40].

3.2 DATA ANALYSIS OF SPECTRAL DATA (FOR THIS RESEARCH)

The spectral and compositional data was subjected to data pretreatment, such as baseline corrections, column centering and scaling. Centering the data by subtracting the column means from each of the elements in the column, corresponds to moving the coordinate system to the center of the data [23]. Scaling standardizes the mean centered data matrix by dividing each column by its variance. Scaling gives each column a variance of 1.0, resulting in the same influence by each variable in the model [23].

A SVD based algorithm for PLS and PCR was used in this research. The codes and procedure followed for the data analysis using this approach are given in the appendix section of this thesis. The SVD approach decomposes the matrix of spectral responses X (a m x n matrix) as:

$$X = U\Sigma V^T \tag{3.13}$$

where

columns of U (a m x m matrix) are orthonormal and are the left singular vectors of X, columns of V (a n x n matrix) are the right singular vectors of X, and Σ (a m x n diagonal matrix) contains the singular values or the square roots of the eigenvalues of X^TX and XX^T which are positive and in descending order.

If m<n and the rank is m, then the m columns of U span the column space of X and the first m columns of V span the row space of X. Furthermore, the columns of U and V are orthonormal (of unit length and perpendicular to each other). i.e.,

$$U^T U = I_{mxm} \tag{3.14}$$

$$V^T V = I_{nxn} \tag{3.15}$$

where

I_{mxm} and I_{nxn} are identity matrices of sizes m and n, respectively

The principal components or factors can be added until the percentage of variation explained by adding additional factors is small, although this often leads to "overfitting" of data. Choosing all the principal components increases the chance of incorporating noise into the model. The calibration fit would be good, while the predictions would not be accurate. The maximum number of factors to be chosen that explain all the variation in the data, is to be less than or equal to the minimum of the number of samples or the number of variables in the model [22].

Overfitting by PLS and PCR occurs when more than the optimum number of principal components are considered in the calibration. On the other hand, the choice of very few principal components results in incorporating little information into the calibration model. This is called "underfitting" [35]. The drawback with considering more than the optimal number of principal components is the inclusion of noise in the calibration model. Cross-validation techniques are often used to determine the optimal number of principal components to be retained in the analysis [14].

The number of principal components that are retained for analysis reduce the dimensionality of the principal component space. The reduced X, i.e. X_r is the projection of the original X onto the subspace spanned by the r columns of the principal component space and is given by:

$$X_r = U_r \Sigma_r V_r^T \tag{3.16}$$

where

U_r, Σ_r, and V_r are the reduced U, V, and Σ formed by retaining only the first r principal components [35].

The estimate of the regression coefficients ($\hat{\beta}$), used for future predictions is given by:

$$\hat{\beta} = X_r^+ Y \tag{3.17}$$

where

$$X_r^+ = V_r \Sigma_r^+ U_r^T \tag{3.18}$$

X_r^+ is the pseudoinverse of X and is calculated using Σ_r^+, a leading diagonal matrix containing the reciprocals of the singular values in Σ_r [35].. The pseudoinverse is used rather than the inverse because only the left inverse of X_r is required.

Due to overlaps of vibrational overtones and combination bands NIR analysis requires the use of absorbances at several wavelengths in the spectrum. The two steps for NIR data analyses used in this research are [14]:

1) Calibration step, in which the wavelength responses are related to sample property using calibration samples.

2) Validation step, to check for the robustness of the calibration model for real time monitoring and to determine its feasibility for the determination of the sample property.

The number of principal components to be considered is determined by the SEC and SEP of the calibration and prediction sets, respectively. Predicted residual sum of squares (PRESS) values which are similar to the SEP are also used to determine the accuracy of the predictions. The prediction errors should be minimum for the optimal number of factors in the validation of the models.

The SEC, SEP, and PRESS values are given by the expressions:

1. Standard Error of Calibration (SEC):

$$SEC = \sqrt{\frac{\sum_{i=1}^{N_c}(Y_{i,c} - \hat{Y}_{i,c})}{(N_c - 1)}} \tag{3.19}$$

where

$Y_{i,c}$ is the actual concentration of sample i in the calibration set

$\hat{Y}_{i,c}$ is the predicted concentration of sample i in the calibration set by the model

N_c is the number of samples in the calibration set

2. Standard Errors of Prediction (SEP):

$$SEP = \sqrt{\frac{\sum_{i=1}^{N_p}(Y_{i,p} - \hat{Y}_{i,p})}{N_p}} \tag{3.20}$$

where

$Y_{i,p}$ is the actual concentration of sample i in the validation set

$\hat{Y}_{i,p}$ is the predicted concentration of sample i in the validation set by the model

N_p is the number of samples in the validation set

3. Predicted Residual Sum of Squares ($PRESS$):

$$PRESS = \sum_{i=1}^{N_{cr}} (Y_{i,cr} - \hat{Y}_{i,cr})^2 = (SEP)^2 (N_p) \qquad (3.21)$$

where

$Y_{i,cr}$ is the actual concentration of sample i in the cross-validation set

$\hat{Y}_{i,cr}$ is the predicted concentration of sample i in the cross-validation set

N_{cr} is the number of samples in the cross-validation set

SEC, SEP and PRESS values are calculated for models using increasingly more factors. The number of the principal components that gives the minimum SEP is taken as the optimal number of factors to be retained in the model.

The ith column of the scores matrix describe the amount of information each sample has in the direction of the ith principal component. The scores for a factor give the relationship between the different samples relative to that principal component. Loadings describe the contribution of the original variables in making up the principal components. Outliers can be detected by considering the spectral residuals, after taking into account the spectral variation accounted for by the optimal number of factors.

PLS and PCR models offer many advantages over other methods depending on the degree of spectral overlap, scattering effects, precision of the reference data and spectrometer noise, etc. Sources of error in the SEC may be due to instrumental considerations, noise, sample inhomogeneity, inaccurate reference measurements, etc.

4. APPLICATIONS OF NIR SPECTROSCOPY

NIR analysis can be used for rapid analysis in a relevant and reliable way for quality analysis and process monitoring. Analytical technology as applied to process situations should be, nondestructive without substantial sample preparation, for effective process control and regulation. NIR spectroscopy offers all these advantages, and is being used in a number of applications.

4.1 POLYMERS

Polymeric compounds can be studied by NIR spectroscopy for useful information regarding composition, functional group analysis, molecular weight, residual monomer content, quantification of blends, crystalline effects and degree of curing, etc. NIR offers advantages with respect to easy sample handling and selection of greater pathlengths compared to the mid-IR [6]. The NIR applications of polymers with emphasis on recent analyses are discussed in this section.

Greive and Doepken (1968) used the absorbance peak at 2140 nm to determine the amount of acrylonitrile-butadiene-styrene (ABS) terpolymer in polyvinyl chloride (PVC) compounds by NIR spectrophotometry. It was pointed out that the bands from 2100 nm to 2200 nm were due to hydrogen bonding of unsaturated compounds, benzene rings and methylene group adjacent to a carbonyl group. These bands were used to determine the amount of ABS in PVC. 80 mil thick samples were used for the NIR analysis [41].

Takeuchi *et al* (1969) studied the combination region from 2200 nm to 2500 nm in the NIR for the spectrophotometric analysis of ethylene-propylene copolymers. Four random ethylene-propylene rubbers (EPR), an isotactic propylene (PP), a high and low density polyethylene (PE), and physical blends of homopolymers were purified, dried in a vacuum oven at 90° C for 24 hours and prepared as 100 to 125 mm thick films. Absorbances at 2275 nm, 2310 nm, 2350 nm, and 2466 nm were used for the analysis. The combination band at 2466 nm, a result of the symmetric methyl stretch at 3472 nm, was found to be most sensitive to propylene content. Shifts in the band at 2310 nm were also observed. It was concluded that the shifts could be used to discriminate random copolymers from block copolymers and physical blends of homopolymers [42].

Crandall *et al* (1975) studied the ultraviolet, visible and NIR spectra of a series of polyamic acids (prepared by various reaction conditions) for characterization purposes. The NIR region was found to be the most suitable for the studies. They also demonstrated that polymerization processes could be followed by observing changes in absorbances in the 1950 nm combination band and in a band at 2300 nm due to the amide group [43].

Crandall and Jagtap (1977) studied the NIR spectra for a number of step reaction and addition polymers for identification and following the course of polymerization processes. The overtone C-H band at 1670 nm to 1700 nm was compared for relative band intensities for different polymers subject to changes in reaction and heat curing conditions. They observed a strong N-H band from 2000 nm to 2100 nm in polyurethanes, ureaformaldehyde and polyamides. Carbonyl band due to unreacted formaldehyde indicated no curing time in the preparation of phenol-formaldehyde resins.

They observed a decrease in bands associated with terminal functional groups with heat curing and increases or no changes in bands associated with linkages in the polymer chain. It was concluded that NIR region could be used for determining the state of cure of resins and identification of polymers [44].

Weyer (1985) used the combination band of the terminal -CH_2 group at 2200 nm to show a decrease in absorption during an epoxy resin curing study. This can be seen in figure 4.1. Copolymer and terpolymers containing the monomer allyl glycidyl ether (AGE) were also analyzed using the absorption bands at 2200 nm and 1630 nm, respectively [6].

Weyer (1986) utilized the zero crossover points in the second derivative NIR reflectance spectra for the analysis of polymer pellets and films. Zero crossover (or node) is defined as the point in the first derivative curve which represents the top of an absorption peak, or the point of inflection in the second derivative spectrum. Zero crossover points in the derivative spectra indicated negligible response to concentration changes at the corresponding wavelength. The first application discussed was the determination of methyl ether ketone (MEK) in a UV-curable, photosensitive mixture of acrylic polymers and monomers. Second derivative spectra indicated that 2294 nm was a zero crossover point for the matrix, whereas MEK exhibited a sharp peak at 2294 nm. Spectral measurements at 2294 nm and 1736 nm gave SEC and SEP of 0.12 and 0.15, respectively, for a set of 14 calibration and validation samples [45].

Peck *et al* (1987) demonstrated the use of Fourier-transform NIR to determine the terminal epoxide equivalent weight in polymer resin systems. NIR absorbance at 2206

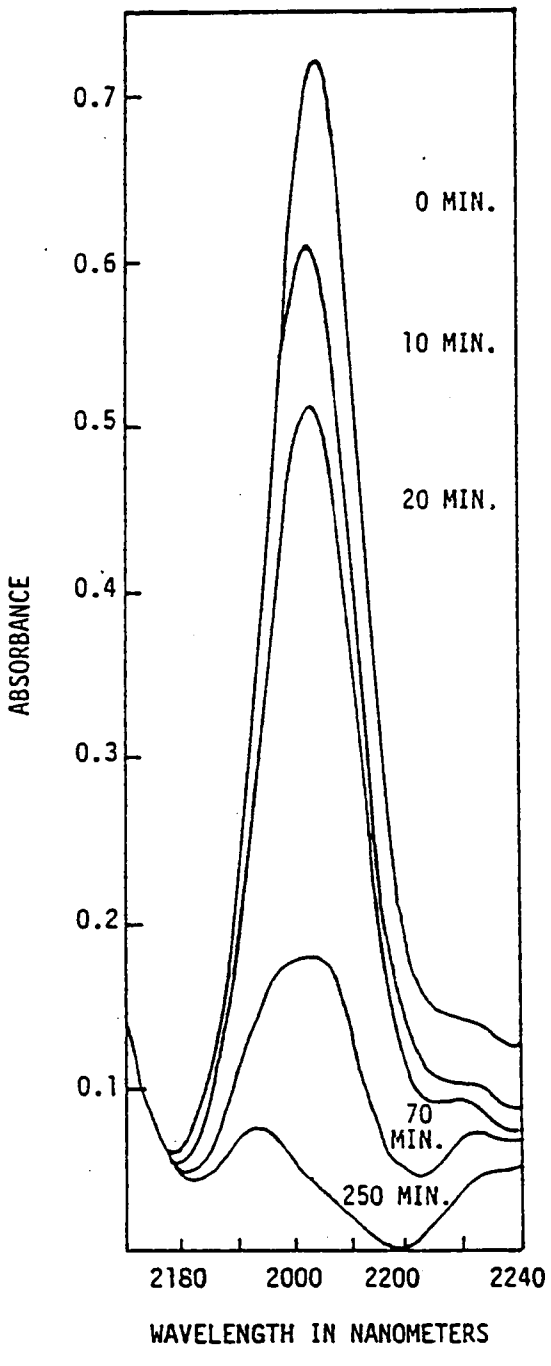


Figure 4.1 Epoxy resin curing study [6].

nm due to the terminal epoxide was chosen for spectral analysis as it was relatively free of interferences. Chloroform solutions of five commercial available resins (derived from bisphenol-A and epichlorohydrin) were analyzed for epoxy equivalent weight. The epoxy concentration levels for these solutions varied from 3.6-20.7 meq epoxy/L chloroform. Absorbance spectra for the samples were obtained by referencing against the chloroform spectrum. The decrease in the epoxy absorbance at 2206 nm was correlated to the increase in epoxide equivalent weight. Furthermore, the spectra of the appropriate amine adducts were subtracted from their epoxide spectrum to isolate the 2206 nm band for all the fine resin systems. Concentrations of one of the resin systems was varied with epoxide equivalent concentration similar to the five resin samples. The varied resin and varied concentration studies exhibited a linear response in the epoxy concentration range 3.6-20.7 meq epoxy/L chloroform [46].

Siesler (1988) demonstrated the use of NIR reflectance spectroscopy and chemometrics for the determination of constituent compositions in liquid mixture of ethanol, dimethyl formamide, ethyl acetate, chloroform and tetrahydrofuran. SEC of 0.05-0.09 and correlation coefficient of 0.99 were obtained. NIR multicomponent analysis of solid mixtures of pyromelliric acid, citric acid, fumaric acid, silica and ceres red based on 28 calibration samples gave SEC of 0.04-1.08 and correlation coefficient of 0.92-0.98 [47].

Miller (1989) used NIR spectroscopy and multivariate methods for providing calibrations for the constituents in ethylene-propylene-diene monomer (EPDM) terpolymers. SEP values of 1.5-3.7 % for ethylene and 1.7-5.0% for propylene were observed by the PLS approach [48]. Bickel (1989) discussed the increased number of on-

line process control applications in polymer, petrochemical, and textile industries using NIR spectroscopy [16].

Miller and Eichinger (1990) demonstrated the use of NIR diffuse reflectance spectroscopy for the characterization of structural features in fibrous and bulk poly(ethylene terepthalate) (PET). NIR diffuse reflectance spectra of PET fibers and bulk PET were obtained and four spectral regions were analyzed by multivariate techniques. The regions from 1570-1850 nm and 2000-2400 nm gave lower SEP and SEC for percent crystallinity compared to regions from 1100-1350 nm and 1850-2000 nm, and hence were considered for further analysis by PLS and PCA [49].

SEP values ranging from 2-3.5% crystallinity were obtained for PET fibers after considering two principal factors of variation in the NIR spectra. PLS on second derivative spectra for region II and IV improved calibration and prediction errors due to removal of baseline variation and enhancement of spectral resolution. It was found that the first principal component was inversely related to orientation in the polymer and the second principal component was inversely related to crystallinity. PCA of the spectra was also used to study the crystallization effects with temperature and detection of moisture in the bulk PET. With the spectral analysis it was demonstrated that NIR spectroscopy could be used to characterize both the intramolecular and intermolecular effects and thus distinguish between crystallinity and orientation [49].

Miller *et al* (1990) [50] further analyzed poly(ether urethane urea) (PEUU) copolymers by NIR spectroscopy to characterize the degree of phase separation and thereby determine the physical properties of the block copolymers. NIR spectra of

urethane model (a reaction product of MDI with ethanol), and urea model (1,3-diethyl urea) compounds in the region 1800-2100 nm were used for the phase separation analysis. Second overtone carbonyl bands at 1918 nm and 2036 nm due to urethane carbonyl and free urea carbonyl were assigned to monitor the phase separation of PEUU copolymers at 100^{o} C. The annealing trend marked by a decrease in absorbance at 2036 nm, and a increase followed by a decrease in absorbance at 1918 nm was consistent with the phase separation mechanism. It was concluded that further study and information was necessary to completely characterize the structural changes with annealing [50].

Diene polymers, such as poly(butadiene), poly(isoprene), and styrene-butadiene copolymers, mostly used in the rubber industry can also be analyzed by NIR spectroscopy [14]. Miller *et al* (1990) used NIR transmission spectroscopy to determine the microstructure and composition of poly(butadiene) (PBD) polymers and styrene-butadiene (SBR) copolymers in bulk and in carbon tetrachloride solution. CLS results in the first overtone region from 1570 nm to 1850 nm predicted 1,2-butadiene within 0.947%, cis-1,4-butadiene within 1.03%, trans-1,4-butadiene within 1.15% and styrene within 1.38% in the PBD and SBR polymers. Sensitivity of NIR spectroscopy to intermolecular interactions was also demonstrated [51].

Miller and Eichinger (1990) analyzed rigid polyurethanes by NIR diffuse reflectance spectroscopy to determine its thermal and compression properties. PCA and PLS results indicated that NIR spectroscopy could determine the compression modulus within 63.6 psi and compression strength within 2.63 psi. The deformation at failure was determined within 1.29% and K-factor was found within 0.0089 Btu-in./^{o}F-h-ft^{2} [52].

Miller *et al* (1990) [53] demonstrated the use of NIR diffuse reflectance spectroscopy for the rapid composition determination of bulk PEUU block copolymers. The PEUU polymers were synthesized from 4,4'-methylenebis (phenylene isocyanate) (MDI), hydroxy-terminated poly(tetramethylene oxide) of approximately 2000g/mol (PTMO-2000), and 1,3-propylenediamine (PD). A hard-segment model compound was prepared by reacting a 1:1 molar mixture of MDI and PD. A soft-segment model was pure PTMO-2000. Six samples ranging from 11.3-42.5% mass hard-segment were used as calibration samples.

Classical least squares (CLS) analysis on log(1/reflectance) data for the calibration of hard and soft-segment concentration in the PEUU copolymers, in the spectral region from 1100-2200 nm was performed. The region from 1350 to 1450 nm was not considered due to instrumental deviations. SEE (standard-error-of-estimate) or SEC of 2.6% mass hard-segment over a range of 31% mass hard-segment was obtained using the CLS model. Further the comparison of the estimated spectra and model compound indicated non-representative sampling and the presence of side products in the polymers as two possible sources of error in the calibration [53].

An excellent review by Miller (1991) [14] demonstrated the sensitivity of NIR spectroscopy to numerous compositional and structural properties of synthetic polymers. The results of the studies can be used to determine specific properties of the polymer system by NIR spectroscopy. The developments in the use of NIR spectroscopy for the non-destructive analysis of synthetic polymers in process and quality control situations was discussed. An account of NIR applications for the study of a wide variety of polymerization reactions was also presented.

Siesler (1991) reviewed NIR spectroscopy of polymers and discussed the impact of chemometric data analysis techniques and fiber optic technology on conventional NIR spectroscopy. NIR studies for the determination of characteristic chemical and physical parameters for poly(acrylonitrile) fibers reflected the good agreement between the actual and predicted values. NIR light fiber spectroscopy and monochromator developments were also presented in the article [54].

Miller and Eichinger (1991) demonstrated the ability of NIR diffuse reflectance spectroscopy to characterize reaction-injection-molded (RIM) polyurethane elastomers. Results obtained by PLS and PCA indicated that changes in composition, density, and phase separation could be accurately determined by NIR spectroscopy [55].

Moisture in polymers can strongly effect polymer processing techniques that require elevated temperatures, such as injection molding, blow-molding, and extrusion. The presence of water can causes degradation during polymer processing operations. Haagen *et al* (1991) demonstrated the use of NIR spectroscopy followed by PCR as an alternative technique for the determination of -OH and -COOH numbers and water content in polyesters. Comparison of obtained results by chemometric analysis of NIR data with standard methods indicated the potential of NIR spectrometry for process control during the polymerization of polyesters [56].

Miller (1992) described the use of non-destructive NIR analysis to improve the understanding of bulk polymeric systems. Process sensing and optimization, product improvement, and structural studies by NIR spectroscopy were also discussed.

Classification, quality, and structural information was obtained from the scores and loadings plots for different polyurethane foams [57].

Mackinson *et al* (1992) demonstrated the feasibility of using multimode silica optical fibers up to 2 km for remote in-line NIR spectroscopic process analysis on a set of aliphatic alcohol mixtures in methanol. The results from the remote in-line NIR measurements compared to the conventional laboratory methods yielded SEP of 3% for 1- propanol and 2- propanol whereas ethanol was predicted with SEP of 5% due to spectral similarity between ethanol and the solvent, methanol [13].

Studies on protein hydration by NIR spectroscopy (1992) were used to distinguish hydrogen bonded water from bulk water. Absorbance peaks due to water, H-bonded to the amino group, were observed at 1406 nm for poly-L-lysine (PLL), at 1408 nm for lysine, and at 1402 nm for n-$BuNH_2$. The study demonstrated the detection of polar-side-chain hydration in polypeptides by NIR spectroscopy [58].

Williams and McPeters (1992) demonstrated the use of NIR spectroscopy for real time in-line monitoring of polymer melt compositions in extruders [1]. They studied the level of methacrylate polymer units in a reactive extrusion process. Design of robust probes capable of withstanding high temperatures and pressures was also undertaken. In the design, a sapphire window was brazed onto the end of a metal housing. A quartz rod, behind the sapphire window was used for light-piping. Their self designed high temperature and high pressure probes were directly placed in the process stream. No waste stream was generated as a result of the sampling arrangement. Longer pathlengths due to low absorptivities in the NIR region helped in maintaining continuous flow of

polymers between the probes. The region around 1400 nm was used for monitoring the level of methacrylate in the copolymer system.

In another study of heterogeneous blends, polymer composition and level of water was monitored by in-line NIR spectroscopy [1]. Difference plots in the region around 1350 nm and 1850 nm indicated negative and positive correlations, respectively with increasing modifier levels. SEP of 0.30 and correlation value of 0.997 were obtained by using PLS and MLR methods. The water level, a good indicator of process performance, was monitored using the combination band at 1900 nm.

Ciurczak (1992) studied acetonitrile (ACN) solutions with water content ranging from 0 to 8% by NIR spectroscopy [59]. The second derivative spectra of water and acetonitrile indicated three regions from wavelengths 1300-1350 nm, 1880-2000 nm and 2380-2400 nm for calibration purposes. Several applications of NIR spectroscopy in various fields were also discussed.

A review article by Brown (1992) [25] discussed on-line applications of NIR spectroscopy for polymeric measurements in real time, indicating the transition of NIR technology from the laboratory, to being a viable technique for process measurements. Kradjel and McDermott (1992) presented a comprehensive account of NIR analysis of polymers [60]. Completion of a three component reactive polymer system (components were not given in the article), was demonstrated by Weyer (1992) [61] by monitoring spectral changes in the regions 1100-2500 nm and 900-1450 nm.

Eschenauer *et al* (1992) discussed the potential of NIR spectroscopy in polymer research by demonstrating its application in the study of the temperature-dependence of hydrogen bonding in polyamides [20]. Application of near infrared spectroscopy in a polymer recycling process for the identification of plastic waste was also presented by screening 30 different polymer types. Grob *et al* (1992) used NIR transmission spectroscopy for monitoring polyol production in a pilot plant. Unreacted epoxide and changes in hydroxyl number were monitored by using a fiber optic transmission probe in the batch reaction. They concluded that monitoring these quantities by NIR spectroscopy would result in increased productivity and reduced raw material wastage [62].

McPeters and Williams (1992) [19] applied NIR spectroscopy for in-line measurements of polymer composition in blends and terpolymers inside an extruder. The polymer blends were a heterogeneous mixture of acrylate/styrene copolymer dispersed in a methacrylate/acrylate copolymer. The terpolymer system was composed of a methacrylate related component, a methacrylate ester and a -OH containing unit. Scattering effect due to mismatched refractive indices in blends was removed by a two point baseline correction, using absorbance values at 1290 nm and 1530 nm.

Absorbance value at 1290 nm was used for baseline correction for terpolymer samples. Positive bands at 1361 nm and 1439 nm and negative bands at 1200 nm and 1407 nm varying from 0-45 wt. % were considered. MLR and PLS methods were applied to the first and second derivative absorbance spectra in the region from 1200 to 1650 nm. SEC values of 0.79 for MLR and 0.78 for PLS using three factors were recorded [19].

For the terpolymer system, increases in the methacrylate component occurred at 1469 nm and 2009 nm while decreases in methacrylate ester occurred at 1350 nm, 1425 nm, and 1949 nm. Large changes in the -OH containing third component showed up at 1444 nm, 1899 nm and 2034 nm. MLR and PLS techniques were applied to second derivative absorbance spectra over the region 1200-1650 nm. PLS method with three factors gave SEC of 0.98 and 0.032 for methacrylate component and -OH containing unit, respectively [19].

Monitoring the polymerization of a monomer to a polymer by NIR spectroscopy was discussed by Miller (1992) [63]. The level of monomer, polymer, and chain transfer agent were monitored continuously in a batch reactor. SEPs of 0.05, 0.10, and 0.05 wt. % were obtained for the monomer, polymer, and chain transfer agent, respectively. It was determined that continuing the reaction after the limiting amount of components is economically infeasible and could be avoided by real-time monitoring of the composition of the components by NIR spectroscopy.

Lee (1993) reviewed an account of the different applications of mid-IR and NIR spectroscopy and compared the two regions for qualitative and quantitative analyses in polymers [64]. It was discussed that due to the high sensitivity in the mid-IR region, only a little amount of material is needed for analysis, although the samples have to specially prepared, i.e. made thinner or diluted. In comparison, the NIR analysis is not as sensitive and does not require special sample preparation, although more sample compared to the mid-IR may be needed for analysis. Min *et al* (1993) measured the changes in concentrations of epoxy, primary and secondary amine groups with time by

NIR spectroscopy. The measurements were used to determine the extent of conversions of elementary reactions during a curing study [65].

Miller *et al* (1993) demonstrated the use of NIR reflective-transmission spectroscopy in the region from 1500 nm to 2500 nm, for the analysis of food packaging laminates containing polyethylene (PE), polyamide-6 (PA-6), and ethylene vinyl alcohol (EVOH) layers. PCR results indicated that the total laminate thickness could be determined to within 2-4 mm, the PE layer thickness percentage to within 0.7-1.8%, and the EVOH layer thickness to within 0.7-0.8 mm [66].

Gossen *et al* (1993) measured the properties for styrene/methyl methacrylate latex during the course of a semi-batch polymerization reaction using NIR spectroscopy. PLS and PCA results predicted standard errors of less than 0.5 wt. % for all the major components, such as water, poly(styrene), poly(methyl methacrylate), styrene and methyl methacrylate [67].

Miller (1993) [29] determined the blend ratios of high density polyethylene (HDPE) and low density polyethylene (LDPE) in extruded films by NIR reflective-transmission spectroscopy. 60-80 mm thick film samples were non-destructively analyzed over the region 2100-2500 nm in 2 nm increments. Spectra for seven different blend ratios of 0, 2.5, 5, 10, 25, 50, and 100% HDPE were analyzed by PCR. Three principal factors were found optimal after cross-validation by two spectral analyses. First, second, and third factors accounted for 46.67%, 49.25%, and 2.56% of the overall spectral variation, respectively.

Calibration and prediction errors of 2.31% and 2.48% HDPE, respectively, were found using three (optimal) factors. The third factor, even though accounting for only 2.56% of the spectral variation, adequately explained the variation among the samples containing 0-50% HDPE. Scores plot for the first two factors indicated differences between the 100% HDPE sample and the samples with 0-50% HDPE [29]. The spectral effects of scattering and degree of crystallinity were used to determine % HDPE in the samples containing 50-100% HDPE. For the samples containing 0-50% HDPE, the % HDPE was related to the methyl group concentration and the degree of crystallinity. Variation between replicate samples was attributed to variations in the direction and degree of molecular orientation in the samples. Interference fringes were found to contribute to the random error in the spectral data. It was suggested that using thicker samples, reducing the noise due to interference fringes, and using a non-linear calibration modeling approach could result in improving the accuracy of the NIR analysis [29].

Long *et al* (1993) monitored the monomer conversion during anionic solution polymerization reaction by NIR spectroscopy. The conversion of vinyl protons in isoprene monomer to methylene protons in polyisoprene was monitored under polymerization conditions in a cyclohexane solution with 10-20% solids. Studies of copolymerization kinetics of isoprene and styrene by anionic polymerization in cyclohexane at 60 ^{o}C, indicated that NIR was capable of detecting sequence distributions for tapered block copolymers, and reactivity ratios for free radical copolymerization [68].

Hansen, Batra *et al* (1994) monitored the concentration of titanium dioxide (TiO_2), a white inorganic filler, in molten poly(ethylene terepthalate) (PET) by studying baseline shifts in the NIR spectra. Two commercial PET resins, one with no TiO_2 and

another with the desired commercial content of TiO_2 were chosen for the analysis. The concentration of TiO_2 was normalized from 0% to 100% in increments of 10%, by taking weighed quantities of the two resins. The 0% concentration was represented by the resin containing no TiO_2, and the 100% concentration was represented by the TiO_2 filled commercial resin. The dry blended pellet samples of the two PET resins, spanning the TiO_2 concentration from 0% to 100% were vacuum dried for 24 hours at 80 ^oC before processing.

TiO_2 caused scattering of light resulting in a baseline shift, and this shift was correlated to its concentration in the sample. SVD based algorithm for PLS regression was used for the multivariate analysis to determine the TiO_2 content in the PET melt. SEP values of about 1% were obtained by considering two principal components (or factors), indicating the robustness of the calibration model [26]. DeThomas *et al* (1994) used NIR spectroscopy for monitoring the production of polyurethanes in real time [69]. Statistical process control charts were used to monitor the polymerization reaction by determining the extent and rate of the reaction.

A series of experiments were performed by Hansen and Khettry (1994) on blends of polystyrene (PS) and polyphenylene oxide (PPO) to demonstrate the viability of *in-situ* process monitoring of molten polymeric processes. The measurements were made in a flow cell located at the exit port of a single screw extruder. Multivariate analysis of spectral data was used to develop robust calibration models for on-line prediction of compositions. They also demonstrated the successful design and use of fiber optic probes which are inserted into the polymer stream at high temperatures, pressures, and severe process conditions [2].

PS/PPO blends with PPO concentration varying from 0 wt % to 85 wt % were used in the experiments. A constant pathlength of 2 mm was used for the in-line measurements. The overtone region from 1600 nm to 1800 nm was used for multivariate analysis. The decrease in the aromatic C-H peak at 1680 of PS is replaced by the aromatic C-H peak of PPO at 1674 nm and the methylene peak of PS at 1763 nm is replaced by the methyl peak of PPO at 1739 nm. This can be seen in figure 4.2 for the different blends in the 1600 nm to 1800 nm range [2]. Cross validation using leave-a-sample (LAS) and leave-a-group (LAG), and validation using a test set resulted in one factor accounting for 98.24% variation in the spectral data. SEP and SEC values of 0.95 and 0.93 wt % PPO respectively were found to be minimum at one factor and increased with considering more principal components due to the inclusion of random noise in the model with subsequent factors. Similar results were obtained for the overtone region from 2050 nm to 2130 nm.

Ghebremeskel *et al* (1994) demonstrated the use of NIR spectroscopy for studies on specific interactions in miscible polymer blends. NIR spectra of isopropanol in a mixture of heptane and ethyl acetate demonstrated NIR spectral shifts as a result of specific interactions. The hydroxyl of the isopropanol and the ester functionality of ethyl acetate resulted in a broad absorption band centered at 1434 nm, indicating the absorptivity of associated hydroxyl was at least twice that of the unassociated species. In another experiment additional absorption at 1481 nm for blends of nylon-6 and zinc salt of sulfonated polystyrene (ZnSPS) was observed at temperatures greater than the melting point of Nylon-6, due to changes in crystallinity and specific interactions [70].

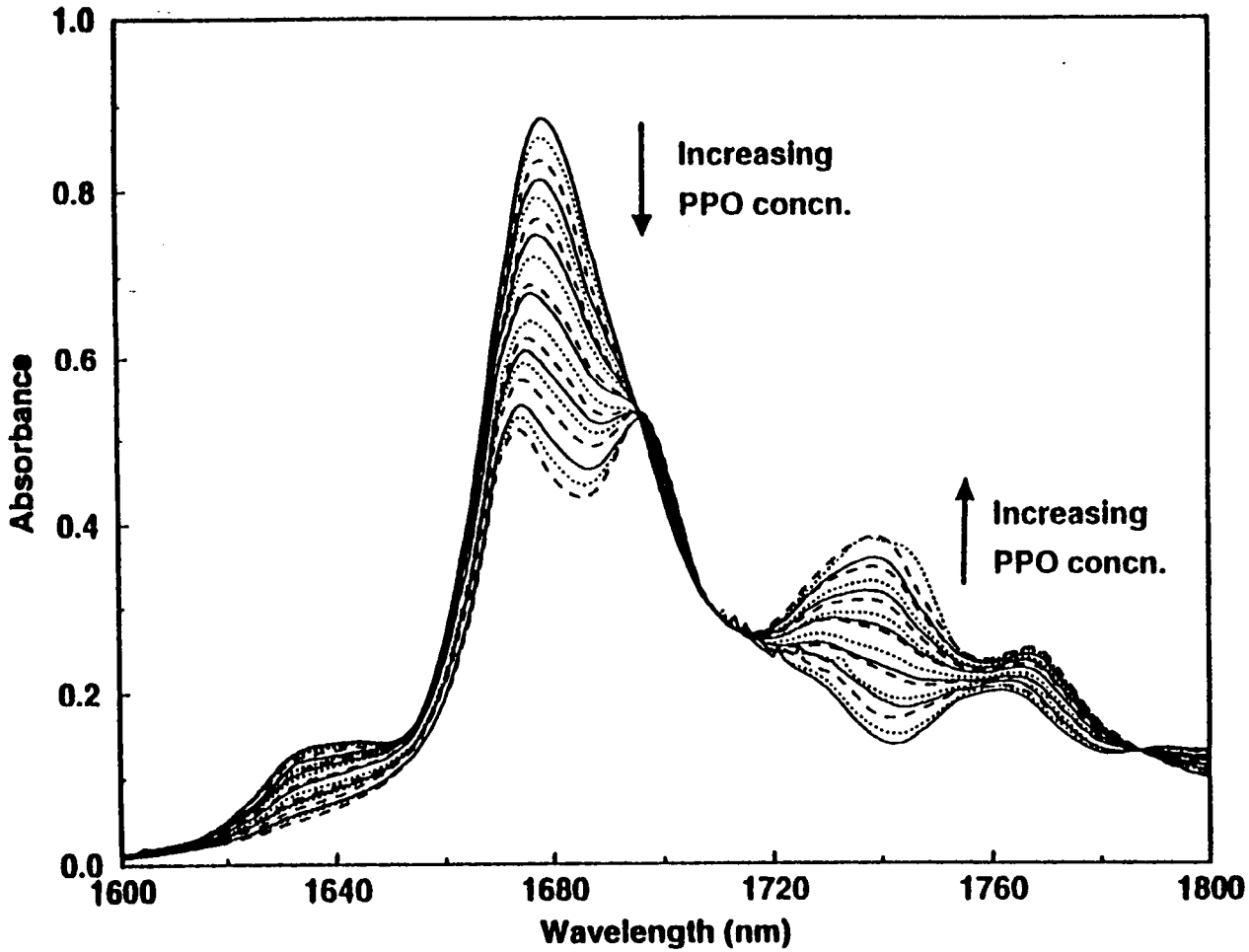


Figure 4.2 PS/PPO blends in the region from 1600 nm to 1800 nm [2].

4.2 MISCELLANEOUS

NIR analysis was applied only to a limited number of problems until the early 1950's due to lack of proper instrumentation. With the developments in NIR instrumentation during the 1950's , it was used for several agricultural applications, along with a wide variety of industrial applications. Some of the agricultural and industrial applications are discussed in this section [7].

Weyer (1985) discussed the extensive use of NIR reflectance measurements in the determination of moisture content in various substances [6]. NIR applications, relating to agricultural products such as grains and oil seeds, were discussed in detail by Stark *et al* (1986) [7]. A comprehensive review on NIR analysis, data treatment, mathematical approaches to calibration, sampling techniques and NIR applications is also presented in the article. Other NIR applications in the field of pharmaceutical, textiles, biomedical and biochemical are also discussed.

Parisi *et al* (1990) used NIR spectroscopy along with fiber optics and multivariate calibration for the on-line determination of fuel quality parameters. Octane number in gasolines and cetane number in diesel fuels were also measured [71].

A review article by Coventry (1991) discussed the developments in sample preparation, analysis, and increased analytical applications of NIR spectroscopy in the food and agricultural, pharmaceutical, chemical, and petrochemical industries. Advantages of on-line analysis for continuous process monitoring for optimum production yield and waste minimization using statistical analysis were also presented [21]. Lang (1991)

discussed the use of Acousto Optic Tuneable Filter (AOTF) based NIR analyzers for in situ monitoring of liquid samples [72].

Baseline offsets due to particle size variations in sucrose was studied by Cuirczak (1992) [59]. Shenk *et al* (1992) discussed application of NIR spectroscopy to agricultural products for the measurement of moisture and protein in grains [73]. The developmental history of NIR analyzers and their on-line applications for gaseous, liquid, and solid samples as applied to process control, product quality, energy conservation, and environmental applications was reviewed by Dailey (1992) [8].

On-line measurements of octane number of gasoline by NIR spectroscopy was presented by Miller (1992) [63]. It was found that NIR analysis was much quicker than the conventional analysis by the octane engine. Figure 4.3 shows the on-line NIR measurements of research octane number (RON) over time. The PLS model for prediction gave SEPs of 0.19 and 0.35 for motor octane number (MON), and research octane number (RON), respectively.

Martin (1992) reviewed the versatility and development of NIR reflectance spectroscopy in several applications. A detailed account of the various chemometric techniques used were also presented in the article [22]. Cermelli *et al* (1992) discussed on-line near infrared analysis for the optimization and control of different petrochemical plants [74].

Weyer (1992) discussed the at-line application of NIR reflectance spectroscopy in the analysis of a propellant, a carbon fiber composite, and a reactive polymer process.

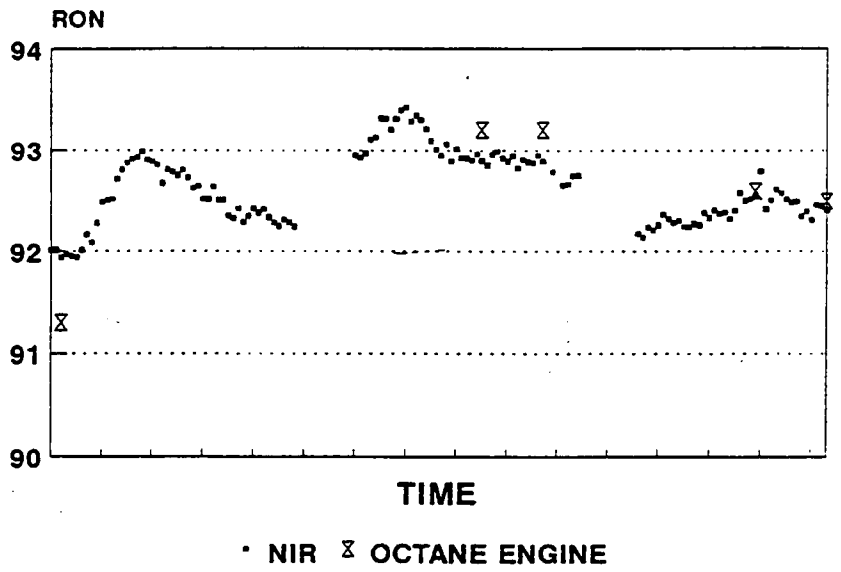


Figure 4.3 On-line NIR measurements of research octane number (RON) over time [63].

Typical composition of a propellant consists of 50% oxidizer, 20-30% aluminum chips (used as fuel), 10% each of plasticizer and binder. The propellant used for the analysis had ammonium sulfate as oxidizer and esters of polyfunctional alcohols as binder and plasticizer. MLR and PLS methods suggested three principal factors of variation in the calibration samples. NIR analysis was used to monitor the level of contaminant on the carbon fiber composite surface, but it was found that optical measurements rather than spectral measurements were sufficient for the problem [61].

Buchanan (1992) reviewed the applications of NIR analysis in the petrochemical industry [75]. It was discussed that as the sources for petrochemical products becomes scarce, analysis at each process step to enhance efficiency would be extremely important. NIR analysis when applied to such processes can be used to enhance process utility. A study for the determination of methanol in gasolines was carried out using fiber optics. SEC of 0.217 and SEP of 0.626 were obtained from the analysis.

Ciurczak(1992) gave an account of the increasing number of NIR analysis in pharmaceuticals [76]. The advantages in terms of minimal sample preparation, lack of expensive and volative solvents, speed of analysis, and modern NIR instrumentation have resulted in the use NIR spectroscopy for analyses in the pharmaceutical industry. Diffee discussed NIR analysis in the tobacco industry [77]. The determination of nicotine is an important analysis in the tobacco industry, as the quality of tobacco is determined largely by its nicotine content. NIR spectroscopy is being used for the determination of nicotine content in tobacco.

Hammersley discussed the immense potential of NIR spectroscopic techniques for the analysis of wool [78]. The estimation of residual grease levels and moisture content in wool can be carried out using NIR analysis. Ghosh and Rodgers [79] discussed the application of NIR spectroscopy in the textile industry for the characterization of raw materials and finished textile products. NIR reflectance spectroscopy can be used to perform a blend analysis of cotton/polyester (PET) blends in 2 minutes, whereas the conventional procedure by dissolving the blend in 70% sulfuric acid solution requires 8 hours before the final result is obtained.

Osborne reviewed the actual and potential uses of NIR spectroscopy in the baking industry for the analysis of ingredients (flour), process intermediates (dough), and final products (bread, biscuits pasta, etc.) [80]. Frankhuizen reviewed NIR analysis of dairy products [81]. Applications include the NIR analysis of milk in terms of fat, protein, and lactose. Analysis of raw materials for the production of cream, cheese, casein, and whey are also important applications of NIR spectroscopy in the dairy industry. Kington and Jones reviewed the use of NIR analysis in the beverage and nutritional formula industry [82]. The constituents in alcoholic beverages (beer, wines, and spirits), nonalcoholic beverages (fruit juices, coffees, teas, and soft drinks), and other products like infant and adult nutritional formulas can also be determined using NIR analysis.

5. EXPERIMENTAL SETUP FOR IN-LINE MONITORING OF POLYMER BLENDS

The objective of the research is to demonstrate the use of NIR spectroscopy for in-line monitoring of polymer blends. The whole assembly for the in-line monitoring, is schematically shown in figure 5.1. The setup for the experiments is discussed in this section.

5.1 EQUIPMENT AND EXPERIMENTAL SETUP

Guided Wave Model 260 spectrophotometer with single fiber optic cables and double insertion optical transmission probes were used in the experiments. Measurements were made in the multifunctional variable pathlength flow cell at the exit port of the variable speed gear pump as shown in figure 5.1. The spectral data was stored on a personal computer (PC) using the Guided Wave Scanner program.

The temperature and pressure in the flow cell is regulated by a control unit. The screw speed and gear pump output is also used for changing and regulating the pressures in the extruder and gear pump. Increasing the screw speed increases the pressure upstream of the gear pump, thereby facilitating back flow in the extruder and resulting in better mixing of the polymers. Back mixing is essential for the blends used in the experiments as the polymer resins were available in the pellet form. Dry nitrogen (N_2) gas is constantly purged in the feed hopper to prevent any moisture absorption from the atmosphere by the sample.

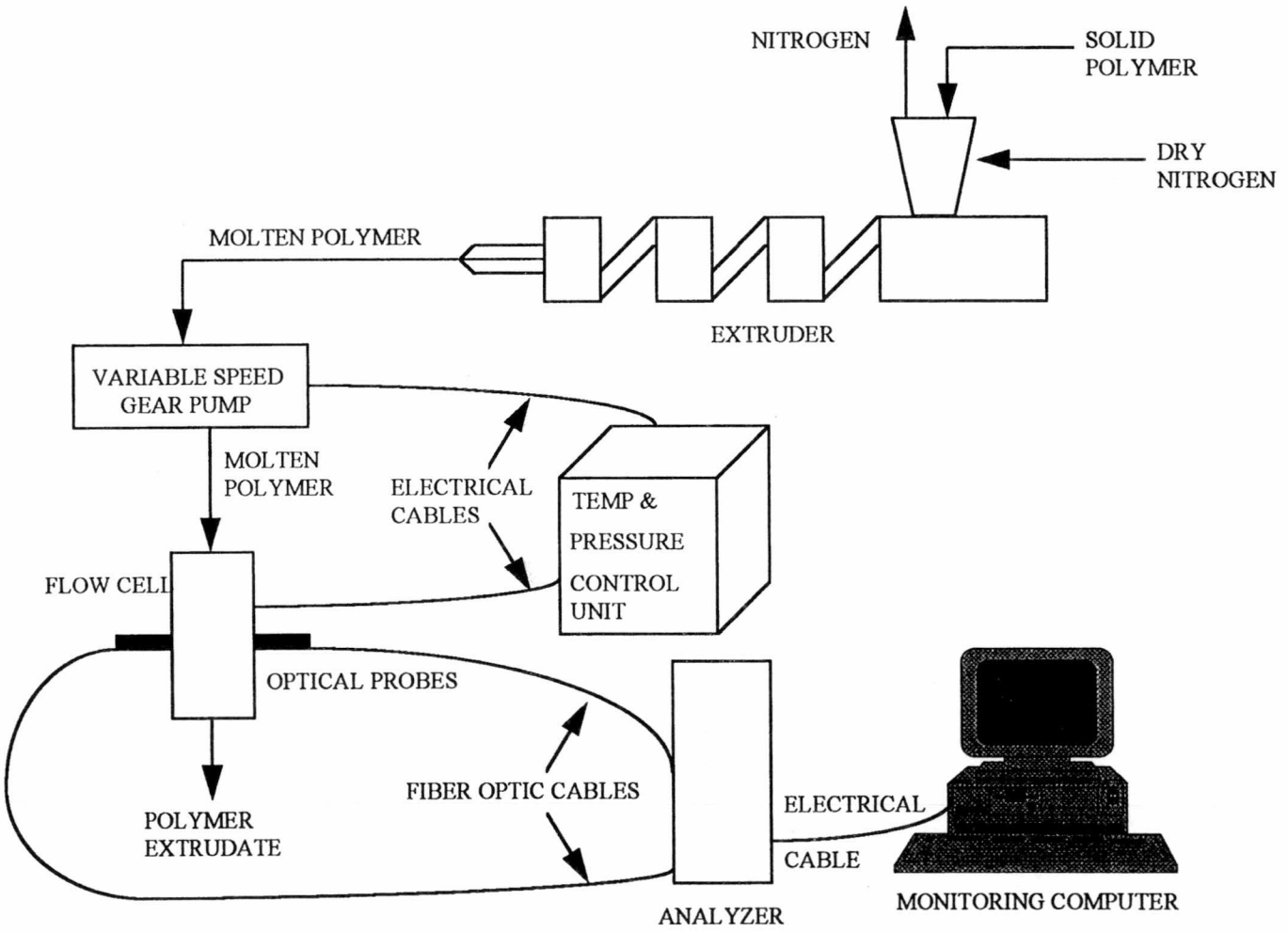


Figure 5.1 Experimental setup for in-line monitoring of molten polymers.

A Brabender laboratory single-screw extruder is used in the experimental setup. The single screw is 3/4 inch (18.75 mm) in diameter and 18.75 inch (476.25 mm) in length. The extruder is divided into four zones; the feed zone and three heating zones 1, 2, and 3. The temperature in the feed zone is kept at 80 ^{o}C using cooling water to facilitate solids conveying in the extruder. The temperatures in the three zones, heating block, and flow cell is regulated by independent controllers. The heating zones in the extruder have a cooling arrangement to maintain desired temperatures.

NIR light is transmitted through the double insertion transmission fiber optic probes installed in the multifunctional variable pathlength flow cell. Collimated beam emerging from one probe is transmitted through the process stream to an identical receiving probe. The distance between the probes or pathlength can be varied from 1 mm to 9.5 mm using spacers. The Guided Wave Model 260 spectrophotometer uses a tungsten halogen lamp and a lead sulfide detector. Guided Wave softwares, Scanner and Examiner, installed on a personal computer are interfaced with the spectrophotometer. These programs are used for data acquisition and manipulation.

5.2 RUGGED PROBES AND OPTICAL FIBERS

Probes

The high temperatures and pressures in the highly viscous molten polymer streams require the fiber optic probes to be capable of withstanding these severe conditions. Hansen *et al* discussed the design and development of fiber optic probes, which were successfully tested at 350 ^{o}C on melts of polystyrene (PS) and

polyphenylene oxide (PPO) blends, in a single screw extruder. Figure 5.2 shows the fiber optic probes used for in-situ measurements [2].

Fibers

Light fiber spectroscopy requires a suitable device for the transfer of light from the spectrometer to the sample and back to the spectrometer. Silicon with excellent transmission characteristics in the visible and NIR region is used as the basic material for such a device; the optical fiber. A fiber consists of a silicon core, a cladding and a protective polymer coating. A typical fiber is shown in figure 5.3 [54]. Losses in the fibers are appreciably lower in the NIR, compared to the mid-NIR region [70].

Schirmer (1986) discussed in-situ composition monitoring in real time for process optimization and control in chemical analyzes using fiber optics [83]. On-line monitoring via fiber optics offers a number of advantages, such as the distance of the instrument from the probes can be several hundred meters, the safe features of the fiber optic link and rapid and accurate measurements. Use of fiber optic probes at high temperatures and pressures in severe process environments, and the accessibility of the ultraviolet, visible, and NIR spectral regions are extremely useful for in-line monitoring. NIR fiber optic spectroscopy offers the advantage of light being brought to the sample from the remotely located analyzer, therefore allowing for *in situ* measurements of the process stream.

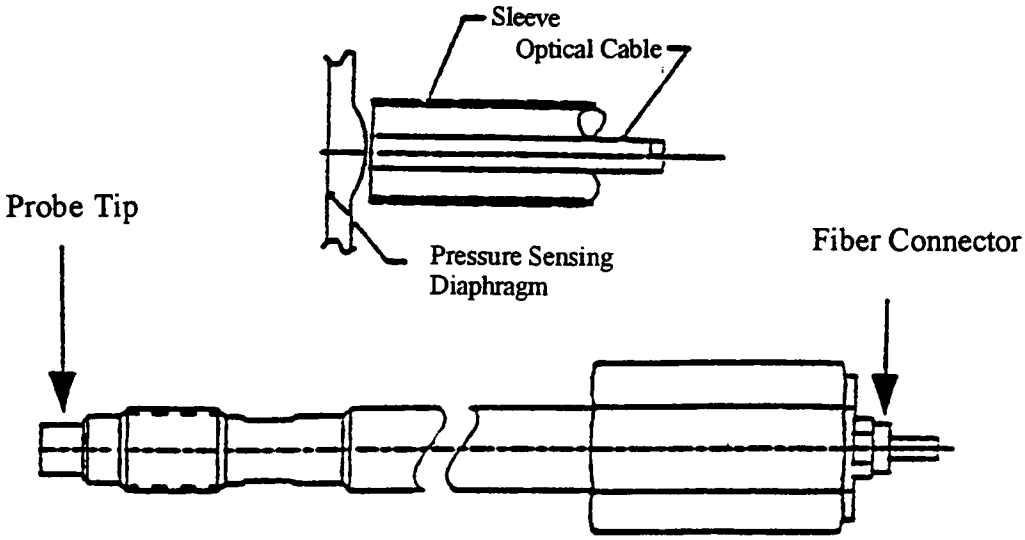


Figure 5.2 Fiber optic probe for *in-situ* monitoring [2].

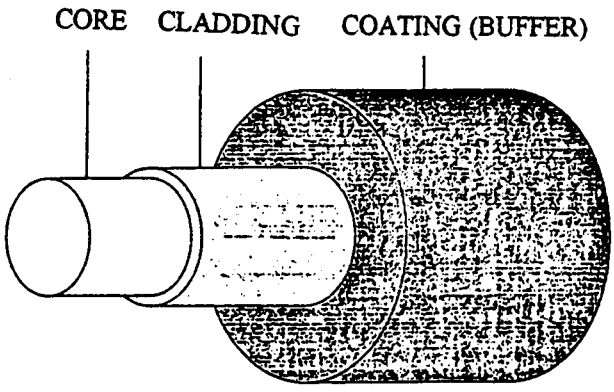


Figure 5.3 Schematic diagram of an optical fiber [54].

5.3 OVERVIEW OF THE POLYMER BLEND SYSTEMS USED FOR EXPERIMENTAL RESEARCH

In-line composition monitoring of partially miscible polymer blends of styrene-acrylonitrile (SAN)/acrylonitrile-butadiene-styrene (ABS), SAN/polycarbonate (PC), and ABS/PC was studied in this research. In the set of experiments for the three blend systems the concentration of the resins were normalized from 0 % to 100 % in increments of 10 %, by taking weighed quantities of the components. Figure 5.4 shows the polymer resins, with the arrow pointing towards the constituent whose concentration is increased in the blend systems. Subsequent chapters discuss in detail experimentation and data analysis for the partially miscible SAN/ABS, SAN/PC, and ABS/PC blends.

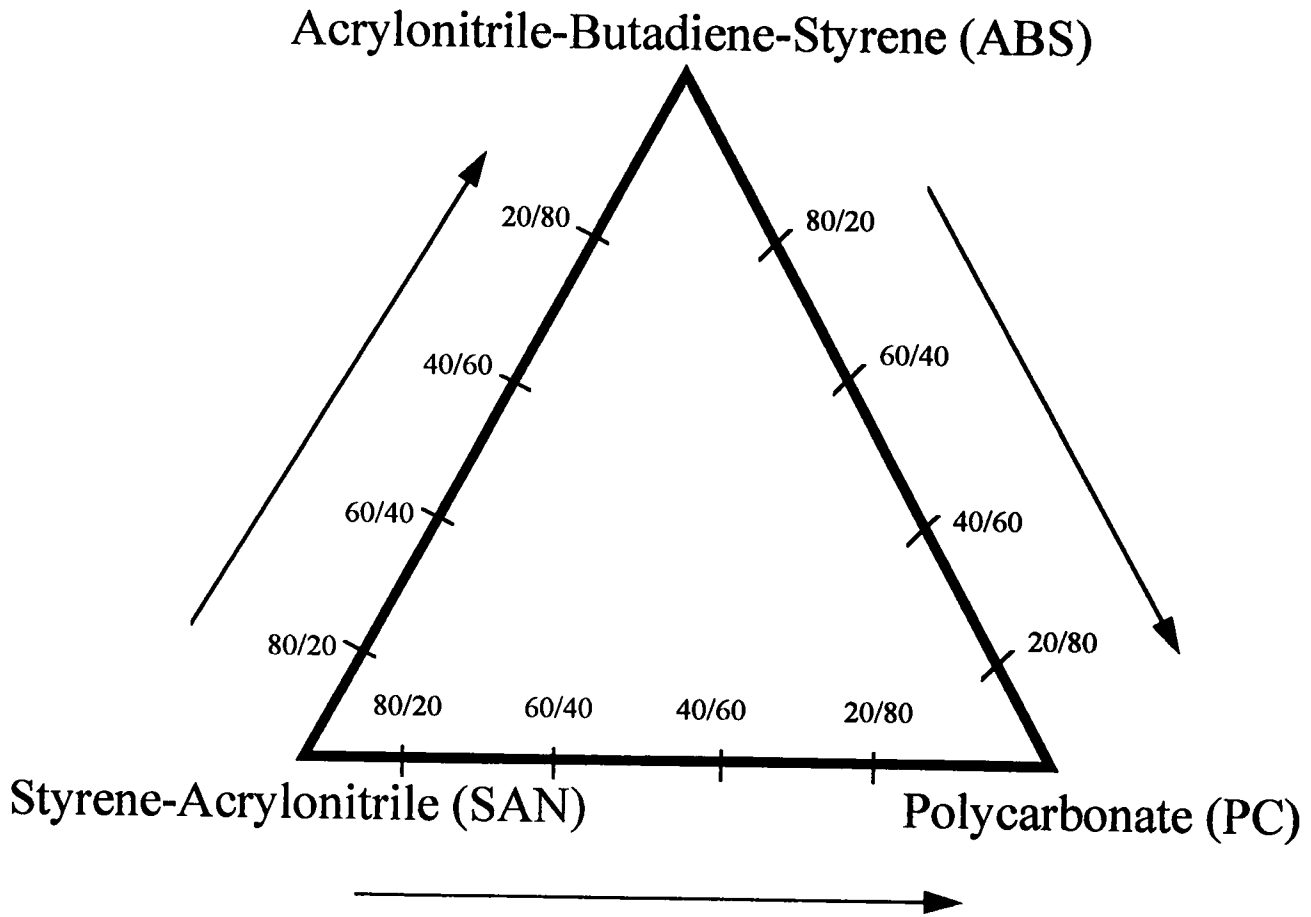


Figure 5.4 Polymer resins in the partially miscible polymer blend systems.

6. IN-LINE MONTORING OF ACRYLONITRILE-BUTADIENE-STYRENE (ABS)/STYRENE-ACRYLONITRILE (SAN) BLENDS

Introduction

Styrenic materials, such as styrene-acrylonitrile (SAN) and acrylonitrile-butadiene styrene (ABS) are an important group of polymers, derived from the styrene, acrylonitrile, and butadiene monomer units. SAN with a T_g of 115 ^oC is a hard, transparent material with excellent heat resistant properties. ABS with a T_g of 110-125 ^oC exhibits excellent balance of properties such as gloss, thermal stability and impact resistance. These properties of SAN and ABS are a result the three monomeric building blocks. The styrene monomer provides rigidity and processability, and the acrylonitrile monomer gives heat stability and chemical resistance. The butadiene monomer in ABS, accounts for the toughness and impact properties of rubber reinforced plastics [84]. Blends, and copolymers of SAN and ABS are found in a number of everyday applications, such as appliances, packages (bottles, nozzles, etc.), automotive parts, and industrial products.

Polymer blends have been a topic of importance in material science during recent years, as blending of different polymers can result in new materials with advantageous properties having great potential for new applications. Compatibility or miscibility can be defined as the ability of two polymers to make a homogeneous mixture which is thermodynamically stable and does not exhibit separation of the components with time [85]. Complete miscibility in a strict thermodynamic sense between two polymers is

extremely rare. Miscible polymer blends are homogeneous systems of mutually compatible polymers.

Miscibility is also understood as the penetration of components on the molecular level, analogous to low molecular weight substances. A blend of compatible polymers exhibit a proportional balance of properties that is directly related to the specific ratio selected. Partial miscibility means that a two-phase structure is generated when two polymers are mixed. Both the phases contain different but limited amounts of each component [86].

As ABS resin has very good impact properties, its blends with other thermoplastic resins are being investigated. Han *et al* (1987) studied the rheological behavior of ABS and poly(methy methacrylate) (PMMA) and found that the rubber particles had little contribution in the compatibility of the ABS/PMMA blends, but the SAN matrix played a major role in compatibilizing ABS resin with PMMA [87].

Kim *et al* (1990) studied the toughening of styrene-maleic anhydride (SMA) copolymers with a SAN-grafted rubber [88]. The acrylonitrile (AN) level of SAN graft was fixed at 22.5 % and the maleic anhydride (MA) content of the SMA matrix was varied from 8 to 25 %. Maximum impact strength was observed when the polymer matrix contained 14-17 % MA. The increase in toughness with MA content between 14-17 % was concluded to be due to the increased miscibility of the SAN with the SMA matrix when the MA and AN contents were about the same in each copolymer.

Molten blends of SAN with SAN-grafted-polybutadiene (PB) (g-ABS) were studied by Kim and Shin (1993) [89]. The effect of rubber concentration on the morphology and mechanical properties of the blends was studied upto 60 wt. % ABS. Lower and higher glass transition temperatures of g-ABS decreased and then increased with the addition of SAN, which was interpreted in terms of graft SAN-PB phase separation.

Barlow (1993) discussed the miscibility of polymer blends and the resulting phase behavior from the thermodynamic state of its components [90]. The formation of miscible blends requires a net exothermic interaction between the molecular groups that comprise the blend components. In the article, a qualitative application of partial miscibility to interfacial adhesion in multiphase polymers was also presented. It was suggested that as the blend components become more nearly miscible, their interfacial adhesion increases.

Machado and Lee (1994) studied the compatabilization of immiscible blends with a mutually miscible third polymer [91]. Four immiscible blend systems, styrene-maleic anhydride (SMA)/SAN, SMA/ABS, poly(vinylidene fluoride)/SAN (PVF_2/SAN), and PVF_2/ABS were investigated in their study. The effect of adding 10 wt. % of poly(methyl methacrylate) (PMMA), a third polymer that is miscible with each blend component, resulted in the improvements of properties such as tensile strength, tensile elongation, and impact strength. They concluded that addition of a relatively minor amount of a mutually miscible component can exhibit substantial interfacial activity which is reflected in the morphology and improved properties of the blends.

Experimental

In the set of experiments for the ABS/SAN blends, the concentration of ABS was normalized from 0 % to 100% in increments of 10%, by taking weighed quantities of commercially available SAN and ABS resins. The 0% concentration of ABS was represented by the pure SAN resin and the 100% concentration of ABS was represented by the pure ABS resin.

The ABS and SAN polymers were available as pellets. The 11 samples which covered the entire range of concentrations from 0 to 100 wt. % ABS, were prepared by carefully weighing the two polymers in the desired ratios. The samples were then mixed by manual shaking in a plastic container. Due to the hygroscopic nature of SAN and ABS, the samples were dried for 16-24 hours, at 180 ^{o}C in a vacuum dryer, before processing. Vacuum drying was carried out after preparing the samples, as the drying temperature and drying time for both the polymers is approximately the same. After vacuum drying, the samples were placed in aluminum foil and kept in an oven to prevent any moisture from being absorbed.

The ABS/SAN blends were extruded at temperature set points of 220 ^{o}C, 230 ^{o}C, and 230 ^{o}C in heating zones 1, 2, and 3, respectively, in the extruder. The temperature in the heating block and flow cell was maintained at 240 ^{o}C, using independent controllers. The mixing of the two polymers was further enhanced in the extruder. The screw speed was maintained between 20-22 r.p.m for the experimental runs. Pressures downstream of the gear pump (figure 5.1) varied from 650-1350 psi, and pressures upstream of the gear

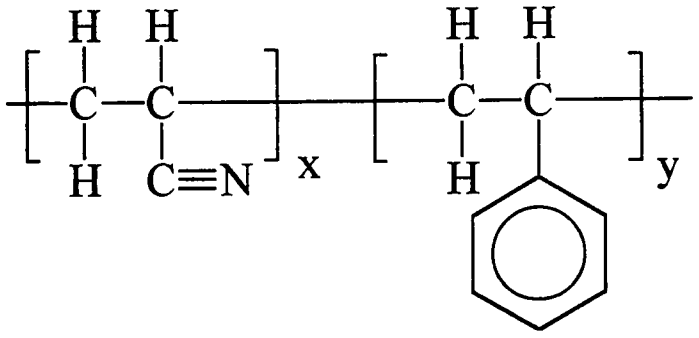
pump varied from 80-220 psi, for the entire range of concentrations. The pressures increased with increasing wt. % ABS in the samples.

The first sample of pure SAN, was run for approximately an hour and a half to flush out any material that might have been present in the extruder, as a result of earlier experiments. Each sample was run for nearly 1 hour in order to flush out the previous sample, and obtain stable and reproducible spectra for the particular blend composition. The NIR spectra was collected in the wavelength range from 1200 nm to 2400 nm with a step size of 1 nm using the Scanner program. A fixed pathlength of 1.5 mm was used for all the ABS/SAN blends to ensure that the maximum absorbance was less than 1.0 absorbance units. Ten representative spectra for each of the samples were saved for qualitative and quantitative analysis.

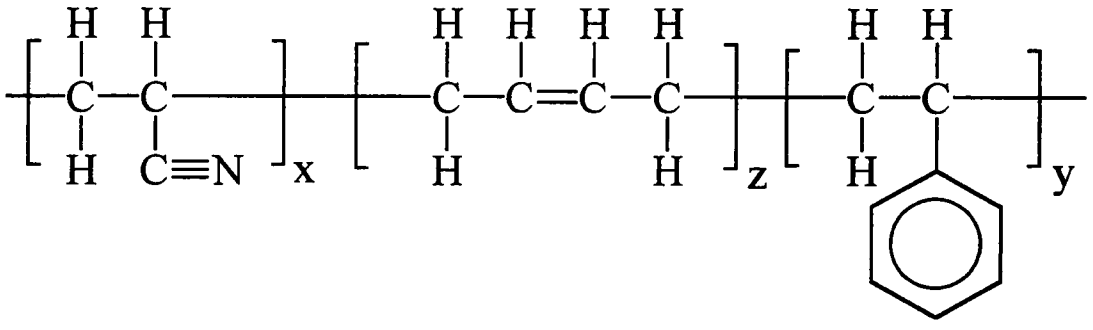
Spectral Analysis

As the NIR region primarily consists of overtone and combinations of C-H, O-H, and N-H stretching and bending vibrations, the structure of the molecules can provide an understanding about the peaks and absorption bands occurring in the NIR. Figure 6.1 illustrates the chemical structures of ABS and SAN. x, y, and z which represent the number of repeat units were not known, although the ratio of the styrene and acrylonitrile (i.e. x/y) in the SAN and ABS resins was the same.

The overtone and combination regions in the ABS/SAN spectra were chosen for the qualitative and quantitative analysis. The region from 1600 nm to 1800 nm shows first overtone bands due to C-H stretch vibrations, while the region from 2000 nm to



Styrene-acrylonitrile (SAN)



Acrylonitrile-butadiene-styrene (ABS)

Figure 6.1 Chemical structures of styrene-acrylonitrile (SAN) and acrylonitrile-butadiene-styrene (ABS). x, y, and z represent the number of repeat units in the two polymers.

2400 nm consists of combination bands as a result of C-H stretch and other modes of vibration [10], as discussed in chapter 2. Figure 6.2 shows overlaid NIR absorbance spectra of the averaged raw data for pure ABS and SAN in the region from 1200 nm to 2400 nm. The spectra of the pure ABS and SAN show differences in the overtone and combination regions of the absorbance spectra. These variations were modeled by multivariate analysis to predict compositions of the ABS/SAN blends.

Results and Discussions

The ten spectra for each of the 11 sample compositions comprised of 1201 absorbance values in the region from 1200 nm to 2400 nm. The absorbance spectra of the averaged raw data for each of the 11 samples, covering the entire range of concentrations are shown in figure 6.3. Due to presence of butadiene monomer (rubber particles) in ABS, scattering and baseline offsets in the spectral data were observed. The overtone and combination regions were selected for the multivariate analysis based on the systematic variations in the two regions. The overtone region was corrected by two point baseline method, using the absorbance values at 1595 nm and 2040 nm. The combination region was also corrected by two point baseline method, using the absorbance values at 2070 nm and 2220 nm.

The 110 baseline corrected spectra, (10 spectra for each blend composition) were then smoothed using Guided Wave Examiner program and visually examined further for non-representative spectra and outliers. Twenty-two spectra were rejected based on these criterion. Eighty-eight spectra (8 for each blend composition) were selected for quantitative analysis by PLS and PCR. The eight spectra for each sample were averaged

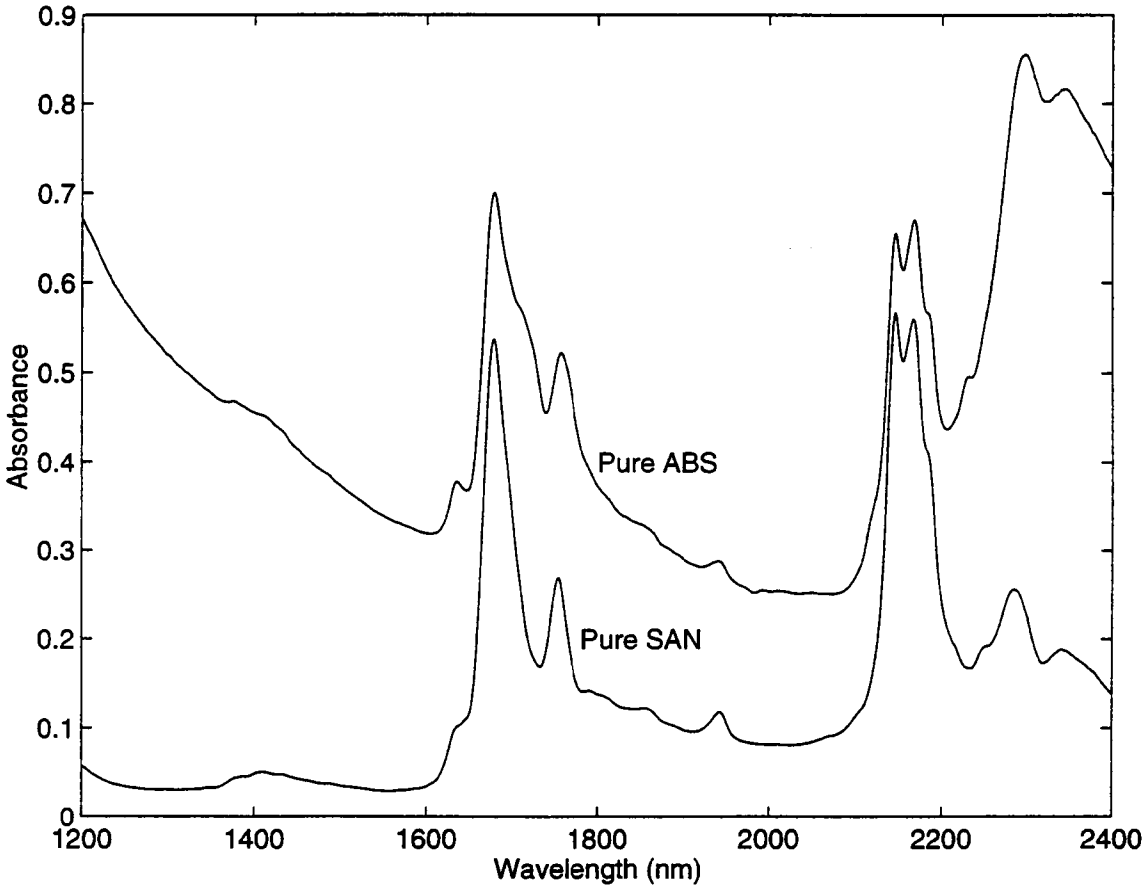


Figure 6.2 Overlaid NIR absorbance spectra (averaged raw data) of pure SAN and pure ABS in the region from 1200 nm to 2400 nm @ 250 ^{o}C.

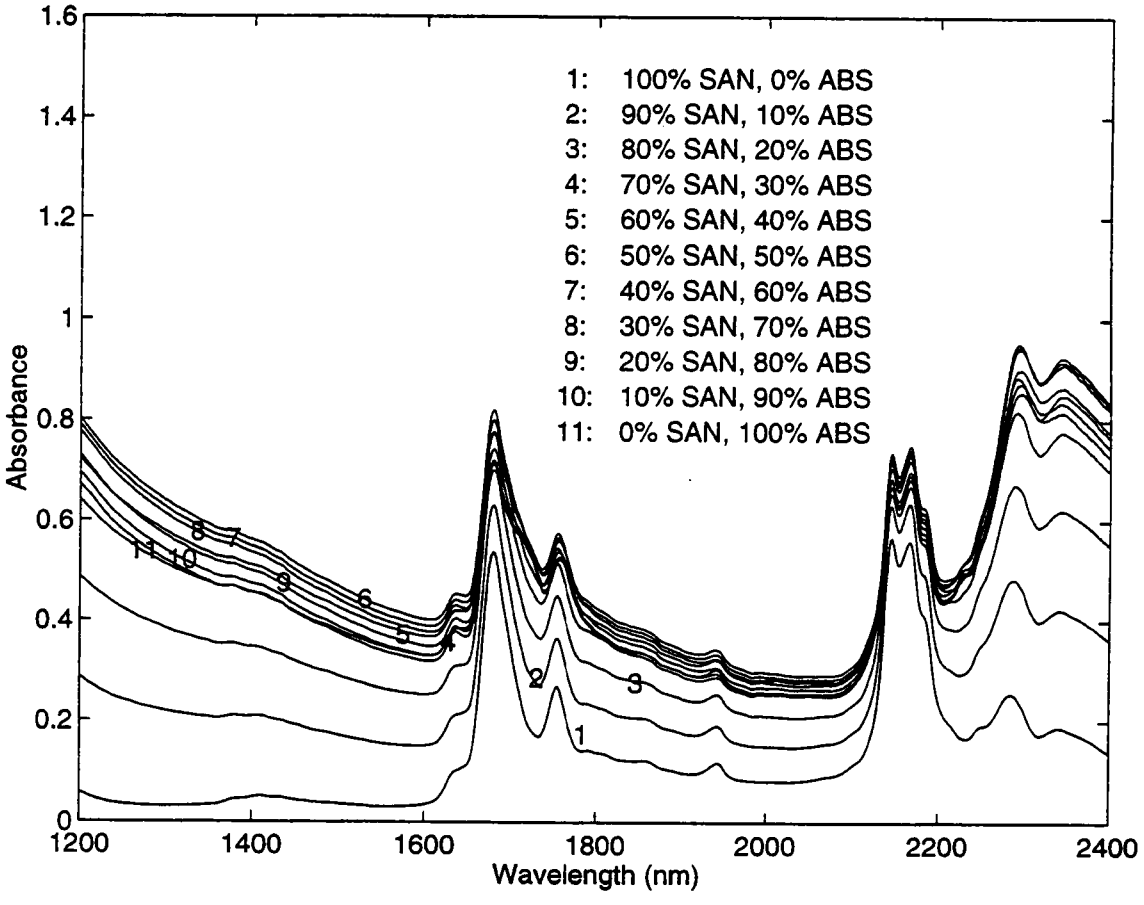


Figure 6.3 Overlaid NIR absorbance spectra (averaged raw data) for each of the ABS/SAN blend compositions in the region from 1200 nm to 2400 nm @ 250 °C.

to obtain an average absorbance spectrum for the particular blend composition. These 11 average absorbance spectra constituted the calibration set. The validation or test set consisted of the 88 spectra selected for the quantitative analysis. The absorbance data for the blends was stored as the X matrix and the corresponding compositional data was stored in the Y matrix.

The data was mean centered by subtracting the column mean from each of the elements in the columns of X and Y. The mean centered data was further normalized with respect to column standard deviation in order to have unit variance to each variable in X and Y. The mean centered and normalized data was then used for building calibration models and then validating the models using PLS, and PCR.

Scattering effects due to butadiene in ABS were observed in the spectra for the ABS/SAN blends. The plot of variance in absorbance at each wavelength for the calibration samples in figure 6.4 shows that the amount of scattering is dependent on the wavelength. The variance in absorbance is highest at 1200 nm and 2400 nm, indicating that the scattering is maximum near the left and right end of the spectra. The systematic trend in the variance in absorption in the region from 1600 nm to 1800 nm as seen in figure 6.4 is not due to scattering but due to changes in the wt. % ABS. It was also seen in figure 6.3, that scattering at the two ends of the spectra increased for samples with increasing wt. % ABS till the sample with 50 wt. % ABS, and then decreased for the remaining five samples.

Wavelengths from 1600 nm to 1800 nm in the overtone region, and 2075 nm to 2215 nm in the combination region were selected as the first and second regions for

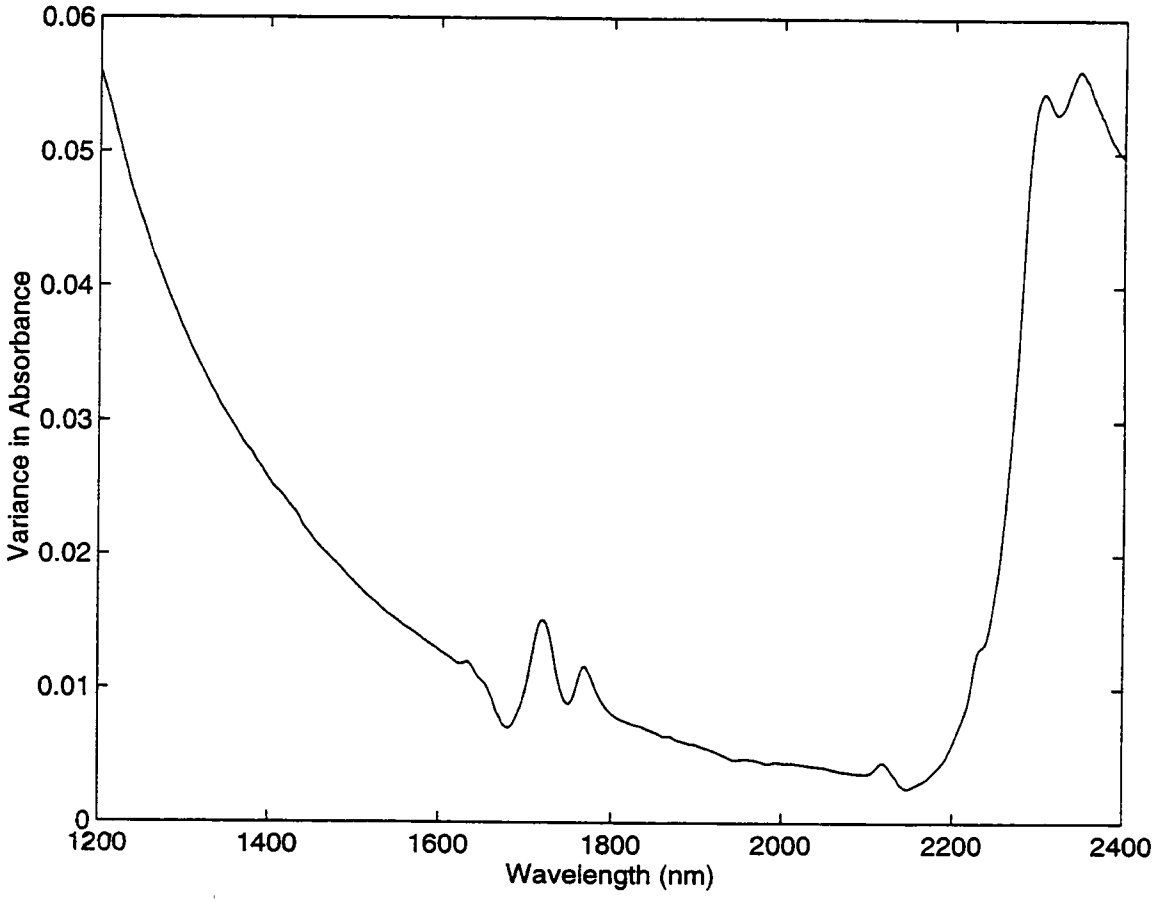


Figure 6.4 Plot of variance in absorbance vs. wavelength for the ABS/SAN blend compositions (averaged raw data) in the region from 1200 nm to 2400 nm @ 250 °C.

analysis by PLS and PCR, due to the systematic variation in the absorbances with concentration changes observed in these regions. Figures 6.5 and 6.6 shows the average, smoothed and baseline corrected spectra for each of the concentrations levels in the overtone and combination regions for the ABS/SAN blends, respectively. Regions with spectral changes due to increasing wt. % ABS in the samples are marked in figures 6.5 and 6.6.

In the analysis of the overtone region, the percent total variance in the X and Y calibration data sets, explainable by the PLS and PCR models with increasing number of factors is given in table 6.1. For the PLS model, the first factor accounts for 96.49 % of the total X-block variance, followed by 2.46 %, and 0.02 % of the total variance accounted by second and third factors, respectively. The percent variances for the 201 wavelengths from 1600 nm to 1800 nm, as explained by the first and second factor is shown in figure 6.7 (a) and figure 6.7 (b), respectively. Most of the variances of the variables were explained by the first factor although the percent variances of some variables was explained only by considering more factors.

As seen in figure 6.7, variances of certain wavelengths from 1630 nm to 1640 nm and from 1745 nm to 1755 nm were explained primarily by the second factor. Intensities at these wavelengths did not exhibit significant spectral variations with concentration changes in wt. % ABS (as seen in figure 6.5), indicating that the second factor did not account for varying ABS concentrations in the ABS/SAN blends. The overall percentage of the explained variance, considering the first two factors, and first three factors is shown in figure 6.8 (a) and figure 6.8 (b), respectively.

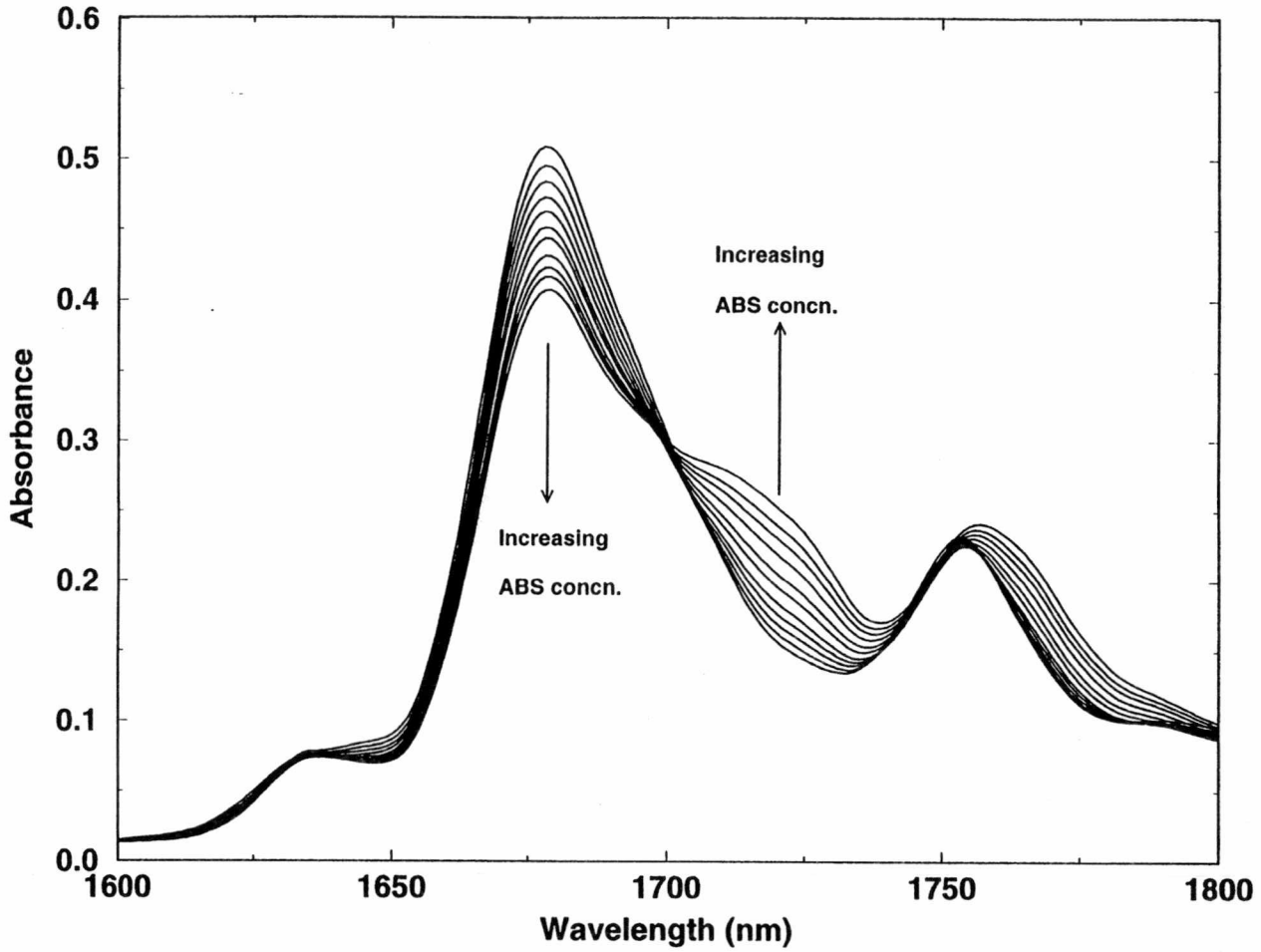


Figure 6.5 Overlaid NIR absorbance spectra (smoothed and baseline corrected data) for each of the ABS/SAN blend compositions in the overtone region from 1600 nm to 1800 nm.

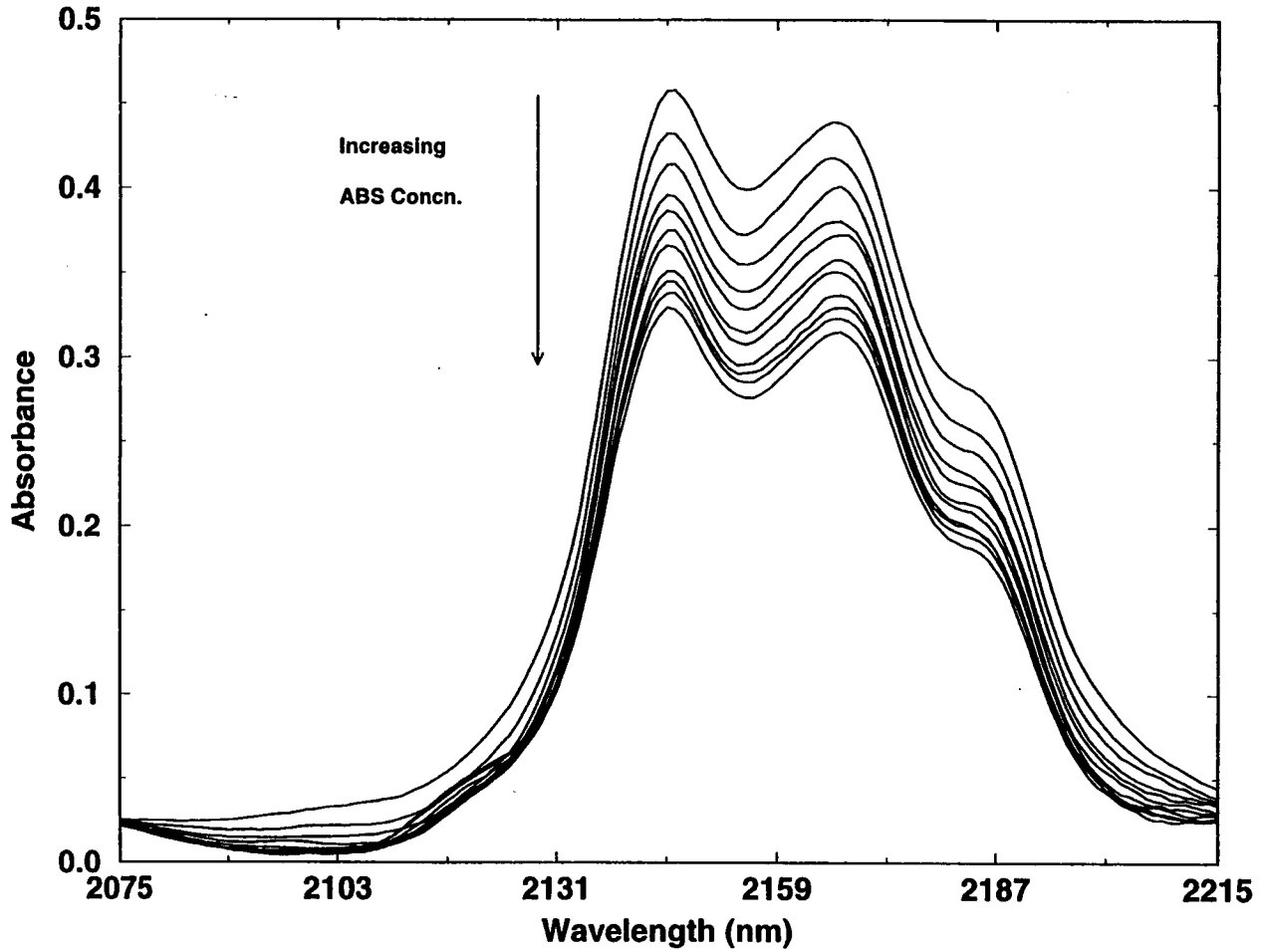


Figure 6.6 Overlaid NIR absorbance spectra (smoothed and baseline corrected data) for each of the ABS/SAN blend compositions in the combination region from 2075 nm to 2215 nm.

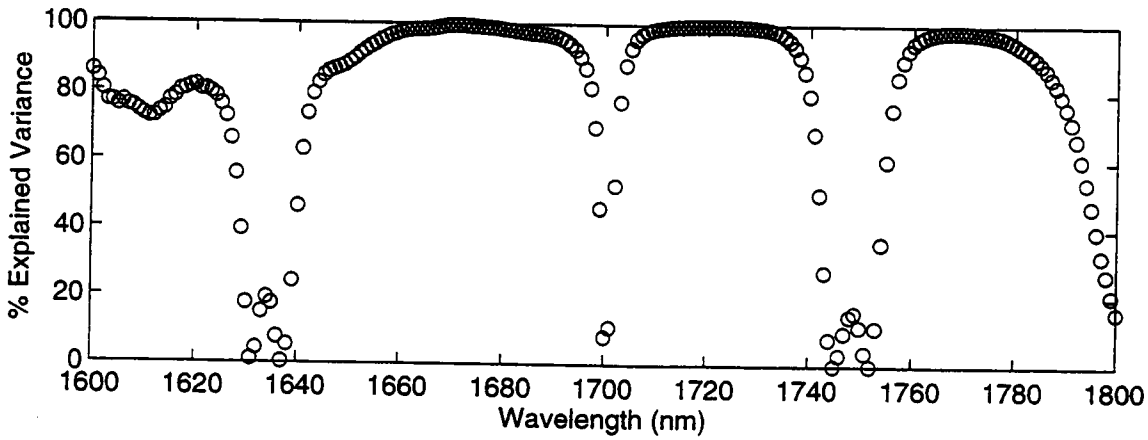
Table 6.1 Percent variances explained by the PLS and PCR models for increasing number of factors in the analysis of the overtone region (1600 nm to 1800 nm) for ABS/SAN blends.

PLS

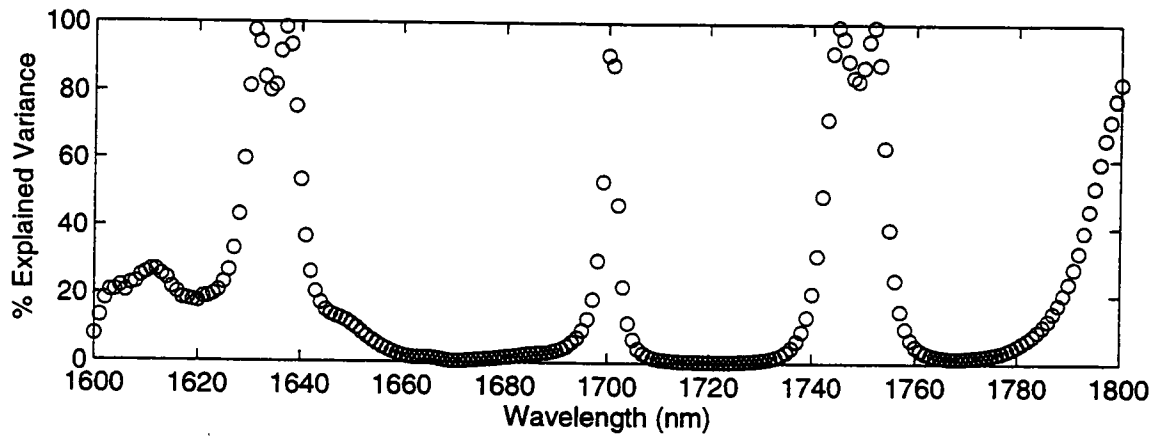
	X-Block (% variance)		Y-Block (% variance)	
Factor	By this Factor	Total	By this Factor	Total
1	97.49	97.49	99.68	99.68
2	2.46	99.96	0.23	99.91
3	0.02	99.98	0.03	99.94
4	0.00	99.99	0.02	99.96
5	0.00	99.99	0.04	100.00

PCR

	X-Block (% variance)		Y-Block (% variance)	
Factor	By this Factor	Total	By this Factor	Total
1	97.49	97.49	99.67	99.67
2	2.46	99.96	0.24	99.91
3	0.02	99.98	0.02	99.93
4	0.01	99.99	0.01	99.94
5	0.00	100.00	0.00	99.94

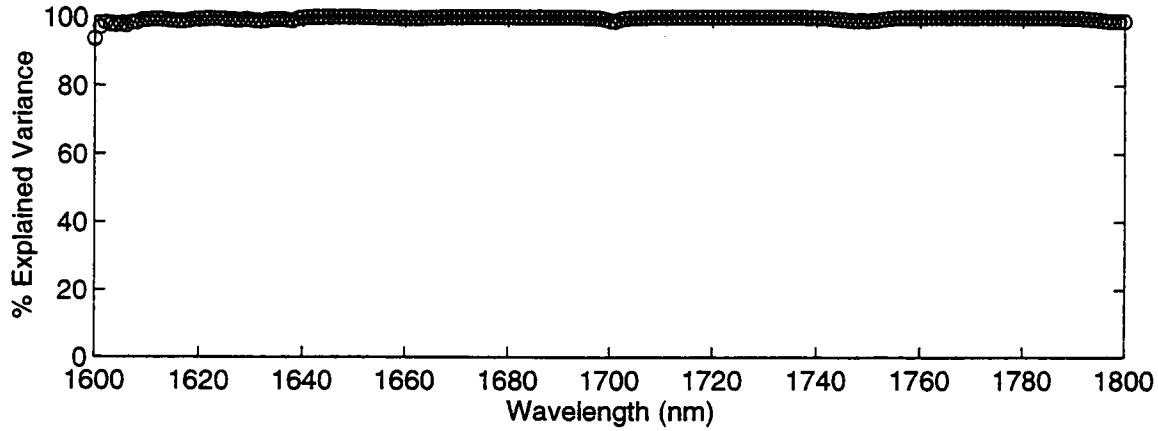


(a) Variances explained by wavelengths after first factor only

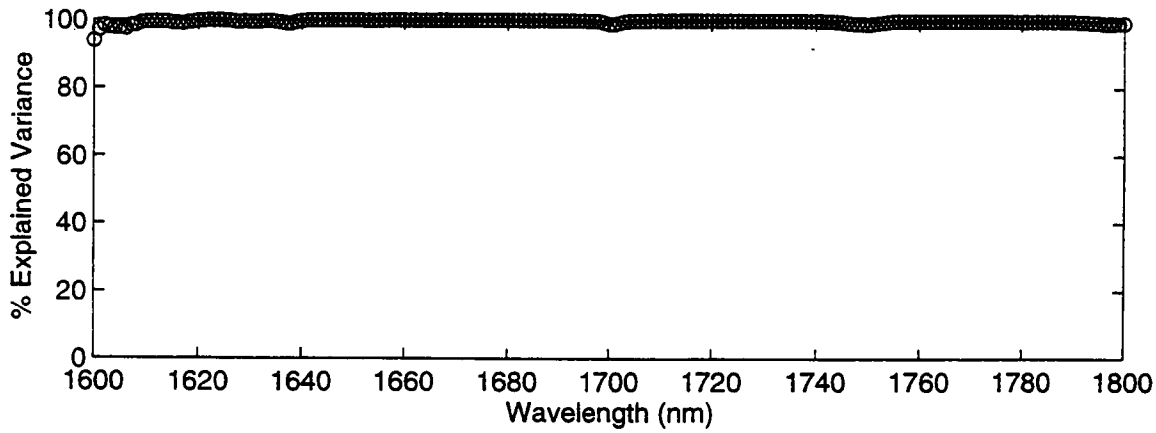


(b) Variances explained by wavelengths after second factor only

Figure 6.7 Variances explained by the wavelengths after considering, (a) First factor only, (b) Second factor only, for the ABS/SAN blends in the region from 1600 nm to 1800 nm.



(a) Variances explained by wavelengths after first and second factors



(b) Varaiances explained by wavelengths after first, second and third factors

Figure 6.8 Overall variances explained by the wavelengths after considering, (a) First two factors, (b) First three factors for the ABS/SAN blends in the region from 1600 nm to 1800 nm.

Cross-validation was used to estimate both the prediction error and the optimal number of factors to be used in the PLS and PCR models. Cross-Validation of the model was done by leave-a-sample (LAS) and leave-a-group (LAG) methods [2]. The LAS approach involved removing one spectrum from the calibration set, performing calibration and then using the model to predict the concentration of the removed spectrum. This procedure was repeated 11 times, equal to the number of spectra in the calibration set.

The LAG approach involved removing the spectra for 20, 40, 60, and 80 wt. % ABS from the calibration set, using the remaining samples to predict the concentration of the left out groups. This procedure was then reversed to predict the concentrations for the samples with 10, 30, 50, 70, and 90 wt. % ABS using the remaining blends. The spectra for pure SAN and pure ABS were included in the LAG approach, as the prediction errors for the extreme concentrations were higher compared to the intermediate concentrations for the ABS/SAN blends. Predicted Residual Sum of Squares (PRESS) values by LAS and LAG were calculated at each factor. The PRESS values for the LAS and LAG for increasing factors are plotted in figure 6.9. The average PRESS values were found to be minimum at 3 factors for both the LAS and LAG cross-validation approaches using PLS.

The model was further tested against the validation or test set to establish its accuracy and robustness. The SEP and SEC values for the test and calibration set, respectively with increasing factors are plotted in figure 6.10. SEC of 0.80 % and SEP of 1.23 % were obtained for 3 factors in the validation step using PLS. The SEP was found to be minimum at 3 factors using PLS. This observation was in agreement with the cross-

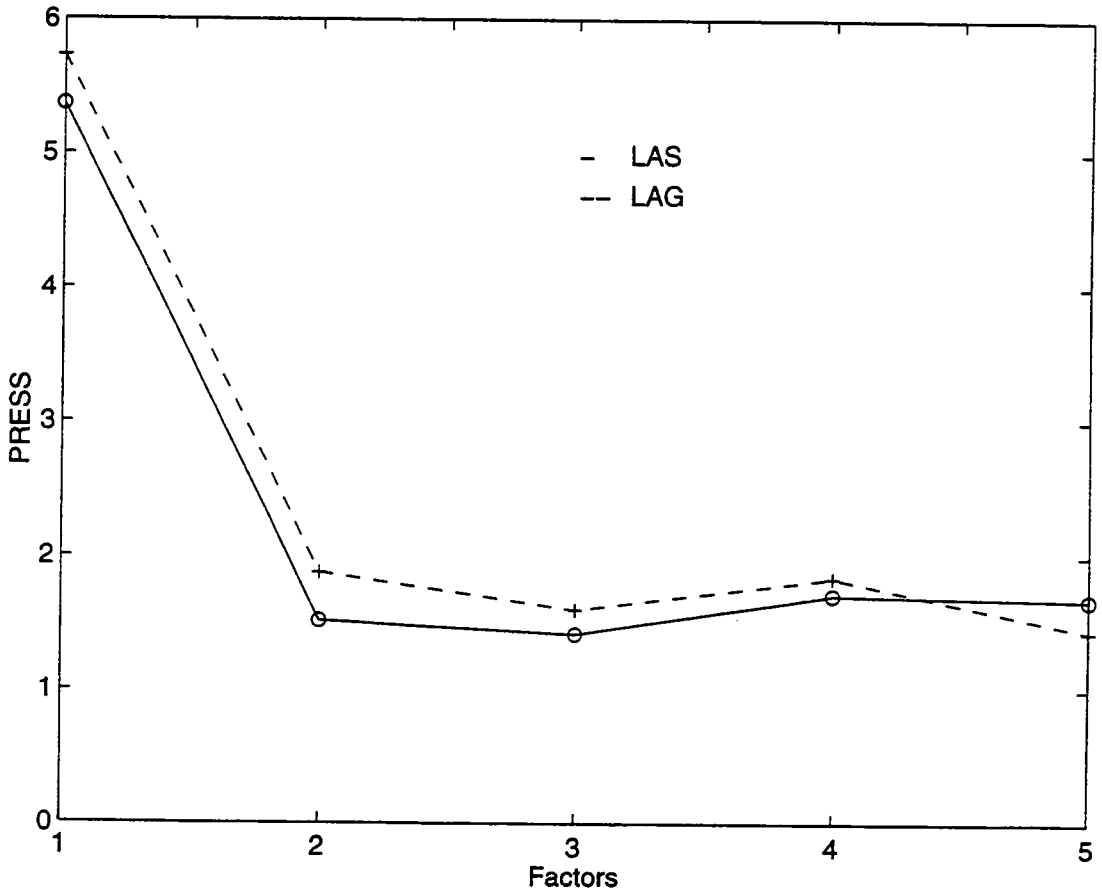


Figure 6.9 PRESS values for leave-a-sample (LAS) and leave-a-group (LAG) cross-validation methods using PLS, for the ABS/SAN blends in the overtone region from 1600 nm to 1800 nm.

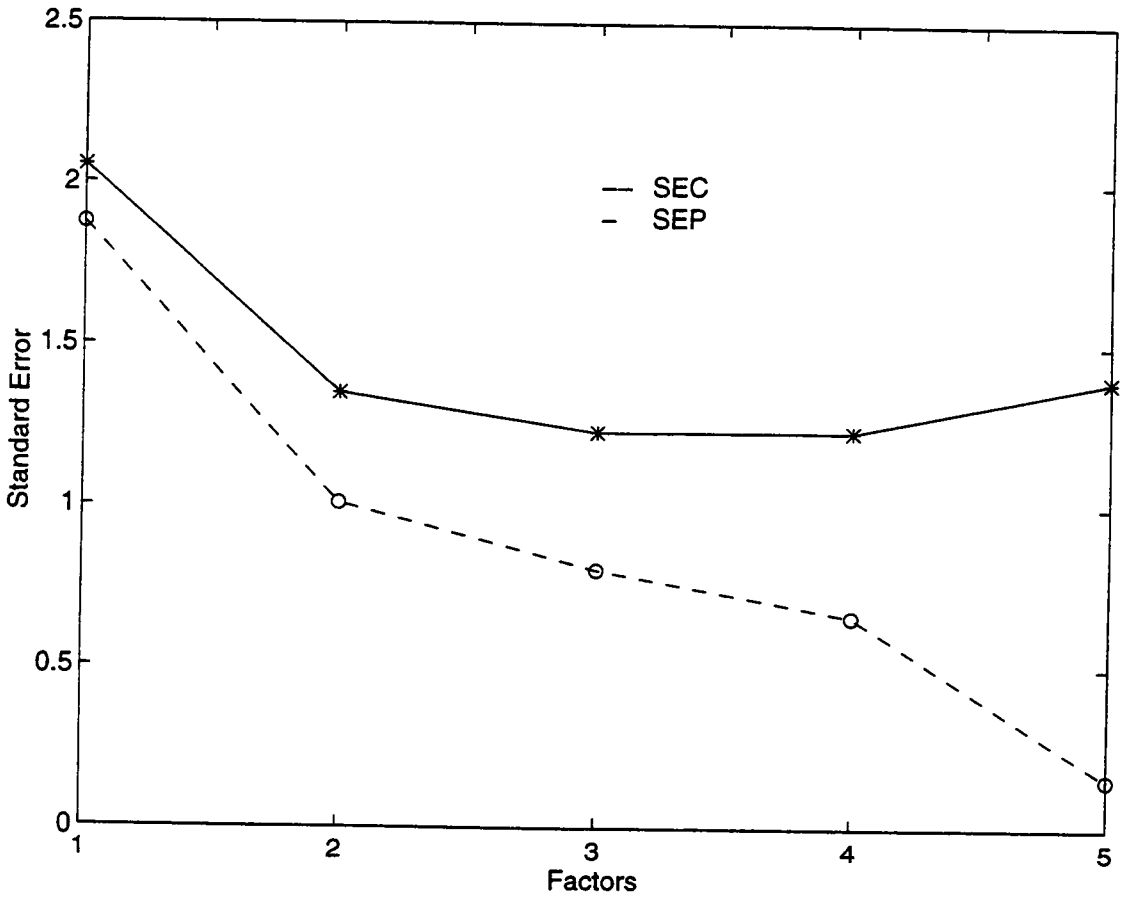


Figure 6.10 Plot of SEC and SEP for calibration and validation sets, respectively, for increasing number of factors using PLS, for the ABS/SAN blends in the overtone region from 1600 nm to 1800 nm.

validation results. It was concluded that 3 factors explain for the variation in the ABS/SAN blends.

PCR needed an addition factor for minimum prediction errors as indicated by the SEP values given in table 6.2. These results suggest that PLS needs fewer factors for the analysis than PCR, which is in agreement with the simulation results reported by Helland [36]. The model predictions for the calibration and validation set for 3 factors using PLS are plotted against the actual concentrations in figures 6.11 and figure 6.12, respectively.

The loadings, which give the relationship between the variables in the data that make up each principal component are plotted for the first, second, and third factors for the ABS/SAN blends in figure 6.13. The loadings for a factor give the contributions of the variables in making up that factor. The loadings for a factor, also help distinguish the positive and negative correlations among the variables. The first factor loadings were seen to decrease around 1680 nm, which is in agreement with the decrease in the peak around 1680 nm, with increasing wt. % ABS (as seen in figure 6.5). Positive correlations in the first factor loadings are seen at 1720 nm and 1770 nm. This trend can also be observed in the spectra of ABS/SAN blends (as seen in figure 6.5), with an increase in the absorbance values at 1720 nm and 1770 nm, with increasing wt. % ABS. Figure 6.13 also indicates that the first factor loadings represent the "mean" or average spectral variations for absorbance, with changes in wt. % ABS in the ABS/SAN blends.

The scores, which give the relationship between the spectra in the data set are plotted for the first, second and third factors in figure 6.14. Scores for the first factor show a step increase with increasing ABS concentration. Trend in second factor scores

Table 6.2 Comparison of calibration and prediction errors using PLS and PCR in the overtone and combination regions for ABS/SAN blends.

PLS

	Overtone Region (1600 nm to 1800 nm)		Combination Region (2075 nm to 2215 nm)	
Factor	SEC	SEP	SEC	SEP
1	1.87	2.05	7.96	7.67
2	1.01	1.35	1.06	1.46
3	0.80	1.23	0.84	1.37
4	0.66	1.24	0.52	1.43
5	0.15	1.39	0.24	1.68

PCR

	Overtone Region (1600 nm to 1800 nm)		Combination Region (2075 nm to 2215 nm)	
Factor	SEC	SEP	SEC	SEP
1	1.91	2.08	8.10	7.80
2	1.01	1.35	1.07	1.46
3	0.88	1.26	1.02	1.46
4	0.83	1.26	0.94	1.38
5	0.83	1.26	0.81	1.39

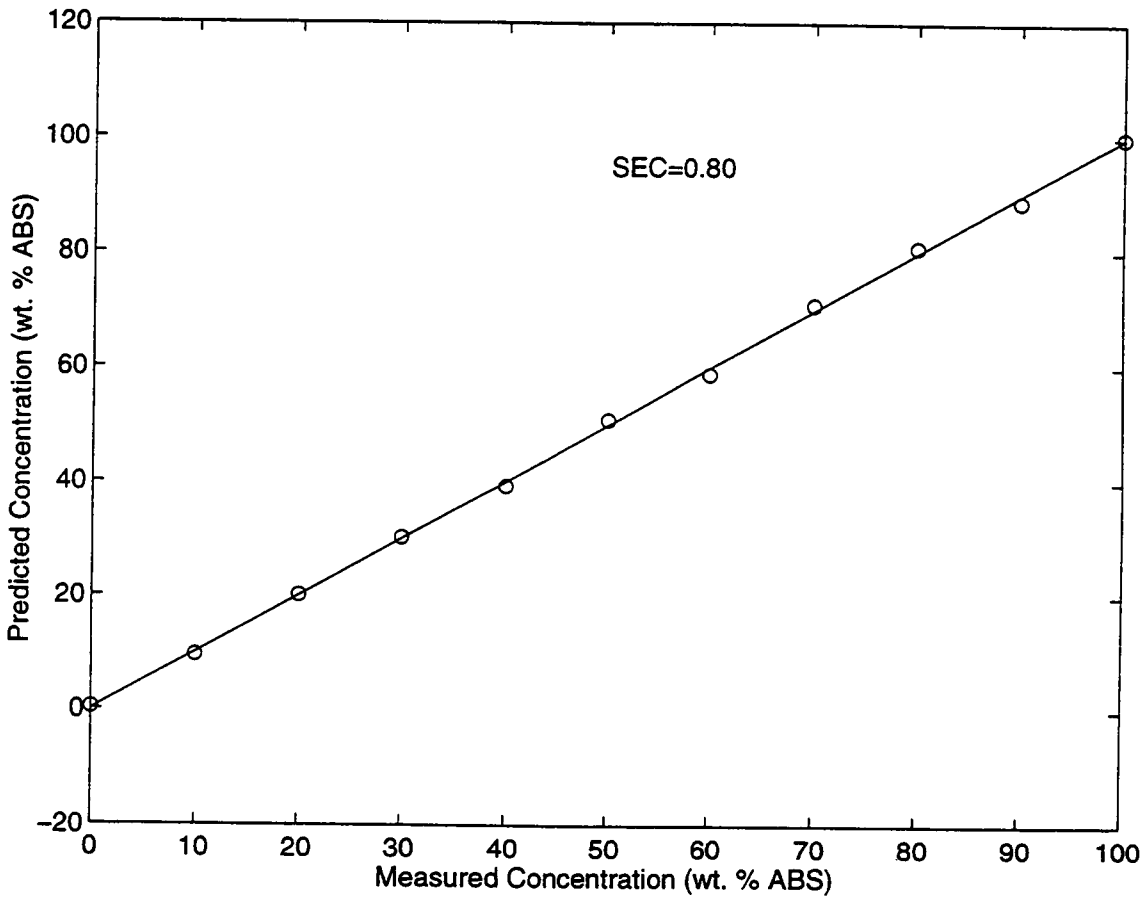


Figure 6.11 Model predictions for the calibration set (based on absorbance data) using PLS, plotted against the reference (actual) concentrations for the ABS/SAN blends in the region from 1600 nm to 1800 nm.

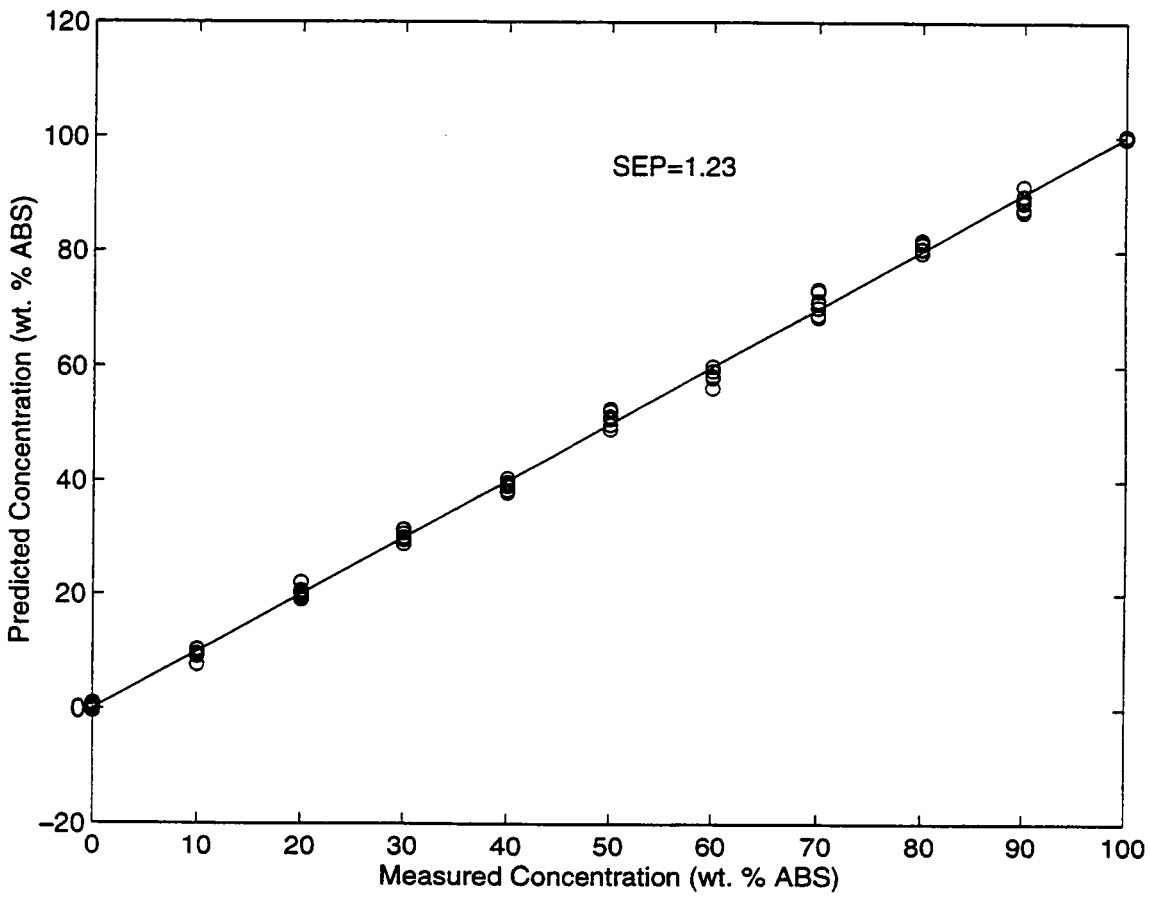


Figure 6.12 Model predictions for the validation set (based on absorbance data) using PLS, plotted against the reference (actual) concentrations for the ABS/SAN blends in the region from 1600 nm to 1800 nm.

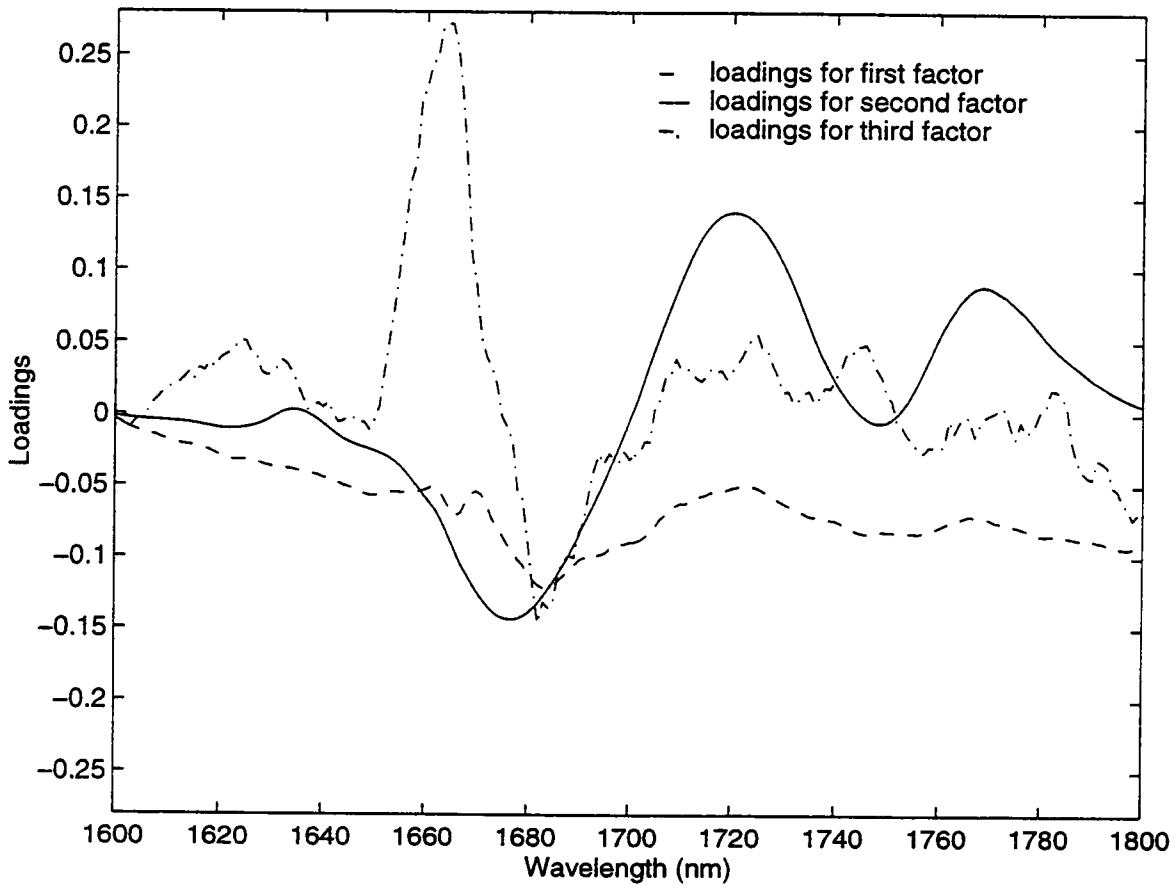


Figure 6.13 Loadings plot for first, second, and third factors for samples in the calibration set (based on absorbance data) using PLS, for ABS/SAN blends in the overtone region from 1600 nm to 1800 nm.

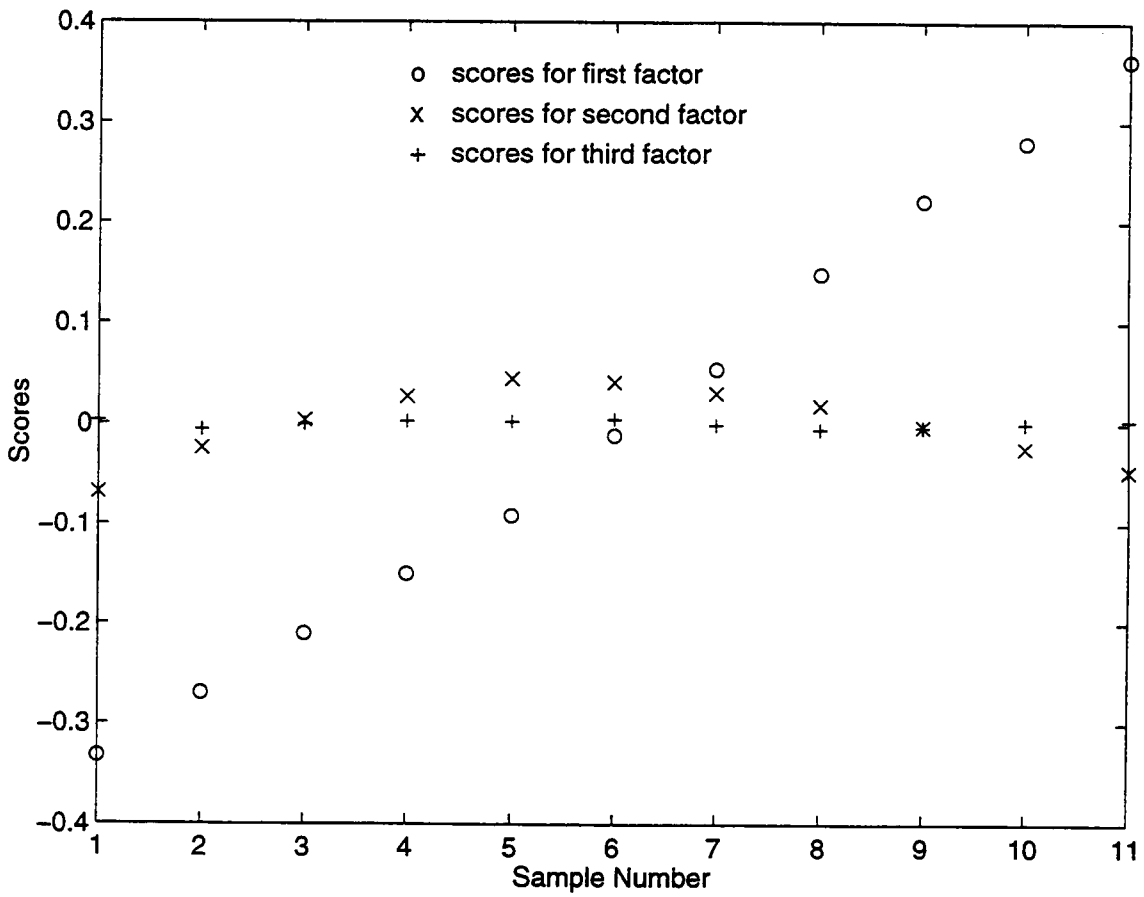


Figure 6.14 Scores plot for first, second, and third factors for samples in the calibration set (based on absorbance data) using PLS, for ABS/SAN blends in the overtone region from 1600 nm to 1800 nm.

were not as regular as the variation observed for the first factor scores. The scores for the second factor increased with increasing wt. % ABS, till the sample with 50 wt. % ABS, and then decreased for the remaining five samples. This variation in second factor scores was similar to the observed scattering trend, mentioned earlier. The third factor scores, although not as significant as the scores for the first and second factors, appeared to follow a sinusoidal trend.

It can be suggested that as there is only one factor of variation (wt. % ABS in the samples) in the ABS/SAN samples, the additional factors could be due to scattering effects, non-linearities, and sample inhomogeneities. Additional factors have to be incorporated in the models as the prediction errors are greater if only one factor is considered. The SEC and SEP values further confirm that the second and third factors cannot be disregarded in the multivariate analysis. This also suggests that the variation explained by the second and third factors for the calibration set is similar to the variation in the test set and cannot be discarded as noise, and should be incorporated in the model for low SEP values.

To demonstrate the variation in the calibration set, the scores for the first, second, and third principal component were plotted in the 3-D transformed space, as shown in figure 6.15. Spectral variation in the data set along the direction of the first factor was maximum, followed by the second and third factor, respectively. 2-D plot of scores for the first factor vs. the scores for the second factor as viewed in the direction of the third factor is given in figure 6.16. 2-D views in the direction of first and second factor are shown in figure 6.17 (a) and figure 6.17 (b), respectively.

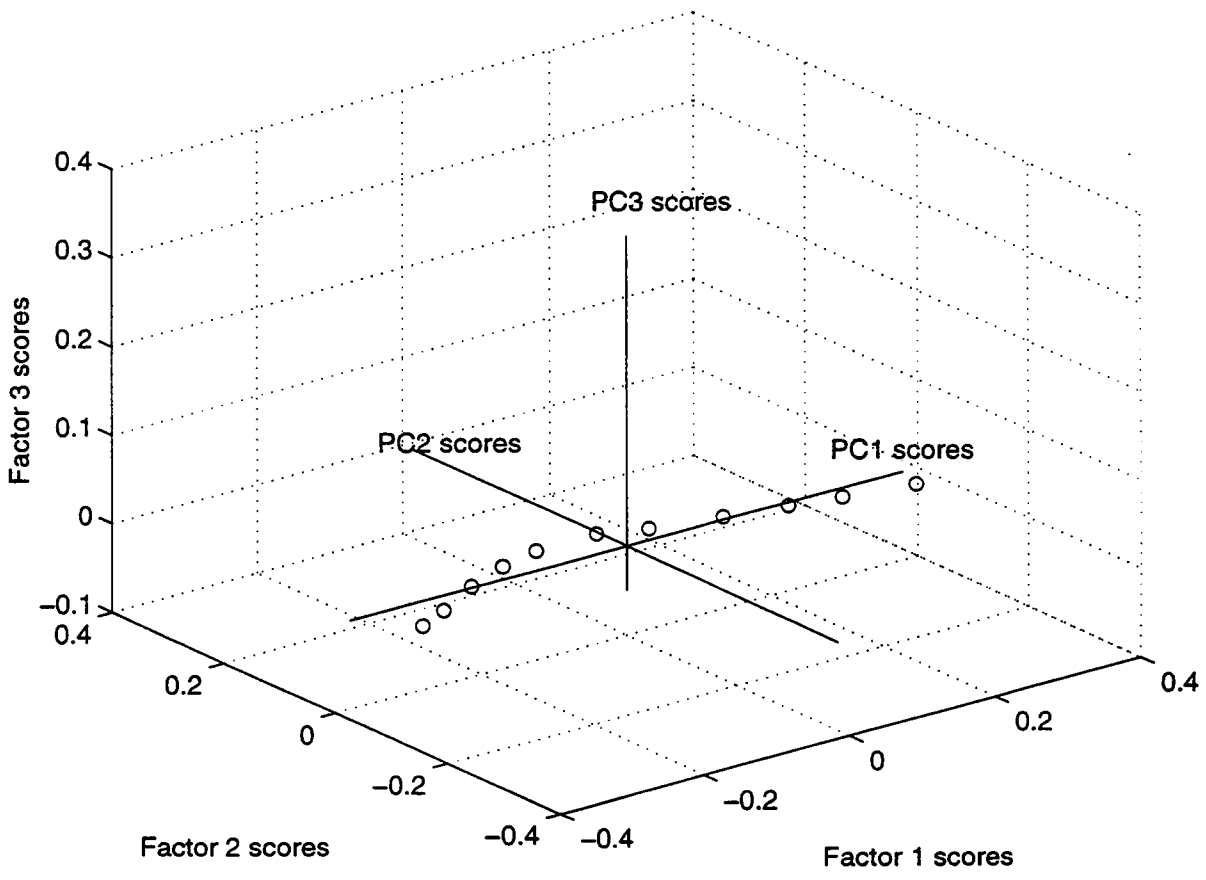


Figure 6.15 First, second, and third factor scores for samples in the calibration set for the ABS/SAN blends using PLS in the region from 1600 nm to 1800 nm.

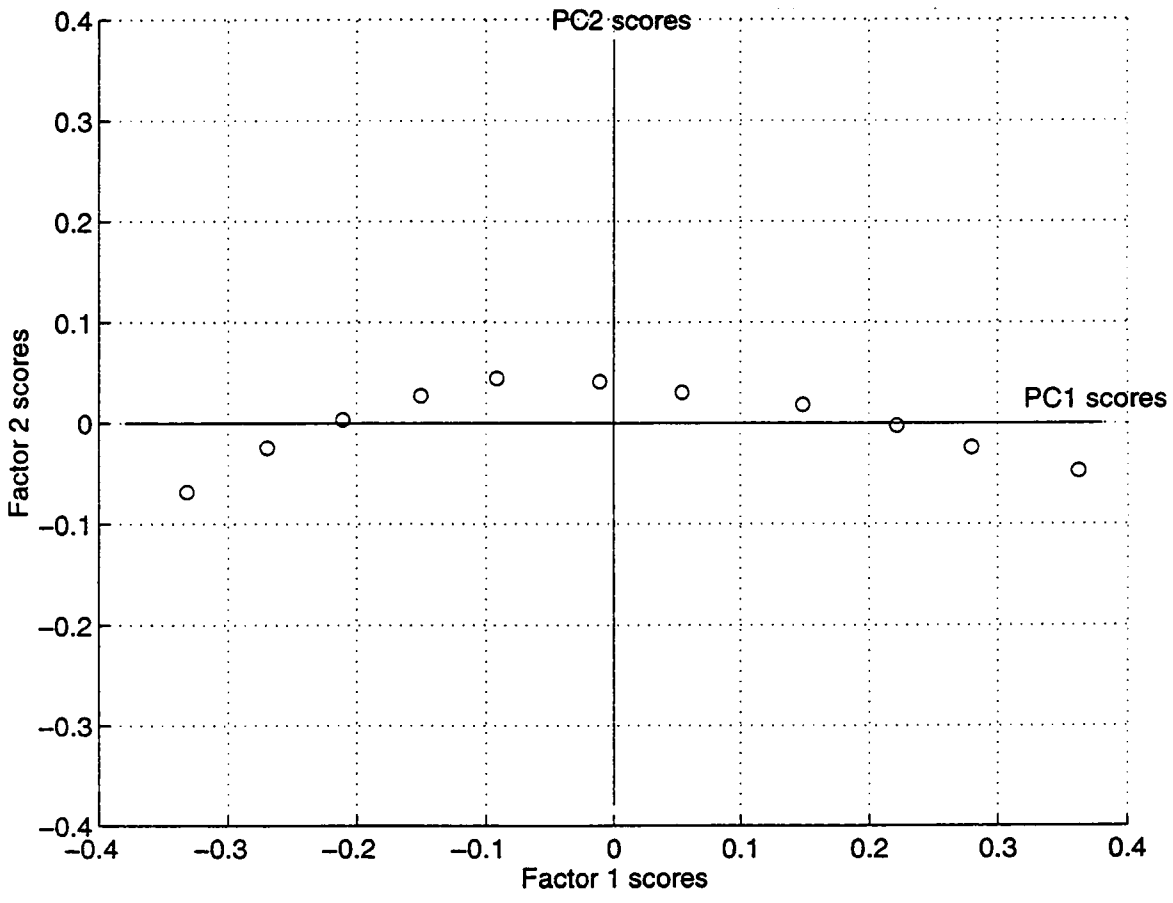
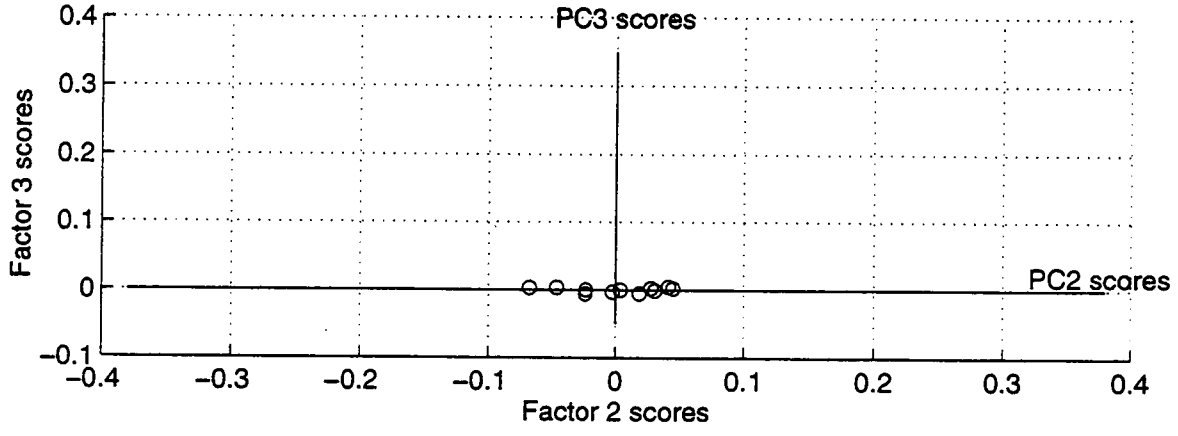
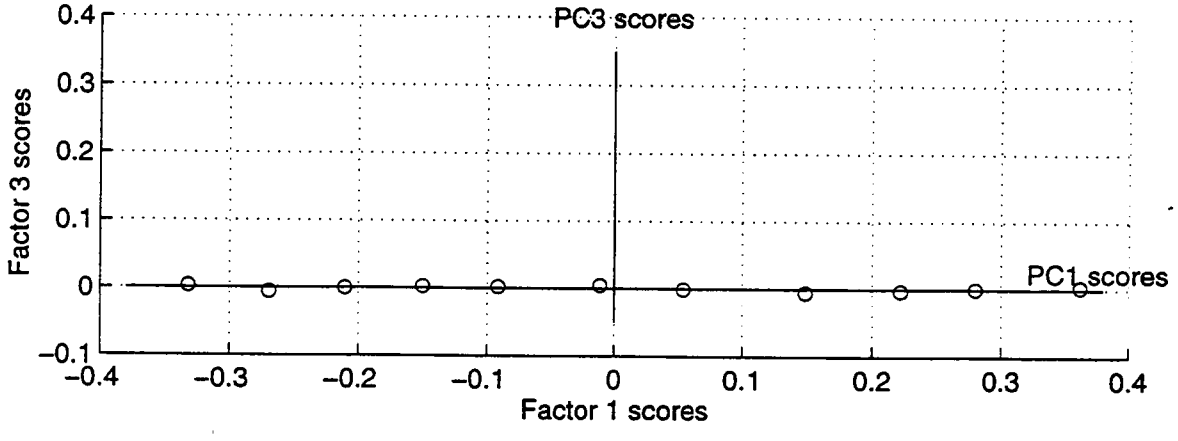


Figure 6.16 First factor vs second factor scores for samples in the calibration set, for the ABS/SAN blends using PLS in the overtone region from 1600 nm to 1800 nm.



(a) Scores for factors, 2 and 3.



(b) Scores for factors, 1 and 3.

Figure 6.17 (a) projection of scores on second and third factors, (b) projection of scores on first and third factors, for the ABS/SAN blends using PLS in the region from 1600 nm to 1800 nm.

Figures 6.15-6.17, provide a better understanding of the spatial distribution of scores in the principal component space. The plot for first factor scores vs. second factor scores using PCR for samples in the calibration set, in the overtone region from 1600 nm to 1800 nm is given in figure 6.18. Comparison of figure 6.16 and figure 6.18 indicates that the scores are nearly identical for the PLS and PCR approaches.

A similar analysis was performed in the combination region from 2075 nm to 2215 nm. This region also gave 3 factors of variation using PLS as a result of cross-validation and validation by the test set. An additional factor was also needed in the combination region, for minimum prediction errors by PCR. The comparison of the SEC and SEP values from the two regions by PLS and PCR is presented in table 6.2.

A full spectrum analysis of the spectral data in the range from 1200 nm to 2400 nm was also performed. As the scattering and sample inhomogeneity effects were more prevalent in the entire range of wavelengths from 1200 nm to 2400 nm, additional factors were required to describe the variations in the spectral data. Table 6.3 gives the explained variance for the full spectrum analysis using PLS and PCR. The increase in the optimal number of factors compared to the overtone and combination regions, indicates that choosing the entire spectrum for composition predictions is not the best choice for analysis as we know that there is only one independent factor of variation (wt. % ABS) in the ABS/SAN blends.

The scores plot for the full spectral analysis (1200 nm to 2400 nm), for the samples in the calibration set is given in figure 6.19. The scores plot clearly shows that the trend for increasing first factor scores with increasing wt. % ABS, as observed in

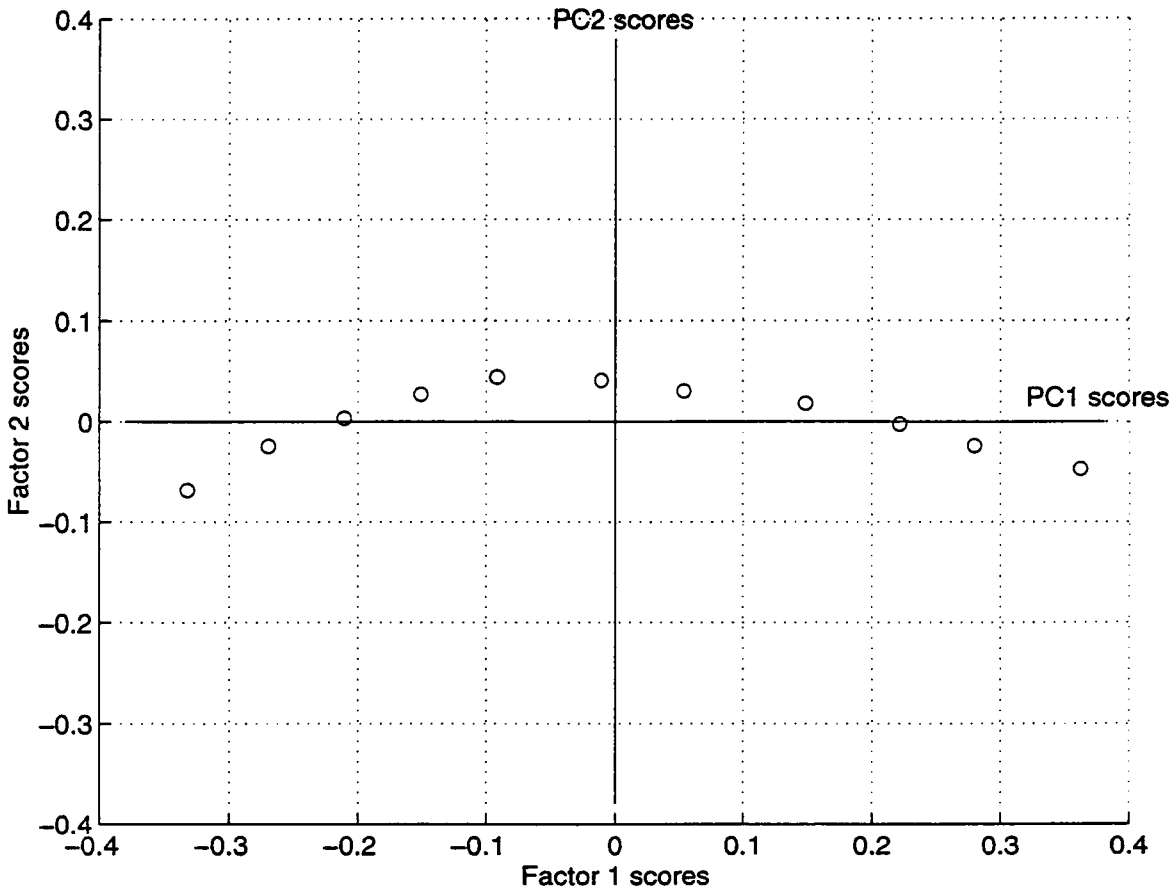


Figure 6.18 First factor vs second factor scores for samples in the calibration set, for the ABS/SAN blends using PCR in the region from 1600 nm to 1800 nm.

Table 6.3 Percent variances explained by the PLS and PCR models for increasing number of factors in the full spectrum analysis (1200 nm to 2400 nm) for ABS/SAN blends.

PLS

	X-Block (% variance)		Y-Block (% variance)	
Factor	By this Factor	Total	By this Factor	Total
1	98.86	98.86	58.75	58.75
2	1.05	99.91	40.51	99.26
3	0.08	99.99	0.57	99.83
4	0.01	100.00	0.12	99.95
5	0.00	100.00	0.05	100.00

PCR

	X-Block (% variance)		Y-Block (% variance)	
Factor	By this Factor	Total	By this Factor	Total
1	98.87	98.87	57.87	57.87
2	1.05	99.91	41.29	99.17
3	0.08	99.99	0.63	99.80
4	0.01	100.00	0.14	99.94
5	0.00	100.00	0.00	99.94

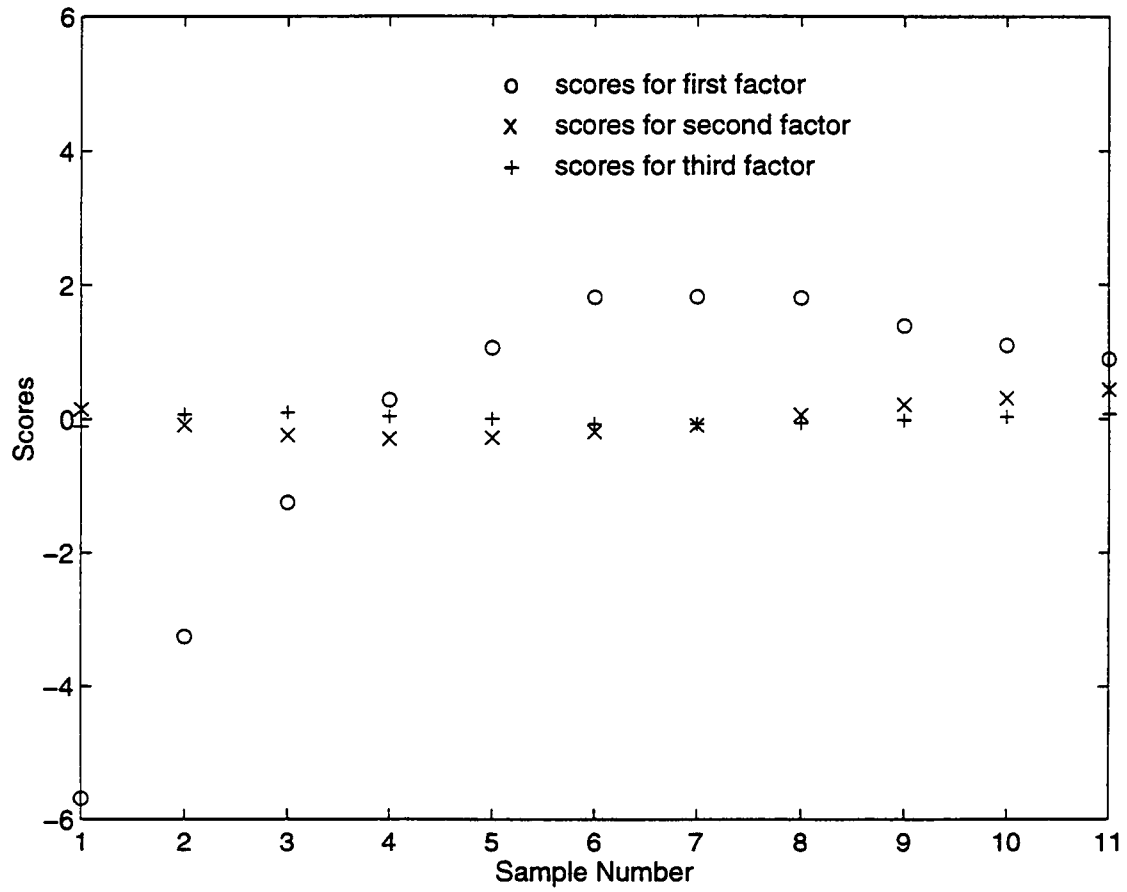


Figure 6.19 Scores plot for first, second, and third factors for full spectral analysis (based on absorbance data) using PLS in the region from 1200 nm to 2400 nm for samples in the calibration set, for ABS/SAN blends.

figure 6.14 is absent, and therefore taking the entire spectral region is not suitable for composition predictions. Although the first factor scores are much larger compared to the second and third factor scores; scattering effects, nonlinearities, and sample inhomogeneities also contribute in making up the first factor. The above discussion shows that the full spectral analysis is not the right choice for composition predictions of unknown samples. Comparison of the SEC and SEP values for the full spectrum analysis by PLS and PCR is given in table 6.4.

Conclusions

It was demonstrated that in-line monitoring of molten polymers coupled with chemometric data analysis techniques can be successfully used for predicting compositions in ABS/SAN blends. Two regions that showed significant changes in absorption characteristics were selected for the analysis by PLS and PCR. Results from both regions indicated that there were three factors of variation in the NIR spectra for the ABS/SAN samples even though there is only one independent known source of variation (wt. % ABS) in the blends. Three factors were used in the development of the calibration models based on the SEC and SEP of 0.80 and 1.23 , respectively, using the PLS approach in the overtone region from 1600 nm to 1800 nm.

As mentioned in an chapter 3, deleting some of the latter factors that account for little variance and which contain mostly noise, does not significantly reduce the amount of useful information in the data. Minimum SEP values obtained by PCR were slightly higher than the minimum SEP values obtained using PLS. A full spectrum analysis was

Table 6.4 Comparison of calibration and prediction errors using PLS and PCR in the region from 1200 nm to 2400 nm for ABS/SAN blends.

	PLS		PCR	
Factor	SEC	SEP	SEC	SEP
1	21.30	20.34	21.53	20.55
2	2.85	3.44	3.03	3.61
3	1.39	1.97	1.48	2.15
4	0.78	1.50	0.83	1.54
5	0.28	1.05	0.82	1.36
6	0.18	1.10	0.80	1.30
7	0.07	1.10	0.79	1.33

also performed, but higher SEP values and more factors, compared to the overtone and combination regions were recorded.

Comparison of scattering in ABS/SAN blends due to rubber particles and in PET resins due to the presence of TiO_2

Hansen, Batra *et al* (1994) studied baseline shifts by monitoring the concentration of titanium dioxide (TiO_2), a white inorganic filler, in molten poly(ethylene terepthalate) (PET). Two commercial PET resins, one with no TiO_2 and another with the desired commercial content of TiO_2 were chosen for the analysis. The concentration of TiO_2 was normalized from 0% to 100% in increments of 10%, by taking weighed quantities of the two resins. The 0% concentration was represented by the resin containing no TiO_2, and the 100% concentration was represented by the TiO_2 filled commercial resin. The dry blended samples of the two PET resins, spanning the TiO_2 concentration from 0% to 100% were vacuum dried for 24 hours at 80 ^oC before processing [26].

The data from the experiments was further analyzed to differentiate between the scattering due to TiO_2, a white inorganic filler, and due to the butadiene in the ABS/SAN blends. NIR absorbance spectra for 85 samples, in the range of 10% to 90% (in 10% increments) normalized TiO_2 concentration was available. The spectra for a particular TiO_2 concentration were averaged to obtain an average spectrum for a given composition. In all 9 average spectra which spanned the range of 10% to 90% normalized TiO_2 concentrations constituted the calibration set. Figure 6.20 shows the overlaid average spectrum for the concentrations from 10% to 90% normalized TiO_2 concentrations.

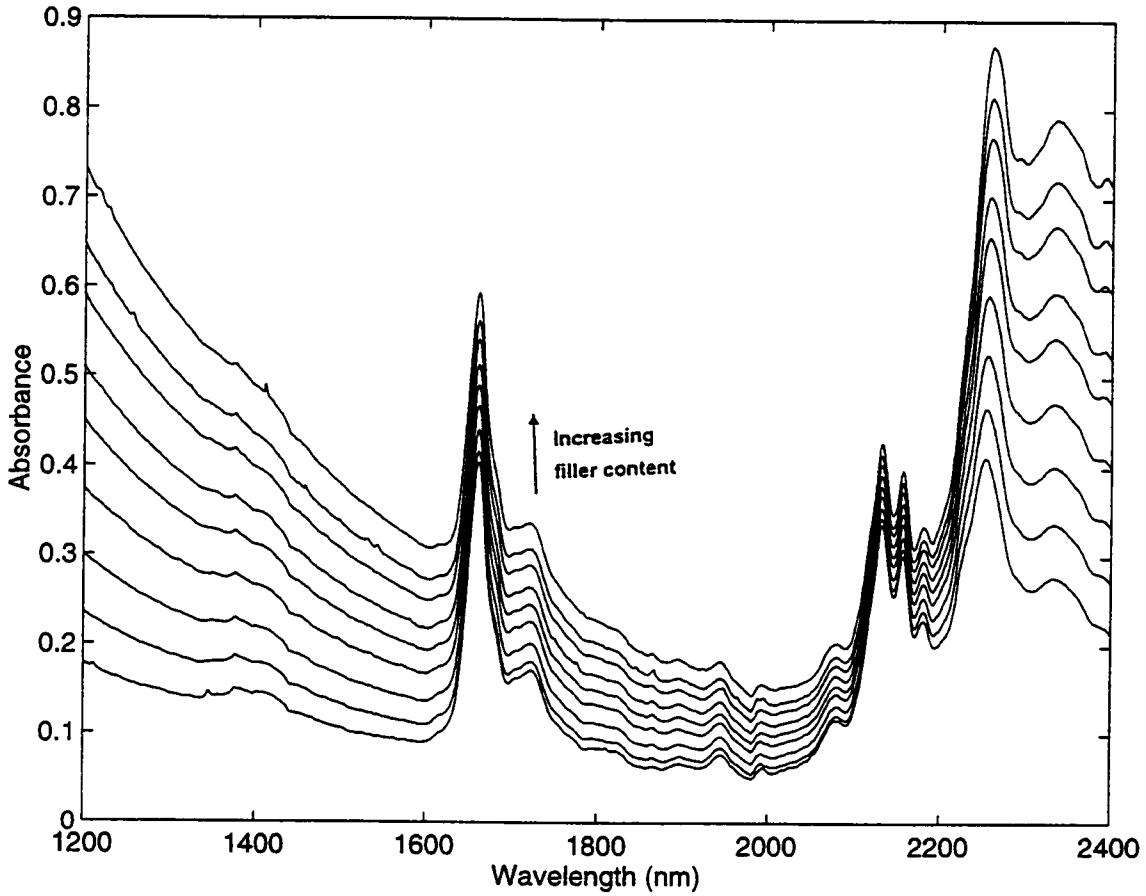


Figure 6.20 Overlaid NIR absorbance spectra (average data) of PET with varying TiO_2 content in the region from 1200 nm to 2400 nm.

The loadings and scores plot are shown in figures 6.21 and 6.22, respectively. The first factor loadings indicate that scattering due to the inorganic filler, caused the baseline shifts. The scores plot shows that the compositional information is present in the first factor scores, although the first factor primarily accounts for scattering effects. This is very different than the scattering observed in the ABS/SAN resins. Figure 6.19 shows that the first factor scores for the ABS/SAN blends do not increase linearly for samples with increasing wt. % ABS. This observation suggests that the first factor may be accounting for more than just composition changes, and hence scattering due to the rubber present in ABS. The spectral changes in the overtone and combination regions were modeled for compositional predictions. Such analysis is not feasible in molten PET filled with TiO_2 as there are baseline shifts with increasing filler content, but no absorption changes in the overtone and combination regions, therefore the entire spectral region from 1200 nm to 2400 nm is considered in the analysis.

Figure 6.23 shows the difference in absorbance for the ABS/SAN blends from 10 to 90 % compared to the absorbance of an ideal blend, based on the absorbances of pure ABS and pure SAN in the region from 1200 nm to 2400 nm. E.g. the difference spectra for a blend containing X % ABS and (100-X) % SAN can be given by:

$$\text{Diff. in Abs. (X \% ABS)} = \text{Abs. (X \% ABS)} - \text{Ideal Abs. (X \% ABS)} \quad (6.1)$$

where:

$$\text{Ideal Abs. (X\% ABS)} = [\text{X\%} \times (\text{Abs. pure ABS}) + (100-\text{X})\% \times (\text{Abs. pure SAN})] \quad (6.2)$$

It can be seen in figure 6.23 that the spectra corresponding to 50 wt. % ABS shows maximum scattering in the regions near 1200 nm and 2400 nm. There is a decrease

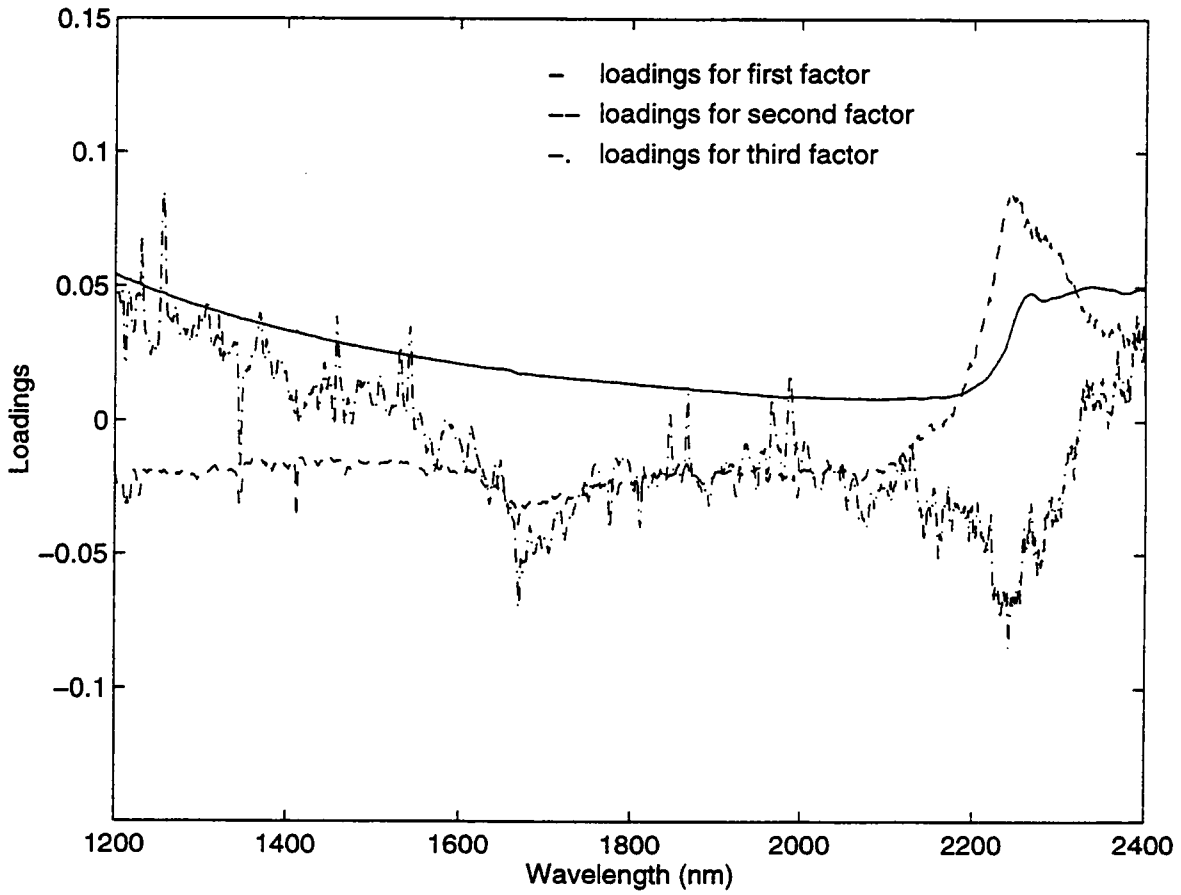


Figure 6.21 Loadings plot for first, second, and third factors for samples in the calibration set (based on absorbance data) using PLS in the region from 1200 nm to 2400 nm, for PET with varying TiO_2 content.

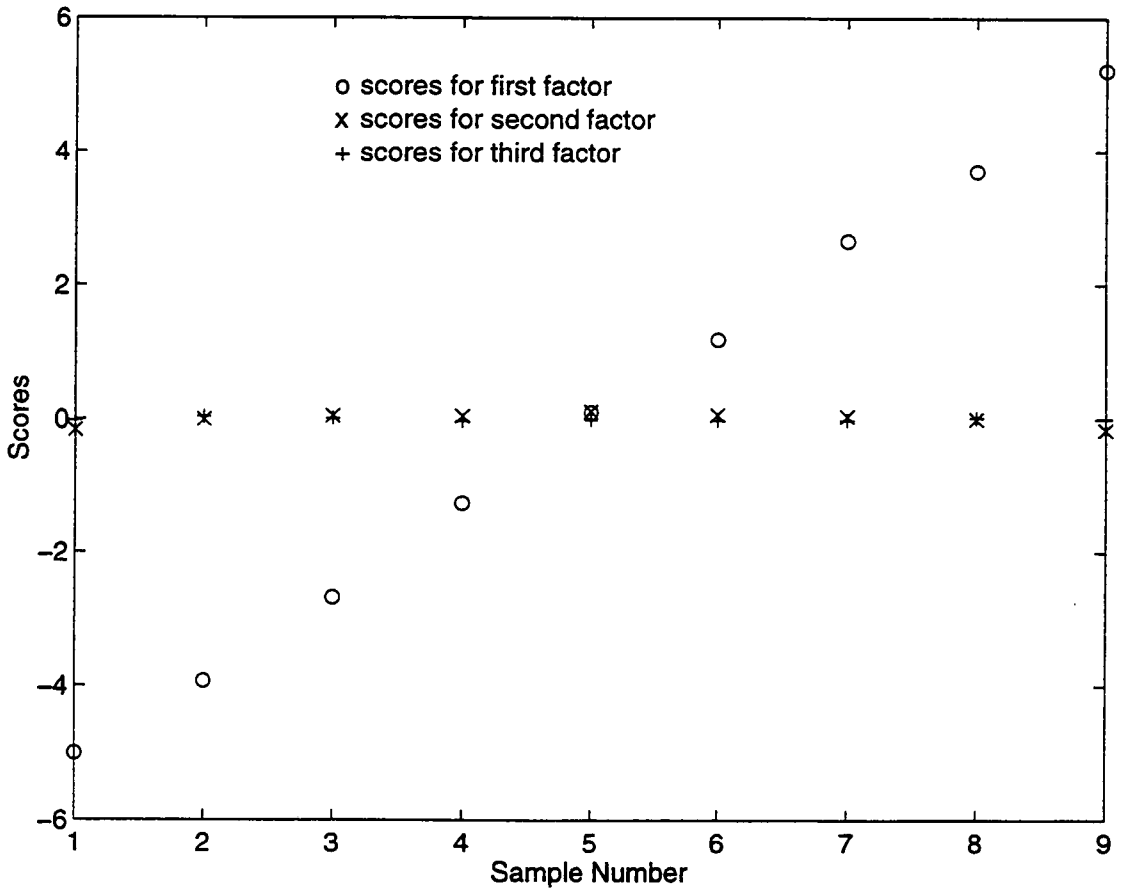


Figure 6.22 Scores plot for first, second, and third factors for samples in the calibration set (based on absorbance data) using PLS in the region from 1200 nm to 2400 nm, for PET with varying TiO_2 content.

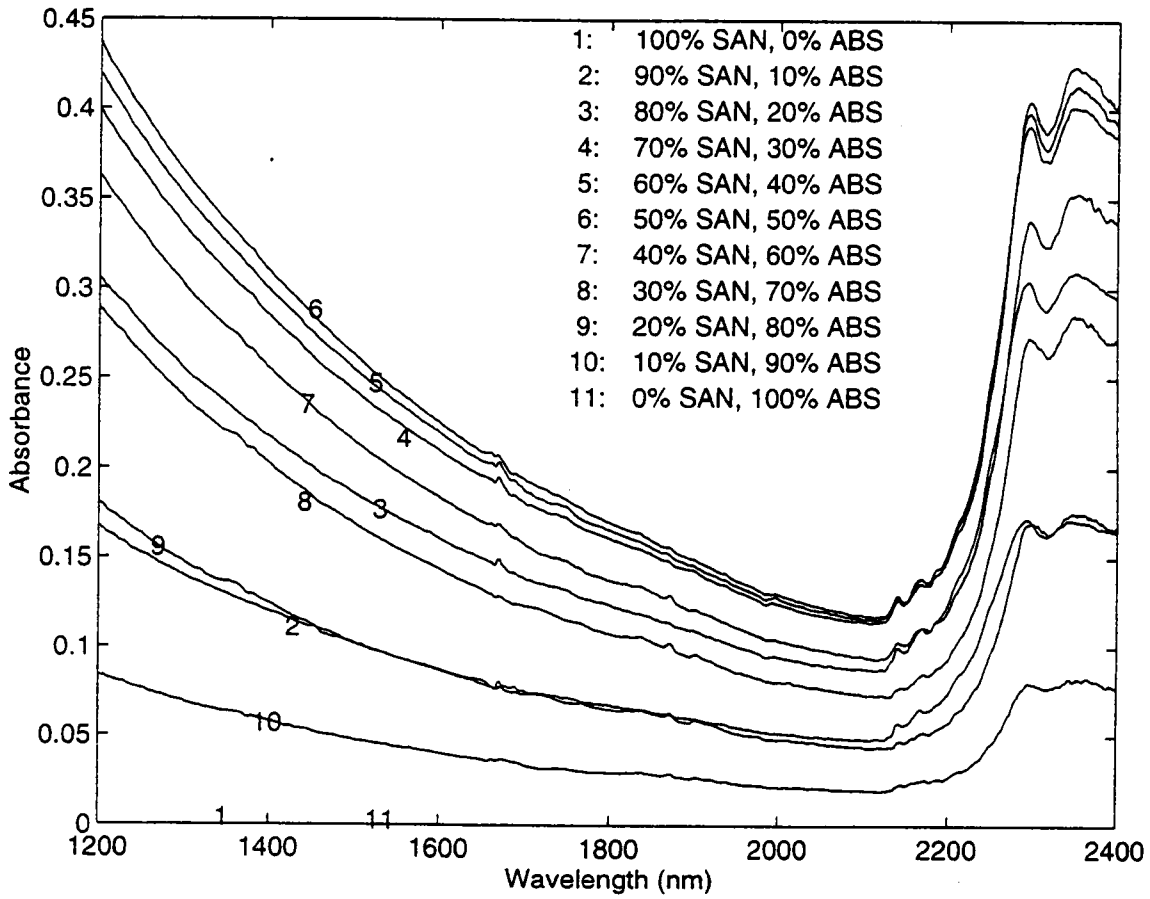


Figure 6.23 Difference in absorbance for the ABS/SAN blends compared to the absorbance of an ideal blend of the same composition (based on the absorbances of pure SAN and pure ABS), in the region from 1200 nm to 2400 nm.

in the scattering, with further increase in wt. % ABS in the ABS/SAN blends. This can also be seen in figure 6.3.

In contrast, figure 6.24 which shows the mean-centered and normalized spectra for PET with increasing TiO_2 in the region from 1200 nm to 2400 nm, suggests that scattering increases linearly with increasing filler content. Therefore it can be concluded that the scattering patterns in ABS/SAN blends with increasing wt. % ABS and in PET with increasing TiO_2 content are different, and factors such as partial miscibility and inhomogeneity effects account for the observed scattering trend in ABS/SAN blends.

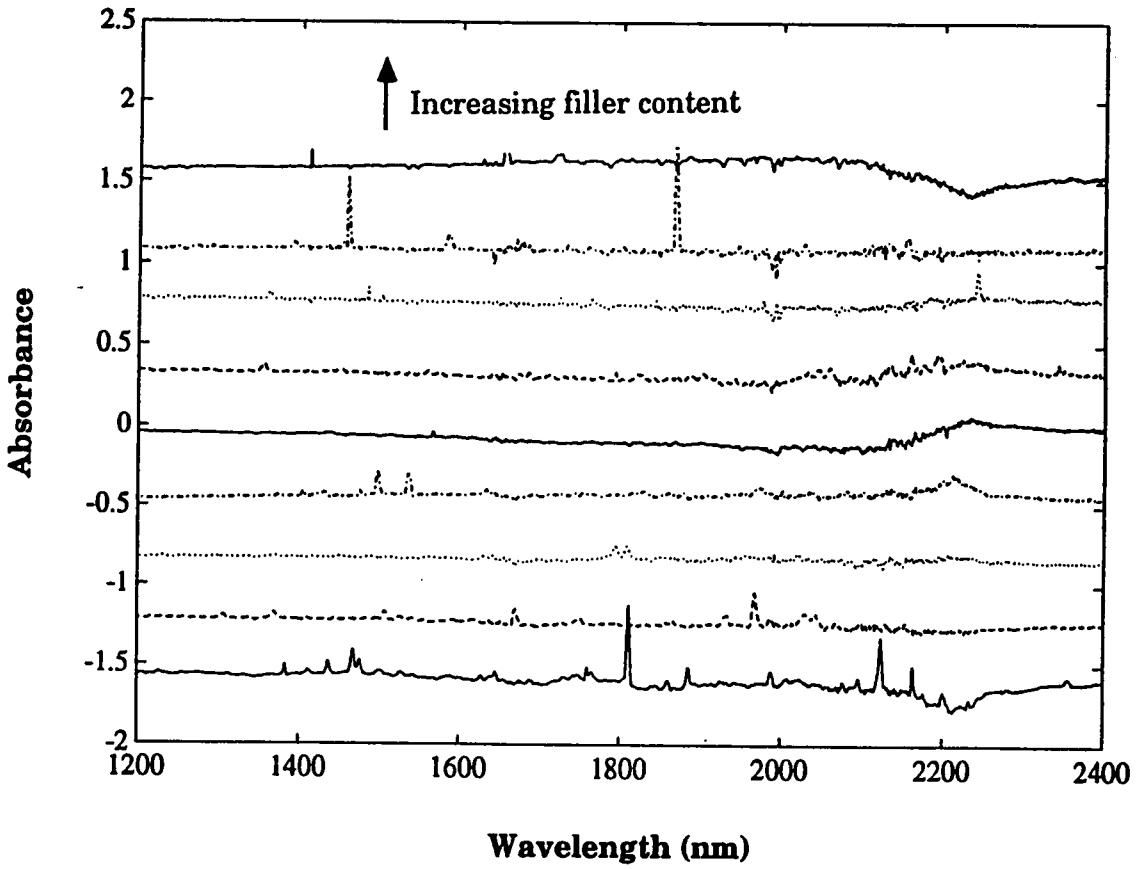


Figure 6.24 Mean-centered and normalized spectra for PET with varying TiO_2 content in the region from 1200 nm to 2400 nm [26].

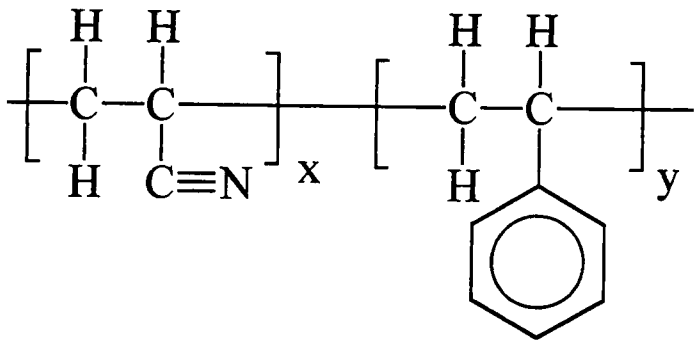
7. IN-LINE MONITORING OF STYRENE-ACRYLONITRILE (SAN)/POLYCARBONATE (PC) BLENDS

Introduction

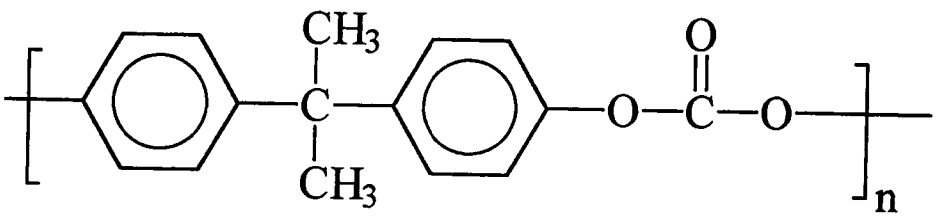
Styrene-acrylonitile (SAN) copolymers are transparent plastics with high heat resistance, excellent gloss and chemical resistance properties. SAN is also characterized by good hardness, rigidity and dimensional stability. Polycarbonate (PC) is classified as an amorphous engineering thermoplastic due to its excellent balance of toughness, clarity, and high-heat deflection temperatures [92]. SAN has a Tg of 115 ^{o}C and PC has a Tg of 150 ^{o}C. The structures for SAN and PC are shown in figure 7.1.

SAN contains the styrene monomer which provides rigidity and processability, and the acrylonitrile monomer which gives heat stability and chemical resistance to the polymer. The carbonate component in the structure of PC, makes it one of the toughest plastics, while the bisphenol component provides the high-heat properties. Blends of SAN/PC have excellent heat resistance, processability and low-temperature impact resistant properties. The blends of SAN/PC are partially miscible. Applications of these copolymers varies from appliances and business machines to specialty commodities like compact discs etc.

SAN/PC blend phase behavior was studied by Paul *et al* (1984) [93]. The miscibility was found to be a function of the acrylonitrile content in SAN, and was explained qualitatively by a binary interaction model. They concluded that ABS with optimum AN content (25-27 wt. % AN) would result in good ABS/PC blends.



Styrene-acrylonitrile (SAN)



Polycarbonate (PC)

Figure 7.1 Chemical structures of styrene-acrylonitrile (SAN) and bisphenol-A polycarbonate (PC). x, y, and n represent the number of repeat units in the two polymers.

Paul and Kim (1992) demonstrated that the SAN/PC blend phase separation temperature decreased as the PC content increased, when the acrylonitrile (AN) levels were kept constant [94]. Trends indicated that addition of AN to the styrene, increases phase separation temperatures ultimately leading to immiscibility. High molecular weight blends of SAN and PC were found to be immiscible, and most favorable interactions were observed for 28 wt. % AN at 140 ^{o}C.

Cheng *et al* (1992) discussed the properties and morphology relationships for ternary blends of PC, SAN, and methacrylated butadiene-styrene (MBS), an impact modifier [95]. Component pair miscibility, interfacial energies and mixing sequence were determined to influence phase morphology and blend properties. Blends prepared by a two-step mixing sequence were found to exhibit better properties than the blends prepared by mixing all components simultaneously. The mechanical properties of binary blends of impact modifiers with a single matrix polymer depends on several aspects of the rubber phase morphology such as particle size, uniformity of particle distribution, rubber phase volume, and particle size distribution. The mechanical properties of ternary blends in the study were found to depend on factors such as, morphology, interfacial adhesion between component pairs, toughness of each matrix component, and chemical and physical nature of the modifier [95].

Kodama (1993) studied the effect of adding short Kevlar fiber on the compatabilization of certain immiscible blends of SAN and PC [96]. SAN/PC mixture at a 1:1 ratio by weight was dissolved in tetrahydrofuran to form a 5 % solution. Kevlar fiber was then added to the solution and dispersed by stirring. It was found that Kevlar

fiber had the effect of partially compatabilizing the SAN/PC blend, in which the blend components interacted with the fiber independently.

Janarthanan *et al* (1993) studied the fracture toughness for SAN/PC blends for five purified SAN materials with a range of 17-31 wt. % AN. Maximum SAN/PC toughness was observed for 24% AN material [97]. Paul *et al* (1993) studied the thermodynamic interactions in SAN/PC blends. The optimum thermodynamic interaction of PC with SAN copolymers was found at 25 wt. % AN content. Critical molecular weight analysis of the PC/SAN blends indicated that when the molecular weights of PC and SAN was reduced to 3000 each, their blends became miscible [98].

Kodama (1993) discussed that the phase morphology of SAN/PC blends change characteristically by annealing at temperatures above the T_g of the component polymers [99]. It was also demonstrated that the solubilization of PC by SAN in SAN-rich phase is greater than that of SAN by PC in PC-rich phase. Watkins and Hobbs (1993) studied the interfacial tensions between PC and a series of SAN blends having styrene/AN ratios varying between 100/0 and 60/40 (wt %). A distinct minimum in the interfacial tension was observed close to the SAN composition giving the highest PC/SAN miscibility at nearly 15% AN [100].

Nachlis *et al* (1994) studied *in-situ* polymerization of bisphenol-A-carbonate cyclic oligomers (BPACY)/SAN copolymer blends [101]. The SAN/PC blends obtained by this process had morphologies that could not be attained by conventional melt blending, due to the extremely fine phase dispersion. Gan and Paul (1994) studied the

phase behavior of blends of glycidal methacrylate (GMA)/styrene copolymers with polycarbonate to evaluate the binary interaction densities for repeat-unit pairs [102].

Experimental

In the series of experiments for in-line monitoring of SAN/PC blends, the concentration of polycarbonate (PC) was normalized from 0% to 100 % in increments of 10%, by taking weighed quantities of commercially available SAN and PC polymer resins. The 0% concentration of PC was represented by the pure SAN resin and the 100% concentration of PC was represented by the pure PC resin.

The SAN and PC polymer resins were available in the pellet form. As both the polymers absorb moisture, they were dried before processing. SAN was vacuum dried at 180 ^{o}C for 16-24 hrs and PC was vacuum dried at 220 ^{o}C for 12-15 hrs. The pure polymers were dried before samples were prepared, as the two polymers have different recommended drying conditions. The 11 samples, representing the entire range of concentrations from 0-100 wt. % SAN and PC were prepared by weighing the dried polymers in the required ratios. The weighed samples were subsequently mixed in a plastic container by manual shaking. The mixed samples were then placed in aluminum foil and kept in an oven to prevent any moisture from being absorbed.

The SAN/PC blends were extruded at temperature set points of 230 ^{o}C, 240 ^{o}C, and 240 ^{o}C in heating zones 1,2, and 3, respectively, in the extruder. The temperatures in the heating block and flow cell were maintained at 250 ^{o}C and 260 ^{o}C, respectively. The mixing of the polymer blends was enhanced in the extruder. The screw speed was

maintained between and 20-22 r.p.m for the experimental runs. Pressures downstream of the gear pump (figure 5.1) varied from 530-1150 psi, and pressures upstream of the gear pump varied from 100-170 psi, for the 11 sample concentrations. The pressures increased with increasing wt. % PC in the samples.

The extruder was flushed with pure SAN (the first sample, representing 0 wt. % PC) for an hour and a half to flush out any polymer present in the extruder as a result of previous experiments. Each subsequent sample was run for nearly one hour to obtain representative spectra for the specific blend concentration.

The NIR spectra was collected in the range from 1200 nm to 2400 nm with a step size of 1 nm using the Scanner program. A fixed pathlength of 1.5 mm was used for the experiments with the SAN/PC blends. At this pathlength the maximum absorbance for the two pure polymers was less than 1.0 absorbance units. Ten representative spectra for each of the 11 blend compositions were saved for qualitative and quantitative analysis.

Spectral Analysis

Primarily, as the near infrared region consists of overtones and combinations of the C-H, O-H, and N-H stretching and bending vibrations, the molecular structure of SAN and PC provides an insight into the absorption bands observed in the region. The chemical structure of SAN and bisphenol-A PC shown in figure 7.1, can be used to explain the absorption bands occurring in the NIR region. x, y and n which represent the number of repeat units, were not known for the two polymers.

The overtone region from 1600 nm to 1800 nm consists of first overtone bands of C-H stretching vibrations. The combination region from 2000 nm to 2400 nm consists of combination bands due to C-H stretching and other modes of vibration [6, 10, 11]. Overlaid spectra for averaged raw data, for pure SAN and PC in the region from 1200 nm to 2400 nm can be seen in figure 7.2. The spectra of the two pure polymers show differences in the overtone and combination regions. These variations in the absorption characteristics of the two resins were modeled by multivariate analysis for composition predictions, for the SAN/PC blends.

Results and Discussions

The ten spectra for each of the 11 samples comprised of 1201 absorbance values in the region from 1200 nm to 2400 nm. The averaged raw data for the 11 samples as shown in figure 7.3 was smoothed using Guided Wave Examiner program, and first derivatives of the average absorbance spectra and the individual absorbance spectra were calculated. Slight variations in the absorbance spectra, such as baseline shifts were observed in the region from 1200 nm to 1600 nm. This non-reproducibility in the spectra can be attributed to sample inhomogeneity, and the immiscible nature of SAN/PC blends. The first derivative of the average and individual absorbance spectra was smoothed further before multivariate data analysis was performed. The effect of the baseline shifts was minimized by taking the first derivative of the spectra.

Figure 7.4 shows the variance in absorbance for the averaged raw data for the SAN/PC blends in the region from 1200 nm to 2400 nm. The variance in absorbance is

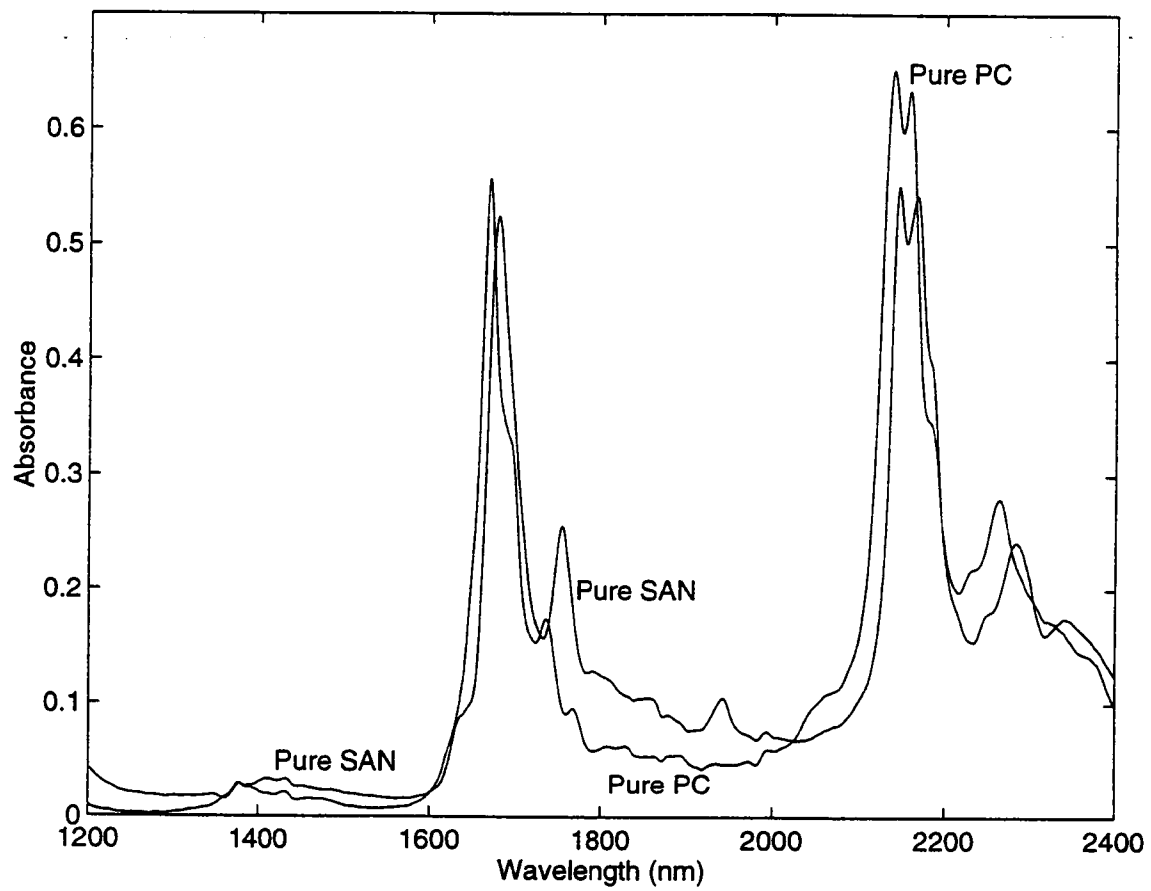


Figure 7.2 Overlaid NIR absorbance spectra (averaged raw data) of pure SAN and pure PC in the region from 1200 nm to 2400 nm @ 260 ^{o}C.

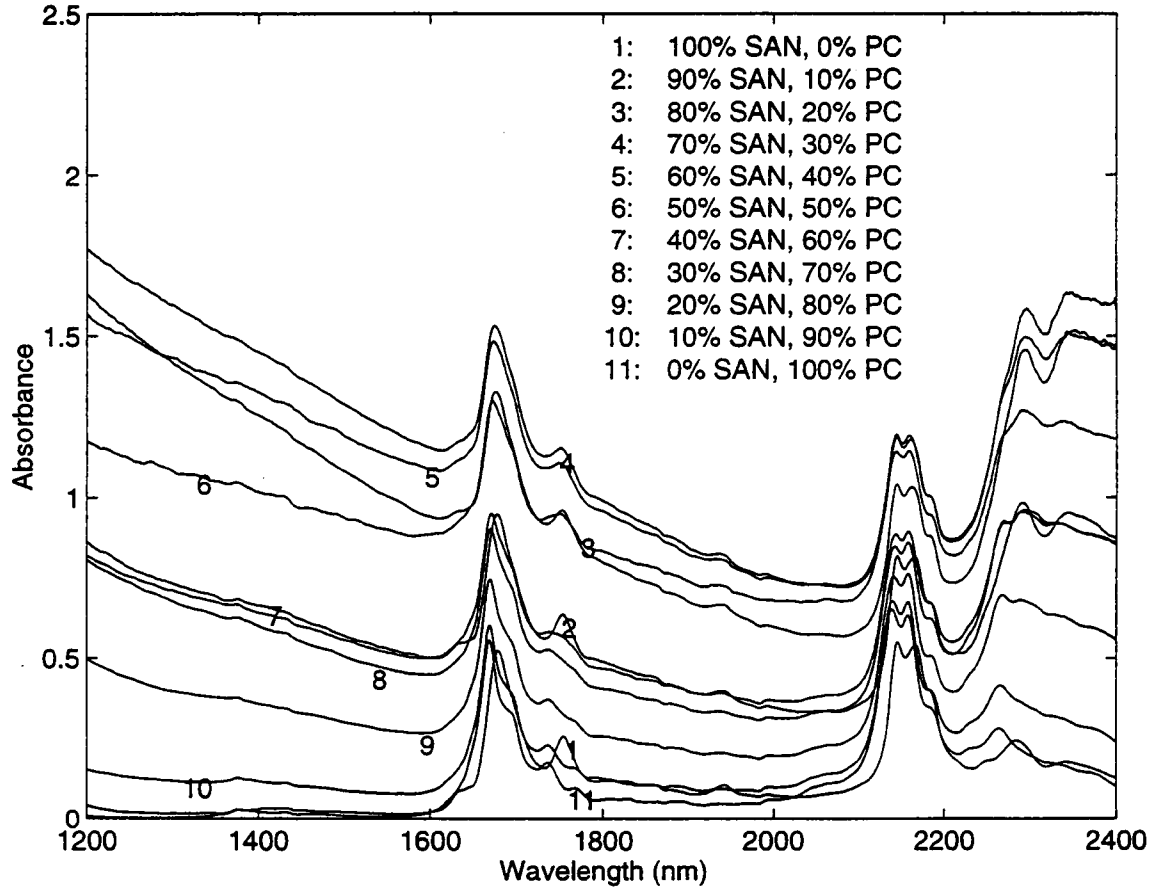


Figure 7.3 Overlaid NIR absorbance spectra (averaged raw data) for each of the SAN/PC blend compositions in the region from 1200 nm to 2400 nm @ 260 °C.

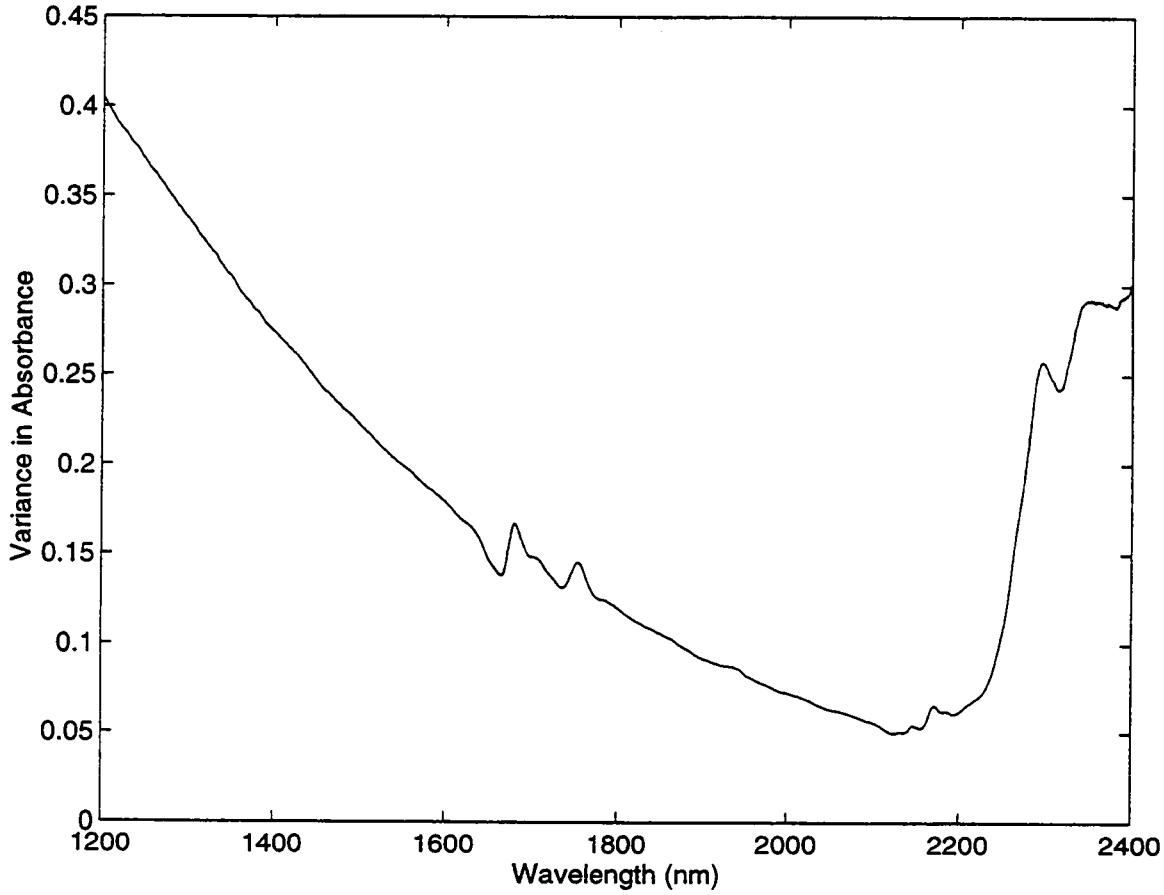


Figure 7.4 Plot of variance in absorbance vs. wavelength for the SAN/PC blend compositions (averaged raw data) in the region from 1200 nm to 2400 nm @ 260 °C.

highest at 1200 nm, indicating that the inhomogeneity effects are maximum near the left end of the spectra.

The 110 first derivative spectra of the individual absorbances (ten for each blend composition) were then examined for non-representative spectra and outliers. Seventy-seven derivative spectra (seven for each blend composition) were selected for the quantitative analysis. The first derivative of the average absorbance spectrum for each of the 11 samples, were used in the calibration step, to account for the spectral variability due to sample inhomogeneity and immiscibility of the SAN/PC blends. Therefore in all, the 11 first derivatives of the average absorbance spectra constituted the calibration set and the validation or test set consisted of the 77 individual first derivative spectra (seven for each blend composition) chosen for the analysis.

Two regions in the spectra for the SAN/PC blends were chosen for the quantitative analysis. Wavelengths from 1600 nm to 1800 nm in the overtone region and wavelengths from 2065 nm to 2185 nm in the combination region were selected for calibration and predictions using PLS and PCR. These regions were selected based on the systematic variation in absorbance values with changes in compositions in the SAN/PC blends. Figure 7.5 shows the first derivative spectra for the 11 calibration samples, overlaid in the overtone region from 1600 nm to 1800 nm. The overlaid first derivative spectra for the calibration samples, in the combination region from 2065 nm to 2185 nm is shown in figure 7.6. Regions with spectral changes due to increasing wt. % PC in the samples are marked in figures 7.5 and 7.6.

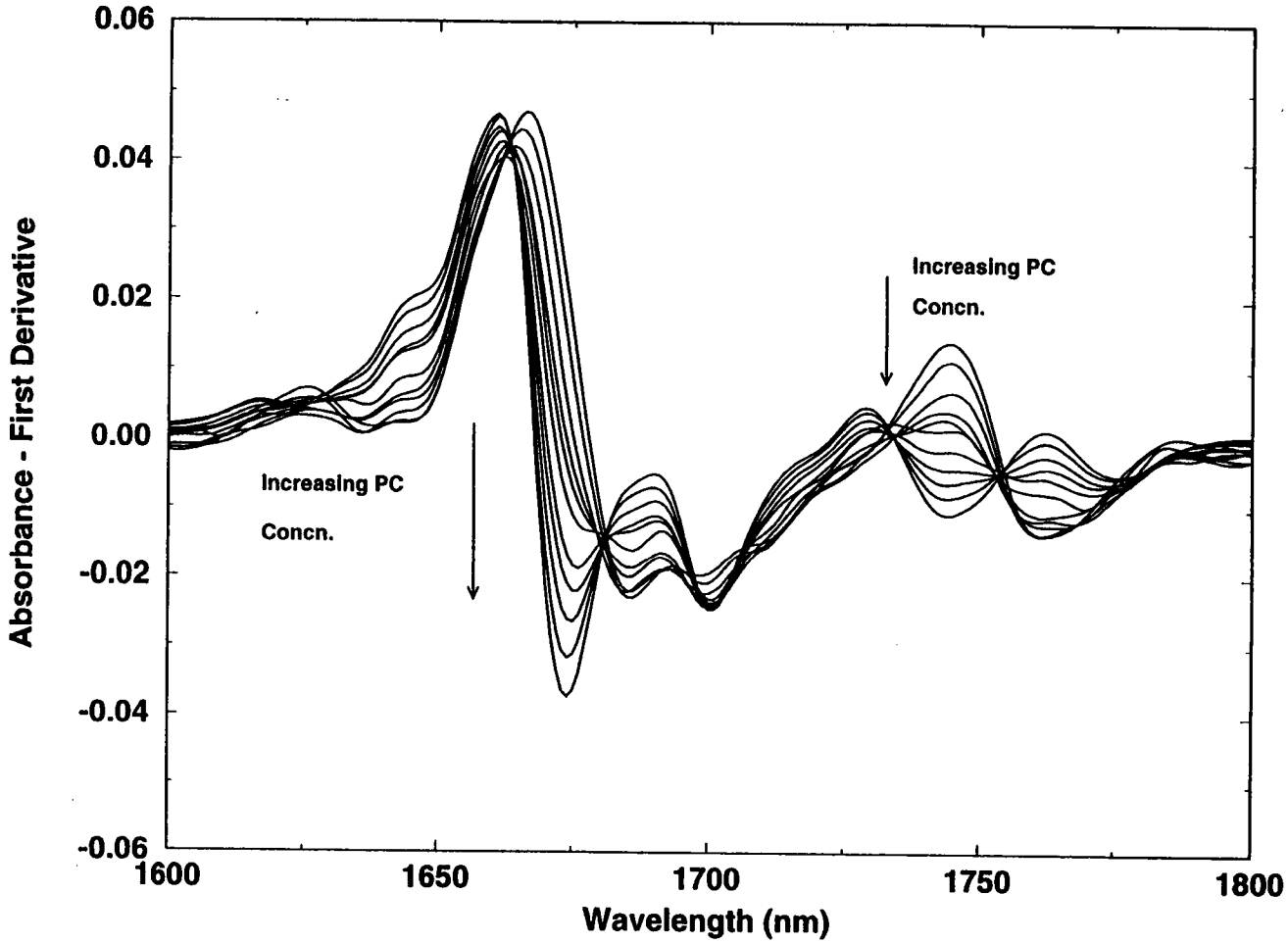


Figure 7.5 Overlaid first derivative NIR absorbance spectra for each of the SAN/PC blend compositions in the overtone region from 1600 nm to 1800 nm.

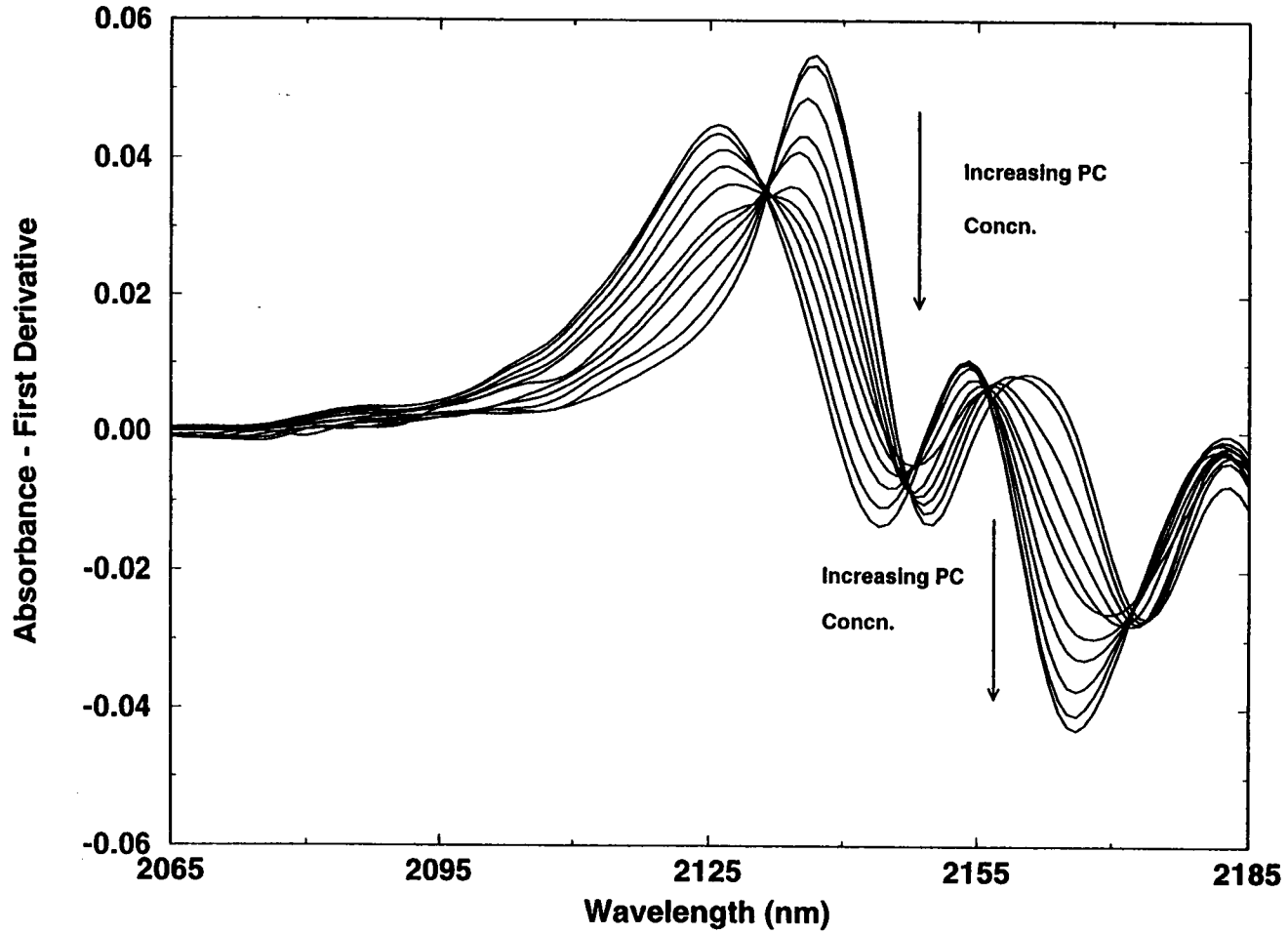


Figure 7.6 Overlaid first derivative NIR absorbance spectra for each of the SAN/PC blends compositions in the combination region from 2065 nm to 2185 nm.

The absorbance data was stored in the X matrix and the corresponding compositional data was stored in the Y matrix. The data was mean centered by subtracting the column mean from each of the elements in the columns of X and Y. The mean centered data was scaled by normalizing each column with respect to the column standard deviation, in order to have unit variance to each variable in X and Y. The mean centered and scaled data was then used for building the calibration models, and then validating them using PLS, and PCR.

In the analysis of the overtone region, the percent variances in X and Y data sets, explainable by the PLS and PCR models, for increasing number of factors is presented in table 7.1. For the PLS model, the first factor accounts for 97.27 % of the total X-block variance, followed by 1.76 % and 0.66 % of the total variance accounted by the second and third factors, respectively. The percent explained variance of the 201 wavelengths corresponding to the wavelengths from 1600 nm to 1800 nm, for the first and second factor is shown in figure 7.7 (a) and 7.7 (b), respectively. Most of the variance of the variables was explained by the first factor, although some variables required additional factors to explain their variance. As seen in figure 7.7, variances of certain wavelengths from 1620 nm to 1628 nm and from 1787 nm to 1793 nm were explained by additional factors. Intensities at these wavelengths did not show significant spectral variations with concentration changes in wt. % PC (as seen in figure 7.5), indicating that factors other than the first factor, did not account for varying PC concentrations in the SAN/PC blends.

The overall percentage of the explained variance, considering the first two factors can be seen in figure 7.8 (a). The first two factors explain most of the variance, however, the third factor is needed to explain the variance of some variables. This can be seen in

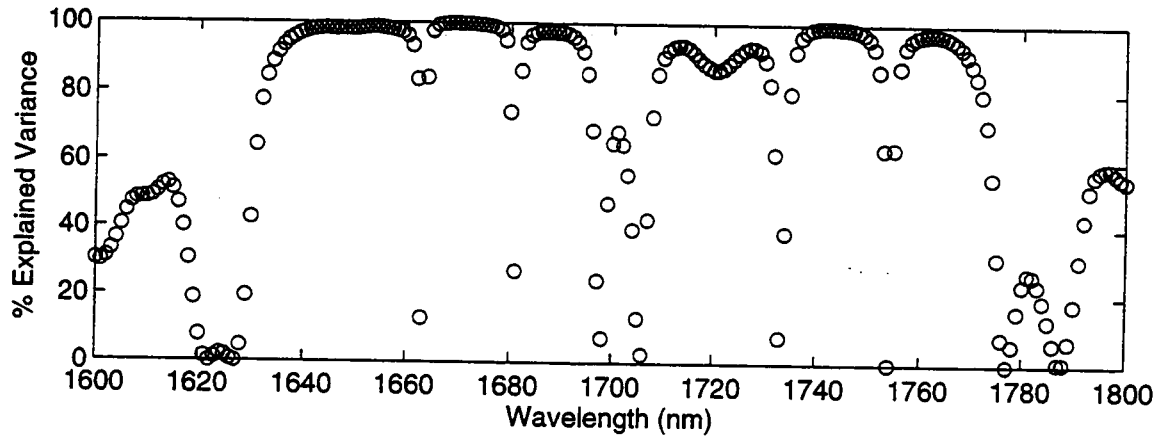
Table 7.1 Percent variances explained by the PLS and PCR models for increasing number of factors in the analysis of the overtone region (1600 nm to 1800 nm) for SAN/PC blends.

PLS

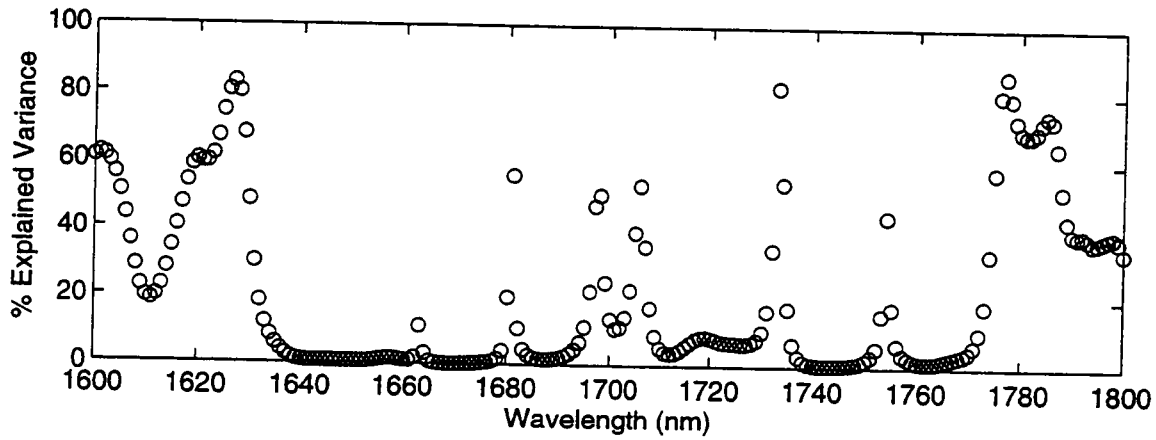
	X-Block (% variance)		Y-Block (% variance)	
Factor	By this Factor	Total	By this Factor	Total
1	97.27	97.27	99.82	99.82
2	1.76	99.03	0.04	99.87
3	0.66	99.69	0.10	99.96
4	0.13	99.83	0.04	100.00
5	0.07	99.90	0.00	100.00
6	0.05	99.94	0.00	100.00

PCR

	X-Block (% variance)		Y-Block (% variance)	
Factor	By this Factor	Total	By this Factor	Total
1	97.27	97.27	99.82	99.82
2	2.27	99.54	0.00	99.82
3	0.21	99.76	0.03	99.85
4	0.09	99.85	0.01	99.86
5	0.07	99.92	0.13	99.99
6	0.03	99.95	0.01	100.00

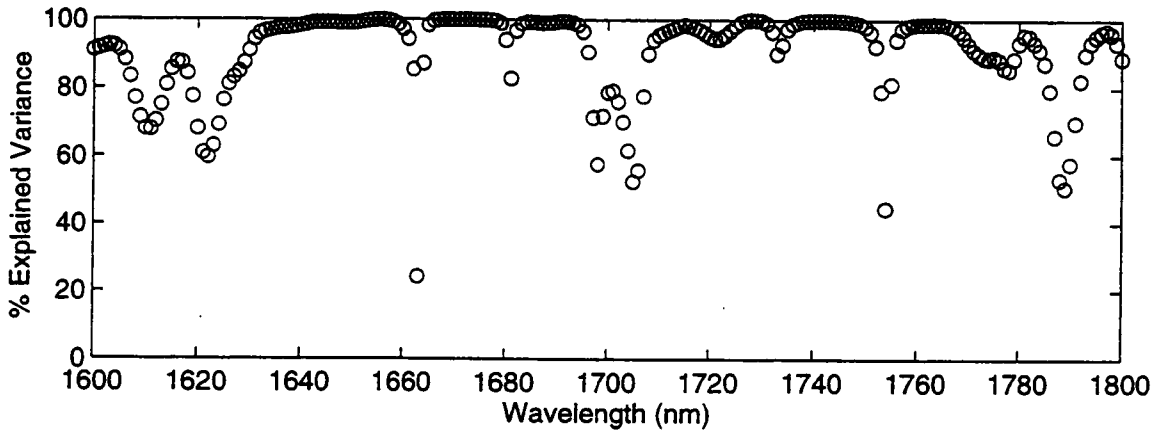


(a) Variances explained by wavelengths after first factor only

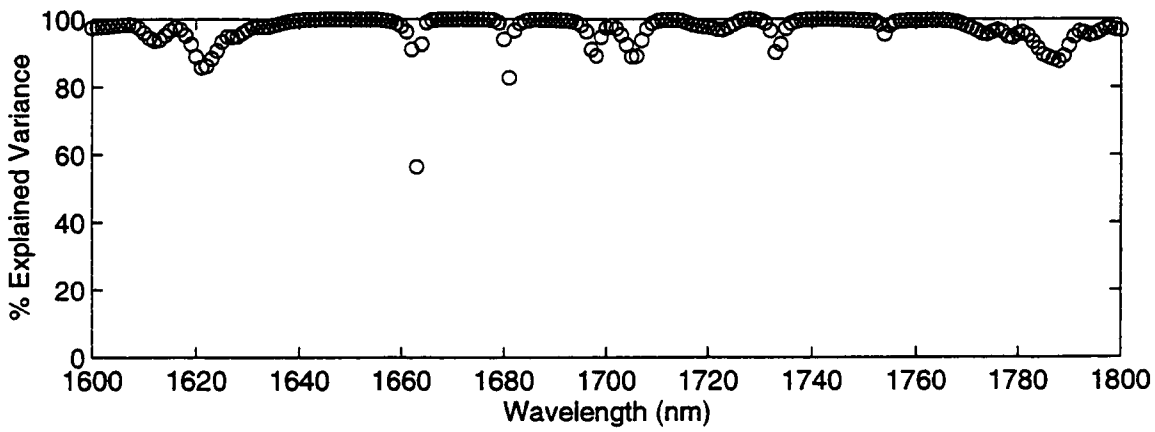


(b) Variances explained by wavelengths after second factor only

Figure 7.7 Variances explained by the wavelengths after considering, (a) First factor only, (b) Second factor only, for the SAN/PC blends in the region from 1600 nm to 1800 nm.



(a) Variances explained by wavelengths after first and second factors



(b) Varaiances explained by wavelengths after first, second and third factors

Figure 7.8 Overall variances explained by the wavelengths after considering, (a) First two factors, (b) First three factors for the SAN/PC blends in the region from 1600 nm to 1800 nm.

figure 7.8 (b) which shows the overall percentage of the explained variance, considering the first three factors.

Cross-validation was used to estimate the prediction errors and determine the optimal number of factors to be used in the calibration models. Cross-validation was carried out using the leave-a-group (LAG) and leave-a-sample (LAS) approaches [2]. The LAS approach involved removing one of the spectra from the calibration set, carrying out the calibration with the remaining spectra and then using the model to predict the concentration of the sample corresponding to the left out spectrum. This procedure was repeated for 9 spectra corresponding to the samples from 10 wt. % PC to 90 wt. % PC.

Prediction errors for the pure samples using the LAS approach were higher compared to the prediction errors for the intermediate compositions. The pure polymers represent the extremities in the calibration data set, therefore if a calibration set comprising of samples from 10 wt. % PC to 100 wt. PC was used to predict the concentration of 0 wt. % PC (pure SAN), the prediction errors would be higher relative to SEPs for other samples.

The LAG approach involved removing the spectra for 20, 40, 60 and 80 wt. % PC from the calibration set, and using the remaining samples to predict their concentrations. This procedure was then reversed to predict the concentrations for the samples with 10, 30, 50, 70 and 90 wt. % PC using the remaining blends. The spectra for pure SAN and PC were included in the LAG approach, as the prediction errors for the extreme concentrations, were found to be higher compared to the intermediate concentrations for the SAN/PC blends. Predicted Residual Sum of Squares (PRESS) values by LAS and

LAG were calculated at each factor. The PRESS values for the LAS and LAG for increasing factors are plotted in figure 7.9. The average PRESS values were found to be minimum at 3 factors for both the LAS and LAG cross-validation approaches using PLS.

The model was further tested against the validation or test set to establish its accuracy and robustness. The SEP and SEC values for the test and calibration set, respectively with increasing factors are plotted in figure 7.10. SEC of 0.65 % and SEP of 1.75 % were obtained for 3 factors in the validation step using PLS. The SEP was found to be minimum at 3 factors using PLS. This observation was in agreement with the cross-validation results. It was concluded that 3 factors explain the variation in the SAN/PC blends.

PCR needed addition factors for minimum prediction errors as indicated by the SEP values given in table 7.2. These results suggest that PLS needs fewer factors for the analysis than PCR, which is in agreement with the simulation results reported by Helland [36]. The model predictions for the calibration and validation set for 3 factors using PLS are plotted against the actual concentrations in figures 7.11 and figure 7.12, respectively.

The loadings, which give the relationship between the variables in the data that make up each principal component are plotted for the first, second, and third factors in figure 7.13. The loadings for a factor give the contributions of the variables in making up that factor. The loadings for a factor, also help distinguish the positive and negative correlations among the variables in the analysis of the first derivative absorbance spectra for the SAN/PC blends. The first factor loadings were seen to decrease around 1670 nm, which is in agreement with the decrease in the first derivative absorbance around 1670 nm,

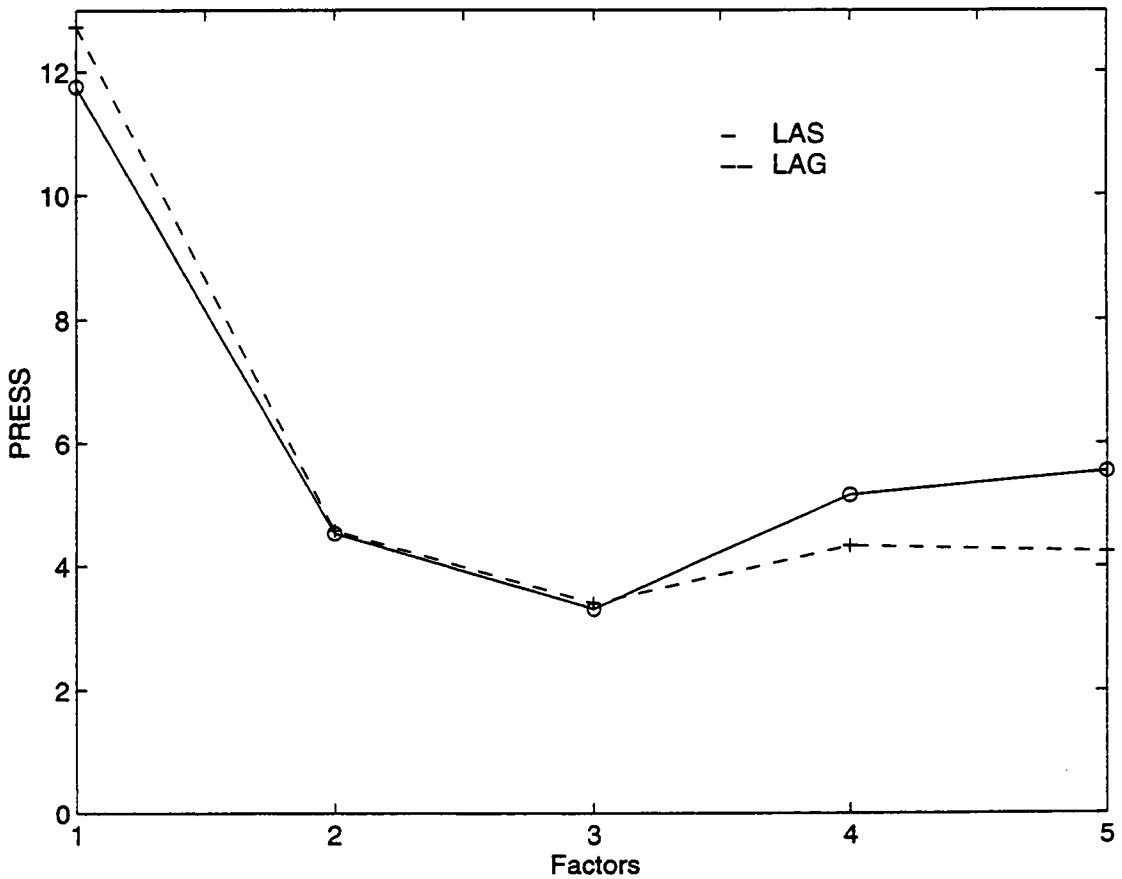


Figure 7.9 PRESS values for leave-a-sample (LAS) and leave-a-group (LAG) cross-validation methods using PLS, for the SAN/PC blends in the overtone region from 1600 nm to 1800 nm.

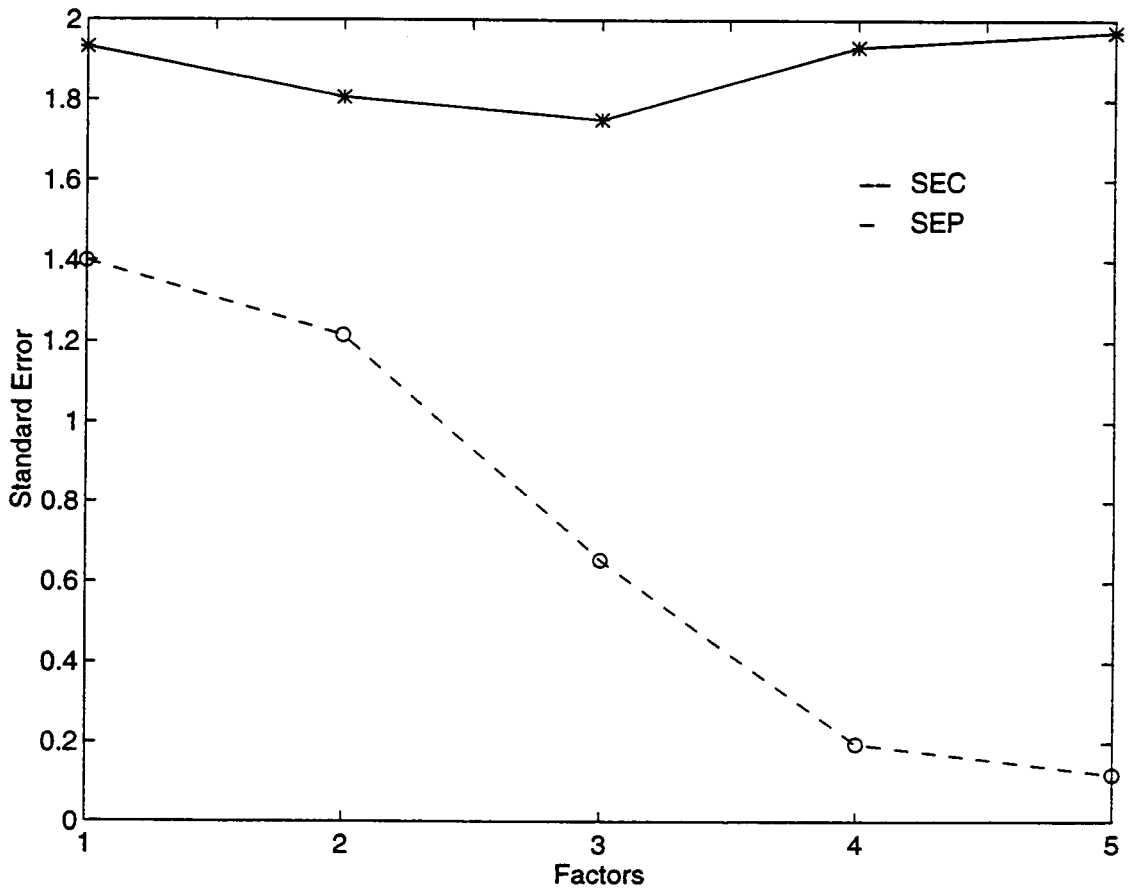


Figure 7.10 Plot of SEC and SEP for calibration and validation sets, respectively, for increasing number of factors using PLS, for the SAN/PC blends in the overtone region from 1600 nm to 1800 nm.

Table 7.2 Comparison of calibration and prediction errors using PLS and PCR in the overtone and combination regions for SAN/PC blends.

PLS

	Overtone Region (1600 nm to 1800 nm)		Combination Region (2065 nm to 2185 nm)	
Factor	SEC	SEP	SEC	SEP
1	1.40	1.93	1.99	2.57
2	1.22	1.81	1.65	2.34
3	0.65	1.75	1.13	2.21
4	0.20	1.93	0.81	2.29
5	0.12	1.97	0.47	2.39
6	0.05	2.02	0.37	2.48

PCR

	Overtone Region (1600 nm to 1800 nm)		Combination Region (2065 nm to 2185 nm)	
Factor	SEC	SEP	SEC	SEP
1	1.40	1.93	1.99	2.57
2	1.40	1.93	1.84	2.48
3	1.29	1.88	1.82	2.48
4	1.25	1.87	1.79	2.45
5	0.31	1.87	1.37	2.42
6	0.18	2.04	1.37	2.42

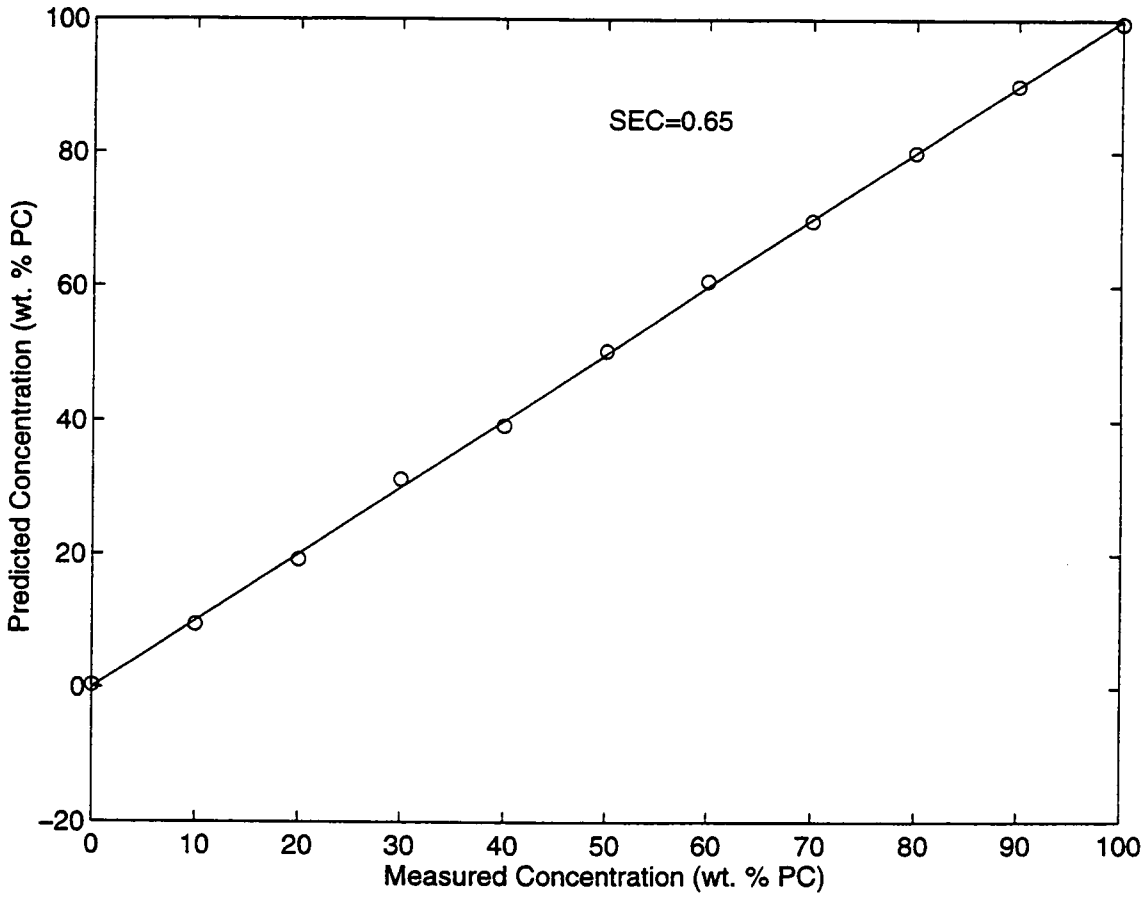


Figure 7.11 Model predictions for the calibration set (based on first derivative absorbance data) using PLS, plotted against the reference (actual) concentrations for the SAN/PC blends in the region from 1600 nm to 1800 nm.

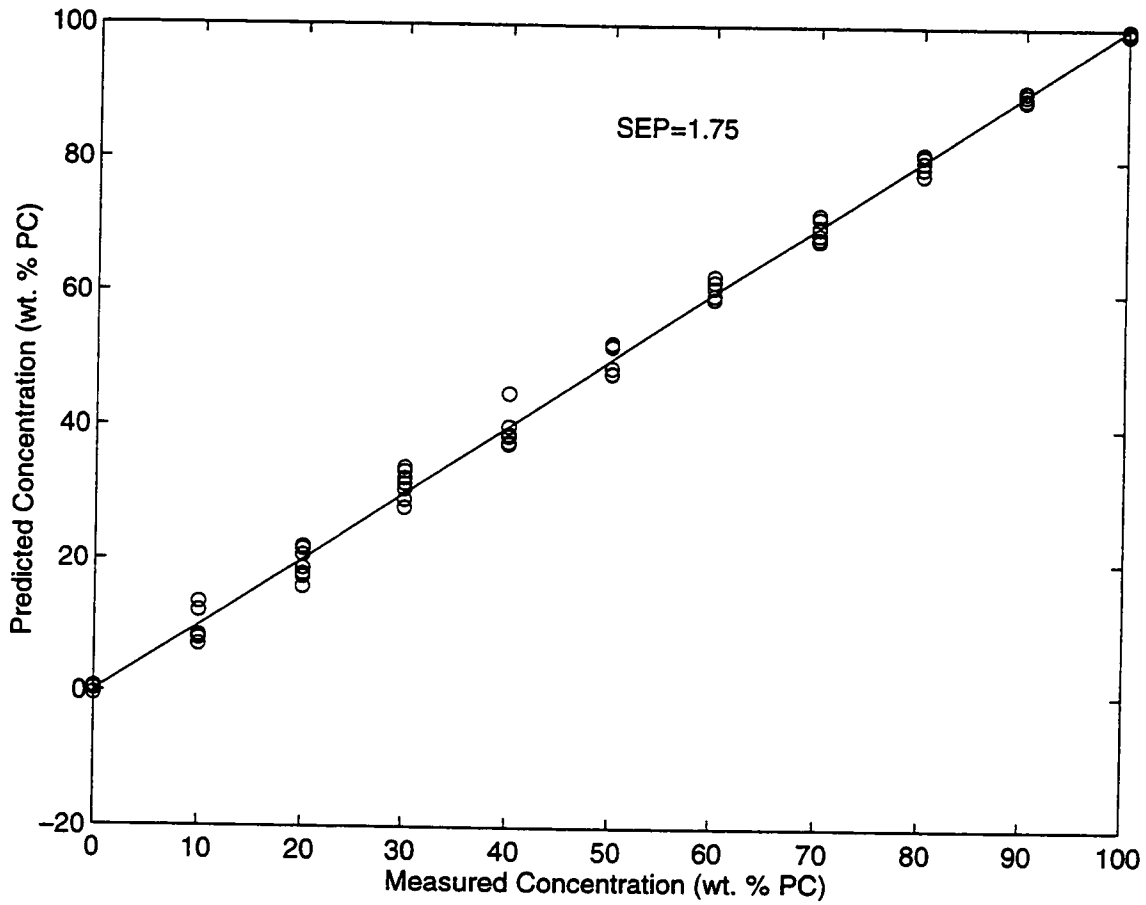


Figure 7.12 Model predictions for the validation set (based on first derivative absorbance data) using PLS, plotted against the reference (actual) concentrations for the SAN/PC blends in the region from 1600 nm to 1800 nm.

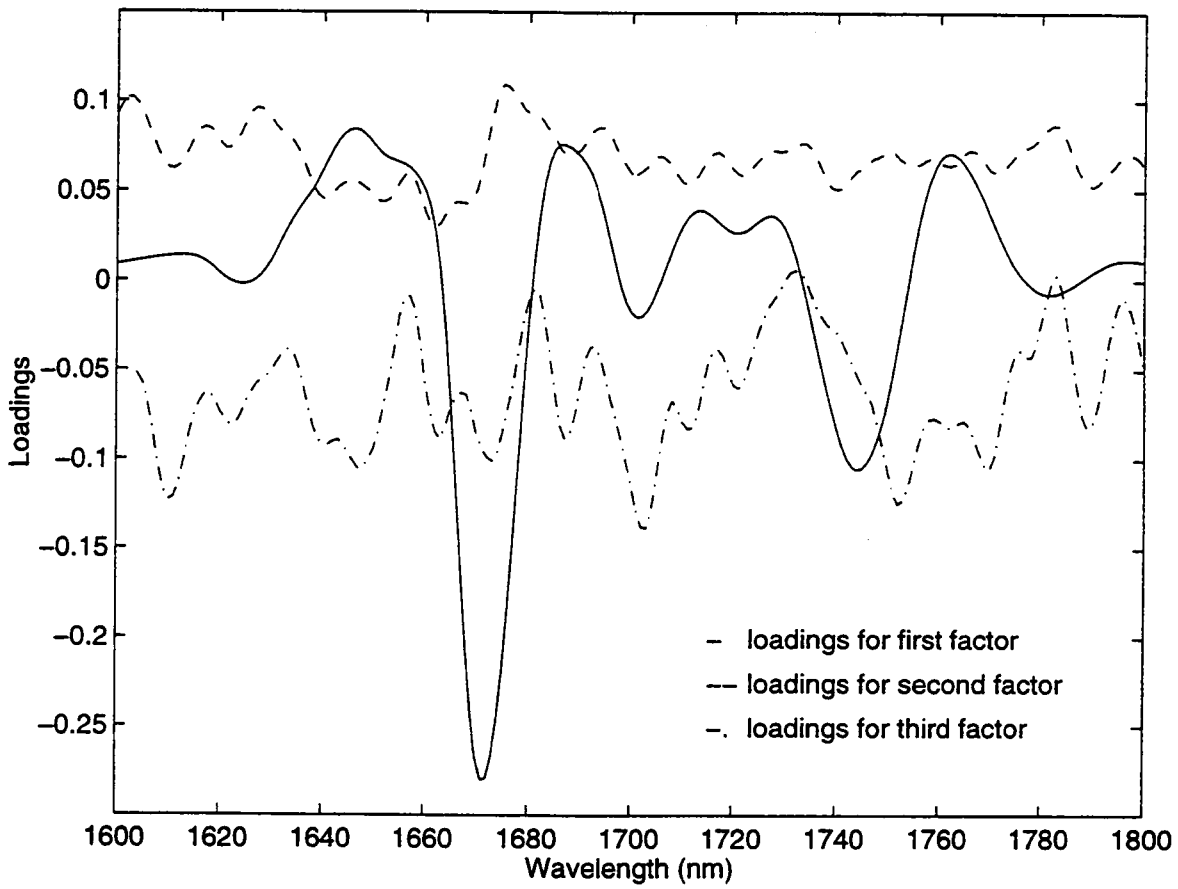


Figure 7.13 Loadings plot for first, second, and third factors for samples in the calibration set (based on first derivative absorbance data) using PLS, for SAN/PC blends in the overtone region from 1600 nm to 1800 nm.

with increasing wt. % PC (as seen in figure 7.5) for the SAN/PC blends. Negative correlations in the first factor loadings are seen at 1740 nm. This trend can also be observed in the first derivative absorbance spectra (as seen in figure 7.5), with a decrease in the first derivative absorbance values at 1740 nm, with increasing wt. % PC. Figure 7.13 also indicates that the first factor loadings represent the "mean" or average spectral variations for first derivative absorbance, with changes in wt. % PC in the SAN/PC blends.

The scores, which give the relationship between the spectra in the data set are plotted for the first, second and third factors in figure 7.14. Scores for the first factor show a step increase with increasing ABS concentration. Trends in second and third factor scores were not as regular as the variation observed for the first factor scores.

It can be suggested that as there is only one independent factor of variation (wt. % PC in the samples) in the SAN/PC samples, the additional factors could be due to non-linearities, and sample inhomogeneities. Additional factors have to be included in the models as the prediction errors are greater if only one factor is considered. The SEC and SEP values confirm that the second and third factors cannot be disregarded in the multivariate analysis. This observation suggests that the variance explained by the second and third factors for the calibration set is similar to the variance in the test set, and the two factors should be incorporated in the model for low SEP values.

To demonstrate the variation in the calibration set, the scores for the first, second, and third principal component were plotted in the 3-D transformed space, as shown in figure 7.15. Spectral variation in the data set along the direction of the first factor was

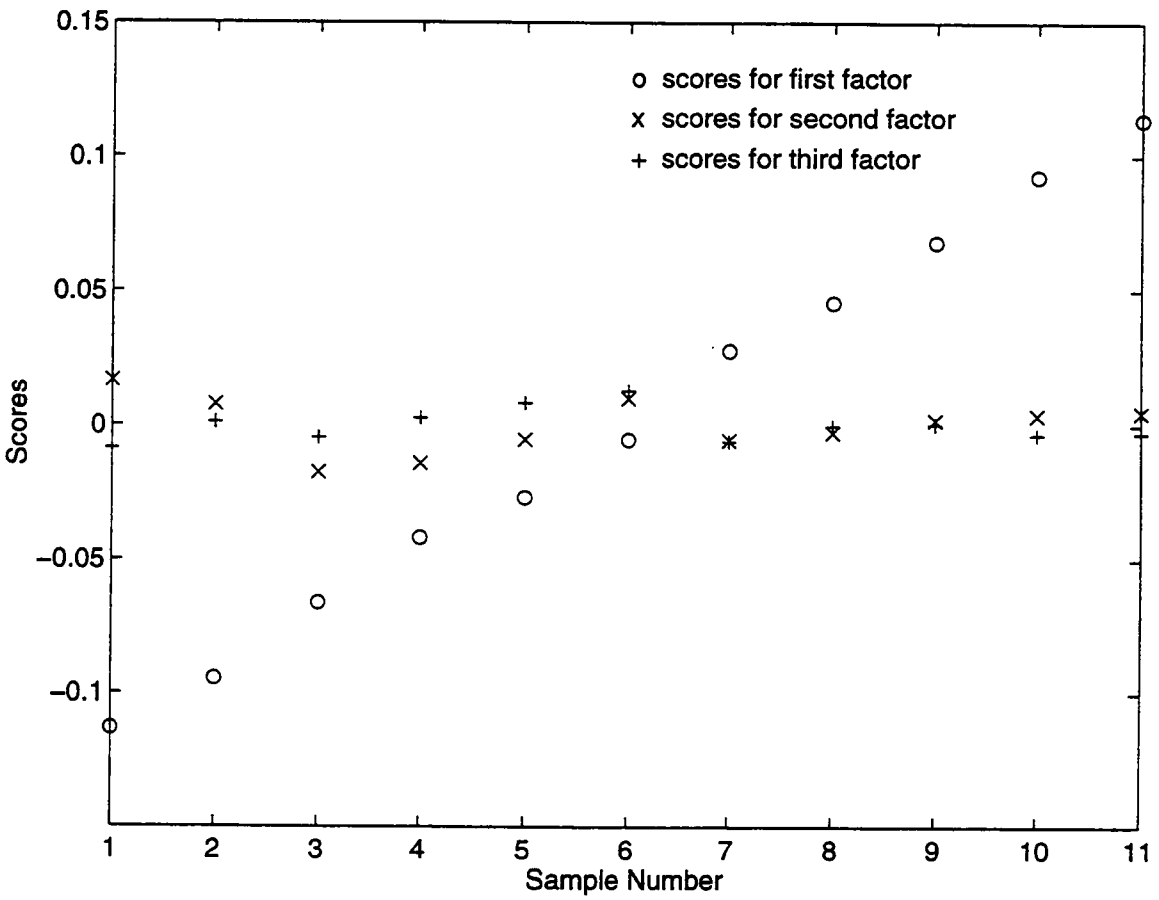


Figure 7.14 Scores plot for first, second, and third factors for samples in the calibration set (based on first derivative absorbance data) using PLS, for SAN/PC blends in the overtone region from 1600 nm to 1800 nm.

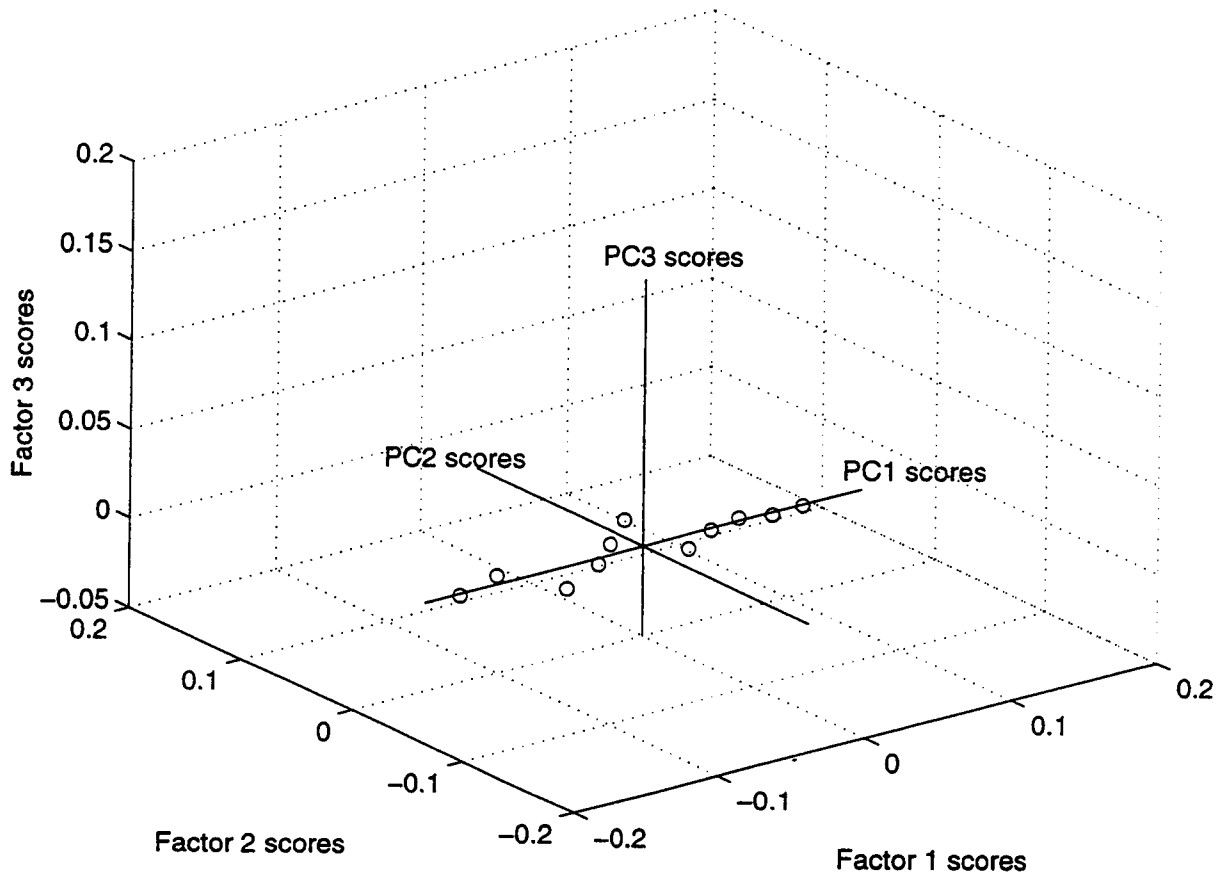


Figure 7.15 First, second, and third factor scores for samples in the calibration set for the SAN/PC blends using PLS in the region from 1600 nm to 1800 nm.

maximum, followed by the second and third factor respectively. 2-D plot of scores for the first factor vs. the scores for the second factor as viewed in the direction of the third factor is given in figure 7.16. 2-D views in the direction of first and second factor are shown in figure 7.17 (a) and figure 7.17 (b), respectively. The scores plots provide a better understanding of the spatial distribution of scores in the principal component space. The plot for first factor scores vs. second factor scores using PCR for samples in the calibration set, from 1600 nm to 1800 nm in the overtone region is given in figure 7.18. Comparison of figure 7.16 and figure 7.18 indicates that the scores values are nearly identical for the PLS and PCR approaches.

A similar analysis was performed in the combination region from 2065 nm to 2185 nm. This region also gave 3 factors of variation using PLS as a result of cross-validation and validation by the test set. Additional factors were needed in the combination region as well, for minimum prediction errors by PCR. The comparison of the SEC and SEP values from the two regions by PLS and PCR are presented in table 7.2.

A full spectrum analysis of the spectral data in the range from 1200 nm to 2400 nm was also performed. As the sample inhomogeneity effects and non-linearities were more prevalent in the entire region from 1200 nm to 2400 nm, an additional factor was required to describe the variation in the spectral data for minimum prediction errors. Table 7.3 gives the explained variance for the full spectrum analysis using PLS and PCR. The increase in the optimal number of factors compared to the overtone and combination regions, indicates that choosing the entire spectrum for composition predictions is not the best choice for analysis as we know that there is essentially one factor of variation (wt. % PC) in the blends.

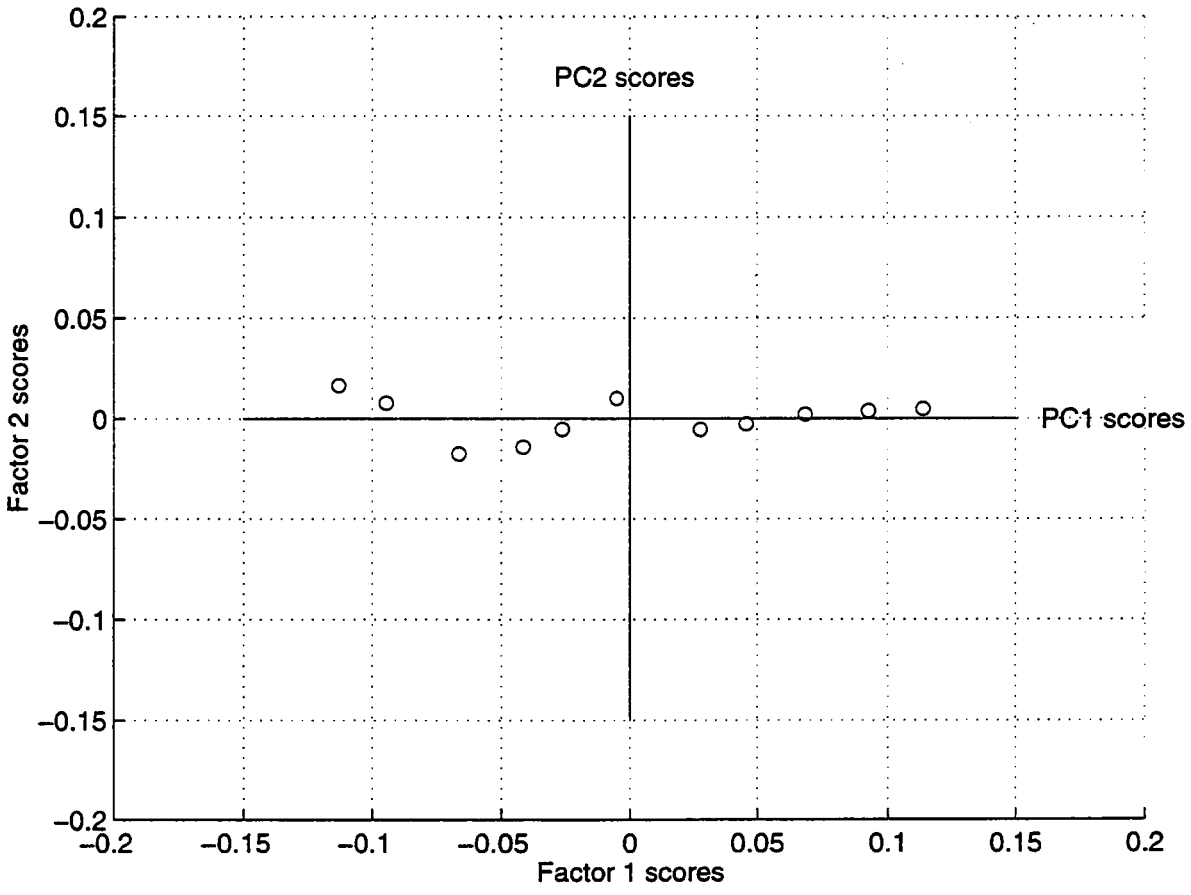
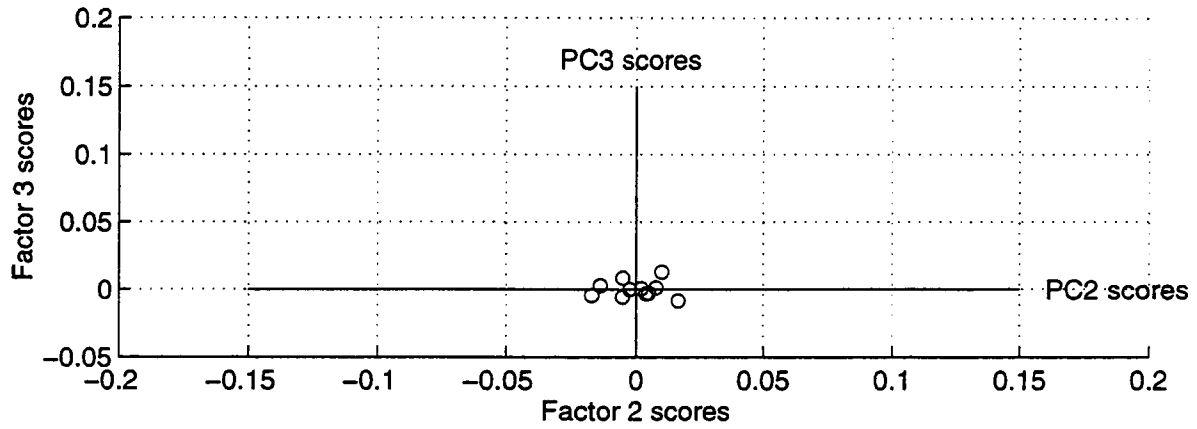
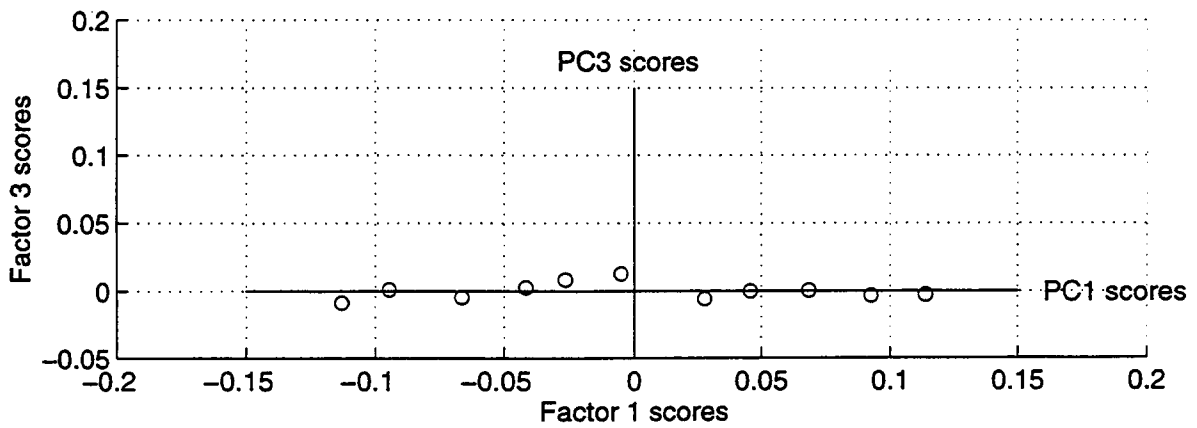


Figure 7.16 First factor vs second factor scores for samples in the calibration set, for the SAN/PC blends using PLS in the overtone region from 1600 nm to 1800 nm.



(a) Scores for factors, 2 and 3.



(b) Scores for factors, 1 and 3.

Figure 7.17 (a) projection of scores on second and third factors, (b) projection of scores on first and third factors, for the SAN/PC blends using PLS in the region from 1600 nm to 1800 nm.

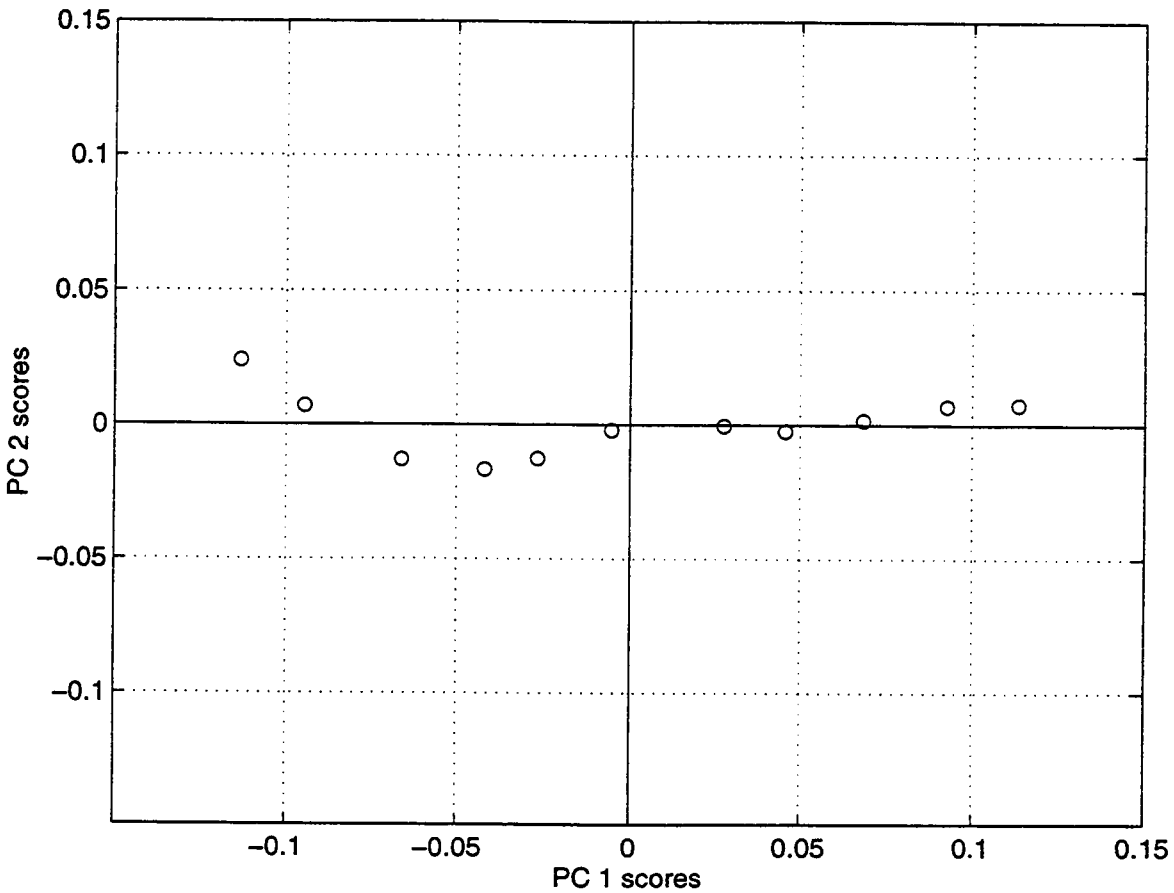


Figure 7.18 First factor vs second factor scores for samples in the calibration set, for the SAN/PC blends using PCR in the region from 1600 nm to 1800 nm.

Table 7.3 Percent variances explained by the PLS and PCR models for increasing number of factors in the full spectrum analysis (1200 nm to 2400 nm) for SAN/PC blends.

PLS

	X-Block (% variance)		Y-Block (% variance)	
Factor	By this Factor	Total	By this Factor	Total
1	76.29	76.29	97.34	97.34
2	19.27	95.56	2.21	99.55
3	2.35	97.96	0.29	99.84
4	0.46	98.37	0.12	99.96
5	0.55	99.91	0.02	99.98
6	0.35	99.26	0.01	99.99

PCR

	X-Block (% variance)		Y-Block (% variance)	
Factor	By this Factor	Total	By this Factor	Total
1	76.43	76.43	95.65	95.65
2	19.16	95.59	3.80	99.44
3	2.34	97.94	0.34	99.78
4	0.70	98.64	0.02	99.80
5	0.48	99.13	0.01	99.81
6	0.43	99.56	0.01	99.82

The scores plot for the full spectral analysis (1200 nm to 2400 nm), for the samples in the calibration set is given in figure 7.19. The scores plot shows that the trend for increasing first factor scores with increasing wt. % PC as observed in figure 7.14 is present, although the increase in scores is not as regular as observed for the overtone region. The second and third factor scores for the entire spectral region as seen in figure 7.19 are greater compared to the second and third factor scores for the overtone region as seen in figure 7.14.

Nonlinearities, and sample inhomogeneities effects which are more pronounced in the region from 1200 nm to 2400 nm, are exhibited by an increase in second and third factor scores. The above discussion shows that the full spectral analysis is not the ideal choice for composition predictions of unknown samples. Comparison of the SEC and SEP values for the full spectrum analysis by PLS and PCR is given in table 7.4.

Figure 7.20 shows the difference in absorbance for the SAN/PC blends from 10 to 90 % compared to the absorbance of an ideal blend, based on the absorbances of pure SAN and pure PC in the region from 1200 nm to 2400 nm. E.g. the difference spectra for a blend containing X % PC and (100-X) % SAN can be given by:

$$\text{Diff. in Abs. (X \% PC)} = \text{Abs. (X \% PC)} - \text{Ideal Abs. (X \% PC)} \qquad (7.1)$$

where:

$$\text{Ideal Abs. (X \% PC)} = [X\% \times (\text{Abs. pure PC}) + (100-X)\% \times (\text{Abs. pure SAN})] \qquad (7.2)$$

The inhomogeniety effects were most pronounced for the sample with 30 wt. % PC. This trend can also be observed in figure 7.3.

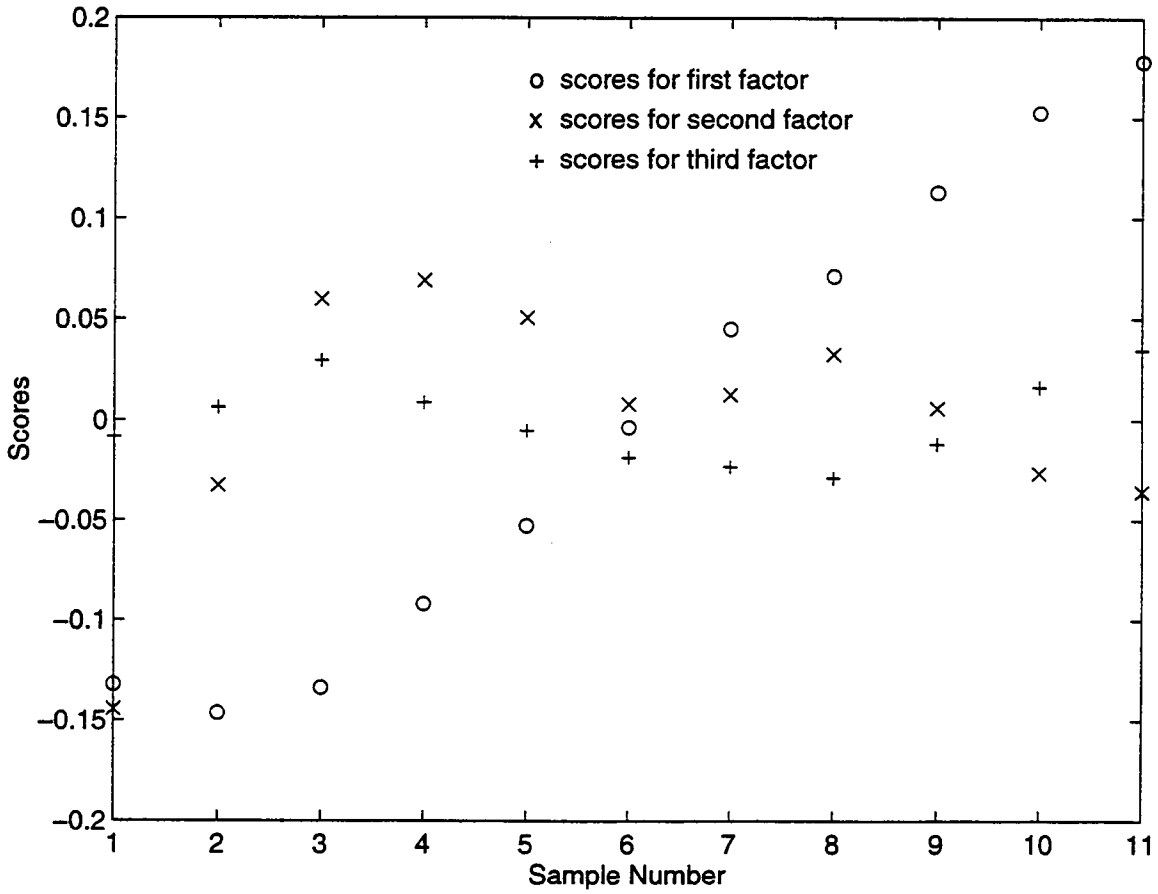


Figure 7.19 Scores plot for first, second, and third factors for full spectral analysis (based on first derivative absorbance data) using PLS in the region from 1200 nm to 2400 nm for samples in the calibration set, for SAN/PC blends.

Table 7.4 Comparison of calibration and prediction errors using PLS and PCR in the region from 1200 nm to 2400 nm for SAN/PC blends.

	PLS		PCR	
Factor	SEC	SEP	SEC	SEP
1	5.41	5.38	6.92	6.78
2	2.23	2.57	2.47	2.78
3	1.32	1.81	1.55	1.98
4	0.65	1.54	1.47	1.91
5	0.48	1.54	1.45	1.92
6	0.39	1.57	1.40	1.85

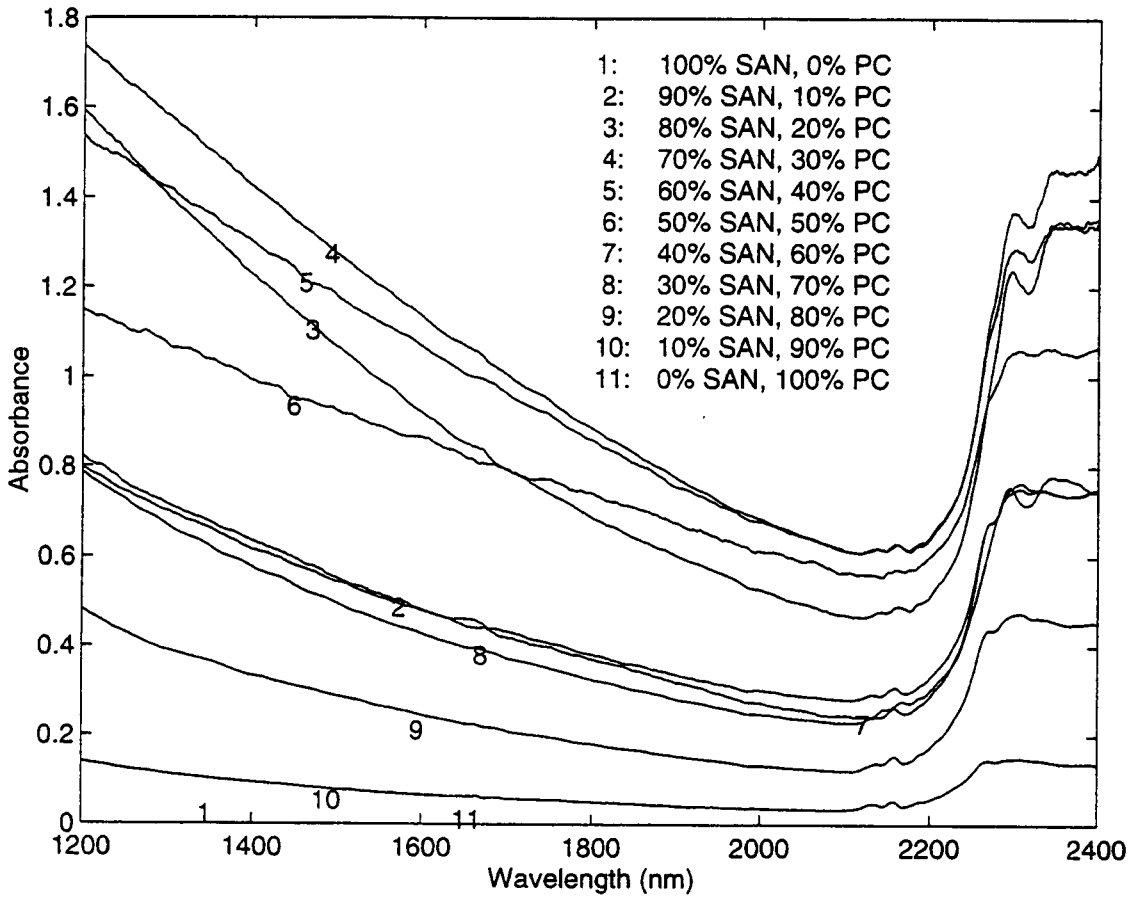


Figure 7.20 Difference in absorbance for the SAN/PC blends compared to the absorbance of an ideal blend of the same composition (based on the absorbances of pure SAN and pure PC), in the region from 1200 nm to 2400 nm.

Conclusions

It was established that in-line monitoring of molten polymers coupled with chemometric data analysis techniques can be successfully used for determining compositions in SAN/PC blends, as well. Two regions that showed significant changes in absorption characteristics were selected for analysis by PLS and PCR. Results from both regions indicated that there were three factors of variation in the NIR spectra for the SAN/PC blends even though there is only one known source of variation (wt. % PC).

Three factors were used in the development of the calibration models based on the SEC and SEP of 0.65 and 1.75 , respectively, using the PLS approach in the overtone region from 1600 nm to 1800 nm. Analysis by PCR required additional factors for minimum SEP. Minimum SEP values obtained by PCR were slightly higher than the minimum SEP values obtained using PLS. The SEC and SEP values obtained by PLS and PCR suggest that PLS is more suited for the analysis as the prediction errors are lower, suggesting that there is significant correlation between the NIR absorbances and concentrations, for the SAN/PC blends.

A full spectrum analysis was also performed, but higher SEP values and an additional factor was required for the analysis, compared to the overtone and combination regions. Certain degree of inconsistency in the spectral data may be due to the polymer samples in the form of pellets. This effect could be minimized by using samples of uniform compositions and measuring the actual extrudate compositions by off-line laboratory methods.

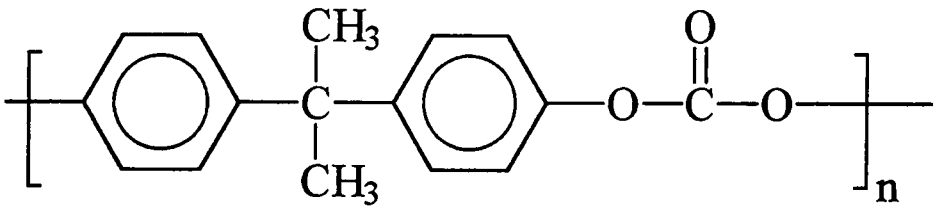
8. IN-LINE MONITORING OF ACRYLONITRILE-BUTADIENE-STYRENE (ABS)/POLYCARBONATE (PC) BLENDS

Introduction

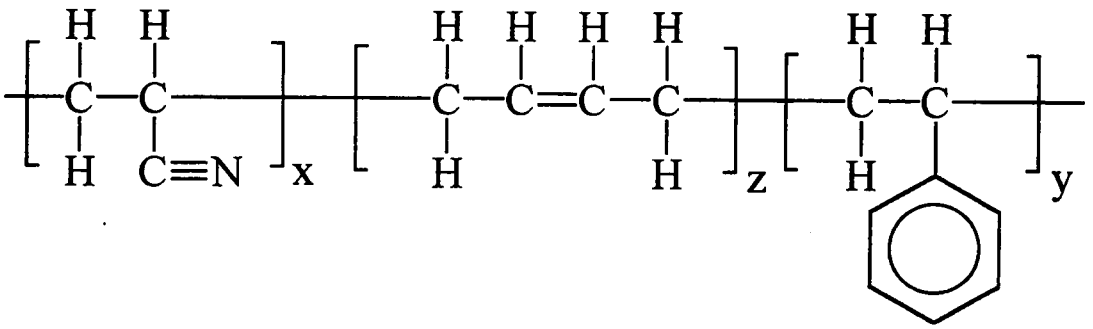
Blends of polycarbonate (PC) and acrylonitrile-butadiene-styrene (ABS) provide a useful balance of toughness, heat resistance, and ease of processing at a lower cost than that of the high performance engineering thermoplastic polycarbonate [103]. Polycarbonates are classified as amorphous engineering thermoplastics that are useful for diverse applications which require high performance polymers. ABS polymers are an important group of styrenic materials, which exhibit excellent balance of properties such as thermal stability, gloss, and impact resistance. Polycarbonate exhibits an excellent balance of toughness, clarity, high-heat deflection temperatures, and processability [92]. ABS has a Tg of 110-125 ^{o}C and PC has a Tg of 150 ^{o}C. The structures for ABS and PC are shown in figure 8.1.

ABS contains three monomeric units, namely the styrene monomer, the acrylonitrile monomer, and the butadiene monomer. The styrene monomer provides rigidity and processability, the acrylonitrile monomer gives heat stability and chemical resistance, and the butadiene monomer provides the toughness and impact resistant properties to ABS. The carbonate component in the structure of PC, makes it one of the toughest plastics, while the bisphenol component provides the high-heat properties.

The development of rubber-toughened thermoplastic resins is an important contribution to the polymer industry. Small amount of discrete rubber particles in a



Polycarbonate (PC)



Acrylonitrile-butadiene-styrene (ABS)

Figure 8.1 Chemical structures of polycarbonate (PC) and acrylonitrile-butadiene-styrene (ABS). x, y, and z represent the number of repeat units in the two polymers.

glassy plastic can significantly improve the crack and impact resistance of otherwise brittle plastics. Polymer blends of PC and ABS, provide products with improved balance in properties at a reduced cost in comparison to that of PC [104]. Blends of ABS/PC have excellent heat resistance, processability and low-temperature impact resistant properties. The blends of ABS/PC are partially miscible. Applications of rubber-modified polycarbonate blends include housings for electrical appliances, radio and television cabinets, automotive and lawn equipment, etc. [105].

Wu *et al* (1993) discussed the effect of polycarbonate molecular weight on polymer blends of PC and ABS [106]. They found that an increase in the molecular weight of PC in PC/ABS blends, resulted in low-temperature fracture toughness improvement but suffered from the disadvantage of higher melt viscosity. The melt viscosities of PC/ABS blends were found to be significantly lower compared to pure PC and even lower than pure ABS in several compositions.

Wu *et al* (1994) discussed the effect of rubber content in ABS on the polymer blends of ABS and polycarbonate (PC). Higher ABS content in the PC/ABS blends provides toughness improvement and heat distortion temperatures. They also pointed out that the toughness advantage by increasing the rubber content in the ABS/PC blends must be compensated by the viscosity increase, and this fact should be considered while selecting the starting materials. Acrylonitrile (AN) content of about 25 wt. % AN in the SAN portion of ABS resulted in the best compatibility of ABS/PC blends [104].

The miscibility between rubber and blend components was found to be the most important factor in controlling the rubber distribution in the ABS/PC blends. Rubber

distribution is important for the resultant properties of the blends. The phase distribution of the added rubber in ABS/PC blends and its effect on toughness improvement was also studied. It was discussed that the melt blended immiscible polymer blends possess complicated phase morphologies depending on a number of factors such as interfacial tension, viscosity ratio, viscosity and elasticity of the two phases, volume fraction, and temperature [104].

Experimental

In the series of experiments for in-line monitoring of ABS/PC blends, the concentration of polycarbonate (PC) was normalized from 0% to 100 % in increments of 10%, by taking weighed quantities of commercially available ABS and PC polymer resins. The 0% concentration of PC was represented by the pure ABS resin and the 100% concentration of PC was represented by the pure PC resin.

The ABS and PC polymer resins were available in the pellet form. As both the polymers absorb moisture, they were dried before processing. ABS was vacuum dried at 180 ^{o}C for 16-24 hrs and PC was vacuum dried at 220 ^{o}C for 12-15 hrs. The pure polymers were dried before samples were prepared, as the two polymers have different recommended drying conditions. The 11 samples, representing the entire range of concentrations from 0-100 wt. % ABS and PC were prepared by weighing the dried polymers in the required ratios. The weighed samples were subsequently mixed in a plastic container by manual shaking. The mixed samples were then placed in aluminum foil and kept in an oven to prevent any moisture from being absorbed.

The ABS/PC blends were extruded at temperature set points of 230 ^{o}C, 240 ^{o}C, and 240 ^{o}C in heating zones 1,2, and 3, respectively, in the extruder. The temperatures in the heating block and flow cell were maintained at 250 ^{o}C and 260 ^{o}C, respectively. The mixing of the polymer blends was enhanced in the extruder. The screw speed was maintained between and 20-22 r.p.m for the experimental runs. Pressures downstream of the gear pump (figure 5.1) varied from 1190-1430 psi, and pressures upstream of the gear pump varied from 180-280 psi, for the 11 sample concentrations.

The extruder was flushed with pure ABS (the first sample, representing 0 wt. % PC) for an hour and a half to flush out any polymer present in the extruder as a result of previous experiments. Each subsequent sample was run for nearly one hour to obtain representative spectra for the specific blend concentration.

The NIR spectra was collected in the range from 1200 nm to 2400 nm with a step size of 1 nm using the Scanner program. A fixed pathlength of 1.5 mm was used for the experiments with the ABS/PC blends. At this pathlength the maximum absorbance for the two pure polymers was less than 1.0 absorbance units, although the maximum absorbances of some of the blend compositions were higher than 1.0 absorbance units. Ten representative spectra for each of the 11 blend compositions were saved for qualitative and quantitative analysis.

Spectral Analysis

Primarily, as the near infrared region consists of overtones and combinations of the C-H, O-H, and N-H stretching and bending vibrations, the molecular structure of

ABS and PC provides an insight into the absorption bands observed in the region. The chemical structure of ABS and bisphenol-A PC shown in figure 8.1, can be used to explain the absorption bands occurring in the NIR region. x, y, z and n which represent the number of repeat units, were not known for the two polymers.

The overtone region from 1600 nm to 1800 nm consists of first overtone bands of C-H stretching vibrations. The combination region from 2000 nm to 2400 nm consists of combination bands due to C-H stretching and other modes of vibration [6, 10, 11]. Overlaid spectra for averaged raw data for pure ABS and PC in the region from 1200 nm to 2400 nm can be seen in figure 8.2. The spectra of the two pure polymers show differences in the overtone and combination regions. These variations in the absorption characteristics of the two resins were modeled by multivariate analysis for composition predictions, for the ABS/PC blends.

Results and Discussions

The ten spectra for each of the 11 samples comprised of 1201 absorbance values in the region from 1200 nm to 2400 nm. The averaged raw data for the 11 samples as shown in figure 8.3 was smoothed using Guided Wave Examiner program, and first derivatives of the average absorbance spectra and individual absorbance spectra were calculated. Slight variations in the absorbance spectra, such as baseline shifts were observed in the region from 1200 nm to 1600 nm. This non-reproducibility in the spectra can be attributed to sample inhomogeneity and immiscible nature of ABS/PC blends. The first derivative of the average absorbance spectra and individual absorbance spectra

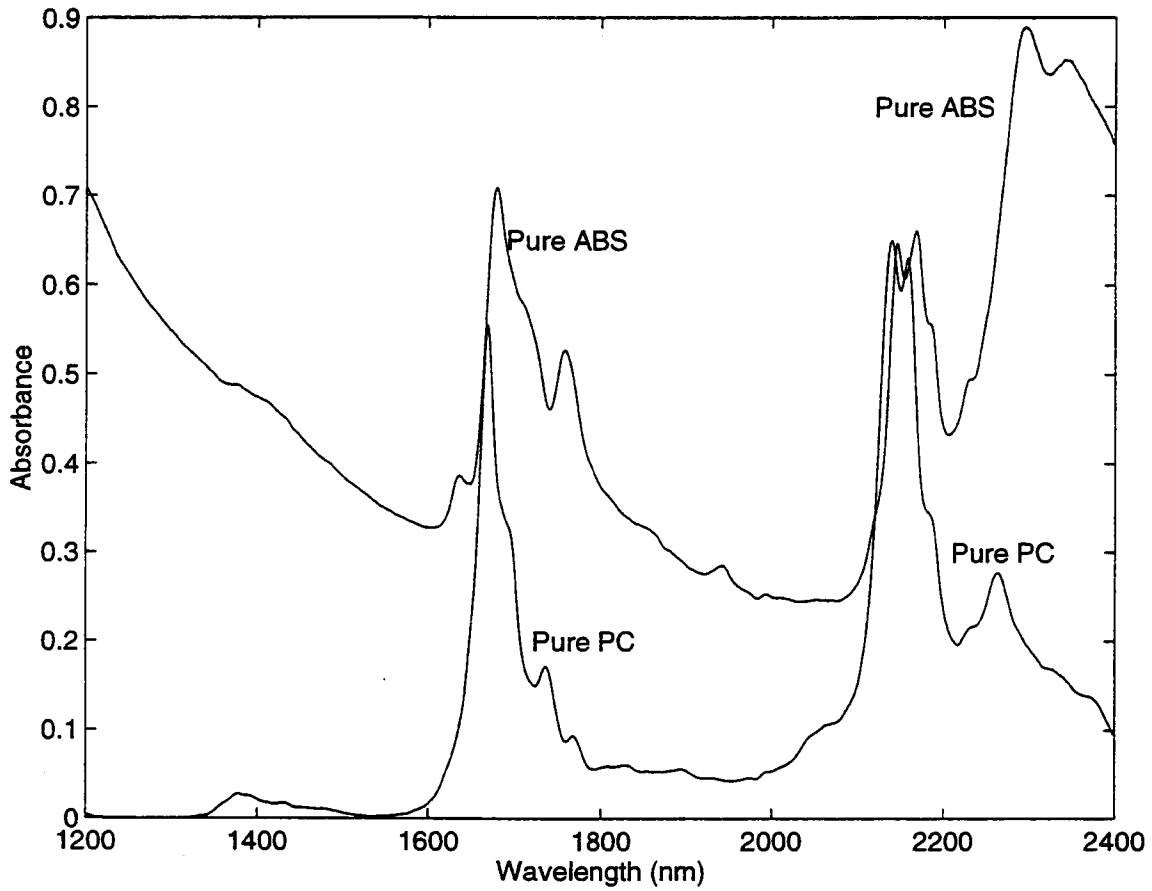


Figure 8.2 Overlaid NIR absorbance spectra (averaged raw data) of pure PC and pure ABS in the region from 1200 nm to 2400 nm @ 260 ^{o}C.

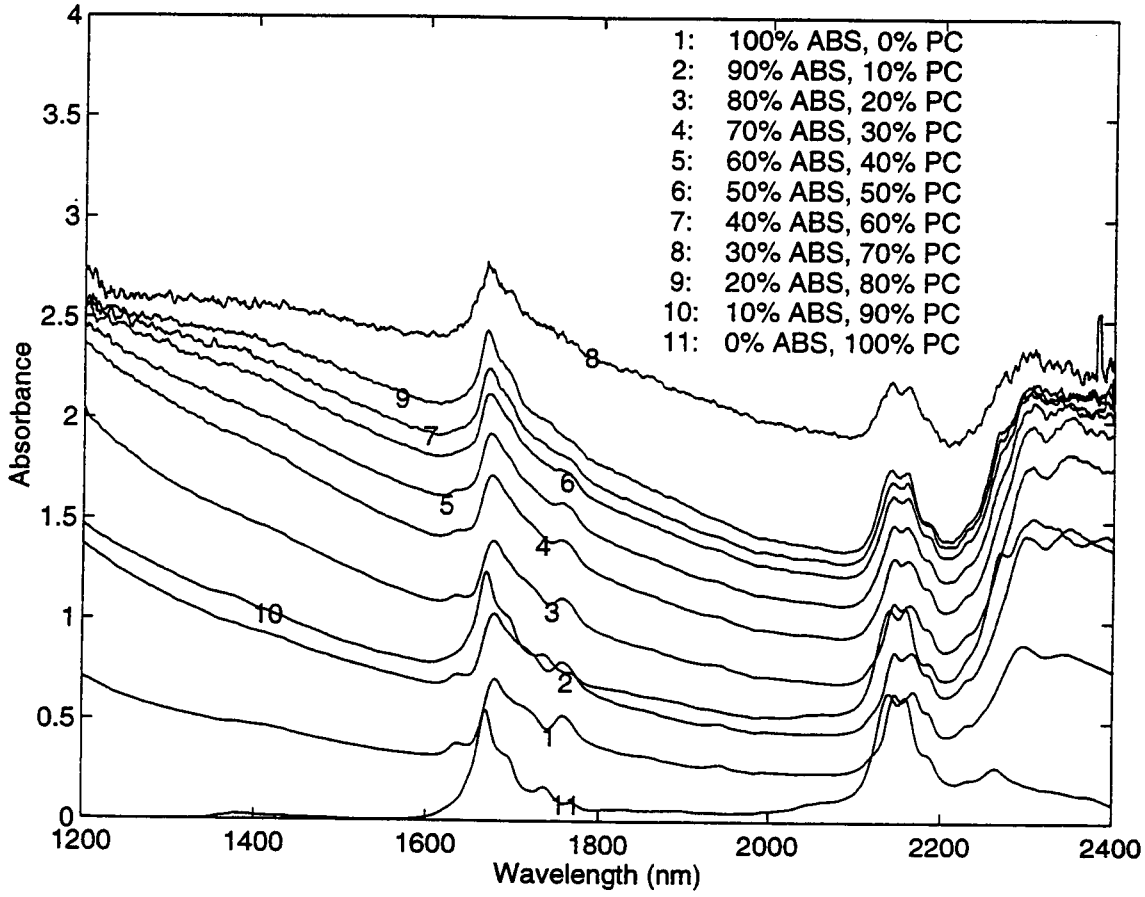


Figure 8.3 Overlaid NIR absorbance spectra (averaged raw data) for each of the ABS/PC blend compositions in the region from 1200 nm to 2400 nm @ 260 °C.

was smoothed further, before multivariate data analysis was performed. The effect of the baseline shifts was minimized by taking the first derivative of the spectra.

Figure 8.4 shows the variance in absorbance for the averaged raw data for the ABS/PC blends in the region from 1200 nm to 2400 nm. The variance in absorbance is highest at 1200 nm indicating that the scattering is maximum near the left end of the spectra.

The 110 first derivative spectra of absorbances (ten for each blend composition) were then examined for non-representative spectra and outliers. Sixty-two derivative spectra were selected for the quantitative analysis. Six representative derivative spectra were chosen for blends with compositions varying from 0-50 wt. % PC and from 80-100 wt. % PC. Four representative spectra were chosen for samples with 60-70 wt. % PC, as there was a lot of noise present in the raw data for these blend concentrations and several spectra could not be used in the data analysis.

The first derivative of the average absorbance spectrum for each of the 11 samples, were used in the calibration step, to account for the spectral variability due to sample inhomogeneity, scattering, and immiscibility of the ABS/PC blends. Therefore in all, 11 first derivatives of the average absorbance spectra constituted the calibration set. The validation or test set consisted of the 62 spectra, selected for quantitative analysis.

Two regions in the spectra for the ABS/PC blends were chosen for the quantitative analysis. Wavelengths from 1600 nm to 1800 nm in the overtone region and wavelengths from 2050 nm to 2200 nm in the combination region were selected for

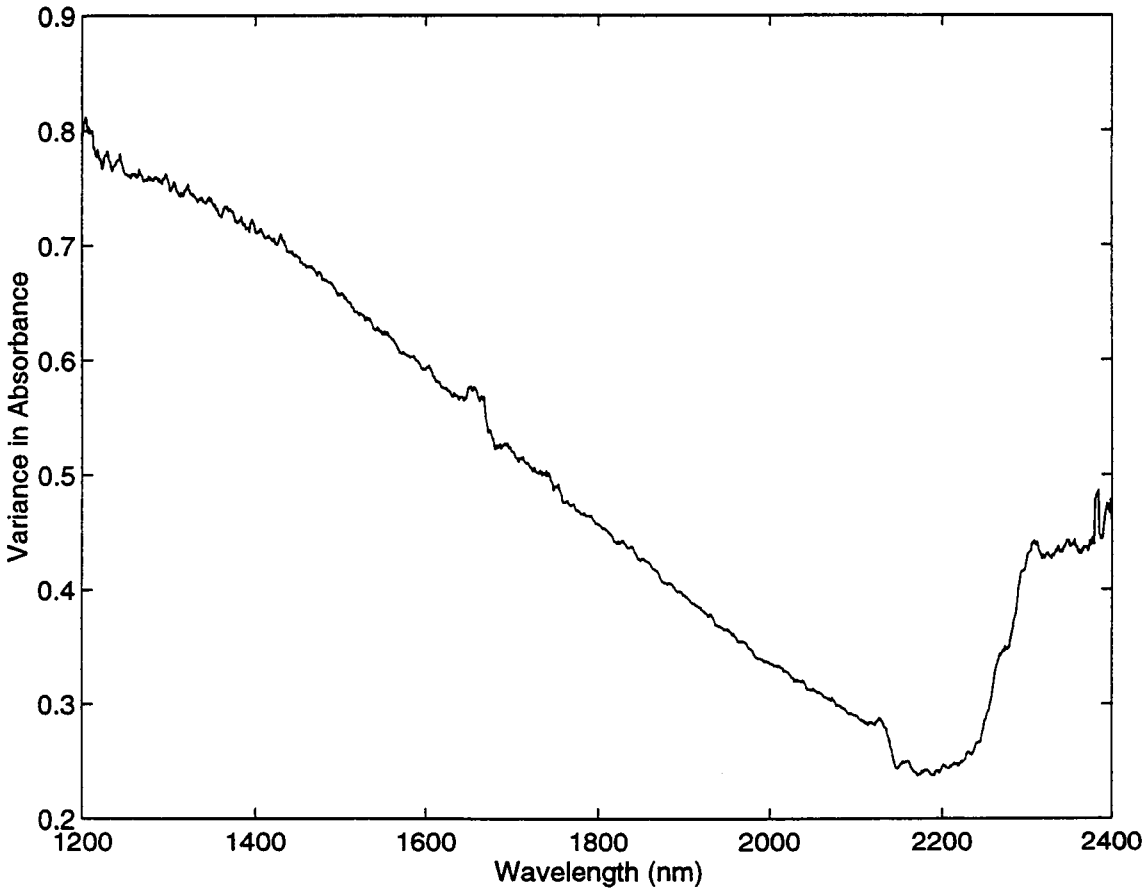


Figure 8.4 Plot of variance in absorbance vs. wavelength for the ABS/PC blend compositions (averaged raw data) in the region from 1200 nm to 2400 nm @ 260 ^{o}C.

calibration and predictions using PLS and PCR. These regions were selected based on the systematic variation in absorbance values with changes in compositions in the ABS/PC blends. Figure 8.5 shows the average first derivative spectra for the 11 samples, overlaid in the overtone region from 1600 nm to 1800 nm. The overlaid average first derivative spectra for the 11 samples, in the combination region from 2050 nm to 2200 nm is shown in figure 8.6. Regions with spectral changes due to increasing wt. % PC in the samples are marked in figures 8.5 and 8.6.

The absorbance data was stored in the X matrix and the corresponding compositional data was stored in the Y matrix. The data was mean centered by subtracting the column mean from each of the elements in the columns of X and Y. The mean centered data was scaled by normalizing each column with respect to the column standard deviation, in order to have unit variance to each variable in X and Y. The mean centered and scaled data was then used for building the calibration models, and then validating them using PLS, and PCR.

In the analysis of the overtone region, the percent variances in X and Y data sets, explainable by the PLS and PCR models, for increasing number of factors is presented in table 8.1. For the PLS model, the first factor accounts for 89.05 % of the total X-block variance, followed by 4.72 % and 5.63 % of the total variance accounted by the second and third factors, respectively. The percent explained variance of the 201 wavelengths corresponding to the wavelenths from 1600 nm to 1800 nm, for the first and second factor is shown in figure 8.7 (a) and 8.7 (b), respectively.

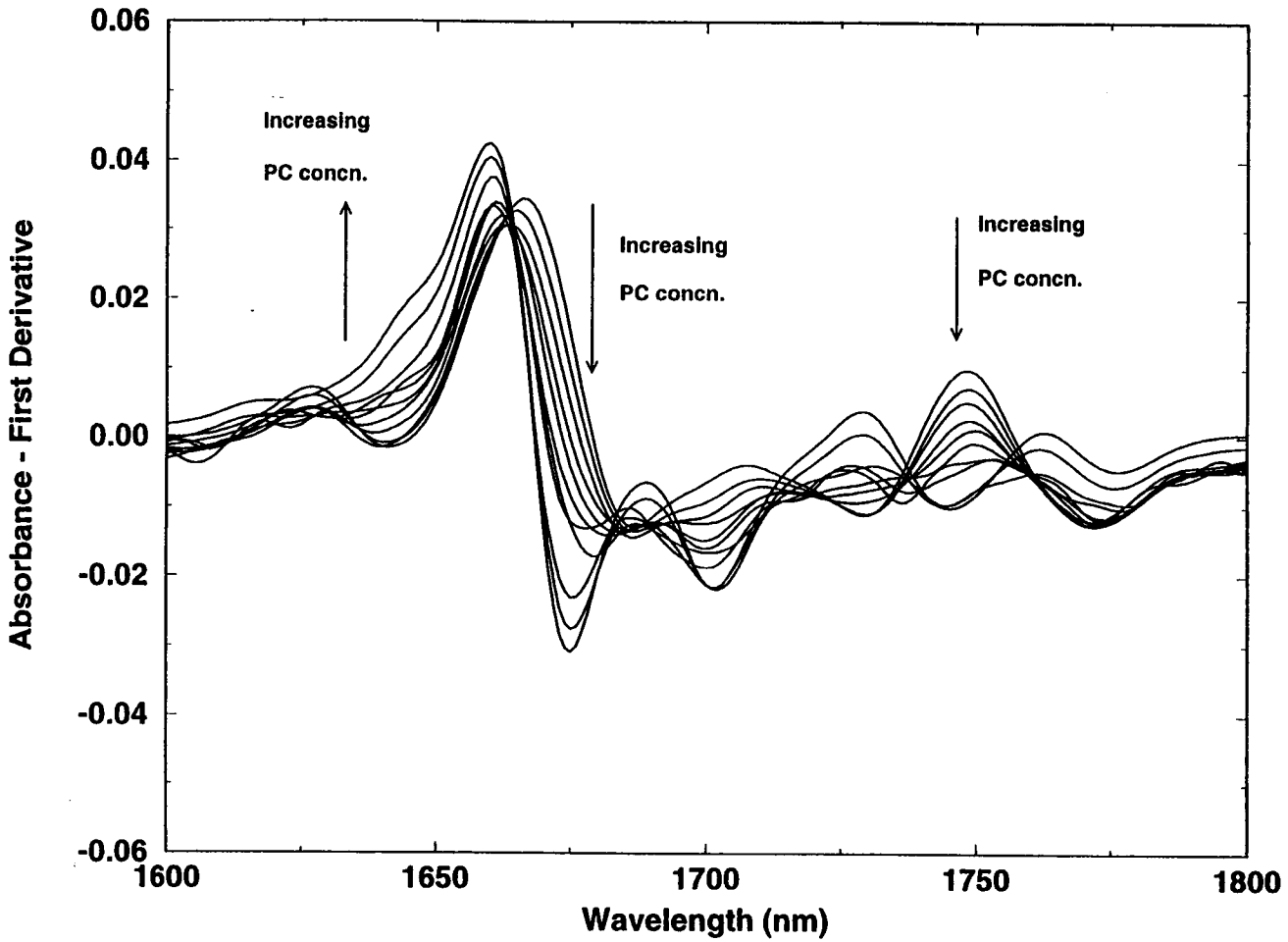


Figure 8.5 Overlaid first derivative NIR absorbance spectra for each of the ABS/PC blends compositions in the overtone region from 1600 nm to 1800 nm.

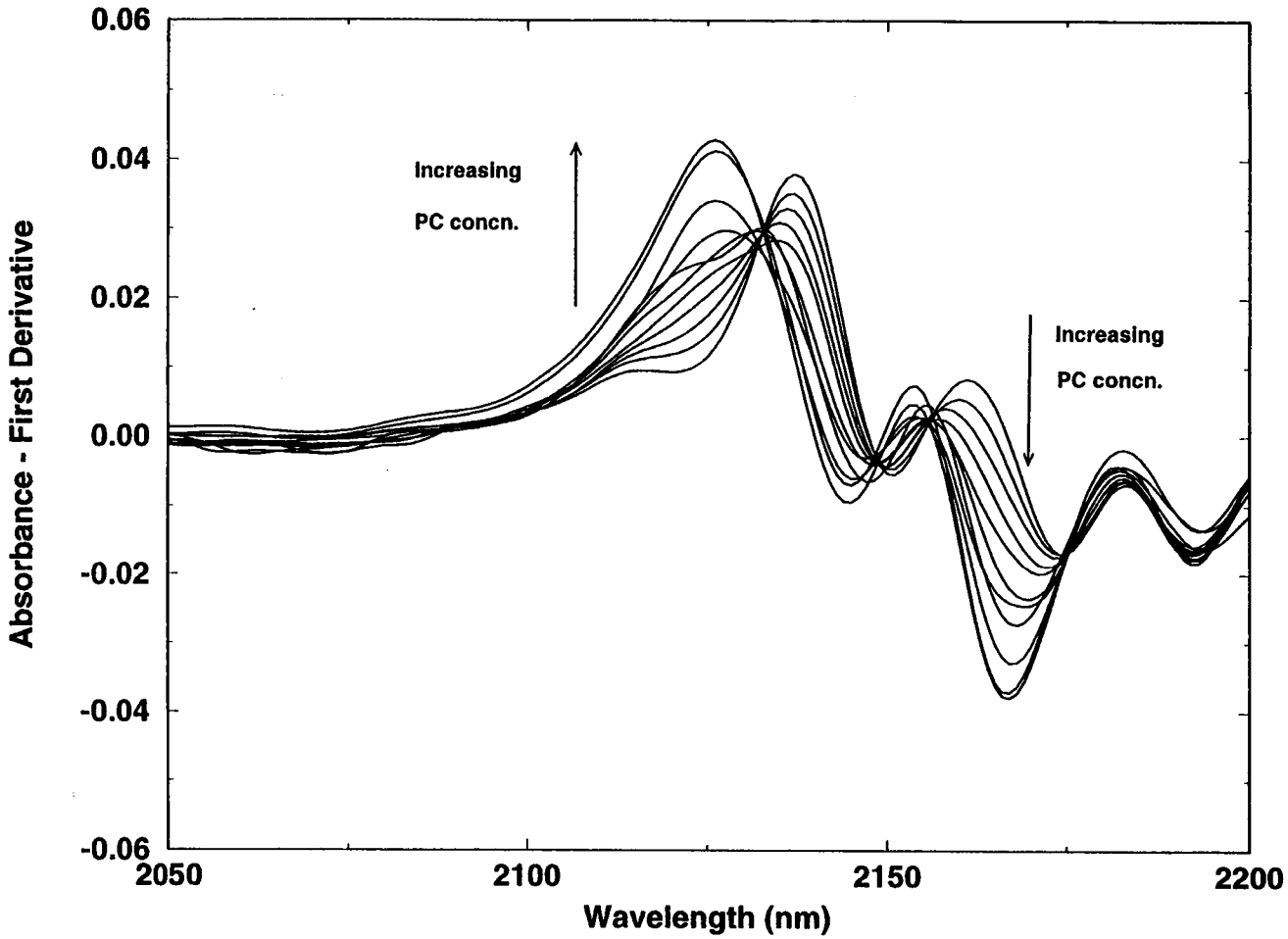


Figure 8.6 Overlaid first derivative NIR absorbance spectra for each of the ABS/PC blend compositions in the combination region from 2050 nm to 2200 nm.

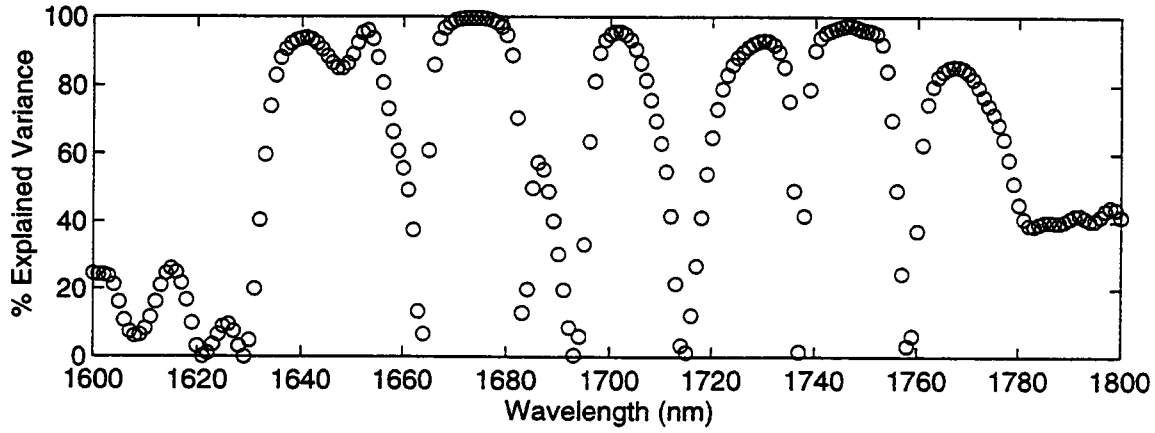
Table 8.1 Percent variances explained by the PLS and PCR models for increasing number of factors in the analysis of the overtone region (1600 nm to 1800 nm) for ABS/PC blends.

PLS

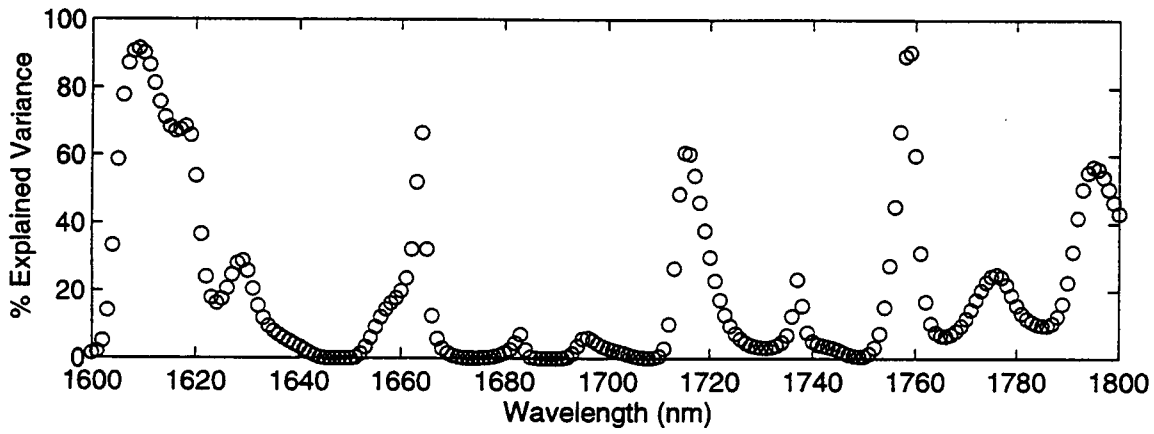
	X-Block (% variance)		Y-Block (% variance)	
Factor	By this Factor	Total	By this Factor	Total
1	89.05	89.05	99.85	99.85
2	4.72	93.77	0.13	99.98
3	5.63	99.40	0.00	99.98
4	0.25	99.65	0.01	99.99
5	0.12	99.77	0.01	99.99

PCR

	X-Block (% variance)		Y-Block (% variance)	
Factor	By this Factor	Total	By this Factor	Total
1	89.05	89.05	99.84	99.84
2	5.90	94.95	0.02	99.85
3	4.48	99.43	0.13	99.98
4	0.25	99.68	0.00	99.98
5	0.14	99.83	0.00	99.98



(a) Variances explained by wavelengths after first factor only



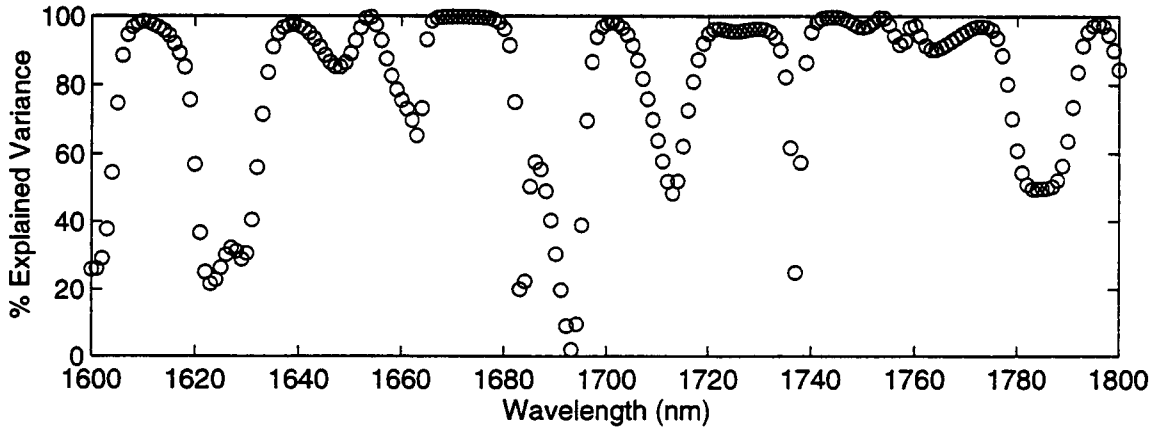
(b) Variances explained by wavelengths after second factor only

Figure 8.7 Variances explained by the wavelengths after considering, (a) First factor only, (b) Second factor only, for the ABS/PC blends in the region from 1600 nm to 1800 nm.

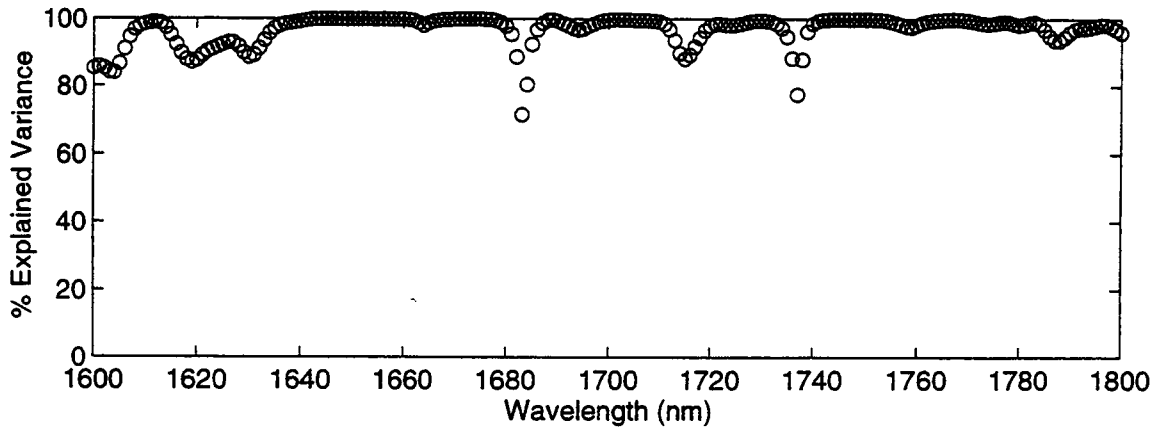
Most of the variance of the variables was explained by the first factor, although some variables required additional factors to explain their variance. As seen in figure 8.7, variances of certain wavelengths from 1600 nm to 1632 nm and from 1780 nm to 1800 nm were explained by additional factors. Intensities at these wavelengths did not exhibit significant spectral variations with concentration changes in wt. % PC (as seen in figure 8.5), indicating that factors other than the first factor, did not account for varying PC concentrations in the ABS/PC blends. The overall percentage of the explained variance, considering the first two factors can be seen in figure 8.8 (a). Figure 8.8 (b) shows the overall percentage of the explained variance, considering the first three factors.

Cross-validation was used to estimate the prediction errors and determine the optimal number of factors to be used in the calibration models. Cross-validation was carried out using the LAG and LAS approaches [2]. The LAS approach involved removing one of the spectra from the calibration set, carrying out the calibration with the remaining spectra and then using the model to predict the concentration of the sample corresponding to the left out spectrum. This procedure was repeated for the 11 spectra in the calibration set corresponding to the samples from 0 wt. % PC to 100 wt. % PC. The prediction errors for the sample with 70 wt. % PC were found to be the highest. Figure 8.3 shows that the spectra for this concentration has maximum noise and scattering among all the samples.

The LAG approach involved removing the spectra for 20 and 40 wt. % PC from the calibration set, and using the remaining samples to predict their concentrations. This procedure was then repeated to predict the concentrations for the samples with 30 and 50 wt. % PC using the remaining blends. The spectra for pure ABS and PC were included in



(a) Variances explained by wavelengths after first and second factors



(b) Varaiances explained by wavelengths after first, second and third factors

Figure 8.8 Overall variances explained by the wavelengths after considering, (a) First two factors, (b) First three factors for the ABS/PC blends in the region from 1600 nm to 1800 nm.

the LAG approach, as the prediction errors for the extreme concentrations, were found to be higher compared to the intermediate concentrations for the ABS/PC blends. PRESS values by LAS and LAG were calculated at each factor. The PRESS values for the LAS and LAG for increasing factors are plotted in figure 8.9. The average PRESS values were found to be minimum at 2 factors for both the LAS and LAG cross-validation approaches using PLS.

The model was further tested against the validation or test set to establish its accuracy and robustness. The SEP and SEC values for the test and calibration set, respectively with increasing factors are plotted in figure 8.10. SEC of 0.49 % and SEP of 3.00 % were obtained for 2 factors in the validation step using PLS. The SEP was found to be minimum at 2 factors using PLS. This observation was in agreement with the cross-validation results. It was concluded that 2 factors explain the variation in the ABS/PC blends. The model predictions for the calibration and validation set for 2 factors using PLS are plotted against the actual concentrations in figures 8.11 and figure 8.12, respectively.

The loadings, which give the relationship between the variables in the data that make up each principal component are plotted for the first and second factors in figure 8.13. The loadings for a factor give the contributions of the variables in making up that factor. The loadings for a factor, also help distinguish the positive and negative correlations among the variables in the analysis of the first derivative absorbance spectra for the ABS/PC blends. The first factor loadings were seen to decrease around 1670 nm, which is in agreement with the decrease in the first derivative absorbance around 1670 nm, with increasing wt. % PC (as seen in figure 8.5) for the ABS/PC blends. Negative

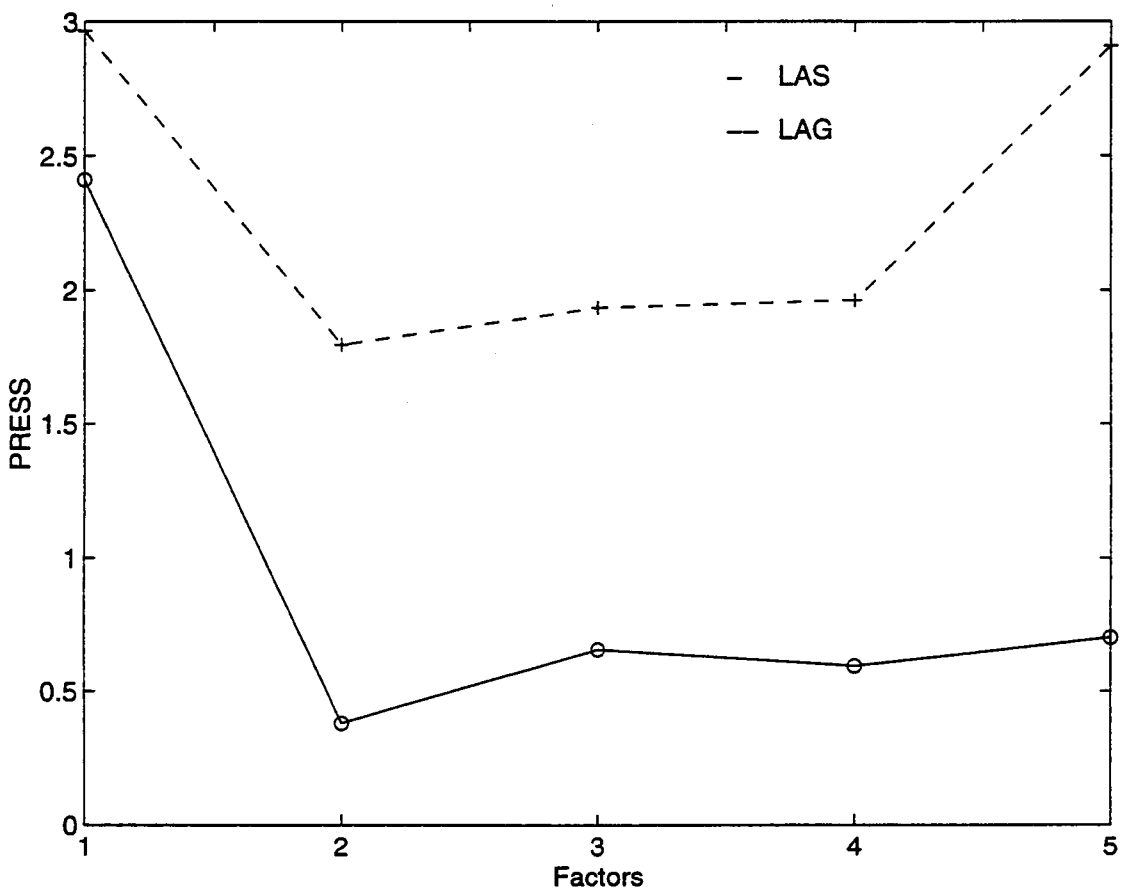


Figure 8.9 PRESS values for leave-a-sample (LAS) and leave-a-group (LAG) cross-validation methods using PLS, for the ABS/PC blends in the overtone region from 1600 nm to 1800 nm.

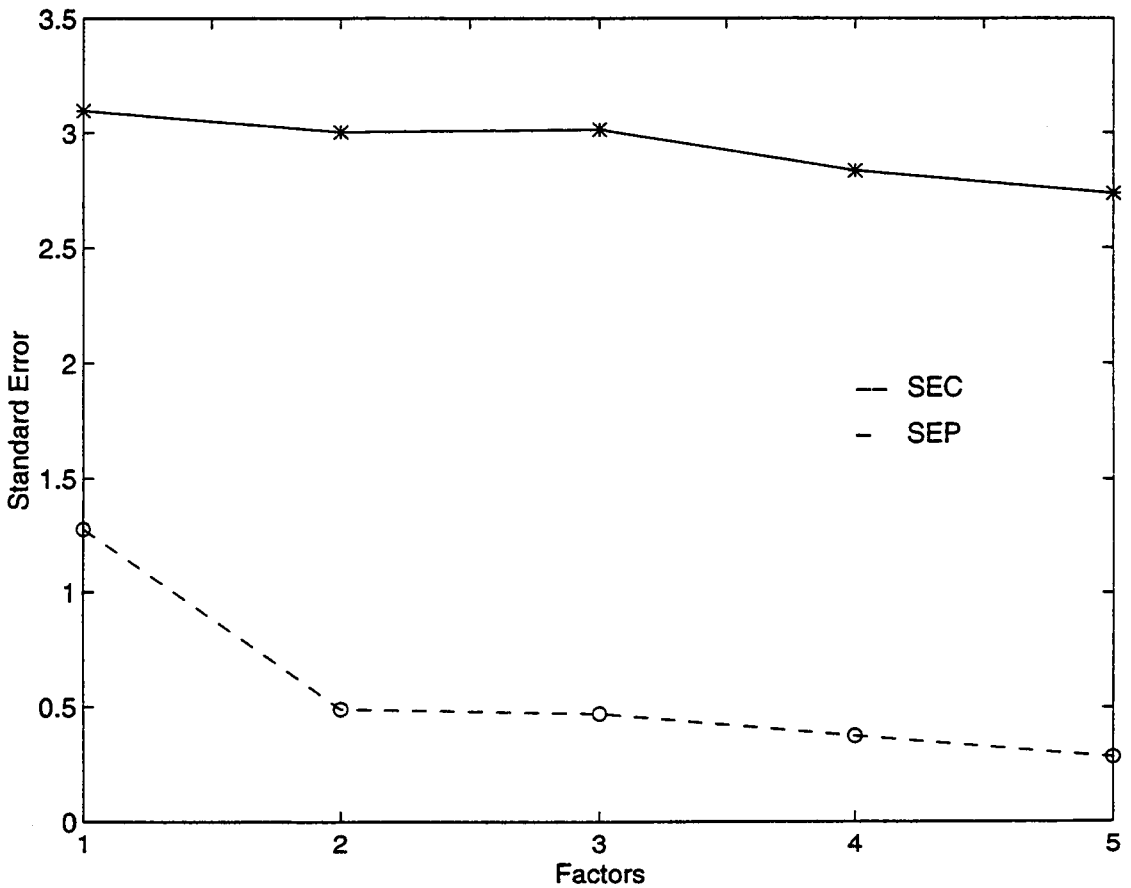


Figure 8.10 Plot of SEC and SEP for calibration and validation sets, respectively, for increasing number of factors using PLS, for the ABS/PC blends in the overtone region from 1600 nm to 1800 nm.

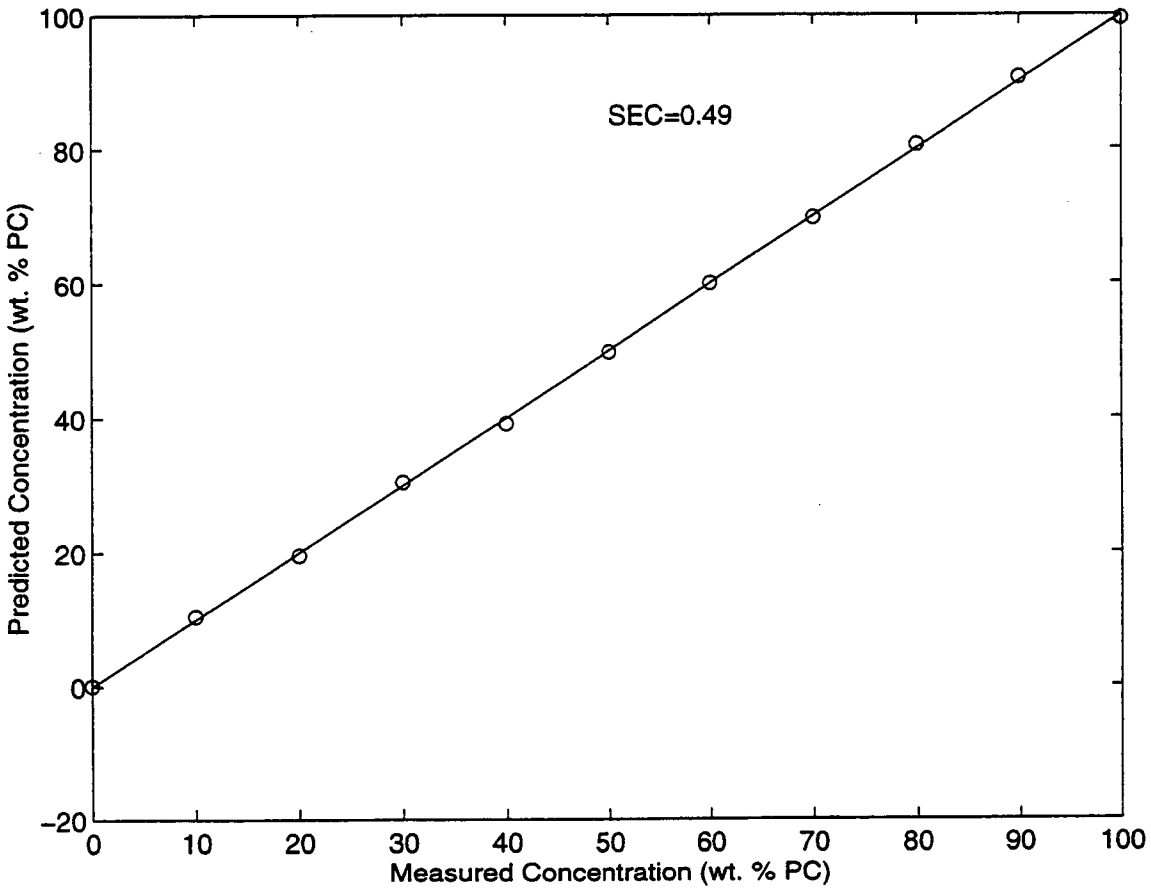


Figure 8.11 Model predictions for the calibration set (based on first derivative absorbance data) using PLS, plotted against the reference (actual) concentrations for the ABS/PC blends in the region from 1600 nm to 1800 nm.

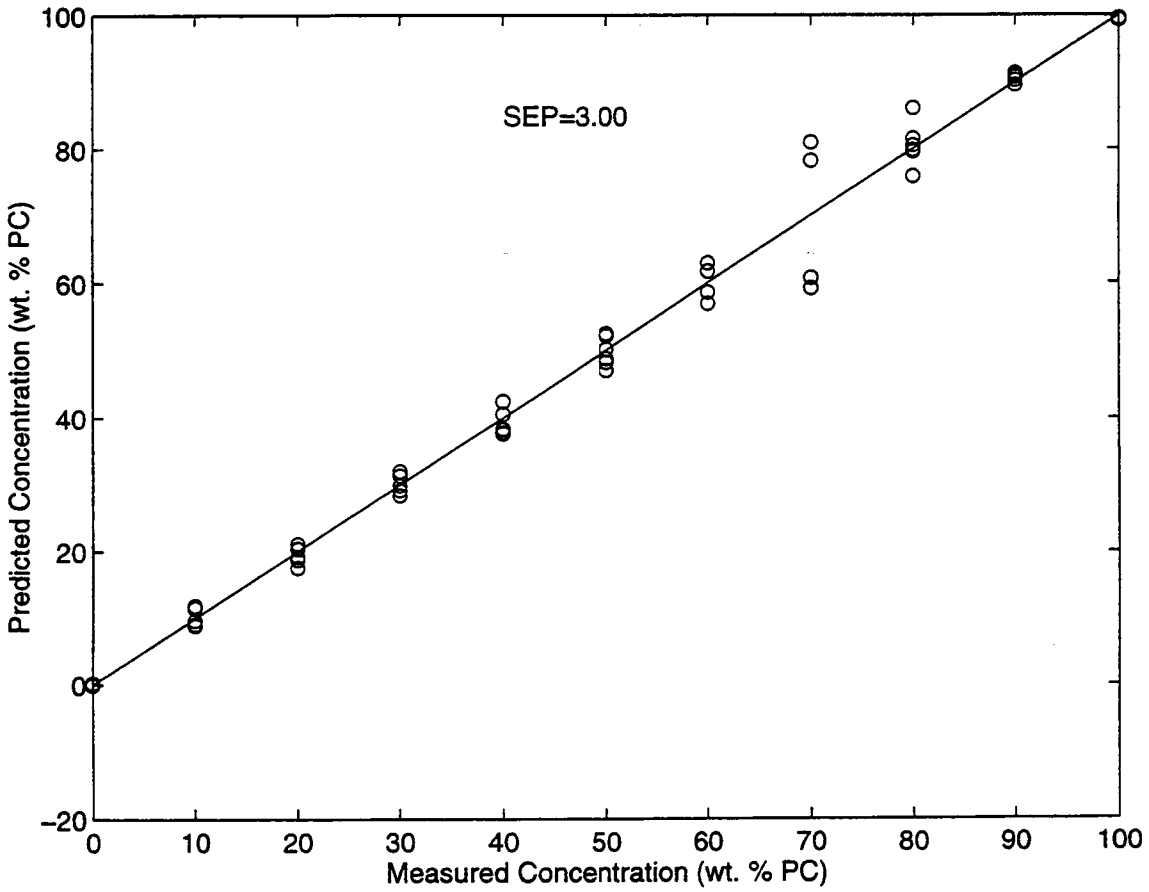


Figure 8.12 Model predictions for the validation set (based on first derivative absorbance data) using PLS, plotted against the reference (actual) concentrations for the ABS/PC blends in the region from 1600 nm to 1800 nm.

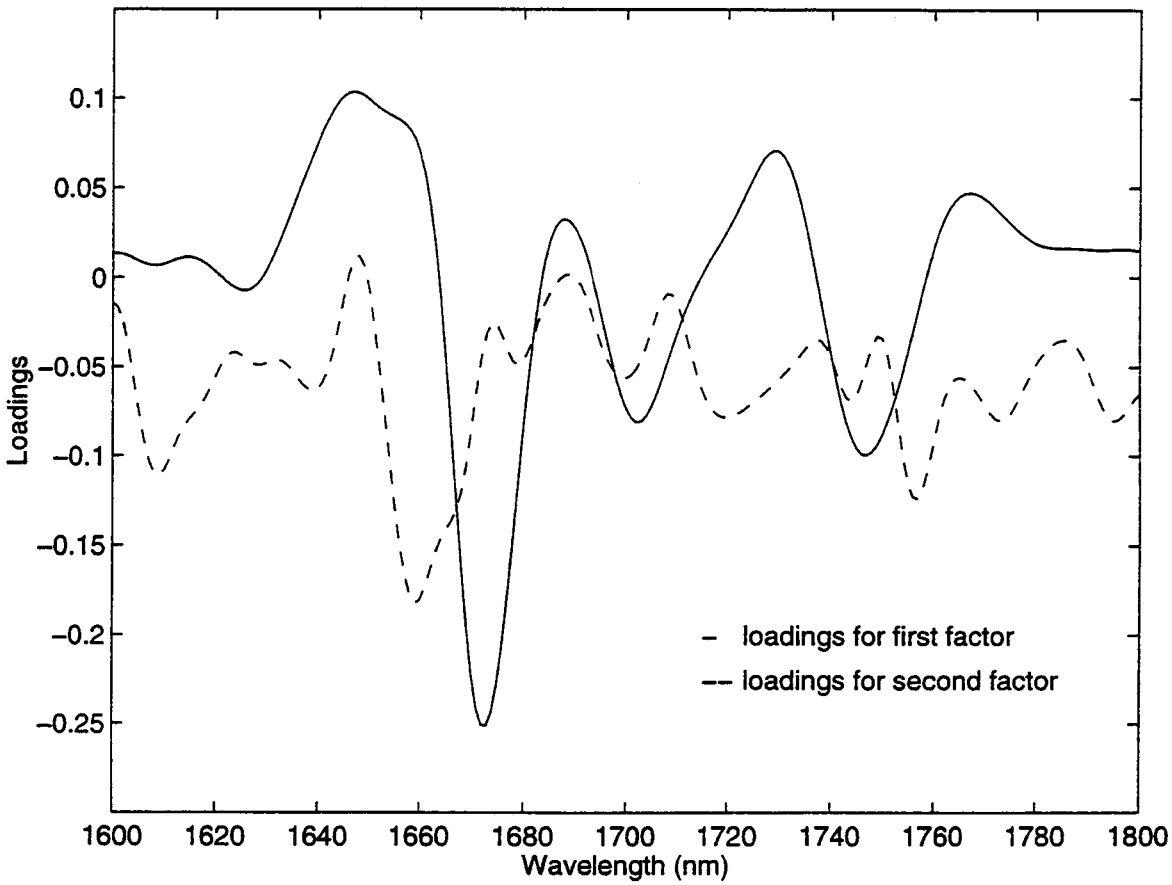


Figure 8.13 Loadings plot for first and second factors for samples in the calibration set (based on first derivative absorbance data) using PLS, for ABS/PC blends in the overtone region from 1600 nm to 1800 nm.

correlations in the first factor loadings are seen at 1740 nm. This trend can also be observed in the first derivative absorbance spectra (as seen in figure 8.5), with a decrease in the first derivative absorbance values at 1745 nm, with increasing wt. % PC. Figure 8.13 also indicates that the first factor loadings represent the "mean" or average spectral variations for first derivative absorbance, with changes in wt. % PC in the ABS/PC blends.

The scores, which give the relationship between the spectra in the data set are plotted for the first and second factors in figure 8.14. Scores for the first factor show a step increase with increasing ABS concentration. Trend in second factor scores was not as regular as the variation observed for the first factor scores. Plot of scores for the first factor vs. the scores for the second factor is given in figure 8.15. The scores plots provide a better understanding of the spatial distribution of scores in the principal component space. It can also be seen in figure 8.15, that the second factor scores increase with increasing wt. % PC till the sample with 70 wt. % PC and then decrease. This trend is similar to the scattering and baseline shifts observed in figure 8.3.

It can be suggested that as there is only one independent factor of variation (wt. % PC in the samples) in the ABS/PC samples, the additional second factor could be due to non-linearities, sample inhomogeneities, and scattering due to the rubber particles in ABS. An additional factor has to be included in the model as the prediction errors are greater if only one factor is considered. The SEC and SEP values confirm that the second factor cannot be disregarded in the multivariate analysis. This observation suggests that the variance explained by the second factor for the calibration set is similar to the variance in

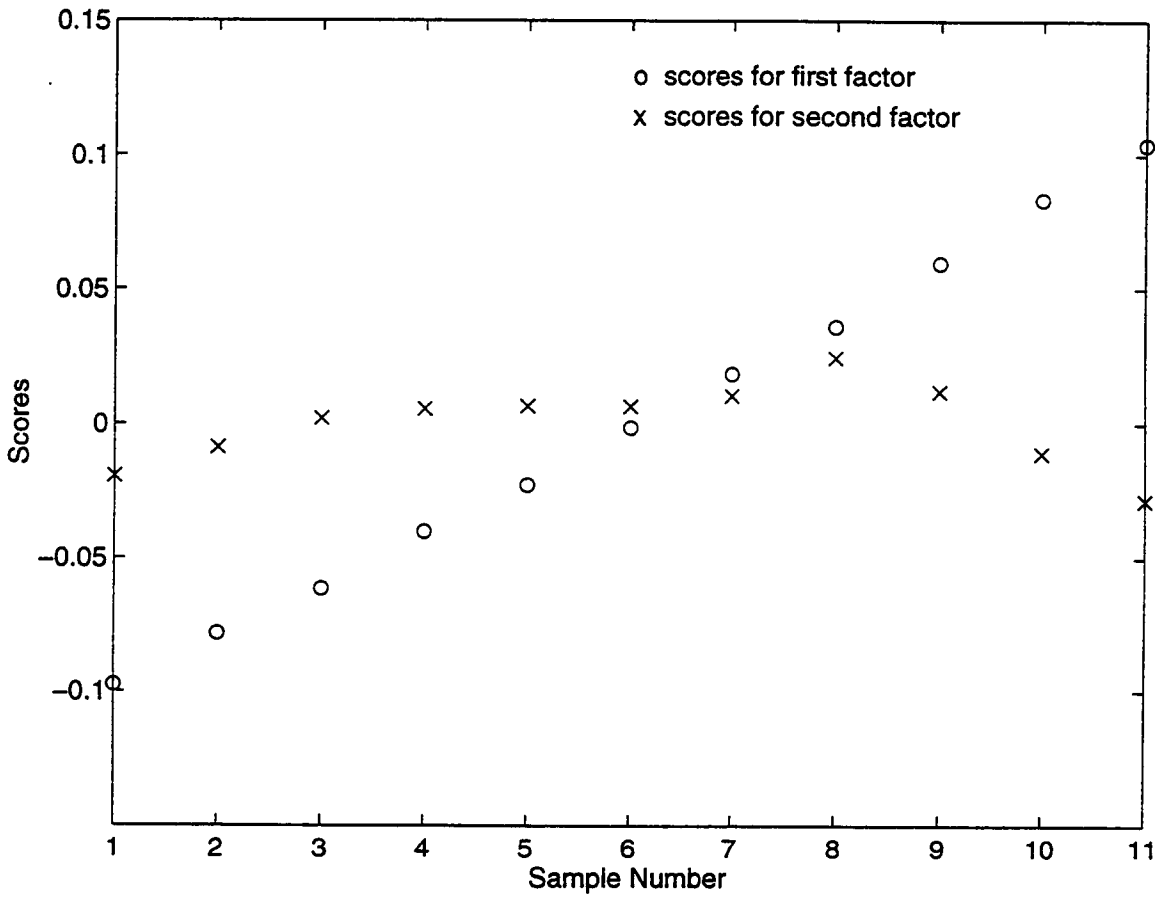


Figure 8.14 First and second factor scores for samples in the calibration set (based on first derivative absorbance data) for the ABS/PC blends using PLS, in the region from 1600 nm to 1800 nm.

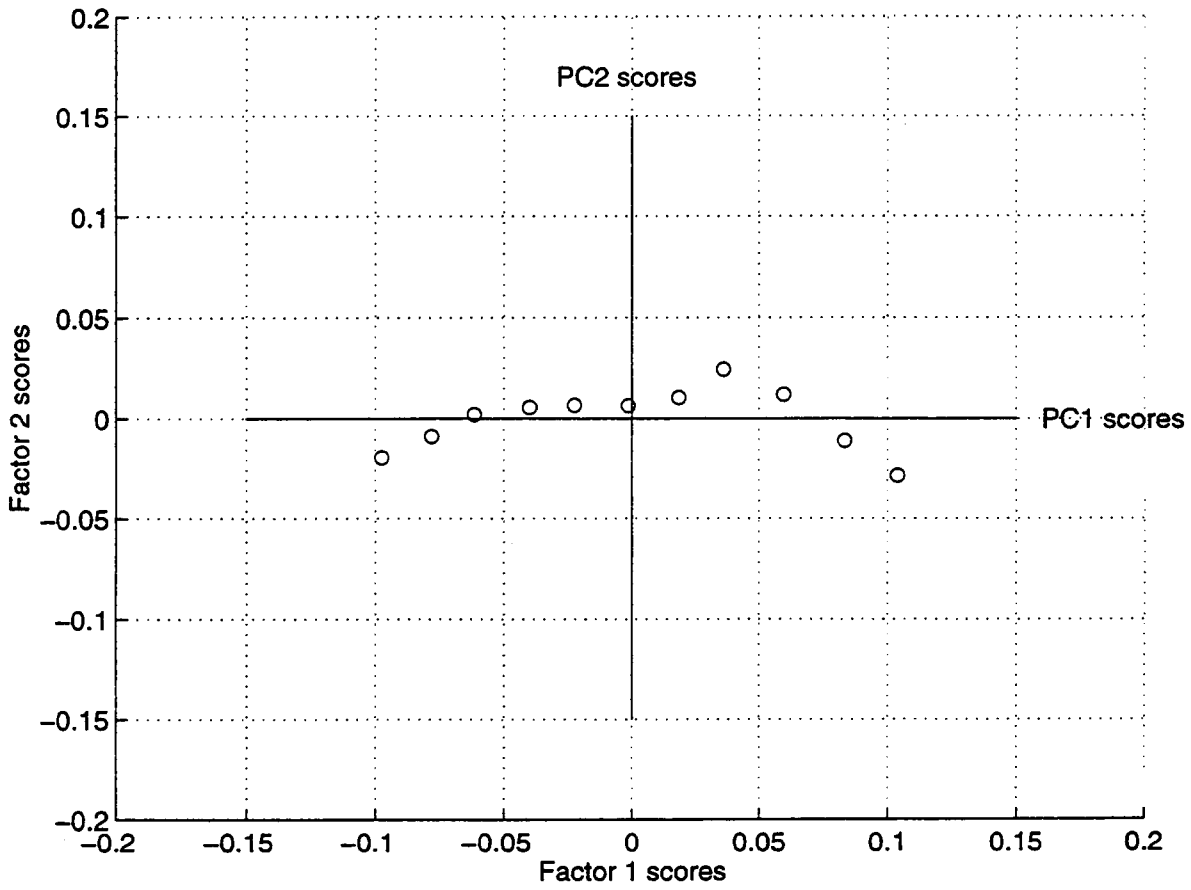


Figure 8.15 First factor vs second factor scores for samples in the calibration set, for the ABS/PC blends using PLS in the overtone region from 1600 nm to 1800 nm.

the test set, and the second factor should be incorporated in the model for low SEP values.

A similar analysis was performed in the combination region from 2050 nm to 2200 nm. This region also gave 2 factors of variation using PLS as a result of cross-validation and validation by the test set. The comparison of the SEC and SEP values from the two regions by PLS and PCR are presented in table 8.2.

A full spectrum analysis of the spectral data in the range from 1200 nm to 2400 nm was also performed. This spectral variation in this region was also accounted for by 2 factors. Table 8.3 gives the explained variance for the full spectrum analysis using PLS and PCR. The scores plot for the full spectral analysis (1200 nm to 2400 nm), for the samples in the calibration set is given in figure 8.16. The scores plot shows that the trend for increasing first factor scores with increasing wt. % PC as observed in figure 8.14 is present, although the increase in scores is not as regular as observed for the overtone region. This implies that the entire spectrum is not the best choice for composition predictions.

The second factor scores for the entire spectral region seen in figure 8.16 are also greater compared to the second factor scores for the overtone region, as seen in figure 8.14. Nonlinearities, sample inhomogeneities, and scattering effects which are more pronounced in the region from 1200 nm to 2400 nm, are exhibited by an increase in second factor scores. The above discussion shows that the full spectral analysis is not the ideal choice for composition predictions of unknown samples. Comparison of the SEC and SEP values for the full spectrum analysis by PLS and PCR is given in table 8.4.

Table 8.2 Comparison of calibration and prediction errors using PLS and PCR in the overtone and combination regions for ABS/PC blends.

PLS

	Overtone Region (1600 nm to 1800 nm)		Combination Region (2050 nm to 2200 nm)	
Factor	SEC	SEP	SEC	SEP
1	1.28	3.01	4.62	4.55
2	0.49	3.00	1.59	2.82
3	0.47	3.01	0.67	2.83
4	0.38	2.84	0.38	2.83
5	0.28	2.74	0.31	2.97

PCR

	Overtone Region (1600 nm to 1800 nm)		Combination Region (2050 nm to 2200 nm)	
Factor	SEC	SEP	SEC	SEP
1	1.34	3.11	5.07	4.88
2	1.27	3.04	1.78	2.91
3	0.48	3.03	0.80	2.85
4	0.45	2.95	0.79	2.83
5	0.42	2.93	0.55	2.68

Table 8.3 Percent variances explained by the PLS and PCR models for increasing number of factors in the full spectrum analysis (1200 nm to 2400 nm) for ABS/PC blends.

PLS

	X-Block (% variance)		Y-Block (% variance)	
Factor	By this Factor	Total	By this Factor	Total
1	50.21	50.21	96.57	96.57
2	19.28	69.49	2.39	98.96
3	8.76	78.25	0.63	99.59
4	6.09	84.34	0.36	99.94
5	9.72	94.07	0.28	99.97

PCR

	X-Block (% variance)		Y-Block (% variance)	
Factor	By this Factor	Total	By this Factor	Total
1	50.47	50.47	93.17	93.17
2	19.87	70.34	4.67	97.83
3	12.20	82.54	0.34	98.18
4	9.98	92.53	0.42	98.60
5	2.94	95.47	0.81	99.41

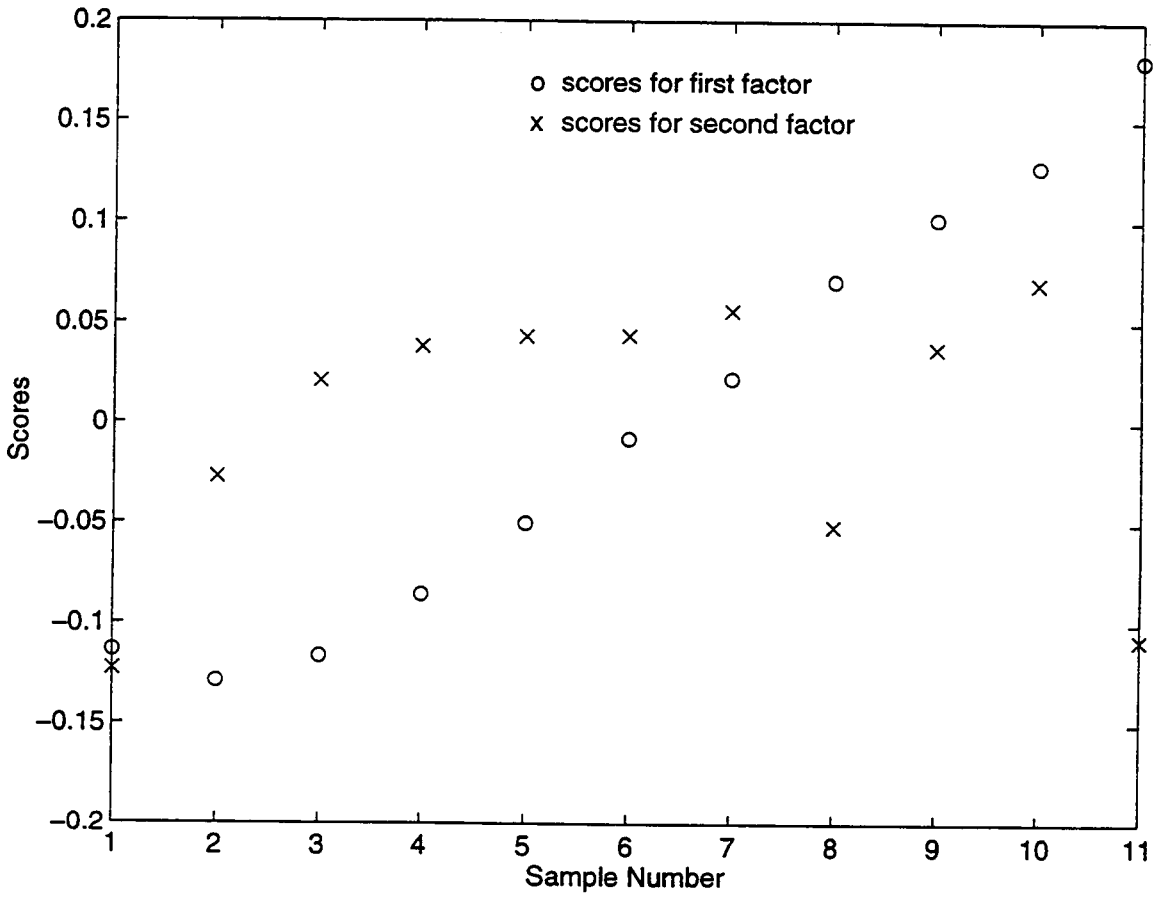


Figure 8.16 Scores plot for first and second factors for full spectral analysis (based on first derivative absorbance data) using PLS in the region from 1200 nm to 2400 nm for samples in the calibration set, for ABS/PC blends.

Table 8.4 Comparison of calibration and prediction errors using PLS and PCR in the region from 1200 nm to 2400 nm for ABS/PC blends.

	PLS		PCR	
Factor	SEC	SEP	SEC	SEP
1	6.14	6.99	8.67	9.26
2	3.39	4.58	4.88	5.39
3	2.14	4.89	4.48	6.06
4	0.81	3.97	3.92	5.14
5	0.59	4.14	2.55	5.23

Figure 8.17 shows the difference in absorbance for the ABS/PC blends from 10 to 90 % compared to the absorbance of an ideal blend, based on the absorbances of pure ABS and pure PC in the region from 1200 nm to 2400 nm. E.g. the difference spectra for a blend containing X % PC and (100-X) % ABS can be given by:

$$\text{Diff. in Abs. (X \% PC)} = \text{Abs. (X \% PC)} - \text{Ideal Abs. (X \% PC)} \quad (8.1)$$

where:

$$\text{Ideal Abs. (X \% PC)} = [X\% \times (\text{Abs. pure PC}) + (100-X)\% \times (\text{Abs. pure ABS})] \quad (8.2)$$

The scattering and inhomogeniety effects were most pronounced for the sample with 70 wt. % PC. This trend can also be observed in figure 8.3.

Conclusions

It was established that in-line monitoring of molten polymers coupled with chemometric data analysis techniques can be successfully used for determining compositions in ABS/PC blends. Two regions that showed significant changes in absorption characteristics were selected for the analysis by PLS and PCR. Results from both regions indicated that there were two factors of variation in the NIR spectra for the ABS/PC blends even though there is only one known source of variation (wt. % PC).

Two factors were used in the development of the calibration models based on the SEC and SEP of 0.49 and 3.00 , respectively, using the PLS approach in the overtone region from 1600 nm to 1800 nm. Minimum SEP values obtained by PCR were slightly higher than the minimum SEP values obtained using PLS. The SEC and SEP values obtained by PLS and PCR suggest that PLS is more suited for the analysis as the

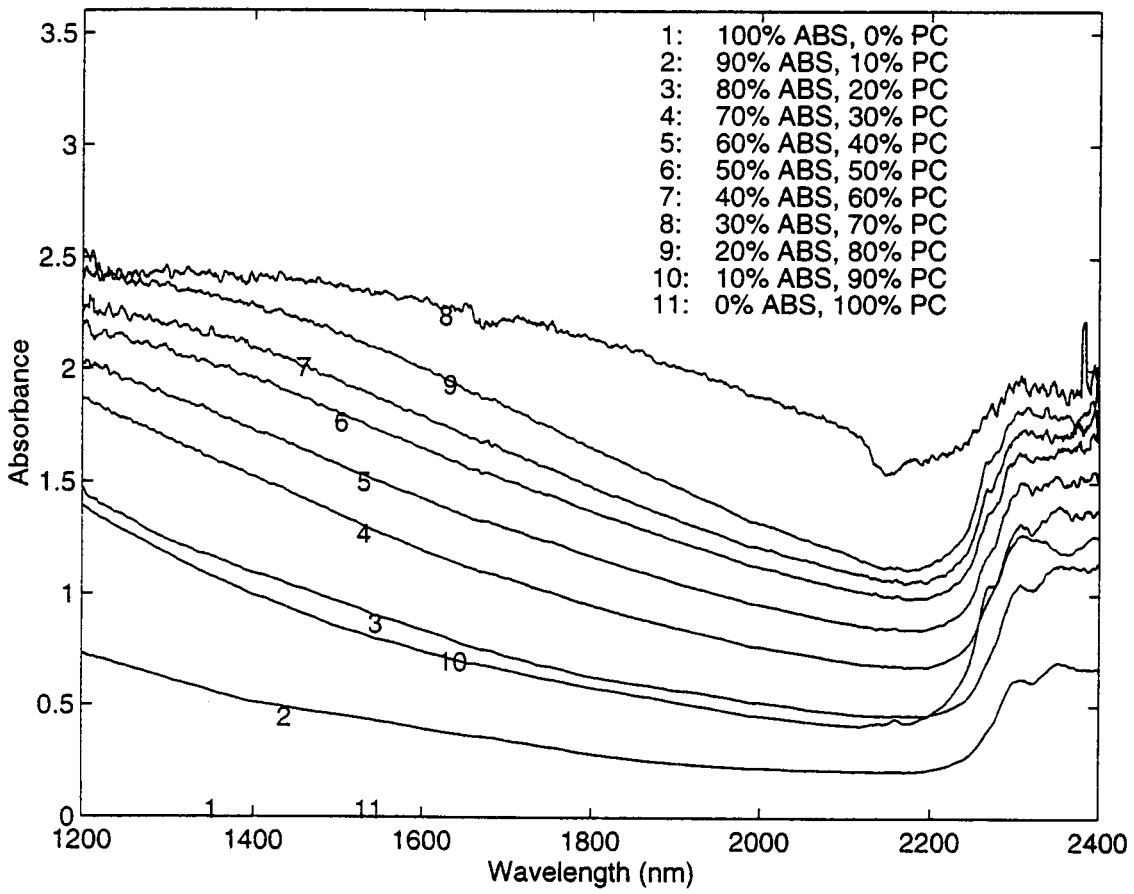


Figure 8.17 Difference in absorbance for the ABS/PC blends compared to the absorbance of an ideal blend of the same composition (based on the absorbances of pure ABS and pure PC), in the region from 1200 nm to 2400 nm.

prediction errors are relatively lower, suggesting that there is significant correlation between the NIR absorbances and concentrations, for the ABS/PC blends. A full spectrum analysis was also performed, but higher SEP values compared to the overtone and combination regions were recorded.

9. CONCLUSIONS AND FUTURE WORK

The results of this research indicate that NIR spectroscopy, combined with multivariate techniques can be successfully used for in-line composition analysis of partially miscible polymer blends. The potential of in-line monitoring of molten polymers by spectroscopic techniques for feedback process control was also demonstrated.

The studies on partially miscible blends of ABS/SAN, SAN/PC, and PC/ABS demonstrated that optical measurements could be made directly in the process stream using rugged fiberoptic probes. Of all the options discussed for process analysis, *in-situ* measurements offered several advantages in terms of speed, cost-effectiveness and accuracy. Rapid analysis in process environments which is extremely important for quality control and optimization, was demonstrated by in-line NIR transmission spectroscopy.

The use of chemometric techniques like PLS and PCR, to extract useful information from large sets of correlated data was also shown. These methods that are employed to distinguish between useful information and noise in the data were extensively used for developing calibration models, based on the NIR absorbance spectra and compositional data of representative samples. The calibration models were subsequently used for predicting compositions of unknown samples when their NIR absorbance spectra was known.

Studies on blends of ABS/SAN in the NIR region from 1200 nm to 2400 nm showed that the overtone region from 1600 nm to 1800 nm and the combination region from 2075 nm to 2215 nm exhibited significant changes in absorption characteristics. These two regions were analyzed by PLS and PCR, using cross-validation and test sets. Three factors were recorded even though there was only one known source of variation (wt. % ABS) in the blends. The additional factors were discussed to be due to scattering effects of the rubber particles in ABS, non-linearities, and sample inhomogeneities.

Loadings and scores plots provided an understanding about the relationship between the variables, and the calibration samples, respectively. SEC and SEP values of 0.83 and 1.34, respectively, (for eight spectra at each blend composition) were obtained using the PLS approach in the overtone region. PCR required an additional factor for minimum SEP values. A full spectrum analysis from 1200 nm to 2400 nm was also performed, but higher SEP values and more factors were recorded, compared to the overtone and combination regions.

A similar analysis was carried out for the partially miscible SAN/PC blends in the NIR region from 1200 nm to 2400 nm. The overtone region from 1600 nm to 1800 nm and the combination region from 2065 nm to 2185 nm, which exhibited significant changes in absorption characteristics, were chosen for analysis by PLS and PCR. First derivative absorbance spectra for these two regions were analyzed by PLS and PCR, using cross-validation and test sets. Three factors were recorded even though there was only one known source of variation (wt. % PC) in the blends. The additional factors were discussed to be due to partial miscibility, non-linearities, and sample inhomogeneities. SEC and SEP values of 0.65 and 1.75, respectively (for seven spectra at each blend

composition), were obtained using the PLS approach in the overtone region from 1600 nm to 1800 nm. PCR required additional factors for minimum SEP values. A full spectrum analysis from 1200 nm to 2400 nm was also performed, but higher SEP values and an additional factor was recorded, compared to the overtone and combination regions.

Studies on blends of PC/ABS in the NIR region from 1200 nm to 2400 nm were also performed. Although the raw data was relatively noisy compared to that of ABS/SAN and SAN/PC blends, smoothing of data, followed by taking first derivative of absorbance data indicated systematic spectral variations with composition changes, in the overtone region from 1600 nm to 1800 nm and from 2050 nm to 2200 nm in the combination region. PLS and PCR analysis in the two regions by cross-validation and validation by test sets resulted in two factors. Although there was only one known source of variation (wt. % PC), the second factor was discussed to be due to partial miscibility, inhomogeneity, non-linearity, and scattering effects. SEC and SEP values of 0.49 and 3.00, respectively, were obtained using the PLS approach in the overtone region from 1600 nm to 1800 nm. Higher SEP values were recorded for the full spectral analysis from 1200 nm to 2400 nm compared to the overtone and combination regions.

Experimentation and analysis of molten polymer blends of ABS/SAN, SAN/PC, and PC/ABS demonstrated that in-line monitoring coupled with multivariate analytical techniques is an extremely useful tool for composition monitoring of molten polymer blends in the process stream using fiber optics. Certain degree of inconsistency could be due to the polymer samples in the form of pellets, resulting in inhomogeneous samples even after mixing, and due to the partial solubility of the polymer blends. This

inconsistency could be minimized by using samples of uniform compositions, and by measuring the actual extrudate composition by off-line analysis.

Future directions in this area include in-line monitoring of the partially miscible molten polymer blends in real-time, followed by process control. Feedback process control can result in improved product quality, reduction in waste, and improved profitability. Use of a twin screw extruder for polymer processing of partially miscible blends can provide better results compared to the single screw extruder, due to better mixing in the twin screw extruder. Unlike conventional dispersion type devices, high-speed scanning and faster instruments for NIR analysis, such as, Fourier transform-near infrared (FT-NIR), and acousto-optical-tunable-filter (AOTF) instruments can also provide numerous applications for real-time monitoring of molten polymers.

REFERENCES

1. Williams, S. & McPeters, H. L. in *Making Light Work: Adv. Near Infrared Spectrosc., Int. Conf. Near Infrared Spectrosc.* (eds Murray, I. & Cowe, I.A.) 544-553 (1992).

2. Hansen, M. G. & Khettry, A. *Polymer Engineering and Science* **34**, 1758-1766 (1994).

3. McClure, W. F. *Analytical Chemistry* **66**, 43A-53A (1994).

4. Burns, D. A. & Margoshes, M. in *Handbook of NIR Analysis* (eds Burns, D.A. & Ciurczak, E.W.) 1-5 (1992).

5. Ciuczak, E. W. in *Handbook of NIR Analysis* (eds Burns, D.A. & Ciurczak, E.W.) 7-11 (1992).

6. Weyer, L. G. *Applied Spectroscopy Reviews* **21**, 1-43 (1985).

7. Stark, E. W., Luchter, K. & Margoshes, M. *Applied Spectroscopy Reviews* **22**, 336-399 (1986).

8. Dialey, W. V. *Process Control and Quality* **3**, 99-106 (1992).

9. Martens, H. & Martens, M. in *Near Infra-Red Spectroscopy: Bridging the Gap Between Data Analysis and NIR Applications* (eds Hildrum, K.I., Isaksson, T., Naes, T. & Tandberg, A.) 1-10 (1992).

10. Goddu, R. F. *Advances in Analytical Chemistry and Instrumentation* **1**, 347-424 (1960).

11. Whetsel, K. B. *Applied Spectroscopy Reviews* **2**, 1-67 (1968).

12. Morrison, R. T. & Boyd, R. N. *Organic Chemistry* (Allyn & Bacon, 1987).

13. Mackinson, R., Brinkworth, S. J., Belchamber, R. M., et al. *Applied Spectroscopy* **46(6)**, 1020-1024 (1994).

14. Miller, C. E. *Applied Spectroscopy Reviews* **26**, 277-339 (1991).

15. LeFebre, D. A. & Thomas, G. P. *Adv. Instrum. Control* **21**, 51-64 (1985).

16. Bickel, A. *I&CS* **62**(July), 45-48 (1989).

17. Kilham, L. B. & Weiss, S. *Modern Plastics* **66**(August), 65(1989).

18. McDermott, L. P. *Adv. Instrum. Control* **45**, 669-677 (1990).

19. McPeters, H. L. & Willams, S. O. *Process Control and Quality* **3**, 75-83 (1992).

20. Eschenauer, U., Siesler, H. W., Henck, O., Huhne, M., Wu, P. & Zebger, I. in *Near Infra-Red Spectroscopy: Bridging the Gap Between Data Analysis and NIR Applications* (eds Hildrum, K.I., Isaksson, T., Naes, T. & Tandberg, A.) 11-18 (1992).

21. Coventry, G. *Manuf. Chem.* **62(4)**, 35-37 (1994).

22. Martin, K. A. *Applied Spectroscopy Reviews* **27(4)**, 325-383 (1992).

23. Wold, S., Esbensen, K. & Geladi, P. *Chemometrics and Intelligent Laboratory Systems* **2**, 37-52 (1987).

24. Beebe, K. R. & Kowalski, B. R. *Analytical Chemistry* **59**, 1007 A-1017 A (1987).

25. Brown, G. K. *Proc. SPIE-Int Soc. Opt. Eng.* **1681**, 304-306 (1992).

26. Batra, J., Khettry, A. & Hansen, M. G. *Polymer Engineering and Science* **34**, 1767-1772 (1994).

27. Kowalski, B. R. & Seasholtz, M. B. *Journal of Chemometrics* **5**, 129-145 (1991).

28. Kresta, J. V., MacGregor, J. F. & Marlin, T. E. *The Canadian Journal of Chemical Engineering* **69**, 35-47 (1991).

29. Miller, C. E. *Applied Spectroscopy* **47**, 222-228 (1993).

30. Pirouette, Multivariate Data Analysis (version 1.2): Infometrix Inc. (1990).

31. Rannar, S., Lindgren, F., Geladi, P. & Wold, S. *Journal of Chemometrics* **8**, 111-125 (1994).

32. Jong, S. d. & Braak, C. J. *Journal of Chemometrics* **8**, 169-174 (1994).

33. Hoskuldsson, A. *Journal of Chemometrics* **2**, 211-228 (1988).

34. Geladi, P. & Kowalski, B. R. *Analytica Chimica Acta* **185**, 1-17 (1986).

35. Lorber, A., Wangen, L. E. & Kowalski, B. R. *Journal of Chemometrics* **1**, 19-31 (1987).

36. Helland, I. S. *Commun. Statist. Simula.* **17**, 581-607 (1988).

37. Martens, H. & Tormod, N. *Multivariate Calibration* (John Wiley & Sons, 1989).

38. Sutter, J. M., Kalivas, J. H. & Lang, P. M. *Journal of Chemometrics* **6**, 217-225 (1992).

39. Jong, S. d. *Chemometrics and Intelligent Laboratory Systems* **18**, 251-263 (1993).

40. Wang, T. W., Khettry, A., Berry, M., & Batra, J., SVDPLS: An Efficient Algorithm for Performing PLS. The First International Chemometrics InterNet Conference, InCINC'94 (1994).

41. Greive, W. H. & Doepken, D. D. *Polymer Engineering and Science* January, 19-23 (1968).

42. Takeuchi, T., Tsuge, S. & Sugimura, Y. *Analytical Chemistry* **41**, 184-186 (1969).

43. Crandall, E. W., Johnson, E. L. & Smith, C. H. *Journal of Applied Polymer Science* **19**, 897-903 (1975).

44. Crandall, E. W. & Jagtap, A. N. *Journal of Applied Polymer Science* **21**, 449-454 (1977).

45. Weyer, L. G. *Journal of Applied Polymer Science* **31**, 2417-2431 (1986).

46. Paputa, M. C. P., Carter, R. O. & Quaderi, S. B. A. *Journal of Applied Polymer Science* **33**, 77-86 (1987).

47. Siesler, H. W. *Mikrochimica Acta* **I**, 117-120 (1988).

48. Miller, C. E. *Applied Spectroscopy* **43**, 1435-1443 (1989).

49. Miller, C. E. & Eichinger, B. E. *Applied Spectroscopy* **44(3)**, 496-504 (1990).

50. Miller, C. E., Edelman, P. G., Ratner, B. D. & Eichinger, B. E. *Applied Spectroscopy* **44**, 581-586 (1990).

51. Miller, C. E., Eichinger, B. E., Gurley, T. W. & Hermiller, J. G. *Analytical Chemistry* **62**, 1778-1785 (1990).

52. Miller, C. E. & Eichinger, B. E. *Applied Spectroscopy* **44**, 887-894 (1990).

53. Miller, C. E., Edelman, P. G. & Ratner, B. D. *Applied Spectroscopy* **44**, 576-580 (1990).

54. Siesler, H. W. *Makromol. Chem. , Macromol. Symp.* **52**, 113-129 (1991).

55. Miller, C. E. & Eichinger, B. E. *Journal of Applied Polymer Science* **42**, 2169-2190 (1991).

56. Haagen, S., Drosdzoik, D., Riemann, G., Wuller, K. & Oelichmann, J. *Proc. SPIE-Int Soc. Opt. Eng.* **1575**, 375-376 (1992).

57. Miller, C. E. in *Making Light Work: Adv. Near Infrared Spectrosc., Int. Conf. Near Infrared Spectrosc.* (eds Murray, I. & Cowe, I.A.) 519-524 (1992).

58. Communication to the editor, *Bipolymers* **II**, 1305-1309 (1992).

59. Ciurczak, E. E. *CHEMTECH* June, 374-380 (1992).

60. Kradgel, C. & McDermott, L. in *Handbook of NIR Analysis* (eds Burns, D.A. & Ciurczak, E.W.) 565-608 (1992).

61. Weyer, L. G. in *Making Light Work: Adv. Near Infrared Spectrosc., Int. Conf. Near Infrared Spectrosc.* (eds Murray, I. & Cowe, I.A.) 430-437 (1992).

62. Grob, R. L., Skahan, D. J., Dix, K. & Nielsen, K. *Process Control and Quality* **2**, 225-235 (1992).

63. Miller, K. L. in *Making Light Work: Adv. Near Infrared Spectrosc., Int. Conf. Near Infrared Spectrosc.* (eds Murray, I. & Cowe, I.A.) 454-460 (1992).

64. Bunding Lee, K. A. *Applied Spectroscopy Reviews* **28(3)**, 231-284 (1993).

65. Min, B.-G., Stachurski, Z. H. & Hodgkin, J. H. *Polymer* **34**, 4908-4912 (1993).

66. Miller, C. E., Svendsen, S. A. & Naes, T. *Applied Spectroscopy* **47**, 346-356 (1993).

67. Gossen, P. D., MacGregor, J. F. & Pelton, R. H. *Applied Spectroscopy* **47**, 1852-1870 (1993).

68. Long, T. E., Liu, H. Y., Schell, B. A., Teegarden, D. M. & Uerz, D. S. *Macromolecules* **26**, 6237-6242 (1993).

69. DeThomas, F. A., Hall, J. W. & Monfre, S. L. *Talanta* **41**, 425-431 (1994).

70. Ghebremeskel, Y., Fields, J. & Garton, A. *Journal of Polymer Science* **32**, 383-386 (1994).

71. Parisi, A. F., Nogueiras, L. & Prieto, H. *Analytica Chimica Acta* **238**, 95-100 (1990).

72. Lang, G. *I&CS* **64**(April), 99-102 (1991).

73. Shenk, J. S., Workman Jr., J. J. & Westerhaus, M. O. in *Handbook of NIR Analysis* (eds Burns, D.A. & Ciurcazk, E.W.) 383-432 (1992).

74. Carmelli, I., Descales, B., Llinas, J. R., Martens, A. & Vidal, J. L. in *Near Infra-Red Spectroscopy: Bridging the Gap Between Data Analysis and NIR Applications* (eds Hildrum, K.I., Isaksson, T., Naes, T. & Tandberg, A.) 395-400 (1992).

75. Buchanan, B. in *Handbook of NIR Analysis* (eds Burns, D.A. & Ciurczak, E.W.) 643-653 (1992).

76. Ciurzak, E. W. in *Handbook of NIR Analysis* (eds Burns, D.A. & Ciurczak, E.W.) 549-563 (1992).

77. Diffee, J. T. in *Handbook of NIR Analysis* (eds Burns, D.A. & Ciurczak, E.W.) 433-473 (1992).

78. Hammersley, M. J. in *Handbook of NIR Analysis* (eds Burns, D.A. & Ciurczak, E.W.) 475-493 (1992).

79. Ghosh, S. & Rodgers, J. in *Handbook of NIR Analysis* (eds Burns, D.A. & Ciurczak, E.W.) 495-526 (1992).

80. Osborne, B. G. in *Handbook of NIR Analysis* (eds Burns, D.A. & Ciurczak, E.W.) 527-547 (1992).

81. Frankhuizen, R. in *Handbook of NIR Analysis* (eds Burns, D.A. & Ciurczak, E.W.) 609-641 (1992).

82. Kington, L. R. & Jones, T. M. in *Handbook of NIR Analysis* (eds Burns, D.A. & Ciurczak, E.W.) 655-662 (1992).

83. Schirmer, R. E. *Adv. Instrum. Control* **41**, 1229-1236 (1986).

84. Montanye, J. R. *Modern Plastics* Mid-Nov, B-15-B-18 (1994).

85. Jalbert, R. L. & Smejkal, J.P. *Modern Plastics Encyclopedia*, 108-110 (1976).

86. Ratzsch, M., Haudel, G., Pompe, G. & Meyer, E. *J. Macromol. Sci.-Chem.* **27**, 1631-1655 (1990).

87. Han, C. D. & Yang, H. H. *Journal of Applied Polymer Science* **33**, 1221-1229 (1987).

88. Kim, J.H., Keskkula, H. & Paul, D.R. *Journal of Applied Polymer Science* **40**, 183-201 (1990).

89. Kim, B. K. & Shin, G. S. *Journal of Applied Polymer Science* **48**, 945-951 (1993).

90. Barlow, J.W. *Makromol. Chem., Macromol. Symp.* **70/71**, 235-244 (1993).

91. Machado, J.M. & Lee, C. S. *Polymer Engineering and Science* **34**, 59-68 (1994).

92. *Modern Plastics Encyclopedia Handbook* (eds Modern Plastics Magazine) (McGraw Hill, 1994).

93. Paul, D. R., Keitz, J. D. & Barlow, J. W. *Journal of Applied Polymer Science* **29**, 3131-3145 (1984).

94. Paul, D. R. & Kim, C. K. *Polymer* **33**, 4941-4950 (1992).

95. Cheng, T.W., Keskkula, H. & Paul, D.R. *Polymer* **33**, 1606-1619 (1992).

96. Kodama, M. *Polymer Journal* **25**, 95-98 (1993).

97. Janarthanan, V., Stein, R. S. & Garrett, P.D. *Journal of Applied Polymer Science* **31**, 1995-2001 (1993).

98. Paul, D.R., Callaghan, T. A. & Takakuwa, K. *Polymer* **34**, 3796-3808 (1993).

99. Kodama, M. *Polymer Engineering and Science* **33**, 1141-1145 (1993).

100. Hobbs, S. Y. & Watkins, V. H. *Polymer* **34**, 3955-3959 (1993).

101. Nachlis, W. L., Kambour, R. P. & MacKnight, W. J. *Polymer* **35**, 3643-3657 (1994).

102. Gan, P. P. & Paul, D. R. *Polymer* **35**, 3513-3524 (1994).

103. Suarez, H., Barlow, J.W. & Paul, D.R. *Journal of Applied Polymer Science* **29**, 3253-3259 (1984).

104. Wu, J. S., Shen, S. C. & Chang, F. C. *Polymer Journal* **26**, 33-42 (1994).

105. Rudd, J. F. (to Dow Chemical Co.), U.S. Patent 4,243,764 (1981).

106. Wu, J., Shen, S. & Chang, F. *Journal of Applied Polymer Science* **50**, 1379-1389 (1993).

107. The Mathworks, Inc., Cochituate Place, 24 Prime Parkway, Natick, MA 01760.

108. Wise, B. M. (Batelle Pacific Northwest Laboratories), Chemometrics Toolbox (1991).

APPENDICES

A. DATA ANALYSIS

This section describes the procedure for the multivariate analysis of the NIR spectral data on the Unix based software MATLAB [107], available on the University's Sun Workstations. Codes for multivariate techniques like partial least squares (PLS) and principal component regression (PCR) were written in the MATLAB environment and were extensively used for data analysis in this research. These codes have been included in this appendix.

The NIR absorbance data files were stored by the Guided Wave Model 260 in ASCII format with the absorbance values saved as a column of data in each data file. These data files contained 15 lines of information regarding date of spectral data collection, starting wavelength, ending wavelength, wavelength increments, etc. The spectral data files were then examined using Guided Wave Examiner program and pretreated for baseline offsets and scattering by first smoothing the data, followed by either a two-point baseline correction or calculation of first derivatives of absorbance spectra. The pretreated data files were then transferred to the Sun Workstations. The initial lines containing the information about the data files had to be deleted in order for the files to be loaded into MATLAB. A C-shell file which is included in this appendix was used to remove the initial lines and store the NIR absorbance data with a .mat extension for data analysis.

After stripping off the first few lines of headers, the spectral data files were loaded individually as a column of 1201 data points corresponding to the absorbance/first derivative absorbance values from 1200 nm to 2400 nm. All the spectral data files for the

calibration and validation sets appeared as a column of data which were then transposed to a row and concatenated to form the absorbance/first derivative absorbance data matrix (X). The X(i,j) element of this matrix corresponded to the absorbance/first derivative absorbance value of the ith spectra at the jth wavelength.

The concentration matrix (Y) was then created manually by inputting the concentration values corresponding to each row (or spectrum) in X. The number of rows in X and Y were same, although the number of columns in X corresponded to the number of wavelengths being selected for calibration and predictions, and the number of columns in Y corresponded to the different constituents whose concentrations were to be calibrated in the model. The calibration data sets (xc and yc) and prediction data sets (xp and yp) created by this approach were then stored in a MATLAB file with .mat extension and subsequently loaded in the codes for data analysis.

The PLS and PCR codes used in this research, along with some codes from a chemometrics toolbox provided by Wise [108], were based on singular value decomposition approach. The codes and routines used in the data analysis along with a brief description of the functions they perform are presented here:

1. strip.script — A C-shell file to remove the first few header lines (created by Guided Wave Scanner) prior to data analysis in MATLAB.
2. pls.m — Main executable file for PLS regression on the spectral and compositional data sets.
3. pcr.m — Main executable file for PCR analysis on the spectral and compositional data sets.

4. auto.m	Function file to calculate the column mean and standard deviation of a data matrix.
5. scale.m	Function file to mean-center a data matrix and normalize it w.r.t. the standard deviation of each column.
6. spls.m	Function file to determine the loadings and scores matrices for the calibration data set using PLS. This file also calculates the regression coefficients of the concentration vs. absorbance data sets.
7. plssvd.m	Subprogram used in the function file spls.m. This subroutine executes the SVD based algorithm for PLS. Eigenvectors of the residual covariance matrix are calculated in this subprogram.
8. rescale.m	Function file to rescale a data matrix using column mean and standard deviation.
9. plspred.m	Function file to calculate the concentration values based on absorbance data and calibration model parameters.
10. spcr.m	Function file to determine the loadings and scores matrices for the calibration data set using PCR. This file also calculates the regression coefficients of the concentration vs. absorbance data sets.
11. lagpls.m	Main executable file for leave-a-group (LAG) approach.
12. laspls.m	Main executable file for leave-a-sample (LAS) approach.
13. anal_plots.m	Function file that uses the results from pls.m and pcr.m to plot scores, loadings, variance, and model predictions for a qualitative and quantitative interpretation of results.

The steps in the data analysis can be summarized as follows:

a. Pretreat raw spectral data for baseline offsets and scattering by smoothing data, followed by baseline corrections/first derivative absorbance calculations.

b. Transfer data files from the personal computer onto the Unix Workstations.

c. Delete the initial information lines (headers) in these data files using a C-shell program, prior to data analysis in MATLAB.

d. Form initial absorbance/first derivative absorbance data matrix (X) and concentration matrix (Y), followed by forming calibration data sets (xc and yc) and prediction data sets (xp and yp). Save data with .mat extension.

e. Load data files into the main executable programs for PLS and PCR. Input number of factors to be used in the initial model.

f. The data files standardized using function files in the main program, are subsequently used to extract factors using SVD based PLS and PCR. Scores and loading matrices are computed by an iterative procedure using the residual covariance matrix approach.

g. Predicted concentrations for the calibration and prediction sets using model parameters, standard errors of calibration (SEC), standard errors of prediction (SEP), and predicted residual sum of squares (PRESS) are calculated for each factor.

h. The optimum number of factors corresponding to the minimum SEP and PRESS values are determined. Repeat steps e-g are by inputting the optimal number of factors in the executable files for PLS and PCR.

i. The final prediction results for the calibration and validation sets corresponding to the optimal number of factors are then determined using the PLS and PCR codes.

j. Interpret (both qualitatively and quantitatively) scores, loadings, variance, model parameters and predictions, , with the help of tables and plots.

B. COMPUTER CODES

```
% File to remove the first 15 lines of the spectral data files created in Guided Wave
% Scanner software for use in MATLAB
######## strip.script #########
/* put all files into subdir then do csh strip.script */
set tmplist=`ls`
echo "List $tmplist"
echo $tmplist | nawk '{for (i = 1; i <= NF; i++){len=length($i); infile=$i;
outfile=substr(infile,1,len) ".dat"; print infile; print outfile; syscom="sed -e 1,15d "infile
">" outfile; print syscom; system(syscom)}}'
```

MATLAB CODES

```
% ######## pls.m #########

% This is the main file for PLS regression for building calibration models based on the
% absorbance and concentration data sets

% (C) Copyright
% Jitender Batra, Pramit Sarma, Atul Khettry and Tse-Wei Wang
% 1994

% modified in part by Manish Sangal
% 1995

        clear;
        t0=clock;

        load data.mat

        mxc = min(size(xc));
        mxp = min(size(xp));

% Mean-centering and normalization of spectral and compositional data

[xcc,mx] = auto(xc);
xpc = scale(xp,mx);
[ycc,my] = auto(yc);

lv = input('How many factors ?')
sec=zeros(1,lv);
```

```
sep=zeros(1,lv);

% Loop in which factors are successively determined. Prediction results for the
% calibration and prediction sets, standard errors of calibration (SEC), standard errors of
% prediction (SEP), and predicted residual sum of squares are calculated:

for j=1:lv,

        [P,Q,W,T,U,b,ssqdif,beta]=spls(xcc,ycc,j);

        xnew = zeros(size(xc));

        for i = 1:j,
                xnew = xnew + T(:,i)*P(:,i)';
        end

        xnew = rescale(xnew,mx);

        residuals=xc-xnew;
        ypc  = plspred(xcc,b,P,Q,W,j);
        sypc = rescale(ypc,my);

        ypred = plspred(xpc,b,P,Q,W,j);
        sypred = rescale(ypred,my);

        sec(1,j) = sqrt(sum((sypc - yc).^2)/(mxc-1));
        sep(1,j) = sqrt(sum((sypred - yp).^2)/mxp);

        AA(:,j)=yp;
        BB(:,j)=sypred;

end

PRESS=sum((AA-BB).^2);

etime(clock,t0)

% This part calculates the scores for the first three factors

f1=T(:,1)*(P(:,1)');
f2=T(:,2)*(P(:,2)');
tf2=T(:,1:2)*(P(:,1:2)');
tf3=T(:,1:3)*(P(:,1:3)');
```

```
% The percentage explained variance of the variables is calculated here:

vxc=diag(cov(xc));

vf1=diag(cov(f1));
vf2=diag(cov(f2));
vtf2=diag(cov(tf2));
vtf3=diag(cov(tf3));

ratio1=100*(vf1./vxc);
ratio2=100*(vf2./vxc);
tratio2=100*(vtf2./vxc);
tratio3=100*(vtf3./vxc);

w=linspace(1,size(xc,2),size(xc,2));
wave=linspace(1600,1800,size(xc,2));
```

```
% ######## spls.m #########

function [P,Q,W,T,U,b,ssqdif,beta] = spls(x,y,lv)

% This PLS program calculates the P, Q, W, T, and U matrices for the given x and y
% blocks and the number of latent variables specified:  1 <= lv <= dim(x); using the SVD
% method.  It also outputs the fraction of variance used in the x and y matrices; the
% equivalent LSR coefs (beta).  Input format is as follows:

% (C) Copyright
% Jitender Batra, Pramit Sarma, Atul Khettry and Tse-Wei Wang

% 1993

[mx,nx] = size(x);
[my,ny] = size(y);

if (nx < lv)
        error('No. of LVs must be <= no. of x-block variables')
end;

X = x;
Y = y;
```

```
P   = zeros(nx,lv);
Q   = zeros(ny,lv);
W   = zeros(nx,lv);
T   = zeros(mx,lv);
U   = zeros(my,lv);
b   = zeros(1,lv);
ssq  = zeros(lv,2);
ssqx = 0;

for i = 1:nx
        ssqx = ssqx + sum(x(:,i).^2);
end;

ssqy = sum(sum(y.^2)');

for i = 1:lv

        [p,q,w,t,u,SR] = plssvd(x,y);
        SR;
        b(1,i) = u'*t/(t'*t);
        x = x - t*p';
        y = y - b(1,i)*t*q';
        ssq(i,1) = (sum(sum(x.^2)'))*100/ssqx;
        ssq(i,2) = (sum(sum(y.^2)'))*100/ssqy;
        T(:,1) = t(:,i);
        U(:,1) = u(:,i);
        P(:,1) = p(:,i);
        W(:,1) = w(:,i);
        Q(:,1) = q(:,i);
end;

% This step computes the regression coefficients (Beta) and the predicted y - block

Beta = W*pinv(X*W)*Y;
ypred = X*Beta;

ssqdif = zeros(lv,2);
ssqdif(1,1) = 100 - ssq(1,1);
ssqdif(1,2) = 100 - ssq(1,2);

for i = 2:lv,
        for j = 1:2,
                ssqdif(i,j) = 100 - ssq(1,1);
```

```
        end;
end;

disp(' ');
disp('          Percent Variance Captured by PLS Model') disp(' ')
disp('                  ------X - Block------                    -----Y - Block------')
disp(' LV#              This LV       Total                      This LV       Total')
disp([(1:lv)' ssqdif(:,1) cumsum(ssqdif(:,1)) ssqdif(:,2) cumsum(ssqdif(:,2))])
```

```
% ######## plssvd.m #########

function [p,q,w,t,u,SR] = plssvd(x,y);

% This program executes the SVD based algorithm for PLS. This runs as a subprogram
% of a main program as it calculates only one latent variable or factor. The format to
% invoke in the main program is: [p,q,w,t,u,SR] = plssvd(x,y)

% (C) Copyright
% Jitender Batra, Pramit Sarma, Atul Khettry, M.G. Hansen, and Tse-Wei Wang
% 1993

% This step calulates the covariance between x and y
        RY = x'*y;
        [my,ny] = size(y);

% If number of y variables is equal to one, svd step is not required. The normalized
% covariance matrix is used to compute the principal component

        if (ny == 1)
                w = RY/norm(RY);
                t = x*w;
                q = 1;
        end;

% If there are more than one y variables, svd of the covariance matrix yields the principal
% component

        if (ny ~= 1)
                [UR,SR,VR] = svd(RY,0);
                w = UR(:,1);
                t = x*w;
```

```
        q = (t'*y)';
        q = (q'/norm(q'))';
    end;

    p = (t'*x/(t'*t))';
```

```
% ####### auto.m #########

function [ax,mx,stdx] = auto(x)

% autoscales matrix x and returns a vector of means (mx) and standard deviations (stdx)
% used in the scaling.  I/O format is:  [ax,mx,stdx] = auto(x)

[m,n] = size(x);

% Copyright
% Barry M. Wise
% 1991

% Calculate the mean and standard deviation of the input data.  Open a matrix with zeros
% for the scaled data (this makes the function faster since it doesn't have to resize y)

mx = mean(x);
stdx = std(x);
ax = zeros(m,n);

for i = 1:m
        ax(i,:) = (x(i,:) - mx)./stdx;
end
```

```
% ####### scale.m #########

function sx = scale(x,means,stds)

% Scales matrix x using means (mx) and standard deviations (stds) specified.  I/O format
% is:  sx = scale(x,means,stds);  If only two input arguments are supplied then the
% function will not do variance scaling, but only vector subtraction.

% I/O format is:  sx = scale(x,means);
```

```
% Copyright
% Barry M. Wise
% 1991

[m,n] = size(x);
sx = zeros(m,n);
if nargin == 3

        for i = 1:m
                sx(i,:) = (x(i,:)-means)./stds;
        end

        else

        for i = 1:m
                sx(i,:) = (x(i,:)-means);
        end
end
```

```
% ######## rescale.m ##########

function rx = rescale(x,mx,stdx)

% Rescales matrix x using the means (mx) and standard deviation (stdx) vectors specified.
% I/O format is: rx = rescale(x,mx,stdx); If only two input arguments are supplied the
% function rescales the means only. The I/O format is then: rx = rescale(x,mx);

% Copyright
% Barry M. Wise
% 1991

[m,n] = size(x);
rx = zeros(m,n);

if nargin == 3
        for i = 1:m
                rx(i,:) = (x(i,:).*stdx)+mx;
        end

        else

        for i = 1:m
```

```
            rx(i,:) = x(i,:)+mx;
        end
end
```

```
% ####### plspred.m #########

function ypred = plspred(x,b,P,Q,W,lv)

% This program uses pls model parameters to predict the responses to a new x block.
% Input/output sequence is:

% Copyright
% Barry M. Wise
% 1991

[mx,nx] = size(x);
[mq,nq]  = size(Q);
that = zeros(mx,lv);
ypred = zeros(mx,mq);

for i = 1:lv
        that(:,i) = x*W(:,i);
        x  = x - that(:,i)*P(:,i)';
end

for i = 1:lv
        ypred = ypred + b(1,i)*that(:,i)*Q(:,1)';
end
```

```
% ####### lagpls.m #########

% This is the main file for PLS regression for building models based on the leave-a-group
% (LAG) approach from the absorbance and concentration data of the calibration set.

% (C) Copyright
% Manish Sangal
% 1995

        clear;
%       t0=clock;
```

```
        load calset.mat

        xc1=XC(:,1:1201);
        yc1=YC(:,1);

t=input('Total number of concentration levels?')
lv = input('How many factors ?')

tsec=zeros(2,lv);
tsep=zeros(2,lv);

% This step determines the two groups from the calibration data set for the LAG
% approach; one as the calibration set the other as the prediction set. This procedure is
% then repeated with the calibration set for the first case as the prediction set for the
% second case and the prediction set for the first case as the calibration set for the second
% case.

for s=1:2;

        if s==1,
        xc=[xc1(1,:);xc1(2:2:(t-1),:);xc1(t,:)];
        xp=xc1(3:2:(t-2),:);
        yc=[yc1(1,:);yc1(2:2:(t-1),:);yc1(t,:)];
        yp=yc1(3:2:(t-2),:);
        end

        if s==2,
        xc=[xc1(1,:);xc1(3:2:(t-2),:);xc1(t,:)];
        xp=xc1(2:2:(t-1),:);
        yc=[yc1(1,:);yc1(3:2:(t-2),:);yc1(t,:)];
        yp=yc1(2:2:(t-1),:);
        end

        mxc = min(size(xc));
        mxp = min(size(xp));

% Mean-centering and normalization of data sets

[xcc,mx] = auto(xc);
xpc = scale(xp,mx);
[ycc,my] = auto(yc);
```

```
sec=zeros(1,lv);
sep=zeros(1,lv);

% Loop in which factors are successively determined. Prediction results for the
% calibration and prediction sets, standard errors of calibration (SEC), standard errors of
% prediction (SEP), and predicted residual sum of squares are calculated here:

for j=1:lv,

[P,Q,W,T,U,b,ssqdif,beta]=spls(xcc,ycc,j);

xnew = zeros(size(xc));

for i = 1:j,
        xnew = xnew + T(:,i)*P(:,i)';
end

xnew = rescale(xnew,mx);
residuals = xc-xnew;
ypc  = plspred(xcc,b,P,Q,W,j);
sypc = rescale(ypc,my);

ypred = plspred(xpc,b,P,Q,W,j);

sypred = rescale(ypred,my);
sec(:,j) = sqrt(sum((sypc - yc).^2)/(mxc-1));
sep(:,j) = sqrt(sum((sypred - yp).^2)/mxp);
AA(:,j)=yp;
BB(:,j)=sypred;

end

PRESS=sum((AA-BB).^2);

TPRESS(s,:)=PRESS;

% The predictions for the two sets of LAG data are calculated in this section.

if s==1,
typc1(:,1)=ypc;
tsypc1(:,1)=sypc;
typred1(:,1)=ypred;
typ1(:,1)=yp;
```

```
tsypred1(:,1)=sypred;
end

if s==2,
typc2(:,1)=ypc;
tsypc2(:,1)=sypc;
typred2(:,1)=ypred;
typ2(:,1)=yp;
tsypred2(:,1)=sypred;
end

tsec(s,:)=sec;
tsep(s,:)=sep;

clear xc xp yc yp

clear PRESS AA BB

clear sep sec ypc sypc ypred sypred residuals

end
% etime(clock,t0)
```

```
% ######## laspls.m #########

% This is the main file for PLS regression for building models based on the leave-a-
% sample (LAS) approach from the absorbance and concentration data of the calibration
% set.

% (C) Copyright
% Manish Sangal
% 1995

        clear;
%       t0=clock;

        load calset.mat

        xc1=XC(:,1:1201);
        yc1=YC(:,1);

t=input('Total number of samples in calibration set?')
```

```
lv = input('How many factors ?')

tsec=zeros(t,lv);
tsep=zeros(t,lv);

% This step determines the two sets for the LAS approach; one as the calibration set
% the other as the prediction set. This procedure is repeated for all the samples in the
% initial calibration set data (calset.mat).

for s=1:t;
        if s==1,
        xc=xc1(2:t,:);
        xp=xc1(1,:);
        yc=yc1(2:t,:);
        yp=yc1(1,:);
        end

        xc=[xc1(1:(s-1),:);xc1((s+1):t,:)];
        xp=xc1(s,:);
        yc=[yc1(1:(s-1),:);yc1((s+1):t,:)];
        yp=yc1(s,:);

        if s==t,
        xc=xc1(1:(t-1),:);
        xp=xc1(t,:);
        yc=yc1(1:(t-1),:);
        yp=yc1(t,:);
        end

        mxc = min(size(xc));
        mxp = min(size(xp));

% Mean-centering and normalization of data sets

[xcc,mx] = auto(xc);
xpc = scale(xp,mx);
[ycc,my] = auto(yc);

sec=zeros(1,lv);
sep=zeros(1,lv);

% Loop in which factors are successively determined. Prediction results for the
% calibration and prediction sets, standard errors of calibration (SEC), standard errors of
```

```
% prediction (SEP), and predicted residual sum of squares are calculated here:

for j=1:lv


[P,Q,W,T,U,b,ssqdif,beta]=spls(xcc,ycc,j);

xnew = zeros(size(xc));

for i = 1:j,
        xnew = xnew + T(:,i)*P(:,i)';
end

xnew = rescale(xnew,mx);
residuals = xc-xnew;
ypc  = plspred(xcc,b,P,Q,W,j);
sypc = rescale(ypc,my);

ypred = plspred(xpc,b,P,Q,W,j);

sypred = rescale(ypred,my);
sec(:,j) = sqrt(sum((sypc - yc).^2)/(mxc-1));
sep(:,j) = sqrt((sypred - yp).^2/mxp);
AA(:,j)=yp;
BB(:,j)=sypred;

end


% The predictions for the LAS approach are calculated in this section.

PRESS=(AA-BB).^2;

TPRESS(s,:)=PRESS;
typc(:,s)=ypc;
tsypc(:,s)=sypc;
typred(:,s)=ypred;
typ(:,s)=yp;
tsypred(:,s)=sypred;
tsec(s,:)=sec;
tsep(s,:)=sep;

clear xc xp yc yp
```

```
clear PRESS AA BB

clear sep sec ypc sypc ypred sypred residuals

end

% etime(clock,t0)

-----------------------------------------------------------------------------------------------

% ######## anal_plots.m ##########

% The data analysis by explanatory plots can be obtained by the given routines. (The
% following example is taken for the ABS/SAN blends in the region from 1600 nm to
% 1800 nm)

% (C) Copyright
% Manish Sangal
% 1995

% Overlaid spectra of ABS/SAN polymer blends (10% concentration increases)

figure(1)

plot(wave,xc(1:2:21,:))
axis([1600 1800 0 0.55])
xlabel('Wavelength (nm)')
ylabel('Absorbance')
text(1671,0.32,'Pure ABS')
text(1680,0.52,'Pure SAN')
text(1715,0.12,'Pure SAN')
text(1725,0.25,'Pure ABS')

%print -deps diag1

%**************************************

figure(2)

% (a) % variances explained by variables for factor 1 only

subplot(2,1,1)
```

```
plot(wave,ratio1,'o')
axis([1600 1800 0 100])
xlabel('Wavelength (nm)')
ylabel('% Explained Variance')

%**********

%  (b) % variances explained by variables for factor 2 only

subplot(2,1,2)
plot(wave,ratio2,'o')
axis([1600 1800 0 100])
xlabel('Wavelength (nm)')
ylabel('% Explained Variance')

%print -deps diag2

%****************************************

figure(3)

%  Total variances explained by variables after (for) 2 factors

subplot(2,1,1)
plot(wave,tratio2,'o')
axis([1600 1800 0 100])
xlabel('Wavelength (nm)')
ylabel('% Explained Variance')

%**********

%  Total variances explained by variables after (for) 3 factors

subplot(2,1,2)
plot(wave,tratio3,'o')
axis([1600 1800 0 100])
xlabel('Wavelength (nm)')
ylabel('% Explained Variance')

%print -deps diag3

%****************************************
```

```
% Plot of SEP and SEC values with increasing number of factors

figure(4)

fac=1:1:5;
plot(fac,sec,'--')
hold on
plot(fac,sec,'o')
plot(fac,sep)
plot(fac,sep,'*')
xlabel('Factors')
ylabel('Standard Error')
text(3,2,'-- SEC')
text(3,1.9,'- SEP')
hold off

%print -deps diag4

%****************************************

% Scores plot (for the calibration samples) for the first three factors

figure(5)

plot3(T(:,1),T(:,2),T(:,3),'o')
hold on
axis([-0.4 .4 -.4 .4 -0.1 .4])
l=[-.38;.38];
m=[0;0];
n=m;
o=[-0.05;.35];
plot3(l,m,n)
plot3(m,l,n)
plot3(m,n,o)
grid on
xlabel('Factor 1 scores')
ylabel('Factor 2 scores')
zlabel('Factor 3 scores')
text(0.32,0.05,0.025,'PC1 scores')
text(-0.05,.38,0.02,'PC2 scores')
text(-0.05,0,0.4,'PC3 scores')

%print -deps diag5
```

```
%****************************************

% Scores plot for factor 1 and factor 2 (as seen from the direction of factor 3)

figure(6)

clf
plot3(T(:,1),T(:,2),T(:,3),'o')
hold on
axis([-0.4 .4 -.4 .4 -0.1 .4])
l=[-.38;.38];
m=[0;0];
n=m;
o=[-0.05;.35];
plot3(l,m,n)
plot3(m,l,n)
plot3(m,n,o)
grid on
hold off
view([0 0 1])
text(.32,0.025,0,'PC1 scores')
text(-0.05,0.4,0,'PC2 scores')
xlabel('Factor 1 scores')
ylabel('Factor 2 scores')
hold off

%print -deps diag6

%****************************************

figure(7)

% Scores plot for factor 2 and factor 3 (as seen from the direction of factor 1)

subplot(2,1,1)
plot3(T(:,1),T(:,2),T(:,3),'o')
hold on
axis([-0.4 .4 -.4 .4 -0.1 .4])
l=[-.38;.38];
m=[0;0];
n=m;
o=[-0.05;.35];
```

```
plot3(l,m,n)
plot3(m,l,n)
plot3(m,n,o)
grid on
hold off
view([1 0 0])
text(0,.32,0.02,'PC2 scores')
text(0,-0.05,0.4,'PC3 scores')
ylabel('Factor 2 scores')
zlabel('Factor 3 scores')

%**********

% Scores plot for factor 1 and factor 3 (as seen from the direction of factor 2)

subplot(2,1,2)
plot3(T(:,1),T(:,2),T(:,3),'o')
hold on
axis([-0.4 .4 -.4 .4 -0.1 .4])
l=[-.38;.38];
m=[0;0];
n=m;
o=[-0.05;.35];
plot3(l,m,n)
plot3(m,l,n)
plot3(m,n,o)
grid on
hold off
view([0 -1 0])
text(0.32,0,0.025,'PC1 scores')
text(-0.05,0,0.4,'PC3 scores')
xlabel('Factor 1 scores')
zlabel('Factor 3 scores')
hold off

%print -deps diag7

**********************************************

% Scores plots for first and second factors versus samples in calibration set

figure(8)
```

```
samp=1:1:11;
plot(samp,T(:,1),'o')
hold on
axis([1 11 -0.4 0.4])
plot(samp,T(:,2),'x')
plot(samp,T(:,3),'+')
text(5,0.35,'o  scores for first factor')
text(5,0.31,'x  scores for second factor')
text(5,0.27,'+  scores for third factor')
xlabel('Sample Number')
ylabel('Scores')
hold off

%print -deps diag8

%*****************************************

% Loadings for first and second factors

figure(9)

plot(wave,P(:,1))
hold on
plot(wave,P(:,2),'--')
plot(wave,P(:,3),'-.')
axis([1600 1800 -0.2 0.2])
xlabel('Wavelength (nm)')
ylabel('Loadings')
text(1755,0.18,'- loadings for first factor')
text(1755,0.16,'-- loadings for second factor')
text(1755,0.14,'-. loadings for third factor')
hold off

%print -deps diag9

%*****************************************

% Model predictions for 88 samples in the validation set

figure(10)

plot(yp,sypred,'o')
a=[0;100];
```

```
b=a;
hold on
plot(a,b)
xlabel('Measured Concentration (wt. % ABS)')
ylabel('Predicted Concentration (wt. % ABS)')
text(50,95,'SEP=1.23')
hold off

%print -deps diag10

%*****************************************

% Model predictions for 11 samples in the calibration set

figure(11)

plot(yc,sypc,'o')
a=[0;100];
b=a;
hold on
plot(a,b)
xlabel('Measured Concentration (wt. % ABS)')
ylabel('Predicted Concentration (wt. % ABS)')
text(50,95,'SEC=0.80')

%print -deps diag11

%*****************************************
```

VITA

Manish Sangal was born in Meerut, India on July 5, 1970. He attended high school at Kendriya Vidyalaya Andrews Ganj, New Delhi, India. He joined Harcourt Butler Technological Institute (HBTI) in August 1988, where he received the Bachelor of Technology degree in Chemical Engineering in May 1992. In January 1993, he joined the University of Tennessee, Knoxville and received the Master of Science in Chemical Engineering in December 1995.